Blast protection with fluids

Tatiana Rigoulet

THESE DE DOCTORAT

NNT : 2023UPAST130

Protection contre les ondes de souffles à l'aide de fluide

Blast protection with fluids

Thèse de doctorat de l'université Paris-Saclay et de la Leibniz Universität Hannover

École doctorale École doctorale n° 579 : Sciences Mécaniques et Energétiques, Matériaux et Géosciences (SMEMaG)
Spécialité de doctorat : Mécanique des solides
Graduate School : Sciences de l'ingénierie et des systèmes. Référent : ENS Paris-Saclay

Thèse préparée dans l'unité de recherche **LMPS - Laboratoire de Mécanique Paris-Saclay** (Université Paris-Saclay, CentraleSupélec, ENS Paris-Saclay, CNRS) et l'**Institut für Kontinuumsmechanik**, sous la direction de **Federica DAGHIA**, directrice de thèse et la co-direction de **Peter WRIGGERS**, co-directeur de thèse

Thèse soutenue à Paris-Saclay, le 31 octobre 2023, par

Tatiana RIGOULET

Composition du jury

Membres du jury avec voix délibérative

Genevieve LANGDON Professeure des Universités, University of Sheffield	Présidente
Philipp JUNKER Professeur des Universités, Leibniz Universität Hannover	Rapporteur & Examinateur
David LECOMPTE Professeur des Universités, Royal Military Academy Brussels	Rapporteur & Examinateur
Michel ARRIGONI Professeur des Universités, ENSTA Bretagne	Examinateur

This work was carried out in three different institutions: the French-German Research Institute of Saint-Louis (ISL), the Laboratoire de Mécanique Paris-Saclay (LMPS) of the Université Paris-Saclay and the Institut für Kontinuumsmechanik (IKM) of the Leibniz Universität Hannover. Both universities are joined in the frame of the French-German doctoral college SNTA with the International Research Training Group 2657.

Acknowledgements

This Franco-German work bears witness to the collaboration between three research institutes in two countries, enriching the research journey with diverse perspectives and insights. The exchange of ideas and the collaborative spirit across borders have significantly contributed to the depth of this research, and for that, I am sincerely thankful.

In expressing my heartfelt appreciation, I extend my thanks to the individuals who have been the driving force behind the completion of this thesis. This experience not only broadened my academic horizons but also fostered meaningful connections with colleagues and mentors.

With profound appreciation, I extend my sincere gratitude to my supervisors, Ludovic BLANC, Federica DAGHIA and Peter WRIGGERS. Your guidance and mentorship has been instrumental in the completion of this work. Your unwavering support, insightful feedback, and encouragement have not only shaped the trajectory of this research but also fostered my intellectual development. Beyond our academic collaboration, working with you has been an absolute pleasure. Your approachability, collaborative spirit, and genuine enthusiasm for the subject matter created an inspiring working environment. I am grateful for the blend of academic rigor and camaraderie that defined our collaboration.

I would like to extend my gratitude to all my colleagues at ISL. Fabien, for always spotting the best desserts in the canteen. Thérèse, for being my companion in all my adventures, from the yoga room to Tokyo. Thierry, Laurent, Yannick, Dominique and many more for sitting through more than 300 experiments with me. And last but not least, Jean-Francois LEGENDRE for welcoming me to the team.

I am immensely grateful for the camaraderie and friendship extended by my fellow PhD students throughout this academic adventure. Floriane, Alexandre, Aurélia, Claire, Héloïse, Julien, Mahmoud, Pierre, Raphaël, Sofiane and many more, thank you for your collective support, shared experiences, and intellectual exchanges. The journey would not have been as the same without your laughter and encouragement. Your friendship has been a cherished aspect of this academic adventure, and I am thankful for the bond we've forged.

To my family, a heartfelt thank you for not just supporting me emotionally but also literally lifting and moving things! Your support, understanding and occasional words of wisdom have made this journey much brighter.

Contents

List of Figures

List of Tables

Introduction

Buried mines and improvised explosive devices are known threats to military vehicles and sensitive infrastructures. The international campaign to ban land mines (ICBL) publishes an annual report [1] monitoring the impact of explosive devices such as improvised explosive devices (IEDs), explosive reminants of war (ERW) or land mines. The effects are quantified trough parameters such as number of states concerned or size of contaminated areas. In 2021, casualties were recorded in 47 states. Protective solutions must consequently be designed to counteract their effects and within the scope of vehicle protection, the protection of vehicle floors becomes particularly relevant.

When a vehicle is subjected to the detonation of an explosive charge under its floor, several structural responses can occur (Figure 1). These can be the deformation or rupture of the vehicle hull and the rapid acceleration of the vehicle, which can cause its overturning in the worst case scenario. These responses are due to the energy and momentum brought by the blast wave. Consequently, protective solutions must be designed to counteract these effects. In the case of experimental investigations, the blast wave energy and momentum cannot be measured directly through sensors, thus most investigations prefer to focus on the blast wave overpressure and local impulse measured on the target surface.

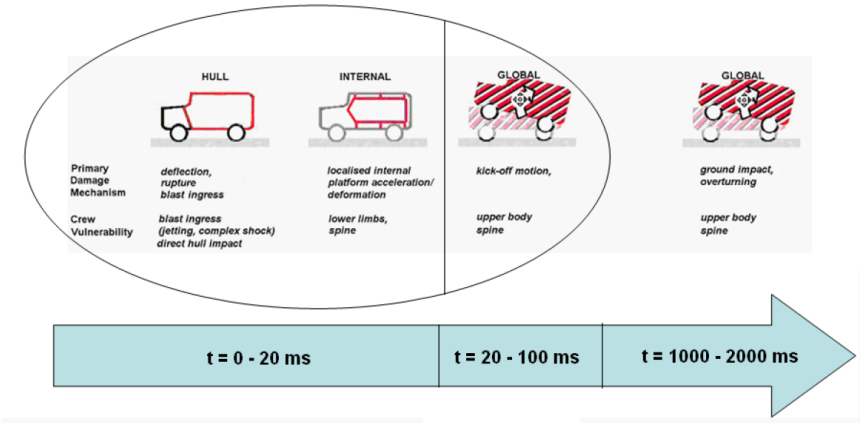

Figure 1: Structural response of a vehicle to blast loading from a buried charge, taken from [2]

Numerous existing designs can be classified based on their approach to control the blast energy and momentum. As an example, the vastly investigated sacrificial cladding aims at dissipating energy through plastic or brittle

deformation of their core, thus applying the pressure load to the target at a lower intensity over a longer duration [3, 4, 5, 6, 7, 8]. Whilst pressure reduction is particularly efficient in reducing the target deflection, the impulse transmitted to the target remains the same and no protection is provided regarding vertical vehicle acceleration.

Very few studies have been performed regarding impulse control. This can be explained by the physical characteristics of impulse. When applied to an object, impulse will cause a change in momentum. Momentum being a vectorial quantity, and momentum conservation being an important principle in physics, not much can be done to control impulse transmission to a target. The beneficial effect of Fluid-Structure Interaction (FSI) is certainly the most impactful method to decrease the impulse seen by the target [9]. As it is set into motion, pressure relief is experienced by the structure as the duration of application of the blast wave exceeds the response time of the target, therefore reducing the transmitted impulse. Another approach would be to redirect the blast flux using geometrical arrangements such as a v-shaped hull. However this can drastically reduce the ground clearance of the vehicle whilst increasing the effect of the threat due to the lower distance between the ground and the protection [10, 11]. Lastly, the impulse can be spread over a larger area, thus achieving lower local impulse values and eventually partially redirecting it away from the structure. Indeed, in the scope of this investigation, impulse will be considered on a local scale, as the integral of the pressure-time signal measured locally on the target. This occurs naturally when the blast wave propagates in free field, but it can be theoretically forced through design. Amongst studies regarding impulse control, the use of fluids has emerged as being an area of interest for research towards new protection solutions. While investigating fluid-filled containers, Bornstein [12, 2] numerically observed that the shock front propagating inside the fluid shows spherical spreading over a larger area. During his study, a number of parameters were considered such as container geometry, fluid properties and distance to the explosive charge. It was concluded by Bornstein that the impulse spreading was one of the many reasons why fluid-filled containers helped decrease the final deflection of the target, but it could not be said how important its role was. Also, this observation was never quantified experimentally (the impulse was not the parameter of interest) and never totally uncoupled from other occurring phenomena, especially energy extraction. Moreover, the main parameter allowing to asses the efficiency of the fluid filled containers for blast mitigation was target deformation. Therefore, only the consequence of the presence of fluid in a protective solution could be observed, and not its cause.

The purpose of this work is to investigate the blast wave transmission within a fluid filled structure itself in order to grasp a better understanding of the mechanisms acting on impulse control. Therefore, it will be possible to give some design guidelines as to the efficient use of fluids in the future development of protective structures.

In the first chapter, a general description of acoustic and blast wave propagation, including the case of a propagation at a material interface, is given. The state of the art regarding mitigation and protection strategies against such a threat is then presented. As this work has a significant experimental component, a literature review for both the generation of a blast loading representative of a buried mine and the measurement of impulse and momentum was carried out. Finally, the main numerical methods allowing the simulation of a blast wave and its interaction with

a structure is reviewed.

In the second chapter, the impulse transmitted to the bottom of a fluid filled container is investigated to highlight the phenomenon of impulse spreading. For this purpose, a novel experimental setup allowing local impulse measurements through pressure sensors at the bottom of the container is presented. The analysis of experimental data is completed by a numerical model, allowing to overcome limitations such as the number of measurement points and to explore a wider range of configurations at a lower cost. Several parameters, such as fluid depth and confinement, are varied in order to asses their influence on impulse spreading. A variation of the degree of fluid confinement is achieved by closing the container with lids of different sizes, thus creating free surface areas through which the fluid can be ejected out of the container. The location of these openings is further investigated through the numerical model. The influence of the water height was studied with two containers of different heights. In this analysis, the rigid and immovable container allowed the investigation of impulse as it could be entirely transmitted to the bottom of the container. However, for a more global understanding of momentum transmission to a structure, an experimental setup that allowed a fluid filled structure to be set into motion had to be studied, which is presented in Chapter 3.

The third chapter aims at providing a more global understanding of momentum transmission. For this purpose, the design of a fluid filled structure that could be mounted onto a blast pendulum is given. The comparison of the maximal angle of elevation of the pendulum for a fluid filled structure and a steel structure of equal weight allows to investigate the effects of the fluid on momentum transmission. In this chapter, the main difficulties of designing such a fluid filled structure are given. The solutions to these difficulties can be seen as similar to the difficulties that will have to be overcome in the integration process of a fluid filled protective structure on a vehicle. Preliminary results show the potential of a fluid based protection for the redirection of local impulse and global momentum transmission.

Chapter 1

Literature review

In the literature review conducted as part of this research, experimental and numerical subjects were of interest. This state of the art begins by describing the formation of shock and blast waves before illustrating the interaction of such a wave with a solid structure or a liquid. Once the interaction between a blast wave and a structure is identified, physical mechanisms in blast protection were described under a general scope, applicable to any structure, and then under the scope of protection against an IED (improvised explosive device). A review of current protective solutions was conducted and allowed to identify the scope under which this research had to be led to improve the understanding of the use of fluids in protective structures against IEDs. Once the scientific need identified, experimental and numerical methods allowing the study of these phenomena were reviewed in an effort to make an informed decision as to the tools selected for this investigation.

1.1 Longitudinal wave in a medium

When energy is added to a medium, the medium tries to reach equilibrium by distributing this energy to the local environment. It creates a mechanical wave: longitudinal (tension/compression) waves, transverse (shear) waves, surface waves. Depending on the energy and the medium characteristics, the mechanical wave propagates either in the form of an acoustic wave or a shock wave. In order to simplify the discussion, only longitudinal waves are discussed in the following.

1.1.1 From an acoustic wave ...

An acoustic wave results from the back-and-forth vibrations of the medium particles in the direction of the wave propagation. Thus, each oscillation of the wave corresponds to a small compression and expansion of the medium. The velocity of an acoustic wave is equal to the sound velocity c of the ambient medium and can be computed using the density of the medium ρ as well as a stiffness measure, namely the bulk modulus K for a fluid and the Young modulus E for a laterally unconstrained solid:

$$c_{fluid} = \sqrt{\frac{K}{\rho}} \tag{1.1}$$

$$c_{solid} = \sqrt{\frac{E}{\rho}} \tag{1.2}$$

1.1.1.1 Acoustic wave propagation in a medium

The d'Alembert equation, or one-way wave equation, is a first order partial differential equation describing a one dimensional wave propagating in a medium. This equation is verified for phenomena such as the propagation of sound.

Considering a section of a medium in which a one-dimensional wave propagates (Figure 1.1), the equation of motion can be written as shown in Equation 1.3 where $\ddot{u}$ is the acceleration. To simplify this equation, the following assumptions can be made:

- assumption of a one dimensional motion and a constant, laterally unconstrained solid section: $S(x) = S(x + dx) = S$
- assumption of small strains : $\rho(x) = \rho(x + dx) = \rho$ and therefore $dm = S\rho dx$
- assumption of small particular velocities: $\ddot{u} = \frac{\partial v}{\partial t}$, where v is the particular velocity

Therefore, the equation of motion can be rewritten as shown in Equation 1.4.

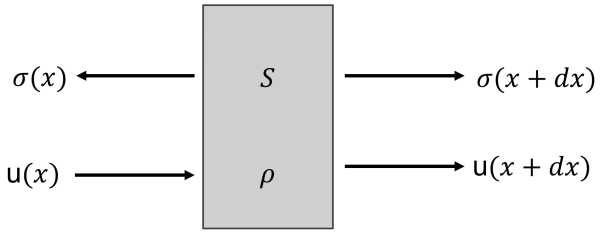

Figure 1.1: Section S of a medium of density ρ with a tension-compression stress σ and a displacement u

$$S(x+dx)\sigma(x+dx) - S(x)\sigma(x) = dm.\ddot{u} \tag{1.3}$$

$$\frac{\partial \sigma}{\partial x} - \rho \frac{\partial v}{\partial t} = 0 \tag{1.4}$$

With consideration of the behavioral law, in the case of an elastic propagation, the derivative of the stress σ relative to the strain ϵ is Young's modulus E. Therefore $\sigma = E\epsilon = E\frac{\partial u}{dx}$, which leads to Equation 1.5

$$\frac{\partial \sigma}{\partial t} - E \frac{\partial v}{\partial x} = 0 \tag{1.5}$$

A convenient representation of this problem is given by the Lagrange diagram (Figure 1.2) where x and t are the horizontal and vertical axes respectively. Here, along a straight path such as $\frac{dx}{dt} = \sqrt{\frac{E}{\rho}}$, Equations 1.4 and 1.5 have a unique solution $(\sigma - \sqrt{E\rho}v) = constant$, and along a path such as $\frac{dx}{dt} = -\sqrt{\frac{E}{\rho}}$, they have a unique solution $(\sigma + \sqrt{E\rho}v) = constant$. In practice, $\sqrt{\frac{E}{\rho}}$ is equal to the speed of sound in the medium c and $\sqrt{E\rho}$ is the impedance Z.

1.1.1.2 Acoustic wave transmission at an interface

The Lagrange diagram can also describe the transmission of an acoustic wave at an interface with the previously described equations, allowing the description of the transmitted and reflected wave. In the following example where an impactor (medium 1) strikes a medium 2 with an initial velocity $v_{impactor}$, to solve for stress σ and particular velocity v transmitted from medium 1 to medium 2, the following boundary conditions were applied:

- no stress is applied at $x = 0$, the impactor moves freely
- the medium 2 is fully constrained at the back end and thus has a null velocity

- stress and velocity are equal at the interface between both mediums

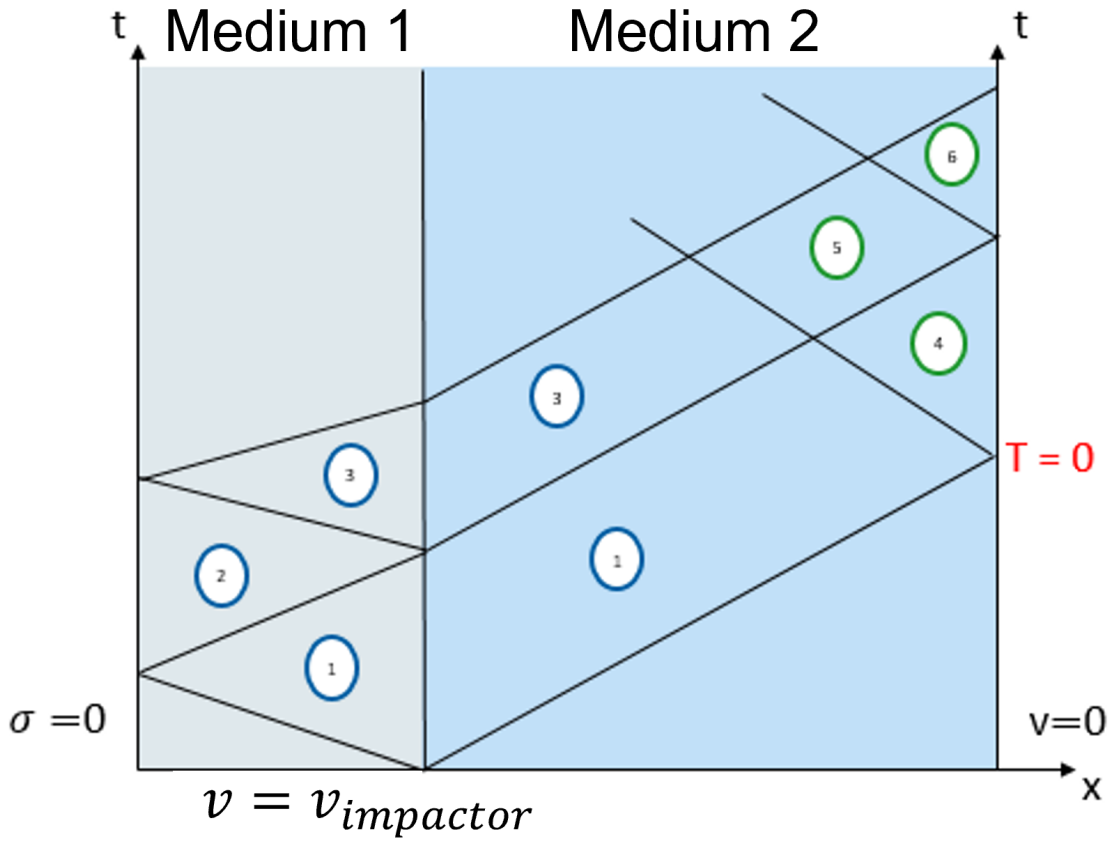

Figure 1.2: Lagrange diagram for the transmission of an acoustic wave at an interface

The different reflections and transmission of the acoustic wave at the interface create different zones in which stress and particular velocity can be calculated using the particular solutions to the partial differential equation described in the previous section. Therefore the stress transmitted by the acoustic wave during the first reflection/transmission can be calculated as follows:

$$1)\ \begin{cases}\sigma - Z_1 v = 0 - Z_1 v_{impactor}\\ \sigma + Z_2 v = 0\end{cases} \rightarrow \begin{cases}(Z_2 + Z_1)v = Z_1 v_{impactor}\\ \sigma = -Z_2 v\end{cases} \rightarrow \begin{cases} v = \frac{Z_1}{Z_2+Z_1} v_{impactor}\\ \sigma = -\frac{Z_2 * Z_1}{Z_2+Z_1} v_{impactor}\end{cases}$$

$$2)\ \begin{cases}\sigma = 0\\ \sigma + Z_1 v = v_{impactor}(-\frac{Z_2 Z_1}{Z_2+Z_1} + \frac{Z_1^2}{Z_2+Z_1})\end{cases} \rightarrow \begin{cases}v = \frac{Z_1 - Z_2}{Z_2+Z_1} v_{impactor}\\ \sigma = 0\end{cases}$$

$$3)\ \begin{cases}\sigma - Z_1 v = -Z_1 \frac{(Z_1 - Z_2)}{Z_2+Z_1} v_{impactor}\\ \sigma + Z_2 v = \left(-\frac{Z_2 Z_1}{Z_2+Z_1} + \frac{Z_1 Z_2}{Z_1+Z_2}\right) v_{impactor} = 0\end{cases} \rightarrow \begin{cases} v = +\frac{Z_1(Z_1 - Z_2)}{(Z_2+Z_1)^2} v_{impactor}\\ \sigma = -\frac{Z_2 Z_1 (Z_1 - Z_2)}{(Z_2+Z_1)^2} v_{impactor}\end{cases}$$

$$4)\ \begin{cases}\sigma - Z_2 v = v_{impactor}(-\frac{Z_2 Z_1}{Z_2+Z_1} - \frac{Z_2 Z_1}{Z_2+Z_1})\\ v = 0\end{cases} \rightarrow \begin{cases} v = 0\\ \sigma = -\frac{2 Z_2 Z_1}{Z_2+Z_1} v_{impactor}\end{cases}$$

Transmission depends on the relative impedance of both mediums. When Z_2 is greater than Z_1, mostly pressure in transmitted to the second medium. On the contrary, when Z_1 is greater than Z_2, mostly velocity in transmitted. The following set of boundary conditions might also be of interest in this work: the first media, initially at rest and in direct contact with the second media, is subjected to a pressure pulse. Using a similar approach, it is possible to calculate the pressure transmission coefficient at the interface between the two medias. The transmitted wave pressure in the second media is equal to $\frac{2Z_2}{Z_1+Z_2}$ times the wave in the first media.

1.1.2 ... to a shock wave

As the energy brought to the system increases, so does the frequency of the oscillation of the medium particles. It does not affect the wave velocity, until the period of the acoustic wave approaches the collision time between the molecules of the medium (in gases), or until the medium is stressed up beyond its elastic limit (in solid and liquid). When it does, the energy brought to the system cannot be dissipated by acoustic waves. It results in the compression of the medium surrounding the source to the point that the resultant compressive heating locally increases the sound speed of the medium. Energy is then transmitted at the local sound velocity, which may be greater than the ambient sound velocity. The energy accumulates at the front of the wave and a shock wave results. By essence, the shock wave is thus characterized by a nearly discontinuous change in pressure, temperature and density of a medium, propagating at a velocity comprised between the bulk sound velocity c_0 of the material at rest and its Chapman-Jouguet's detonation wave velocity $D_{CJ} = c + u$ (u being the material velocity). In other words, a shock wave propagates supersonically in the initial medium and subsonically in the shocked medium.

1.1.2.1 Shock wave propagation in a medium

The Rankine-Hugoniot jump conditions describe the relationship between the states on either sides of a shock wave in a one-dimensional flow in fluids or a one dimensional deformation in solids. The Rankine-Hugoniot conditions can be expressed using conservation of mass, conservation of momentum and conservation of energy. This was presented by Arrigoni in [13].

These relations are valid when assuming 4 hypotheses:

- A shocked solid behaves like a isotropic fluid (for a given point in this fluid, the pressure for this point is equal in every direction).
- The given medium behaves like a fluid.
- The shock produces a virtually perfect discontinuity (perfectly straight shock front, the pressure rise time is virtually equal to zero and stable).
- The heat exchange with the external environment is neglected.

The propagation of a shock wave can be schematically illustrated as shown in Figure 1.3, with P the pressure, u the material velocity, D the velocity of the shock front bringing a medium from a state 0 to a state 1, ρ the density and S the section of the considered medium. When a pressure P_1 is applied to an environment, the shock front propagates at a velocity of $D + u_0$. The medium 0, initially at a velocity u_0, will thus acquire a material velocity equal to $u = u_1 - u_0$ where u is known as the jump condition, a discontinuity due to the abrupt change of the characteristic speeds at the upstream and downstream conditions of the shock front.

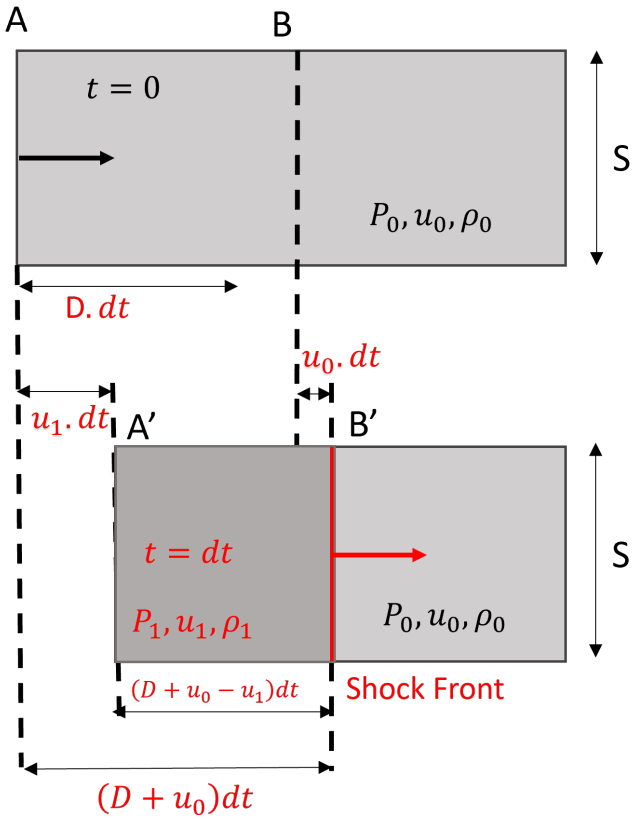

Figure 1.3: Propagation of a shock wave in a medium

When studying mechanical shock waves, 3 equations have to be resolved: conservation of mass, momentum and energy.

Conservation of mass

At a given time, when considering the medium the shock wave is traveling through as a closed entity, the mass of the fluid that has been set into motion by the wave equals to the mass of the fluid that has been compressed (Equation 1.6). The conservation of mass on both sides of the shock front can be written as shown in Equation 1.7, which is the first of three Rankine-Hugoniot relations.

$$\rho_0 . S . D . t = \rho_1 . S . (D + u_0 - u_1) . t \tag{1.6}$$

$$\rho_0 . D = \rho_1 . (D + u_0 - u_1) \tag{1.7}$$

Conservation of momentum

By writing the law of conservation of momentum on a section of fluid, the external forces P_0 and P_1 act on the section of dimension S and mass m during a duration dt and are equal to the product of m by the acceleration (Equation 1.8).

$$\sum \vec{F} = m\vec{a} \Rightarrow S(P_1 - P_0) = \rho_0 SDdt\frac{du}{dt} \tag{1.8}$$

Therefore the second Rankine-Hugoniot relation can be expressed as shown in Equation 1.9

$$P_1 - P_0 = \rho_0.D.(u_1 - u_0) \tag{1.9}$$

Conservation of energy

The variation of energy of a system is equal to work W and heat exchange Q. Whilst heat exchange can be neglected, work is due to the compression of the medium, through external work $P_1 S u_1 t$ and $-P_0 S u_0 t$. This energy variation is also equal to the variation in kinetic energy $\Delta E_k = \frac{1}{2}(u_1^2 - u_0^2)\rho_0 SDt$ and the internal energy $\Delta U = (E_1 - E_0)\rho_0 SDt$ (Equation 1.10).

$$\Delta E = W + Q = \Delta E_k + \Delta U \tag{1.10}$$

By transforming this equation and according to the previous conservation principles, the third Rankine-Hugoniot relation regarding energy conservation can be established (Equation 1.11), where ν is the specific volume defined as $\nu = \frac{1}{\rho}$.

$$E_1 - E_0 = 1/2.(P_1 + P_0).(\nu_0 - \nu_1) \tag{1.11}$$

When the variation in pressure, material velocity and density are small, the Rankine-Hugoniot relation regarding energy conservation can be rewritten (Equation 1.12).

$$dE = -Pd\nu \tag{1.12}$$

Equation of state

However, the Rankine-Hugoniot relations are not sufficient for a full description of the variables determining the thermodynamic state (P,E,ν) and the kinetic variables (D,u). Therefore, an equation of state has to be introduced. For gases, the linear polynomial equation of state or the ideal gas equation of state can be used. A description of these equations is given in [14].

The linear polynomial equation of state (which can be used for gases as well as fluids such as water) gives the pressure as a function of constants C_0 to C_6, the specific internal energy E and $\mu = \frac{\rho}{\rho_0} - 1$ where $\frac{\rho}{\rho_0}$ is the ratio between the current density to the reference density (Equation 1.13).

$$P = C_0 + C_1\mu + C_2\mu^2 + C_3\mu^3 + (C_4 + C_5\mu + C_6\mu^2)E \tag{1.13}$$

The ideal gas equation of state can be recovered from Equation 1.13 by setting $C_0 = C_1 = C_2 = C_3 = C_6 = 0$ and $C_4 = C_5 = \gamma - 1$. The constant adiabatic index is defined as $\gamma = \frac{C_p}{C_v}$ where C_p is the heat capacity at constant pressure and C_v is the heat capacity at constant volume. Therefore, the pressure of an ideal gas is given by Equation 2.1.

$$P = (\gamma - 1)\frac{\rho}{\rho_0}E \tag{1.14}$$

For a full description of the aforementioned five variables, one more equation is needed. A link between D and the particle velocity u exists, as described in Equation 1.15, where s is a dimensionless constant of the material.

$$D = c_0 + s(u_1 - u_0) \tag{1.15}$$

With the Rankine-Hugoniot relations, the equation of state and Equation 1.15, it becomes possible to represent the variables describing the thermodynamic state of the system with Hugoniot curves or polar shock diagrams.

1.1.2.2 Shock wave transmission at an interface

The phenomena occurring when a shock wave travels through different solid media is well described by Arrigoni in his lecture about shock waves in materials [13]. When a shock wave passes through two or more solid mediums having different characteristics, the incident shock wave is reflected at each interface. During this reflection, a rebound shock wave with the opposite direction to the first one is generated in the first medium and a transmitted new shock wave with different characteristics starts its propagation in the second medium. In the case of a flat 1D shock, the characteristics of the reflected and transmitted waves depend on the difference in impedance between the materials at the interface. A polar shock diagram represents the states (P,u) of a medium which has been subjected to a shock wave. Therefore, the material velocity u can be determined knowing the pressure P. The polar shock curve can be calculated with Equation1.16.

$$P - P_0 = \rho_0 c_0 u + \rho_0 s u^2 \tag{1.16}$$

In Figure 1.4, a bi-material target is shown. An incident shock wave hits material A. The thermodynamic state of material A after being subjected to a shock of intensity P_1 can be read on the polar shock diagram shown in Figure 1.5, thus enabling us to determine the material velocity u_1 corresponding to P_1. When the shock wave reaches the interface between the two materials, the incident shock wave is transmitted to material B and reflected into material A accordingly to the impedance mismatch. The state of material B is determined by using the symmetric polar diagram of the material A, called A'. The thermodynamic state of material B can be read at the intersection of the polar diagrams A' and B. Hence, the pressure P_2 and material velocity u_2 were able to be determined accordingly

to the impedance mismatch at the interface of materials A and B.

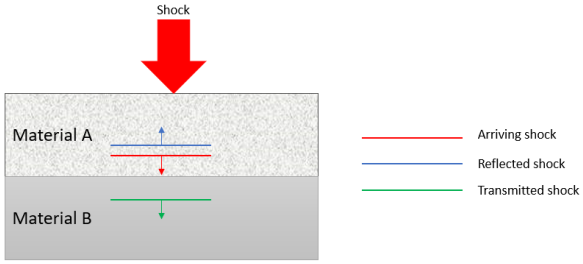

Figure 1.4: Multi material target with flat interface

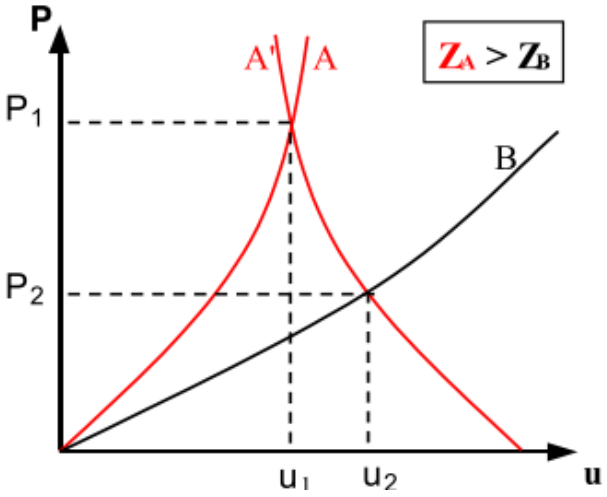

Figure 1.5: Polar shock diagram, taken from [13]

Therefore, the effect of the impedance mismatch can be characterized according to the relative impedance mismatch of the two mediums:

- For $Z_1 >> Z_2$ an important material velocity transmission with little pressure transmission will occur
- For $Z_2 >> Z_1$ an important pressure transmission and little material velocity transmission will occur

1.2 Particular case: the blast wave

Investigations on shock waves are made using specific laboratory equipment such as shock tube for air shock wave, or plate impact for solid shock wave. These shockwaves are followed by an expansion wave thanks to which the stress returns to its ambient value [15, 16]. In air, the combination of a shock wave and its expansion wave is a phenomenon called blast wave. At large distances from the explosion center, the pressure expands below ambient such that the blast wave has a negative phase as well as a positive phase. The pressure-time curve of such a blast wave is shown in Figure 1.6 and is described by several parameters:

- the overpressure ΔP, which is the magnitude of the pressure rise as defined by $\Delta P = P_s - P_0$ with P_s the peak overpressure and P_0 the ambient pressure
- t_a the time of shock arrival
- t^+ the positive phase duration
- t^- the negative phase duration
- i_i the incident specific impulse, defined by the area under the pressure-time curve. It depends on the peak overpressure, the phase duration and the rate of decay of the overpressure. In this work, impulse will refer to the area under the pressure curve during the positive phase i_i^+, thus neglecting the decrease brought by the negative phase i_i^- of the blast wave.

Eventually, the blast wave decays to an acoustic wave traveling at the speed of sound in the air (340 m/s).

The damage potential of a blast wave depends mainly on the overpressure and impulse, a particular object will suffer damage when the impulse and overpressure both exceed damage threshold values. The influence of these two parameters can be illustrated on a P.I. diagram (Figure 1.7).

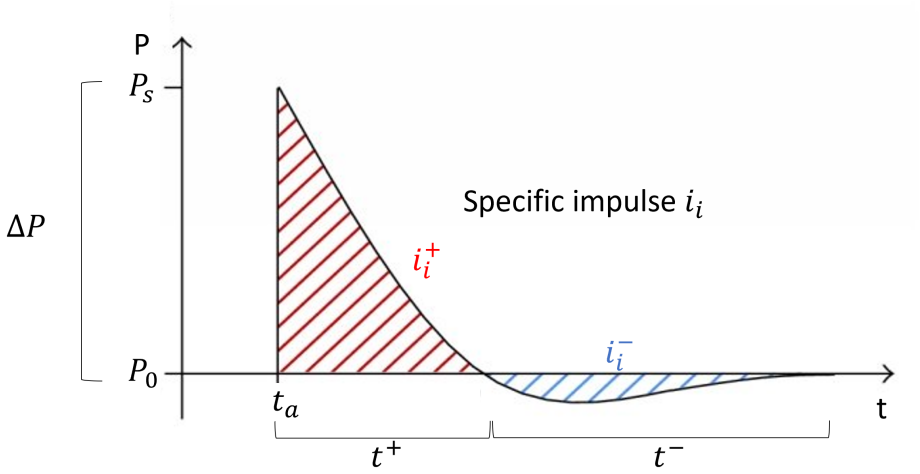

Figure 1.6: Pressure time curve of a blast wave

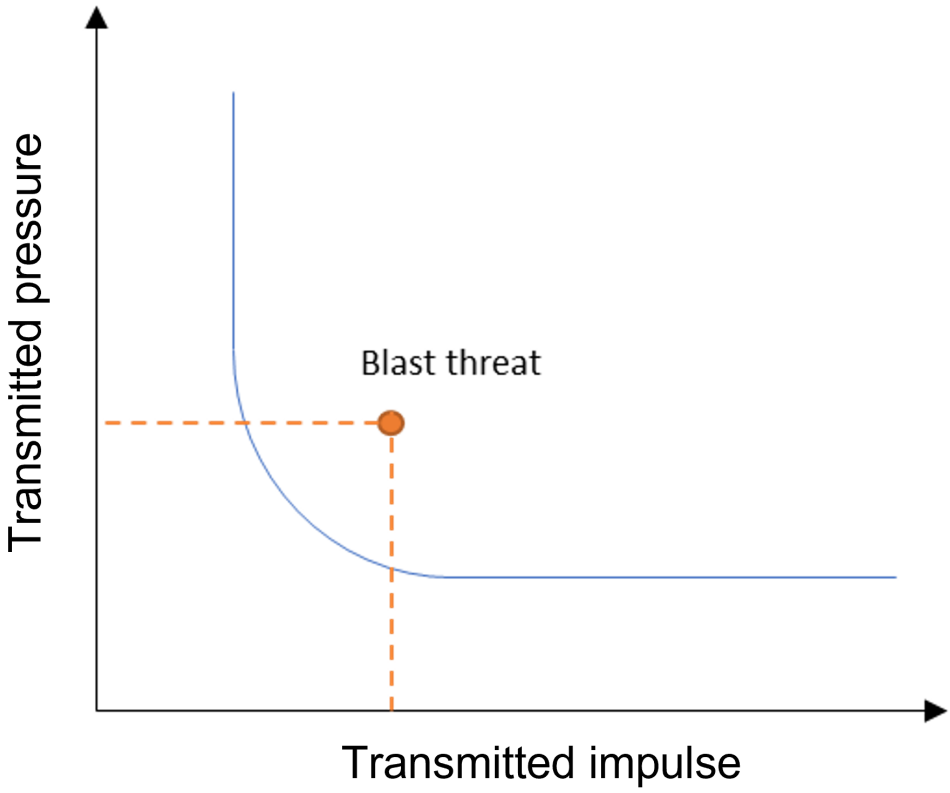

Figure 1.7: P.I. diagram with an ISO damage curve. For a given pair of impulse and pressure values, the blast threat will cause damage to the target if the values are above the ISO curve.

1.2.1 Analytical description of a blast wave

The pressure-time curve of a blast wave can be described analytically with the Friedlander waveform (Equation 1.17) where k is a decay coefficient of the waveform. This decay coefficient can be calculated through non-linear fitting of an experimental pressure time curve over the positive phase duration. Positive impulse, calculated as the area under the pressure-time curve of the positive phase duration, is defined in Equation 1.18.

$$P(t) = P_s e^{-k\frac{t}{t^+}}(1 - \frac{t}{t^+}) \tag{1.17}$$

$$i^+ = \int_{t_a}^{t_a+t^+} P(t)\,dt = \frac{P_s t^+}{k^2}[k - 1 + e^{-k}] \tag{1.18}$$

To complete the analytical approach, scaling laws exist to compute the value of the shock parameters (P_s, i^+, t^+) versus the distance and weight of the explosive. Such scaling laws were introduced by Hopkinson [17] and Cranz [18] and state that during the detonation of two charges of the same explosive and similar geometry but of different weight, a similar blast wave is produced at a scaled distance Z (Equation 1.19) as a function of R, the distance from the detonation source to the point of interest, and W, the mass of the explosive.

$$Z = \frac{R}{\sqrt[3]{W}} \tag{1.19}$$

The Hopkinson scaling law, illustrated in Figure 1.8, states that at a point situated at a distance d from an explosion of energy E and radius R, a shock wave will have an overpressure ΔP, a positive and a negative time phase (t^+ and t^-) and a positive and negative impulse (i^+ and i^-). Now if we consider a new point situated at a distance kd from an explosion of energy k^3E and radius kR, the shock wave will have the same overpressure ΔP, a positive and a negative time phase (kt^+ and kt^-) and a positive and negative impulse (ki^+ and $ki^=$). Therefore, overpressure, impulse and time phase duration can be expressed for different scales, k being the scaling factor.

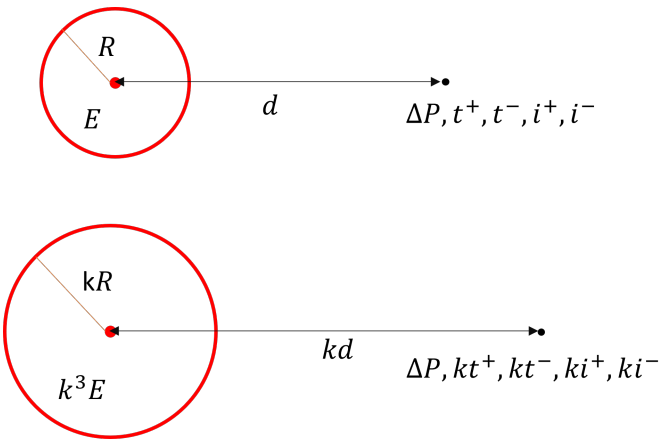

Figure 1.8: Hopkinson scaling law

By combining these spatial models with the temporal model of Friedlander it is possible to give an accurate description of the blast propagation in free-field.

1.2.2 Relationship between overpressure, impulse, energy and momentum

Experimentally, energy and momentum are quantities that cannot directly be measured. Therefore this section will describe the link between pressure, impulse, energy and momentum.

1.2.2.1 From pressure measurement to energy

The direct experimental measurement of a blast wave energy transmitted to a target is not possible. There however exist alternatives to accurately estimate this energy in simple configurations.

The point source solution: Taylor [19], Von Neumann [20] and Sedov [21] proposed that all of the explosion energy E is released homogeneously, instantaneously and at a single point in space. This also means that the energy released by a charge can be calculated using only a few parameters: the position reached by the blast wave r, the time it took to reach its position t, the density of the ambient air ρ_0, and a dimensionless constant C (between 1 and 1.1 in air). Therefore the energy can be calculated as shown in Equation 1.20.

$$E = \frac{\rho_0 r^5}{t^2 C^5} \tag{1.20}$$

Using a video recording of the blast wave propagation, it is consequently possible to estimate the energy released by the explosion, then, by assuming an homogeneous spreading, the energy E_t transmitted to the target of area A (Figure 1.9) would be equivalent to the energy included in the solid angle volume encapsulating this area (Equation 1.21).

$$E_t = E\frac{rA/3}{4/3\pi r^3} \tag{1.21}$$

Using the same approach, and by assuming that the propagation velocity D of the shock front is equal to $D = \frac{dr}{dt}$, it is also possible thanks to Rankine-Hugoniot to link the energy released by the explosion to the shock front pressure P using $P = \frac{2}{\gamma-1}\rho_0 D^2$ (Equation 1.22). This description assumes that all of the blast wave energy is mainly located in the shock front.

$$E = \rho_0 t^3 \left(\frac{5D}{2C}\right)^5 = \rho_0 t^3 \left(\frac{5\sqrt{\frac{P}{2/(\gamma-1)\rho_0}}}{2C}\right)^5 \tag{1.22}$$

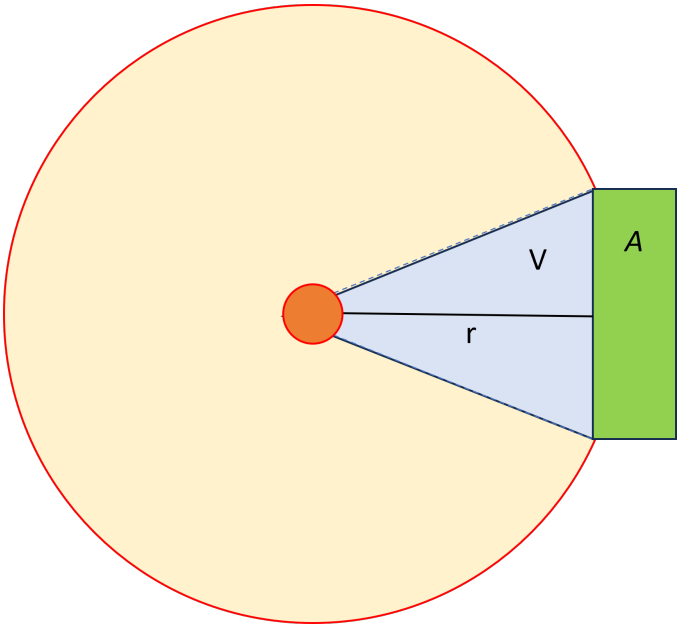

Figure 1.9: Schematic representation of the point source solution

The signal intensity: A second approach derived from the definition of the signal intensity can be used. The goal is to consider the propagation of the pressure wave $P(t)$ in a medium of density ρ and celerity c as shown in Equation 1.23. This description assumes a planar wave thus overestimating the energy.

$$E = \frac{1}{\rho c} \int_0^t |P(t)^2| \, dt \tag{1.23}$$

1.2.2.2 From incident pressure to momentum

Momentum p is a vector quantity resulting of the product of the mass m of a punctual mass and a velocity v as shown in Equation 1.24.

$$p = mv \tag{1.24}$$

Newton's second principle states that force is equal to the time derivative of momentum (Equation 1.25).

$$\frac{dp}{dt} = F \tag{1.25}$$

For an object of initial momentum p_0 at a time t_0 ($p_0 = p(t_0)$) to which a force F is applied during $t_1 - t_0$, the integral of this force during this duration can be written as shown in Equation 1.26, where I is the load impulse.

$$I = \int_{t_0}^{t_1} F(t) \, dt \tag{1.26}$$

Therefore, momentum and load impulse can be linked as shown in Equation 1.27.

$$I = \int_{t_0}^{t_1} \frac{dp(t)}{dt}\, dt = p(t_1) - p(t_0) = \Delta p \tag{1.27}$$

In the case of a blast wave, which is assumed uniformly distributed over a rigid surface S, the incident blast impulse i_i can be expressed as shown in Equation 1.28.

$$i_i(t) = \frac{1}{S} \int_{t_0}^{t_1} F(t)\, dt = \frac{p(t_1) - p(t_0)}{S} \tag{1.28}$$

Therefore, knowing the incident blast impulse $i_i(t)$ and the initial momentum of air, which is usually neglected, it is possible to calculate the variation of momentum through time (Equation 1.29)

$$p_i(t) \approx S i_i(t) \tag{1.29}$$

However, a clear definition of the incident blast impulse i_i must be given. Generally, it is assumed that the incident blast impulse is equal to the integral of the free-field pressure-time signal. However, the impulse due to the flux of the particles that are displaced by the blast is not seen by a free field pressure sensor and is therefore neglected in the traditional definition of impulse. Therefore, it is more accurate to define a total blast impulse i_{tot} (Equation 1.30). Therefore, the total momentum brought on by the blast wave is more accurately defined as shown in Equation 1.31.

$$i_{tot} = i_i + i_{particles} \tag{1.30}$$

$$p_i(t) = S i_{tot}(t) > S i_i(t) \tag{1.31}$$

1.2.2.3 From reflected pressure to momentum

Kambouchev [22] investigated the interaction of blast waves propagating in a highly compressible medium, such as air, and structures. Focus was drawn on impulse transmission from the blast wave to the structure. It was shown that in the case of a reflection of a blast wave on a rigid boundary, there is an incident blast impulse i_i (in this case the impulse due to the mass flux of the particles will be neglected discussed in the previous paragraph) and a reflected impulse i_r applied on the rigid boundary by the blast (Equation 1.32). Therefore, the impulse in the case of a reflection of a blast is not due solely to the incident momentum p_i but also due to the reflected momentum p_r (Equation 1.33).

$$i_r = \frac{p_r + p_i}{S} \tag{1.32}$$

$$p_r \approx S i_r - p_i \tag{1.33}$$

In [22] a framing of the value of the momentum in case of reflection was given (Equation 1.34) which accounts for the cases where the structure cannot be considered a rigid boundary. The momentum of a perfectly reflected wave is comprised between 1/3 and 1 of the incident blast momentum. The reflected impulse applied on the rigid boundary would be between 4/3 and 2 (Equation 1.35).

$$0.33 p_i < p_r < 1 p_i \tag{1.34}$$

$$1.33 p_i < i_t < 2 p_i \tag{1.35}$$

1.3 Blast protection

Protection of a target in a near-field blast environment can intervene on different levels: it can act on the detonation, the propagation of the shock wave, in this case the blast is mitigated or attenuated, or on the target itself, in this case the term of blast protection would be most appropriate. Whilst this work focuses on blast protection, by offering solutions of target protection using fluids, a review of blast mitigation mechanisms has been conducted as well, as these could be transferable to target protection.

1.3.1 Physical mechanisms in blast mitigation and protection

1.3.1.1 Acting on the detonation process

Water mist The use of water mists has been investigated as a way to act on the detonation of an explosive charge. Work by Schunck [23] studied the blast mitigation in a water mist, finding that the shock wave was delayed due to the presence of the water mist. It was also found that the size of the droplets had an impact on the peak overpressure with a reduction of the peak overpressure ranging from 20% to 40 % and a maximal impulse reduction by around 20% to 30%. The presence of the water mist reduced the oxygen supply and thus acted on the formation of the fire ball.

1.3.1.2 Acting on the blast wave in air

Natural decay Following the detonation of an explosive charge in air (or water), a spherical blast wave propagates. Therefore, with increasing distance the energy released by the explosive charge spreads over a larger volume. Thus, the wave intensity is reduced and parameters like overpressure will follow the same intensity decrease over distance. Since the blast intensity decreases with r^3, increasing the distance from an explosion is very efficient as a protection measure.

Reflection, diffraction, rarefaction When a blast interacts with a structure, different phenomena may occur beyond the simple reflection. Rarefaction waves were described by Rigby [24]. A rarefaction, or clearing, wave is generated when a shock wave interacts with the edge of a structure. At the free edge, a reflected shock is generated and moves away from the target surface while an incident wave diffracts around the edge of the structure. This generates a pressure imbalance between the two waves and the flow between the two pressure regions. A rarefaction wave is generated at the free edge and travels along the target surface back towards the center of the target, reducing the pressure and impulse action in the target. Figure 1.10 presents a schematic of this mechanism for an incident shock wave and a far-field blast loading scenario, depending on the size of the obstacle and the time scale of the event. The rarefaction wave reduces the pressure acting on the target.

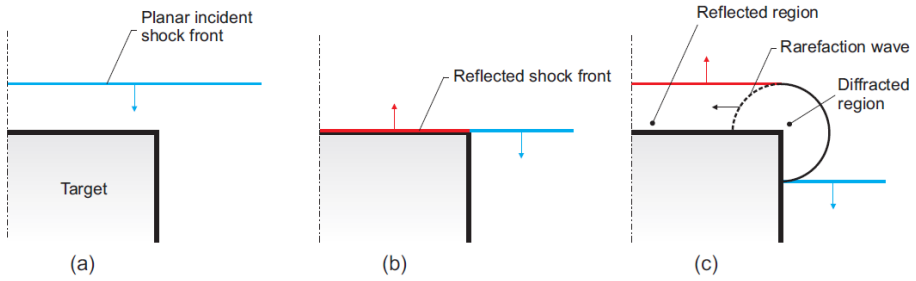

Figure 1.10: Schematic representation of a rerefaction wave forming at the edge og a target [24]

Putting an adequate obstacle between the charge and the target can help alleviate the pressure applied on the target. The shadowing mechanism finds its application primarily in far-field blast mitigation. It occurs when an obstacle is placed in the path of a blast wave. A link between the shadow region and the dimensions of the structure was established by Needham [16]. He defined the low pressure shadow region as being 4 to 5 times the dimension of the structure in the direction perpendicular to the flow.

An experiment designed by Needham compared the appearance of the diffracted shock wave passing beyond a steel structure and a balsa wood structure. No difference was detected in the appearance of the diffracted shock wave. As such, the composition of the structure does not appear to have to be rigid in order to generate a shadowing effect on a blast wave.

The shadowing effect was described by Bornstein [2] as being dependent on the geometry of the structure constituting the obstacle. Figure 1.11 shows the interaction of a detonation product and a fluid filled container. The schematic highlights the shadowing mechanisms generated by an obstacle.

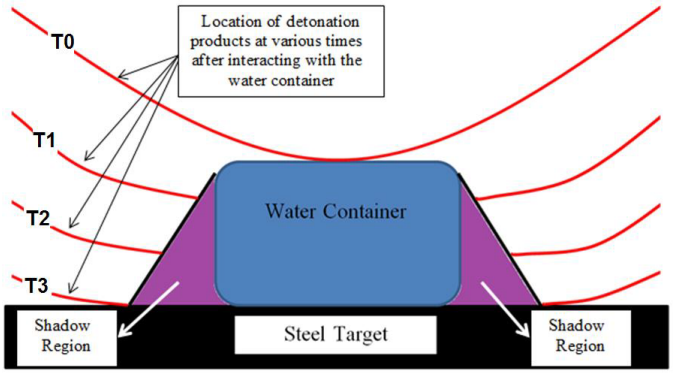

Figure 1.11: Schematic representation of the blast wave at varying times following the interaction with a structure, highlighting the shadow regions, taken from [12]

Beneficial aspect of fluid structure interaction Fluid structure interaction (FSI) is the interaction of some movable or deformable structure with an internal or surrounding fluid flow. Effects of FSI can be exploited to be beneficial by disturbing the interaction of a blast wave with the target, and thus the impulse seen by the target [9]. Following

its interaction with a blast wave, the target will be set into motion. If the target acquires a high enough velocity, the duration of application of the blast wave will be higher than the response time of the plate, thus the impulse transmitted to the target is diminished. It was discussed in Section 1.2.2.3 that the momentum transferred to a rigid body is equal to 2 times the momentum brought on by the blast wave. In the case of a deformable body, it is possible to reduce this value to somewhere between 1.33 and 2. This can be observed experimentally for the free-standing plate problem [25], but also by measuring the deformation of a clamped target through digital image correlation, and computing the impulse using the local velocity of each point [3].

1.3.1.3 Acting on the compression wave in a solid or liquid

Shock impedance mismatch Shock impedance refers to the opposition that a material presents to transmission of a shock wave and is defined as $Z = \rho_0.D$ where ρ_0 is the initial density of a given material and D is the shock velocity at a given particle velocity. It should be noted that the shock impedance is often replaced with the acoustic impedance $Z = \rho_0 c_0$, easier to use analytically. This is reasonable for low shock pressure as the particle velocity would be largely inferior to the shock wave velocity. The higher the ratio of impedance between two media, the more the blast wave will be reflected. For example, the ratio of impedance between air and steel is $1.8.10^5$ which means that the shock wave will be almost completely reflected from the plate surface. By multiplying the layer and variation of impedance, it is possible to trap several waves in the materials, decreasing the peak stress applied to the target by spreading it over time, or even dissipating the wave through the layer deformation.

Energy dissipation A structure subjected to a blast wave can also be protected through the dissipation of the energy brought on by the blast wave. This can be achieved through plastic deformation or delamination of a material.

1.3.2 Threat characterization

Whilst these protection mechanisms are applicable to general air blast scenarios, this work focuses on land mines and improvised explosive devices (IEDs) as a source for the blast. When the detonation of an IED occurs, two different types of loading take place. A very localized and directional blast wave is produced, causing a very high blast load over a concentrated area and impact loading occurs through fragments. This investigation will focus of the blast loading.

Following the detonation of an IED, a vehicle structure can have different responses. Whilst some, like rupture or deformation of the vehicle floor, are mostly associated to overpressure, the vertical acceleration or overturning of the vehicle is due to the impulse transmitted to the structure. The mine blast output was investigated by Bergeron [26]. Whilst the effects are highly dependent of how the mine is buried, two main phases on target loading due to the explosion of buried mines were identified:

- a first over pressure peak due to the blast wave generated by the explosive charge itself

- a secondary pressure loading on the target due to the ejection of the medium the mine is placed in (sand in the case of this study). This secondary loading can be influenced by the properties of the medium (presence of gravel, humidity of the sand) and the depth of burial of the mine. Therefore, the impulse being transmitted to the target increases with the impact of the sand.

A typical pressure time history of the loading due to a buried mine is shown in Figure 1.12.

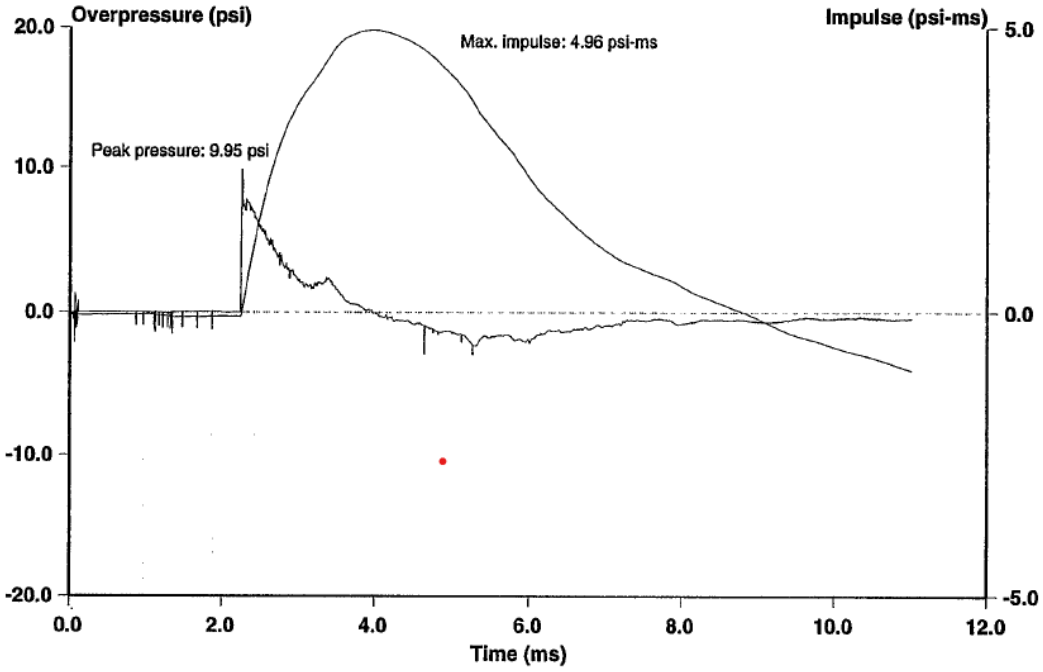

Figure 1.12: Pressure and impulse time history recorded by a pressure sensor in air located 118 mm above ground for a 100 g charge of C4 burried at a depth of 80 mm in silica sand.

In order to test protective structures for their resistance to buried mines, a standard is defined by the STANAG 4569 document (Figure 1.13).

Level		AT mine explosion	
4	4b	explosion under the vehicle centre	AT 10 kg TNT
	4a	explosion under the wheel/caterpillar	
3	3b	explosion under the vehicle centre	AT 8 kg TNT
	3a	explosion under the wheel/caterpillar	
2	2b	explosion under the vehicle centre	AT 6 kg TNT
	2a	explosion under the wheel/caterpillar	

Figure 1.13: Standard testing levels defined by STANAG 4569 for the test of armored vehicles

1.3.3 Current blast protection acting on the target

As a response to these effects, solutions have been implemented. The most straightforward solution being the protection of the vehicle with a monolithic armor panel. Whilst easy to implement, this solution is not viable, especially in the case of a vehicle, as it reduces its mobility drastically and does not provide a satisfactory weight to protection ratio. Therefore, solutions with a more advanced design aim at protecting structure, and in particular vehicles, from the effects of an IED, both by acting on energy and momentum transmitted to the target.

1.3.3.1 Energy control

Vehicle hull shaping The shape of the vehicle floor itself can be used to redirect the energy released by the detonation of an IED under a vehicle. Paykani and Chung [10, 11] described such a solution, where a V-shape was utilized, as described in Figure 1.14. However, this solution is efficient only when the charge is placed in an ideal location underneath the target, directly under the V-shape.

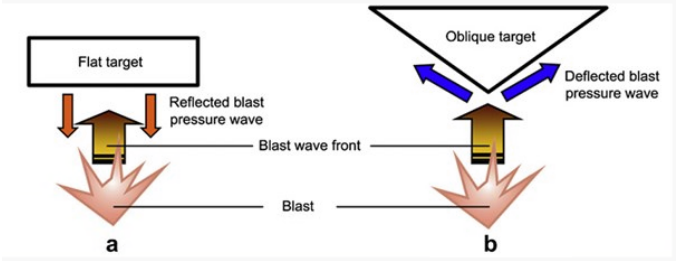

Figure 1.14: Schematic illustration of the redirection of the blast wave through a v-shaped target. Taken from [11]

Heider [27] investigated V-shaped vehicle hulls experimentally and numerically through a scaled model. The numerical model focused on the parameter of ground clearance between the ground and the vehicle floor (Figure 1.15). It was found that a v-shaped vehicle floor reduces the transmitted momentum by about 40%, independent of the ground clearance (Figure 1.16a), and also reduces the global acceleration significantly (Figure 1.16b).

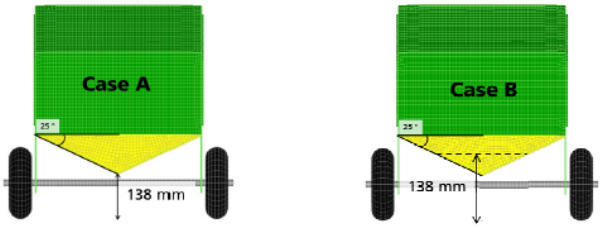

Figure 1.15: Numerical models of the vehicles used by Heider [27] for the investigation of the influence of ground clearance for v-shaped vehicle hulls

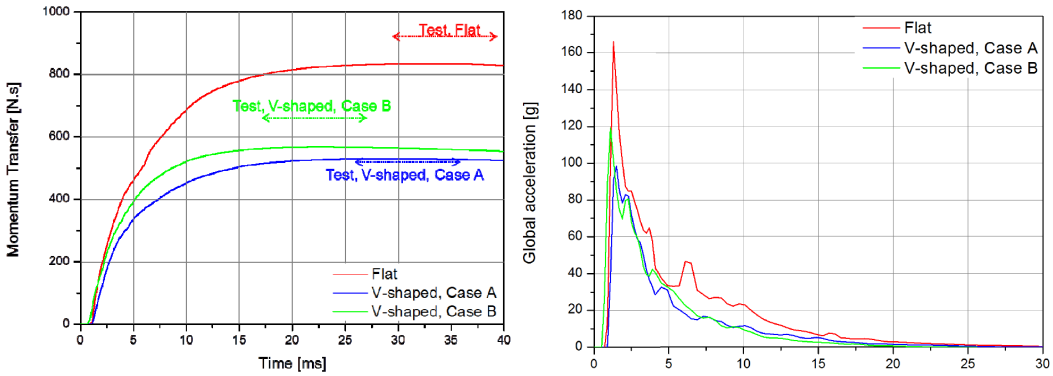

(a) Momentum transfer (b) Global vehicle acceleration

Figure 1.16: Simulation results from [27]

Layered panels Layered panels are a commonly used solution for protection against blast waves. A layered panel consists of a crushable core, or absorber, located between a front plate and a back plate. This core can be made out of different materials (honeycomb structure, foam...) and is crushed by the displacement of the front plate following its interaction with the shock wave. The goal of this structure is to use the core crushing phase to dissipate energy through plastic or brittle deformation of the core, thus the pressure load is applied to the target at a lower intensity over a longer duration (Figure 1.17) [3, 4, 5, 6, 7, 8].

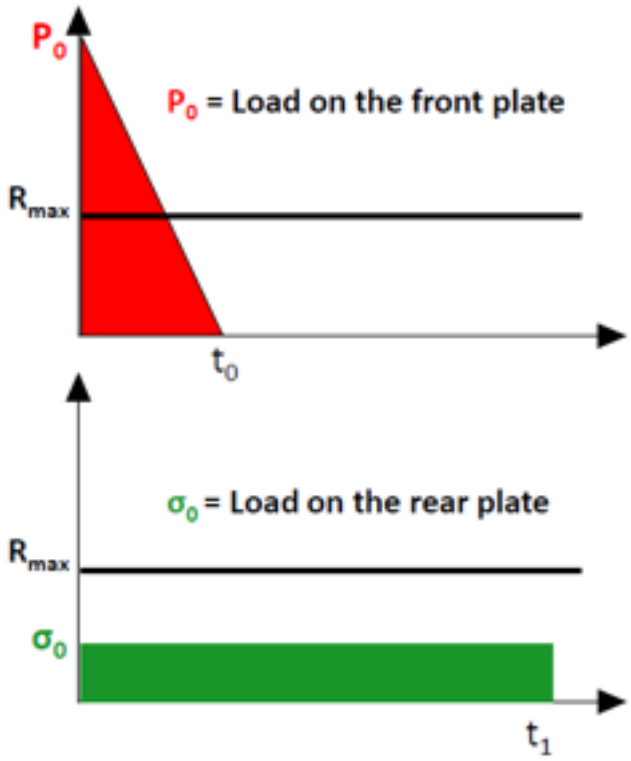

Figure 1.17: Pressure load applied to the front and back plates of a layered panel

The transmitted impulse is generally not affected by such design, but it has been shown that by voluntarily weakening the rigidity of the system, while keeping in check the energy transmitted by the blast wave, it could be possible to reduce the transmitted impulse through the beneficial aspect of fluid-structure interaction [9, 28, 25].

Fluids for personal protective equipment As there are currently few studies making use of fluids for vehicle protection in the literature, other areas of application were also looked at. For example, studies on the use of fluids for blast protection have been preformed in the field of personal protective equipment.

A study by Chen [29] considered a new body armor design equipped with a system of fluid filled tubing fit with and end cap in order to allow the ejection of said fluid. The experimental setup described in Figure 1.18a shows the pressure sensors located in front and behind the sample of the protective equipment, thus allowing the measurement of the peak overpressure reduction due to the sample. This body armor equipped with fluid filled tubing was designed as an overpressure transformer to transfer kinetic energy of shock waves into hydraulic energy in the plastic tubing. The hydraulic energy is redirected through the plastic tubing openings at the lower end, fit with plastic caps. This permits the fluid to be quickly released (Figure 1.18b). For the body armor, the peak overpressure reduction was measured behind the sample. The theory motivating this experiment was that a transformation of the energy generated by the shock wave into hydraulic energy allowed its extraction through the release of water. Measurements were taken at the rear of the sample and are summarized in Table 1.1. Results showed a significant

Table 1.1: Experimental results from [29]

	In front of sample	Behind sample		
		Empty tubing	Empty tubing and kevlar	Filled tubing and kevlar
Measured pressure (psi)	10.14	5.33	0.27	0.27

reduction of the peak overpressure, from 10,14 psi measured by the front sensor to 0,27 psi measured behind the sample. However, experiments were also performed with the empty tubing alone, and a similar reduction of overpressure could be measured (0,25 psi). This begs the question of the role the water ejection mechanism plays in the reduction of the peak overpressure.

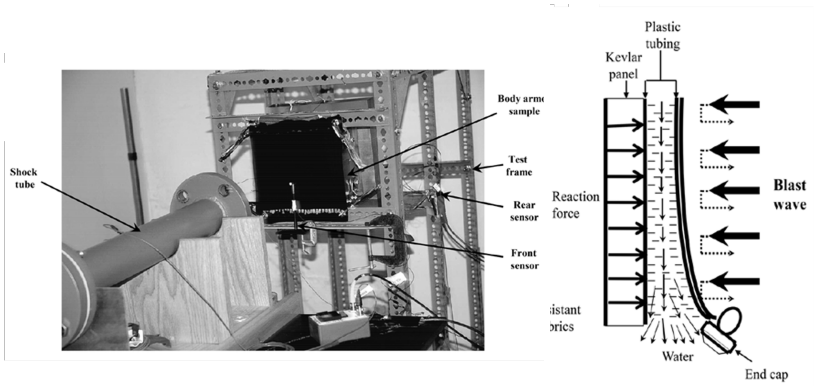

(a) Experimental setup (b) Schematic illustration of the tubing setup

Figure 1.18: Test setup for vests equipped with fluid filled tubing

Previous work by Young [30] investigated the use of fluids to fill a helmet liner in order to maximize the performance characteristics of the helmet when subject to a blast wave. During this investigation, a panel of microcellular, energy-absorbent foam was designed with a cavity that could be filled by a variety of materials as shown in Figure 1.19.

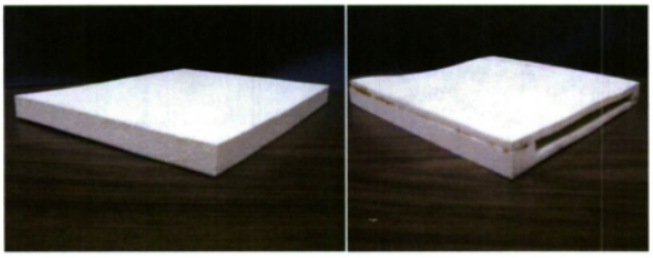

Figure 1.19: Liner structure filled with fluid in the helmet design [30]

The materials tested were both solid fillers (aerogel, glass beads) and liquid fillers (water, glycerin, AgileZorb). In order to quantify the efficiency of the filled panels, a pressure gauge was placed exactly behind the center of the sample. It was found that the most efficient mitigation was provided by AgileZorb. AgileZorb has nano-sized pores suspended in non-wetting liquid. When the pressure exceeds a threshold, because of capillary effect, the liquid

goes inside the pores, resulting in energy dissipation. When choosing a fluid to fill the foam channels, the approach was that the mitigation effects would increase with the energy transfer within the material. When using water, peak overpressure magnitudes were cut in half. The general trend highlighted by the experiments conducted by Young were that high density and low porosity materials provide higher pressure attenuation by increasing the rise time and duration of the blast. However, it must be noted that in this investigation, the variable attesting the efficiency of a given filler is the value of the peak pressure of the remaining blast wave having passed through the fluid filled foam sample. Hence, the main factor impacting the blast mitigation efficiency is the mismatch of impedance between air and the tested filler.

1.3.3.2 Momentum control

Dynamic impulse compensation concept One study taking into consideration the issue of the direction of the momentum transmission was conducted by Denefled [31] with what was called a Dynamic Impulse Compensation concept (DIC). The DIC method is based on the idea of compensating the momentum generated by the IED by a gun type system ejecting a mass in the opposite direction from the blast. This is done by ejecting a massive steel projectile (13% of the total mass of the scaled vehicle model) from a gun type system which will compensate the momentum generated by the blast and accelerate the vehicle in the opposite direction. The experimental setup (Figure 1.20a) had an ejection unit mounted in the center of the vehicle whist the numerical model (1.20b) had 4 DIC ejection units allowing more flexibility in the study, especially when encountering a case of asymmetric IED placement under the vehicle floor.

(a) Experimental setup (b) Numerical setup

Figure 1.20: Vehicle equipped with a gun type system for dynamic momentum compensation. Taken from [31]

Experimentally, a reduction of 70% of the jump height could be achieved (Figure 1.21a). Using the numerical model, it was evaluated whether the occupant loading (loading on the lumbar spine region and lower legs) as well as global vehicle motion could be reduced using DIC. Subsequent to the detonation of an IED, the phenomena on the vehicle structure are as follows: the whole momentum is transferred onto the structure within 40ms after detonation. The vehicle is the in a free flight phase and falls back on the ground after 700ms. The resulting forces acting on the vehicle are reduced from a peak value of 14kN to 8kN with DIC (Figure 1.21b).

However, current technological limitations do not allow the detection of an IED and initiation of the DIC system

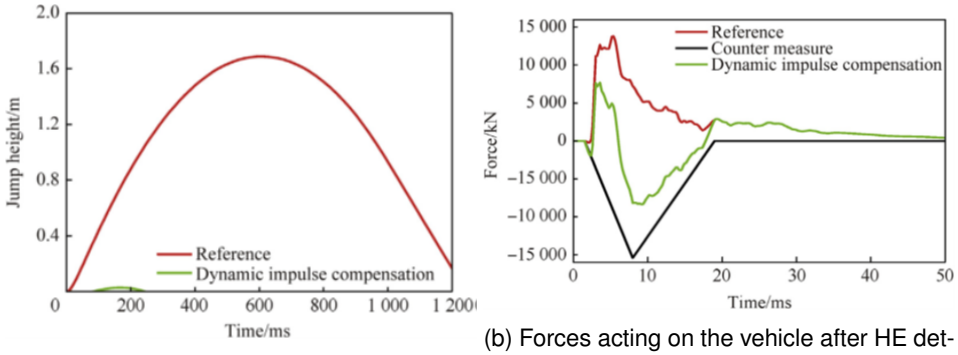

(a) Jump height using DIC

(b) Forces acting on the vehicle after HE detonation

Figure 1.21: Experimental results regarding the used of a dynamic impulse compensation system [31]

to occur in a timely manner for this to be an efficient solution. Thus, a core being able to redirect this momentum in different directions should be designed. To eliminate the need for separate initiation, this core should be easily set in motion, such as a fluid for example.

Kinetic energy defeat device The kinetic energy defeat device (KEDD) is a novel device which uses non-viscous liquids arranged in a periodic array to redirect the kinetic energy generated by a projectile through the formation of high-speed jets. This redirection of energy occurs perpendicular to the incoming projectile when the liquid is shock loaded in compression. It aims at slowing the velocity on incoming projectiles, thus reducing the damage to the structure. The KEDD system has been studied by Wolfson [32], both experimentally and numerically. A computational problem was formulated by Wolfson using the code CTH to determine the capacity of a KEDD to reduce the velocity of the incoming projectile. In this setup, a circular steel impacting disk (the flyer plate) travels at 800m/s and impacts a cylinder of water resting on a second circular steel disk (rear disk). The dimensions of the elements, as described in Figure 1.22, ensure that the weight of the water equals the weight of the two disks.

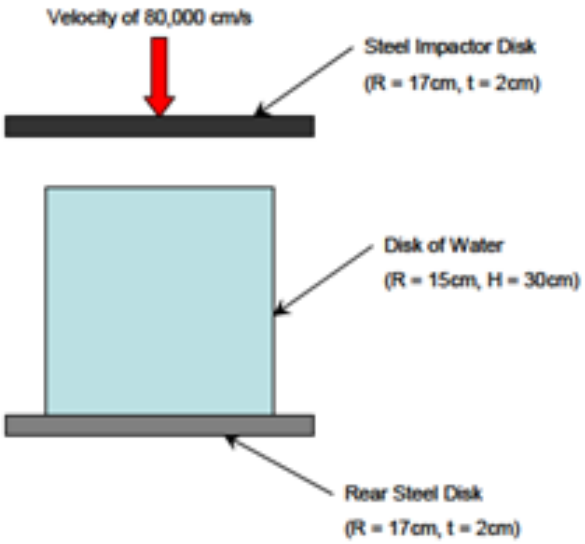

Figure 1.22: Numerical model of the kinetic energy defeat device (KEDD) as described by Wolfson [32]

This numerical simulation was reproduced by the author in the frame of this investigation with the code Impetus AFEA, described in more detail in Section 1.5, as it could be a good starting point for the design of a momentum redirection system. The MAT FLUID command was used to define the material properties of water, with a density $\rho = 1000kg/m^3$, a linear bulk modulus $K = 2.2e^9Pa$ and a dynamic viscosity $\mu = 8.9e^{-4}Pa.s$. A Gruneisen equation of state to determine the pressure levels in the fluid completes this material definition with the linear Hugoniot slope coefficient $S = 1.237$ and a Guneisen gamma of 1.54. When defining the material properties for the plates using the steel S235 present in the Impetus AFEA library, the front and back plates underwent significant deformation as shown in Figure 1.23. This deformation was not present in the simulations performed by Wolfson, thus the plates were defined as rigid in Impetus AFEA (Figure 1.24a).

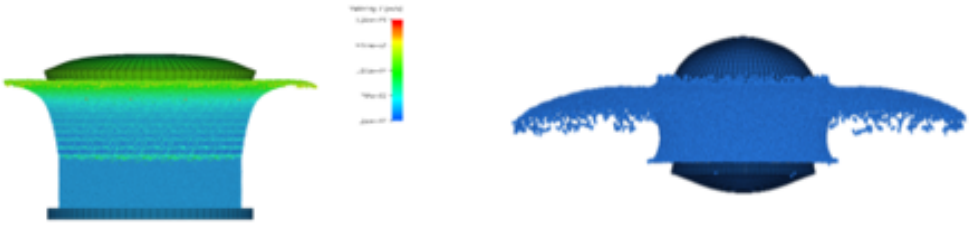

Figure 1.23: Deformation of the steel flyer and rear disk in the numerical simulation in Impetus AFEA

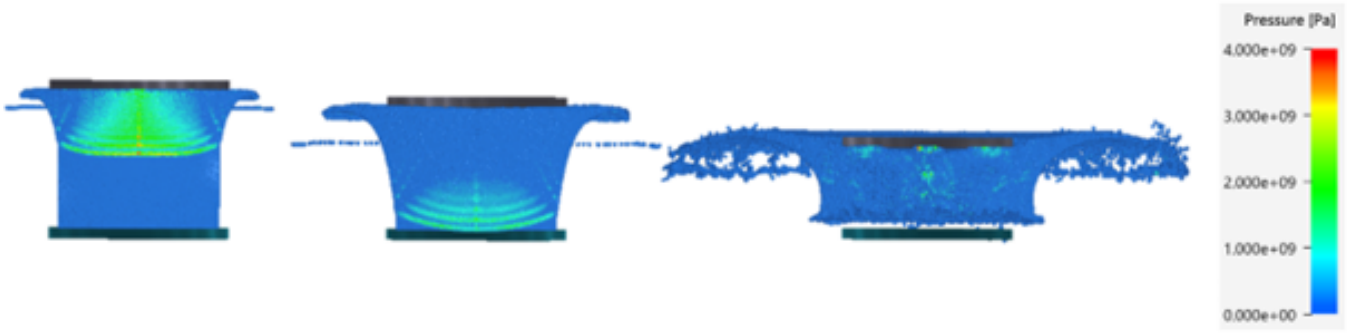

(a) Reproduction of the numerical simulation using Impetus AFEA

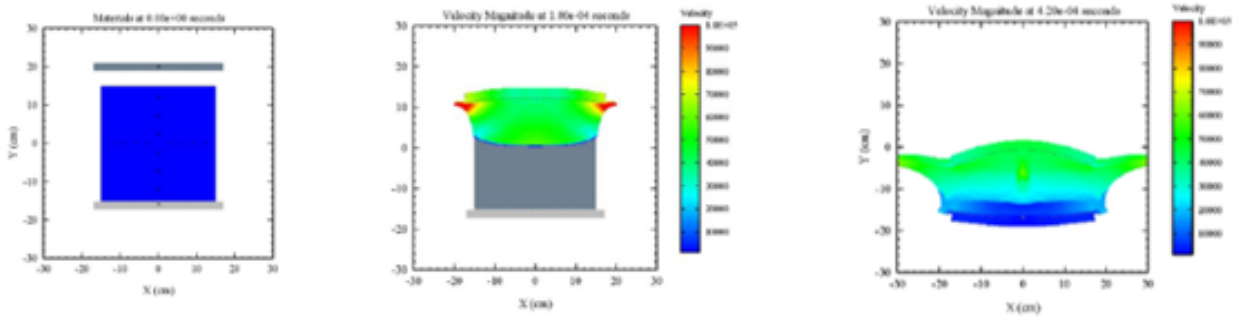

(b) Numerical simulation performed by Wolfson [32]

Figure 1.24: Numerical simulation of the spreading of the water column following the impact of the flyer plate of the KEDD

Wolfson found that the velocity of the flying plate and the rear plate changed through the interaction with the cylinder of water. The initial velocity of the flying plate was set to 800m/s, after the interaction, the back plate and flying plate both travel at the same speed of 200 m/s (a reduction of 75% of the initial velocity) (Figure 1.25b). When comparing the simulation results obtained by Wolfson and Impetus AFEA, it is noticeable that the bottom plate behaves differently. Indeed, the bottom plate stays in constant contact with the water column in the simulation performed by Wolfson as shown in Figure 1.24b. However, with Impetus AFEA a pressure wave is generated from the impact of the flying plate at 800 m/s onto the water column. This impact sets the bottom plate in motion, thus preventing both plate velocities from converging to a common value similarly to the calculations performed by Wolfson. Simulation results from Impetus AFEA (Figure 1.25a), show that the top plate is decelerated to 382 m/s and the bottom plate is accelerated to 114 m/s after the impact. The front plate decelerates a second times as soon as it is intercepted by the wave reflected on the bottom plate.

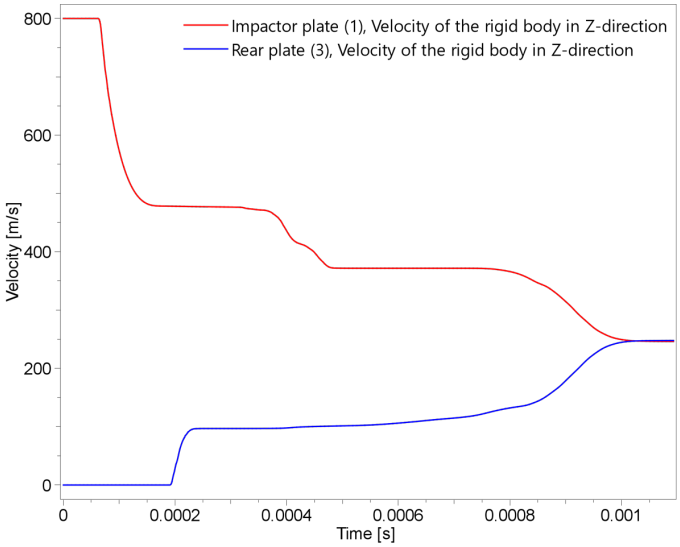

(a) Reproduction of the simulation with Impetus AFEA

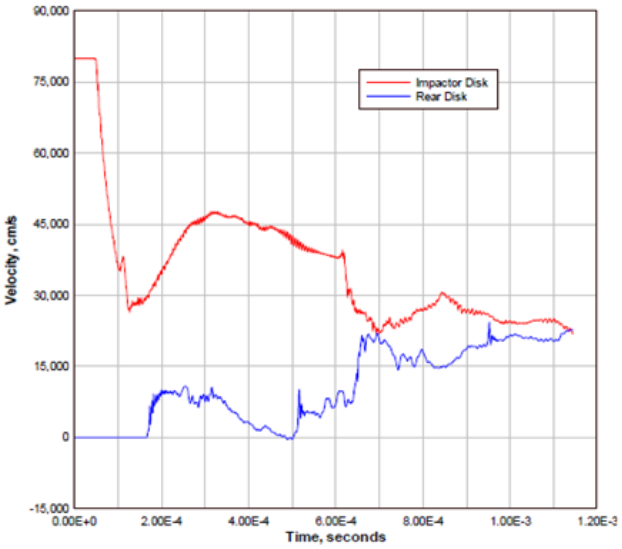

(b) Simulation performed by Wolfson [32]

Figure 1.25: Numerical results of the impactor and rear plate velocity [32]

Momentum conservation dictates that the impactor momentum is transferred to the rest of the system during the impact. A quick calculation shows that the momentum of the rear plate is four times lower than the initial momentum of the impactor. The missing momentum is located in the impactor through its residual velocity, and in the water. However, by reproducing the model using impetus, it can be shown that the water spread over a surface larger than the rear plate, indicating that its momentum will never be transmitted to it. This beg the question: is it possible to use the water ability to spread over in order to locally reduce the impulse, or even the total momentum transmitted to a target ?

The concept of the KEDD was also investigated experimentally with a variation in the number and placement of several water filled tubes, placed in between a top (flyer) plate and a bottom plate (Figure 1.26). The parameter of observation in this study was the damage of the bottom steel plate for varying KEDD configurations. Compared to a baseline test without KEDDs, the damage and strain rate of the bottom plate could be significantly reduced (whilst plates of the baseline test failed, plates used in the same configuration but with KEDDs were still partially intact). This study also included an experimental investigation in which the water was replaced by sand. In that case, the KEDD was not efficient in reducing damage to the target (bottom plate) and was found to even increase the strain rate.

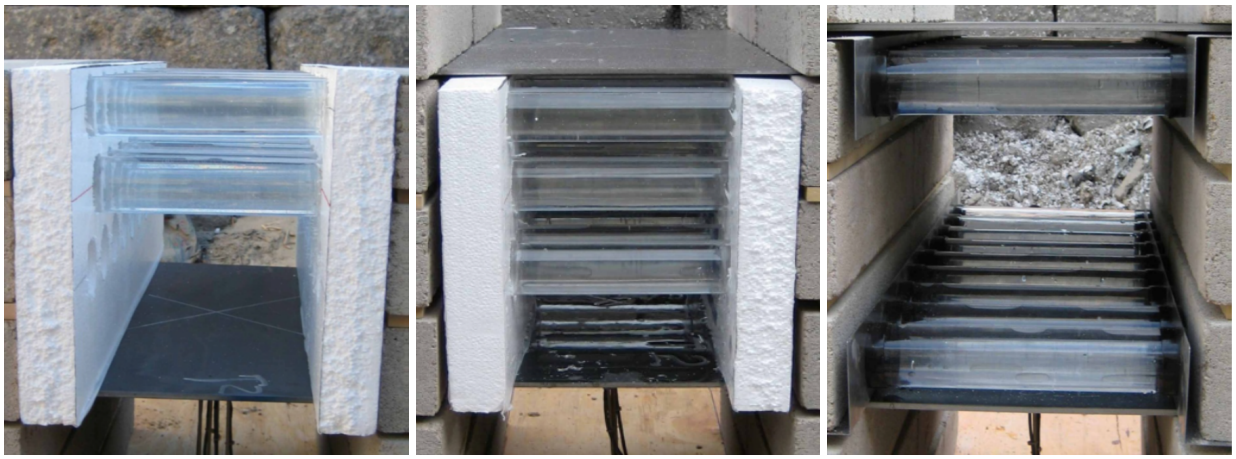

(a) 2 rows close to the top plate (b) 3 rows close to the top plate (c) 2 rows close to the top and bottom plate

Figure 1.26: Different KEDD layouts as tested experimentally by Wolfson [32]

Water filled containers Another study focused on the use of fluids for target protection. Bornstein [2] focused on the potential for water filled containers to mitigate blast loading on armored vehicles by comparing the effects of an empty container, a water filled container with varying geometries and a water filled container at a standoff distance from the target. This study investigated the deformation of a steel plate located under the water filled container.

Near-field blast mitigation provided by a range of container geometries was investigated experimentally by Bornstein [12] the best performing quadrangular water-filled container and novel shaped containers such as cone, in-

verted cone, diamond and mushroom as shown in Figure 1.27.

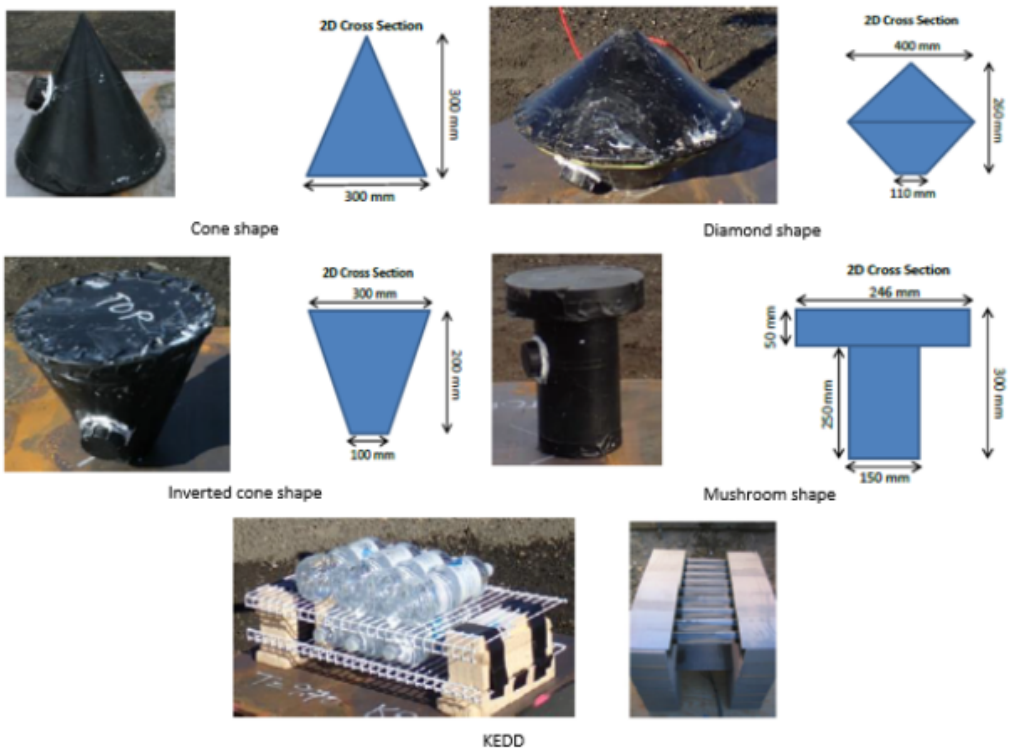

Figure 1.27: Geometries used for the evaluation of the effect of container geometry by Bornstein [12]

The cone shaped container permitted an analogous approach to the V-shaped hull whereas the inverted cone took advantage of the shadowing and spreading mechanisms of the quadrangular shape at a reduced mass. The inverted cone shape presented a large surface area to the detonation product and minimal contact to the target. The diamond shape was chosen to obtain a potential reduction in momentum transfer by angling the surface of the container to the incident shock wave and detonation products. The mushroom shape was used to fully take advantage of the shadowing and spreading effects of the quadrangular container at a reduced mass as the study had shown that there are diminishing effects in terms of blast protection when increasing mitigant mass. Finally, the previously described kinetic energy defeat device (KEDD) consisting of an arrangement of water filled cylinders designed to enhance the spreading mitigation mechanism was examined. A larger number of cylinders were stacked above to mimic an inverted V-shape thought to provide benefits through the shadowing mechanism. This study found that whilst the quadrangular water-filled container provided the best reduction in dynamic deformation, when considering the mass efficiency of blast mitigation, the mushroom shaped container had the highest reduction in deformation per kg of water. However, the cone shaped container provided no mitigation at all, showing that the shadowing mitigation mechanism is more effective at reducing deformation than deflecting the detonation product. Furthermore it was shown that when keeping a constant volume of fluid, a higher more narrow water column had provided better target protection than a thinner layer of fluid covering more surface area.

Bornstein also experimentally investigated the effect of five different filler materials on the deformation of a steel plate subject to blast loading in the near field [33]. Five different materials providing a variety of sound speed values and levels of compressibility were used:

- Bulk water: bulk water was used to provide a baseline level of performance. It was postulated by Bornstein that a lower sound speed reduces the speed of the pressure wave traveling through the fluid, giving rarefaction waves greater time to reduce the impulse delivered to the target.
- Aerated water: aerated water provides a reduced sound speed compared to bulk water (1500 m/s for bulk water and 50 m/s for aerated water) and a different level of compressibility.
- Dry sand: it was found that the porosity and density of sand were key properties and resulted in enhanced mitigation when compared to water.
- Expanded polystyrene (EPS): The H-grade expanded polystyrene block was used to maintain the shadowing effect of the water filled container at a reduced weight.
- EPS + Water: a combination of both these materials was used to maintain the shadowing effect whilst maintaining the same geometry that affected shadowing and to provide a compressible fill.
- Shear thickening fluid (STF): the STF was used to examine the effect of increased fluid density on the rarefaction mechanism.

As a result of this investigation, it was found that the sand was the best performing mitigant. However, when evaluating the mass efficiency of the different fluids, sand did not provide the best performance on a mass basis. Rather, the EPS + Water mixture was found to be the most efficient, followed by bulk water.

In this section, mechanisms allowing blast protection and mitigation were given. The characterization of the threat in this particular study, the buried mine, showed that one possible response of a vehicle to the explosion is its vertical acceleration, linked to momentum transmission to the structure. Current protection solutions for targets were reviewed, both regarding energy and momentum. Whilst not extensively studied at the moment, the use of fluids such as water was identified as one possible solution for momentum control. The investigation of the kinetic energy defeat device (KEDD) showed some promising results by spreading the fluid over a larger surface than the surface of the target. Therefore, several questions need to be answered: is it possible to use spreading mechanisms in water to locally reduce the impulse, or even the total momentum transmitted to a target ? How can we identify the mechanisms occurring in the fluid that are beneficial to momentum transmission in order to take advantage of them ?

The goal of this work is partly to answer these questions. In the next section, different experimental and numerical tools will be described and the most adequate one will be chosen to answer these questions.

1.4 Experimental setups for the investigation of momentum and fluids under blast loading

1.4.1 Generation of a blast load

As stated previously, this work focuses on the effects following the detonation of an IED. Thus, an experimental way of applying a blast load of high intensity to a specific area has to be found. Different methods of generating a blast load will be described in this section.

1.4.1.1 Detonation in free field

The most straightforward solution to generate a blast load is through detonation in free field. One possibility to generate this blast load is through the detonation of a gas mixture. However, studies focusing on this type of detonation often regard accidental detonation of gas and their impact on industrial structure [34] or are performed at a small scale for the characterization of the gaseous mixture itself [35, 36]. This method is however seldom used for an experimental assessment of the protection capabilities of a novel structures. In contrast, numerous experimental investigations with the goal of assessing the protection capabilities of novel structures against the effects of blast make use of the detonation of a condensed explosive in the free field [37, 38, 7]. However, the generation of a blast load through detonation in a free field poses some experimental difficulties:

- as a spherical blast wave is generated in free field, the loading on the tested structure is not uniformly distributed, which adds a difficulty in the interpretation regarding the response of the structure to be tested
- in the scope of this study, focusing on land mines, the blast loading generated by the detonation of a condensed explosive in the free field may be insufficient, or would require high quantities of explosives

1.4.1.2 Steel pots

Whilst the detonation in free field may not be adapted in the case of the study of a novel protective design for the aforementioned reasons, when a structure is tested once the design process had become closer to vehicle integration, steel pots are often used for the test of military vehicles [39, 40]. The AEP-55 document [41] states that the blast effect of a buried TNT surrogate mine overburden with 10 cm water saturated sandy gravel can also be generated using a PETN-B (a plastic explosive containing 86% PETN where $m_{TNT} = 1,19 m_{PETN-B}$) surrogate charge positioned in a steel pot. A steel pot has a specified geometry (Figure 1.28) and it is obligatory to apply an air gap of 50 mm around the charge. Due to these strict specifications, the use of steel pots provides a unified method for testing structures against the effects of the detonation of a buried explosive charge.

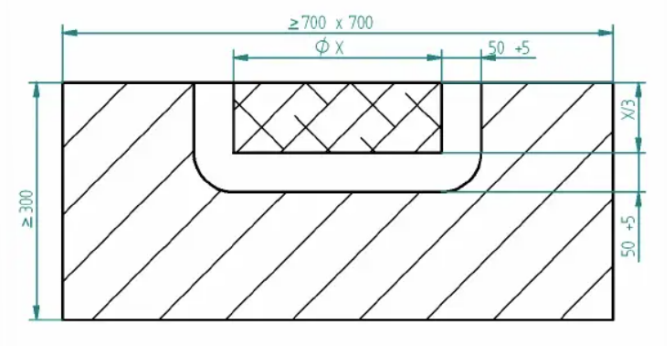

Figure 1.28: Geometrical specifications of a steel pot

1.4.1.3 Shock tubes

Shock tubes have been used for more than a century, with the first description of a shock tube in 1899 by Vieille [42], and have been extensively used for the study of materials under blast loading in a laboratory setting [43, 44]. A shock tube has three main sections: a driver and a driven section as well as a diaphragm (Figure 1.29). To generate a shock wave, the pressure in the driver section is increased until the diaphragm bursts, creating a shock wave propagating though the driven section. In contrary to a free field detonation, the shock tube generates a planar shock wave, thus loading the tested sample in a uniform way. Whilst the shock wave generated by a shock tube can vary depending on the design details of the shock tube, the general pressure-time history in the driven section of the tube, depicted in Figure 1.30, shows that the pressure signal has a virtually instantaneous rise time and can be maintained over several milliseconds. The peak pressure produced by a shock tube is highly dependent on the design of the tube. For the purpose of providing an example, an oxy-acetylene driven laboratory shock tube developed by Courtney [45], provided a peak pressure value in the range of 2 to 11 bar. These characteristics however do not allow for realistic experimental testing of a structure against the effects of an IED, as the shock wave produced by the shock tube does not provide the characteristic decay in the pressure profile of a blast wave and does not provide a peak pressure of a sufficient intensity. Modern shock tubes are now also able to generate a blast profile, whose intensity is however still largely inferior to what can be achieve with explosive driven shock tubes.

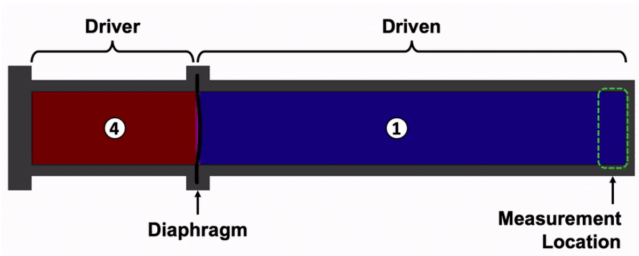

Figure 1.29: Shematic representation of a shock tube

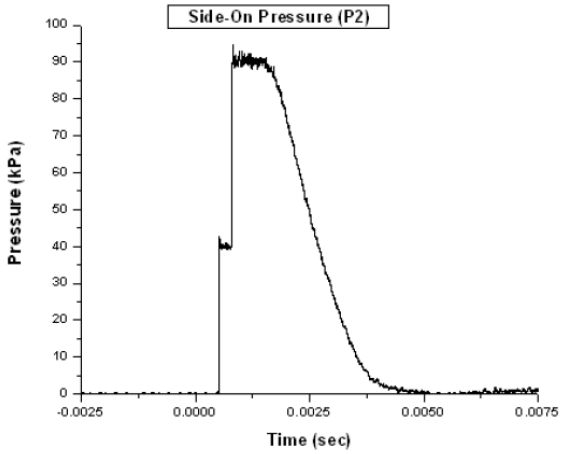

Figure 1.30: Pressure-time history of the pressure sensor located in the driver section with no material in the shock tube (bare end plate) as presented in [46]

1.4.1.4 Explosive driven shock tubes

Explosive driven shock tubes (EDST) are relatively simple experimental setups. An explosive charge is placed at a certain stand-off distance from the entrance of a tube of a given section. After detonation of the explosive charge, a planar blast load is generated at the exit of the tube. Numerous protective structures have been tested using this experimental setup [28, 47] as they provide a repeatable, planar blast wave having the characteristic pressure time history of that generated by an explosive charge such as a buried mine or improvised explosive device.

After detonation of an explosive charge, positioned at a certain stand-off distance, the confined channel of the EDST leads to the development of a planar blast wave. For a small charge, the pressure and impulse profile at the exit of the tube will be much higher than for the detonation of the same charge in air.

1.4.1.5 Choice of blast generator in the scope of this work

Considering that this study focuses on the detonation of land mines or improvised explosive devices, a blast generation through the use of an explosive driven shock tube (EDST) reproduces the effects of the threat most accurately. An EDST was previously used at ISL by Blanc [25]. Figure 1.31 shows a schematic representation of the dimensions of this particular EDST.

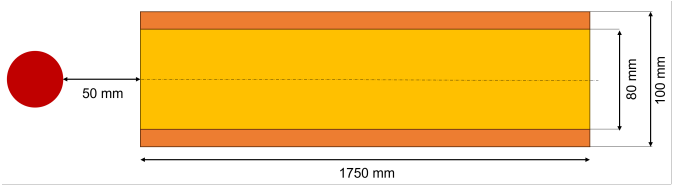

Figure 1.31: Schematic of the geometry of the EDST used by Blanc [25]

Table 1.2: Parameters of the incident and reflected blast load at the exit of the tube as described by Blanc [25]

Charge mass (g)	Free field		Reflected blast	
	Overpressure (bar)	Impulse (bar.ms)	Overpressure (bar)	Impulse (bar.ms)
15	7.99	3.09	38.72	16.98
30	14.29	5.15	79.69	26.54
50	22.53	7.42	131.55	39.76

The charge masses used by Blanc were of 15, 30 and 50 grams of C4. Table 1.2 shows the maximal over pressure and impulse of the blast wave at the exit of the tube. The free field blast load parameters were measured by a blast pencil and the reflected blast load parameters were measured by a pressure transducer while the exit of the tube was closed with a rigid plate.

The United Facilities Criteria (UFC) [48] gives the positive shock wave parameters for a spherical TNT Explosion in Free Air at Sea Level as a function of the scaled distance Z. Knowing the peak over pressure at the exit of the tube, the scaled distance and incident specific impulse $i_s = \frac{I}{\sqrt[3]{m}}$, where m is the mass of the explosive, can be determined from Figure 1.32. Therefore, knowing the impulse I at the exit of the tube, it can be determined which mass of explosive will give the same over pressure value in free field as the value obtained at the end of the tube, at a certain distance:

- for 15 g of C4 the same over pressure is achieved for a free field explosion for 91.1 kg of TNT at a distance of 3.6 m
- for 30 g of C4 the same over pressure is achieved for a free field explosion for 184 kg of TNT at a distance of 3.58 m
- for 50 g of C4 the same over pressure is achieved for a free field explosion for 188 kg of TNT at a distance of 3 m

Therefore, the use of an EDST allows to replicate the high intensity localized blast loads generated by an IED whilst using small charges for the purpose of academic experiments.

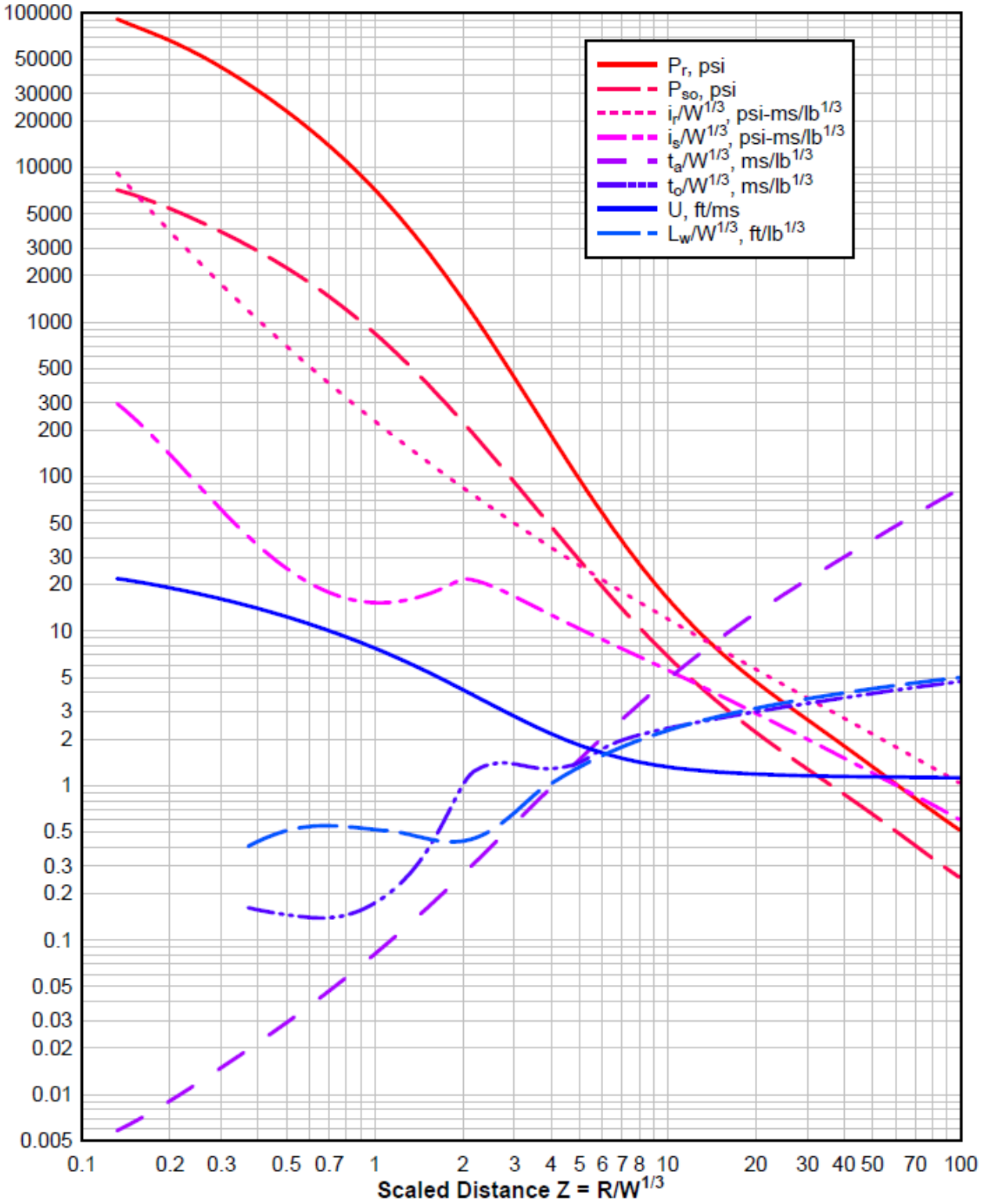

Figure 1.32: Positive phase shock wave parameters for a spherical TNT explosion in free air at sea level, taken from [48]

1.4.2 Pressure measurements in fluids

A pressure sensor converts changes in pressure of a gas or a liquid into an electrical signal and is therefore ideal for monitoring dynamic pressure events. Pressure sensors have a sensing element of constant area and respond to force applied to this area by fluid pressure, which will deflect the diaphragm inside the pressure transducer. This deflection is measured and converted into an electrical output. Pressure measurement in a fluid in the case of the behavior of the blast wave at an air-water interface is scarcely documented, thus giving little information on the use of pressure sensors inside a fluid to measure such phenomena. In an investigation performed by Henderson [49], the refraction of a shock wave at an air-water interface was studied. As detailed in the previous sections, a shock wave propagating in a medium of low density impinging on a second medium of much higher density will be reflected as it passes from one medium to another. In the case of an air-water interface, there is a large difference in the shock impedance. As such, the reflection is somewhat similar to that of a shock in a gas reflecting of a rigid surface, the impedance of the water ($1.510^6\ Pa.s/m$ at 1 atm and 15C) being three orders of magnitude greater than that of air (410 $Pa.s/m$ at 1 atm and 15C). In this way, water is an almost rigid body.

Experimental data was obtained by Peckham [50] in order to characterize the shock wave induced in the water directly below an explosion in air. In this experimental study, the air blast and underwater shock were measured. The measurements were made by underwater pressure sensors as shown in Figure 1.33. Several sensor positions were used extending from a point almost directly under the charge to about 3 meters under the water surface.

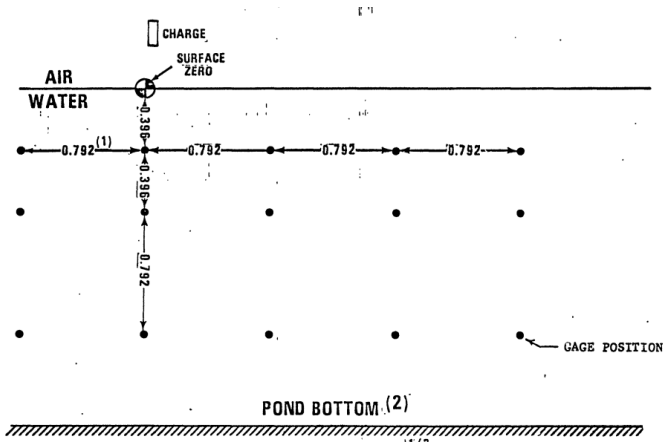

Figure 1.33: Experimental setup for the investigation of the air to water blast wave transfer [50].

The study showed that the pressure-time curves are made up of multiple pressure pulses. These multiple pulses result in part from the perturbations on the air blast shock front and the explosion products front. These perturbations reflecting of the interface act as separate sources for the underwater shock wave. Thus, the underwater pressure-time history shows several pressure peaks corresponding to the arrival of the shock generated by each perturbation.

Indeed, a blast can be equivalent to a succession of shock of decreasing intensity, wanting to compress the media in which the shock is propagating. A subsequent compression wave can only further compress the media if

its intensity is high enough to compress a media that was already in a stage of compression due to the passing of the first compression wave, therefore justifying the observation of multiple pressure pulses.

1.4.3 Measurement of momentum

Measurement of momentum in a fluid can be challenging, which is why pressure (and thus impulse) measurements, as described in Section 1.4.2, will be implemented in the experimental setups described in Chapter 2. However, the global momentum transmission from a blast wave to a structure can be experimentally investigated with the use of a ballistic pendulum (in this case more accurately described as a blast pendulum). This experimental solution is selected for the work described in Chapter 3.

1.4.3.1 The ballistic pendulum

The ballistic pendulum, first described by Robins [51], is a measurement device comprising a suspended target into which a projectile, such as a bullet, can be fired (Figure 1.34). This device allows the measurement of the velocity of said projectile by determining the momentum transferred to the target from the amplitude of the pendulum swing. The initial velocity of the bullet can be easily deduced from the angle of the pendulum motion by conservation of mechanical energy and momentum conservation.

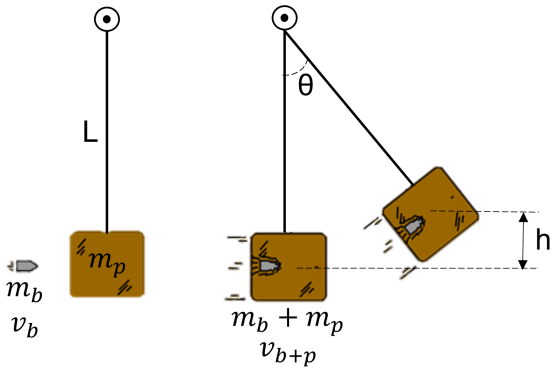

Figure 1.34: Schematic of a ballistic pendulum before and after impact of a projectile. With m_p and m_b the mass of the pendulum and the bullet, v_p and v_b the velocity of the pendulum and the bullet,Θ the angle of the pendulum , h the height difference after displacement of the pendulum

For the initial position of the pendulum, the initial kinetic energy is $E_{k\ initial} = \frac{1}{2}(m_b + m_p)v_{b+p}^2$ whilst the initial potential energy is $U_{initial} = 0$. For the final position of the pendulum (when the maximal potential energy has been reached), the kinetic energy is $E_{k\ final} = 0$ and the potential energy is $U_{final} = (m_b + m_p)gh$. By energy conservation, $E_{k\ initial} = U_{final}$ (Equation 1.36).

$$\frac{1}{2}(m_b + m_p)v_{b+p}^2 = (m_b + m_p)gh \Rightarrow v_{b+p} = \sqrt{2gh} \text{ with } h = L(1 - cos(\Theta)) \tag{1.36}$$

Momentum conservation states that the momentum of the bullet before impact equates to the momentum of the bullet-pendulum system (Equation 1.37).

$$m_b v_b = (m_b + m_p) v_{b+p} \tag{1.37}$$

Therefore, the initial velocity of the bullet can be calculated (Equation1.38).

$$v_b = \frac{m_b + m_p}{m_b} \sqrt{2gh} \tag{1.38}$$

1.4.3.2 The blast pendulum

Properties of a blast wave regarding impulse can also be investigated through a blast pendulum. In that case, the blast pendulum is set into a motion following the interaction with a blast wave generated by a spherical charge placed at a given distance from a square load impact plate. Similarly to the ballistic pendulum, the blast pendulum allows to link the movement of the suspended body to the impulse transmitted by the blast. A blast pendulum can have a rotational movement, as was the case with the ballistic pendulum previously described, or a translational motion.

Such a pendulum was studied by Snyman [52]. This blast pendulum used horizontal motion (Figure 1.35). This setup has the advantage of not having to interpret the results with rotational components as the impulse imparted by the charge can be directly correlated to the horizontal displacement of the beam measured via laser displacement and rapid camera imaging. Moreover, it is possible to use an explosive driven shock tube, rather than a spherical charge, to apply the blast wave to the load impact plate. As seen in the previous section, this allows for a uniform loading of the test plate. Contrary to the ballistic pendulum, it should be noted that the motion of the blast pendulum is not only due to the blast applied on the square load impact plate, but also by the blast applied on the rotating arm. The contribution of the blast applied to the arm towards the total impulse transmission depends on the geometry of the pendulum. For the pendulum used by Reck [53] around 15% of the impulse originates from the blast load applied on the arm of a rotational pendulum.

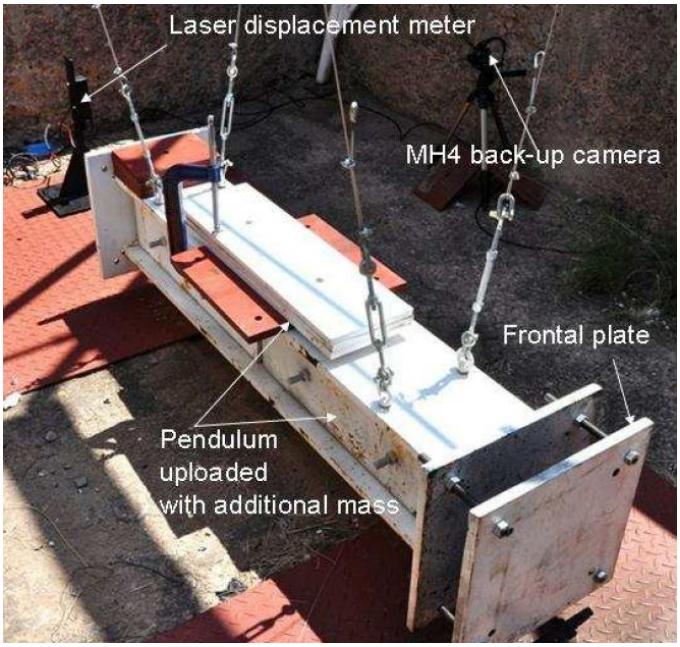

Figure 1.35: Experimental setup of a blast pendulum with horizontal displacement [52]

1.4.3.3 Experimental setup for momentum investigation in the scope of this work

A blast pendulum had been previously been used by Reck [53] at ISL. In that case, the blast pendulum is set into a rotational motion following the interaction with a blast wave generated by a spherical charge placed at a given distance from a square load impact plate. Similarly to the ballistic pendulum, the blast pendulum allows to link the movement of the suspended body (more specifically its rotational angle) to the transmitted impulse. Figures 1.36a and 1.36b show the geometry of the pendulum, where:

- P is the center of rotation of the pendulum on the pendulum axis
- ω is the angular velocity
- CM is the center of mass of the pendulum, with s the distance between P and CM, b the distance between P and the center of the square load impact area of the pendulum

For a blast pendulum, an analytical description aims at establishing a link between pendulum motion and blast wave impulse.

Firstly, the change of angular momentum, ΔL can be written as Equation 1.39 where $r_\perp$ is the lever arm distance between the center of rotation P and the point of application of the force, I is the load impulse, J is the moment of inertia.

$$\Delta L = r_\perp I = J\Delta\omega \tag{1.39}$$

(a) Pendulum used at ISL

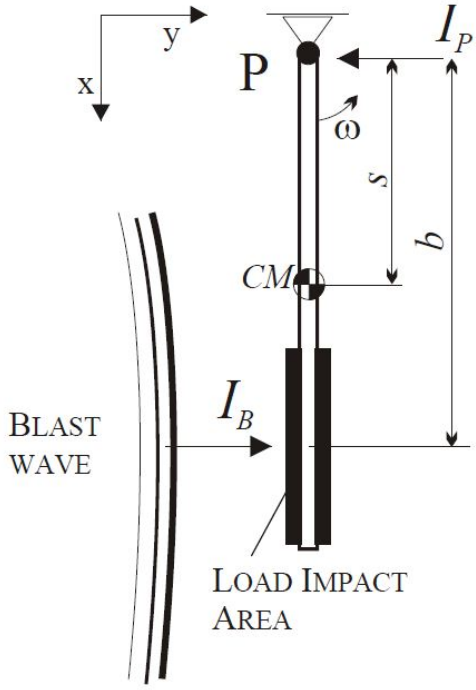

(b) Schematic of the geometry of the pendulum

Figure 1.36: Blast pendulum used experimentally for the investigation of momentum transmission

In this particular case, $r_\perp = b$, and therefore the blast wave load impulse ca be expressed as shown in Equation 1.40, where $\omega_0 = 0$ is the initial velocity of the pendulum.

$$I_b = \frac{J_{Pz}(\omega - \omega_0)}{b} \tag{1.40}$$

Considering energy conservation, the kinetic energy is equal to the potential energy when the pendulum comes to a stop (1.41).

$$E_k = U = \frac{J_{Pz}\omega^2}{2} = mgh \text{ where } h = s(1 - cos(\Omega_{max})) \tag{1.41}$$

Where Ω_{max} is the angle of the pendulum with respect to the vertical position.

Finally, the blast wave load impulse can be expressed as shown in Equation 1.42

$$I_b = \frac{1}{b}\sqrt{2J_{Pz}mgs(1 - cos(\Omega_{max}))} \tag{1.42}$$

Making the assumption that the impact plate is loaded homogeneously and that the impulse effects of the pendulum arms are negligible, an impulse i_b can be defined (Equation 1.43).

$$i_b = \frac{I_b}{A} \text{ where } A \text{ is the surface of the load impact area} \tag{1.43}$$

In this Section, different experimental setups to generate a blast load were reviewed. Considering the threat characterization made in Section 1.3.2, the blast load that has to be generated in the scope of this work has to be of high intensity and localized to a small area. The explosive driven shock tube (EDST) satisfies these two criteria and will therefore be used to generate the blast load in subsequent experimental setups whenever possible. As mentioned previously, the mechanisms occurring in the fluid itself are of interest in this work. Therefore, pressure measurement will be made in the fluid for a local comprehension of the occurring phenomena. Whilst not extensively documented, some elements of literature reported on previous usage of pressure sensors in a fluid environment in the particular case of an aerial detonation of an explosive charge above water. As the pressure sensor is submerged in a fluid, stainless steel sensors in particular seem to be a good option for this investigation. An experimental setup involving an EDST and local pressure measurements in the fluid is discussed in Chapter 2 to investigate the spreading of impulse. For a more global comprehension of momentum transmission, an experimental setup allowing the motion of the protective structure has to be used. The blast pendulum was identified as being an adequate solution, with different geometrical configurations begin related in literature. For this work, experiments were performed on the rotational pendulum previously used at ISL. The blast pendulum experiments to investigate global momentum transmission are discussed in Chapter 3.

1.5 Numerical modeling of blast waves and fluids

Numerical simulations were used to overcome experimental limitations, mainly regarding the finite number of pressure measurement points with the aforementioned pressure sensors. In the frame of this work, two main phenomena need to be simulated: the simulation of a blast wave and the interaction between a structure and a fluid (in our case water). In this section, different methods for blast generation as well as fluid-structure coupling are given in order to choose the methods best suited for the problematic of this study.

1.5.1 Numerical simulation of a blast wave

For the numerical simulation of a blast wave, different approaches can be taken. A summary of these methods has previously been given by Larcher [54] and Blanc [55]. These methods range from the most representative of the real occurrences of the formation of a blast wave to the most simplified but time saving methods:

Numerical simulation of the combustion process The numerical simulation of the entire chemical process involved in an explosion to the formation of a blast wave can be set up. This can be done by combustion codes but is rarely used in the scope of testing protective solutions.

Numerical simulation of an ideal detonation The numerical simulation of the ideal detonation model. In this case, the specific energy and volume of the explosive charge has to be defined in the model. The blast wave propagates as a discontinuity at the Chapman-Jouguet velocity (a propagation velocity at which the blast wave just reaches the speed of sound) and energy release is considered instantaneous (or custom defined). An equation of state to describe detonation products is needed. The John-Wilkins-Lee (JWL) equation of state is often used. The JWL equation of state defines the pressure as stated in Equation 1.44, where A, B and e_0 have units of pressure, $R1$, $R2$, ω and V are dimensionless.

$$p = A(1 - \frac{\omega}{R_1 V})e^{-R_1 V} + B(1 - \frac{\omega}{R_2 V})e^{-R_2 V} + \frac{\omega e_0}{V} \tag{1.44}$$

The term used in the JWL equation of state are the following:

- V is the ratio between ρ_e and ρ, ρ_e being the density of the explosive solid part and ρ the density of the detonation products
- R_1, R_2 and ω are dimensionless parameters and A and B are parameters with units of pressure. These explosive constants are typically determined experimentally by a controlled cylinder expansion test [56].
- e_0 is the chemical energy per unit volume of the explosive

Numerical simulation of corpuscles The corpuscular method is a method based on the kinetic molecular theory, investigated by Olovsson [57], that allows for a numerical treatment of gas volumes on a macroscopic level.

The kinetic molecular theory is the study of gas molecules and their interaction, leading to ideal gas laws. Bernoulli first proposed a theory in which the air pressure against a piston is build from the perfectly elastic collision of discrete molecules. Maxwell derived an expression for the molecular velocity distribution at thermal equilibrium (Equation 1.45) where $f(v)$ is the probability density function for the molecular velocity, M is the molar mass, R is the universal gas constant and T it the temperature.

$$f(v) = 4\pi(\frac{M}{2\pi RT})^{3/2} v^2 e^{-\frac{Mv^2}{2RT}} \tag{1.45}$$

The thermal velocity can be expressed as shown in Equation 1.46.

$$v_{RMS} = \sqrt{\int_0^\infty v^2 f(v)\, dv} = \frac{3RT}{M} \tag{1.46}$$

The mean-free path l and the frequency of collision f_c can be expressed as a function of the molecular radius r_p and the number of molecules per unit volume n (Equations 1.47 and 1.48).

$$l = \frac{1}{\sqrt{2}\pi n r^2} \tag{1.47}$$

$$f_c = n {r_p}^2 \sqrt{\frac{8\pi RT}{M}} \tag{1.48}$$

For the numerical simulation of a blast, not every single molecule can be modeled. Thus, some assumptions need to be made:

- each particle represents many molecules
- particles are rigid and given a spherical shape to improve contact calculations
- for each particle, there is a balance between translational kinetic energy W_t and spin/vibration energy W_s, determined directly from the heat capacity at constant pressure C_p and at constant volume C_v where $\gamma = \frac{C_p}{C_v}$. This balance was described by Olovsson in [57] (Equation 1.49).

$$\frac{W_s}{W_t} = \frac{5 - 3\gamma}{3\gamma - 3} \tag{1.49}$$

The energy redistribution between two particles when a collision occurs is calculated in such a way that, when impact between particle occurs, the kinetic energy W_t changes and the spin/vibration energy W_s remains unchanged. The ratio $\frac{W_s}{W_t}$ is disrupted and the energy is redistributed to maintain a constant ratio. To ensure an accurate interaction, the particle radius is adjusted to obtain a reasonable mean-free-path.

Direct application of an ideal analytical blast load This numerical method for simulating blast waves omits the simulation of the detonation itself, saving on computational cost. This method uses analytical models of the properties of the blast wave generated by a given charge for a given distance. A limit to the models validity is generally given by the code, as the model will not take into account the effects of the fire ball. For example, in LS-DYNA, the *LOAD BLAST ENHANCED command is valid for a scaled distance Z between $0.147m/kg^{1/3}$ and $40m/kg^{1/3}$ (where $Z = \frac{R}{M_{EqTNT}}^{1/3}$, R the distance from the charge center and M_{EqTNT} the equivalent TNT mass).

Direct application of an experimental blast load measurment The solution with the least computational cost is the direct application of the loading generated by the blast wave onto the structure. This is possible when this loading is very well known, for example in a case where sufficient experimental data is present.

1.5.2 Element formulation

The behavior of a shock wave propagating in a fluid is described by the Navier-Stokes equations, a partial differential equation describing the motion of viscous fluid substances. However, in most numerical models, viscosity is not taken into account, therefore simplifying the Navier-Stokes equations in Euler equations. In a finite element description of the fluid, the Euler equations are solved in each element by conservation of mass, momentum and energy (Equations 1.50, 1.51, 1.52) at each time step.

$$\frac{\partial \rho}{\partial t} + \nabla \cdot (\rho V) = 0 \tag{1.50}$$

$$\frac{\partial (\rho V)}{\partial t} + \nabla \cdot (\rho V V) = -\nabla P + \rho g \tag{1.51}$$

$$\frac{\partial (\rho E)}{\partial t} + \nabla \cdot (\rho E V) = -\nabla \cdot (P V) + \rho g \cdot V \tag{1.52}$$

The variables in this equation are:

- t the time (s)
- ρ the density ($kg.m^{-3}$)
- V the Eulerian particle velocity ($m.s^{-1}$)
- P the thermodynamic pressure (Pa)
- g gravity ($m.s^{-2}$)
- E the total energy per unit volume ($J.Kg^{-1}$)

That being said, these 3 equations do not allow the resolution of the problem (4 variables, 3 equations). To that end, an equation of state must be added to the system.

As stated previously, the fluid transport equations are solved for each element of the finite volume description. In order to describe the ALE element formulation, the Lagrangian and Eulerian element formulations must first be described.

1.5.2.1 Lagrangian description

In a Lagrangian description, the nodes of the mesh are attached to material points. During a loading, as the body deforms, both the nodes and the material points change position, thus, the position of a material point relative to a node stays the same. A node contains the same material throughout the calculation. A representation of the Lagrangian mesh is shown in Figure 1.37.

Whilst the Lagrangian formulation presents some advantages (boundary nodes stay on the boundary, therefore boundary conditions are easily applied), the main disadvantage of this formulation resides in the fact that severe mesh distortion, especially during large deformation can occur. This can result in a loss of accuracy and in a time step approaching zero.

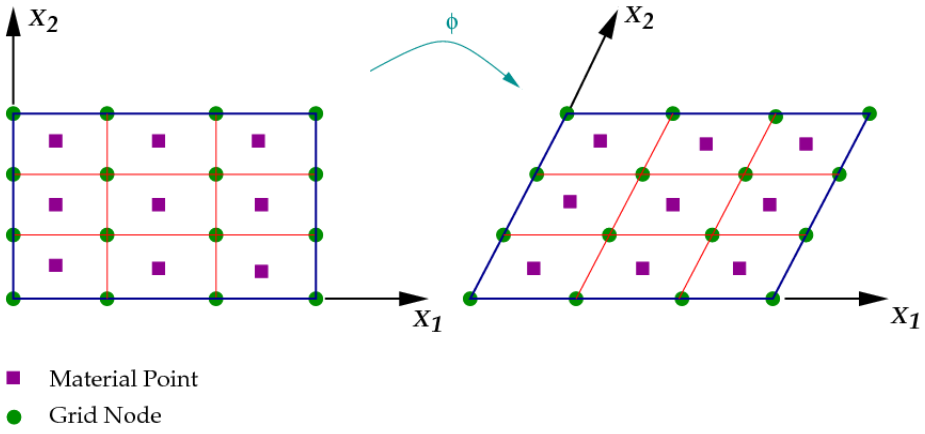

Figure 1.37: Lagrangian element description

1.5.2.2 Eulerian description

On the other hand, the Eulerian mesh is a background mesh. The body, constituted of its material points, flows through the mesh as it deforms. Whilst the nodes remain fixed in space, the material points are fixed on a virtual mesh that move through the background mesh, thus the position of the material points relative to the nodes varies in time. One node will not always contain the same material point throughout the simulation.

Material deformation can be described in two steps. First, the material is deformed in a way similar to the Lagrangian approach. Then, these virtually Lagrangian elements are advected back onto the fixed Eulerian mesh.

A representation of the Eulerian mesh is shown in Figure 1.38.

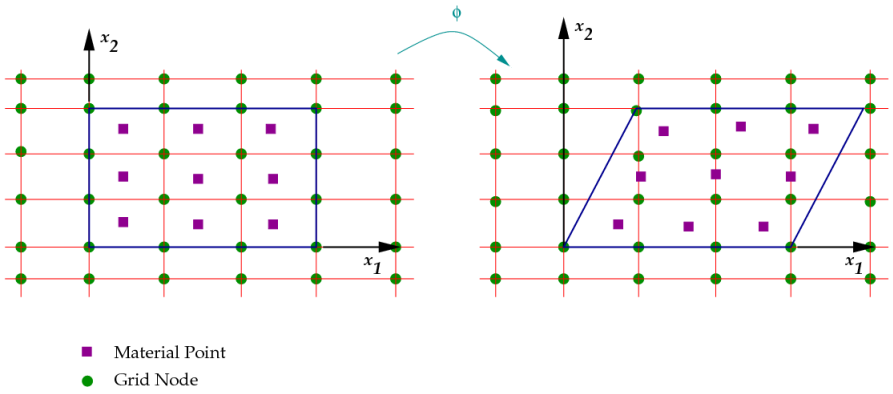

Figure 1.38: Eulerian element description

As the mesh is fixed in space, there is no mesh distortion. However, the domain that needs to be modeled is larger as the body must not leave the domain.

1.5.2.3 Arbitrary Lagrangian Eulerian description

When describing the ALE element formulation, two overlapping meshes have to be taken into account. One is a background reference mesh that can move freely in space. The other is a virtual mesh onto which the material points are attached. This virtual mesh flows through the background reference mesh.

The deformation can be visualized in two steps. First, the material is deformed in a Lagrangian step similarly to the Lagrangian formulation. Then, these virtual Lagrangian elements are advected onto the moving background reference mesh.

Hence, the Eulerian method is a subset of the ALE method where the reference mesh stays fixed in space, the main difference between these methods being the different amounts of material being advected through the meshes due to the reference mesh position.

For the resolution of fluid-structure interaction problems in this study, the ALE element formulation has been used as it is attractive for simulating blast events because excessive mesh deformations associated with Lagrangian formulations are avoided due to the advection re-mapping process. Furthermore, the ALE method is capable of handling multi-material formulations and tracking material interfaces more accurately than a purely Eulerian element formulation.

1.5.2.4 Smooth Particle Hydrodynamics (SPH)

The smooth particle hydrodynamics (SPH) method is often used for simulating mechanics of a continuum media such as fluid flows. It is a mesh free Lagrangian method evaluating spatial derivatives of flow properties such as density and velocity, which makes it suited to simulate problems dominated by complex boundary dynamics. The

SPH method works by dividing the fluid into a set of discrete moving elements, referred to as particles. Each particle serves as a mass point and interpolation point, therefore the properties of one particular particle are calculated based on the information from neighboring particles, which is known as kernel interpolation. This kernel also ensures the smoothing of the discrete values (density, pressure) of each element over a finite region to provide a smooth interpolated filed. An advantage of this method is that it guarantees conservation of mass without extra computation since the particles themselves represent mass.

In Impetus AFEA an improved SPH method, Gamma-SPH, is used. This new method aims at improving the SPH formulation by adding a stabilization term proportional to the pressure difference between two neighboring particles. An illustration of the effects of this stabilization term on the pressure generated by inside a water filled tank, simulated by Limido [58], is shown in Figure 1.39.

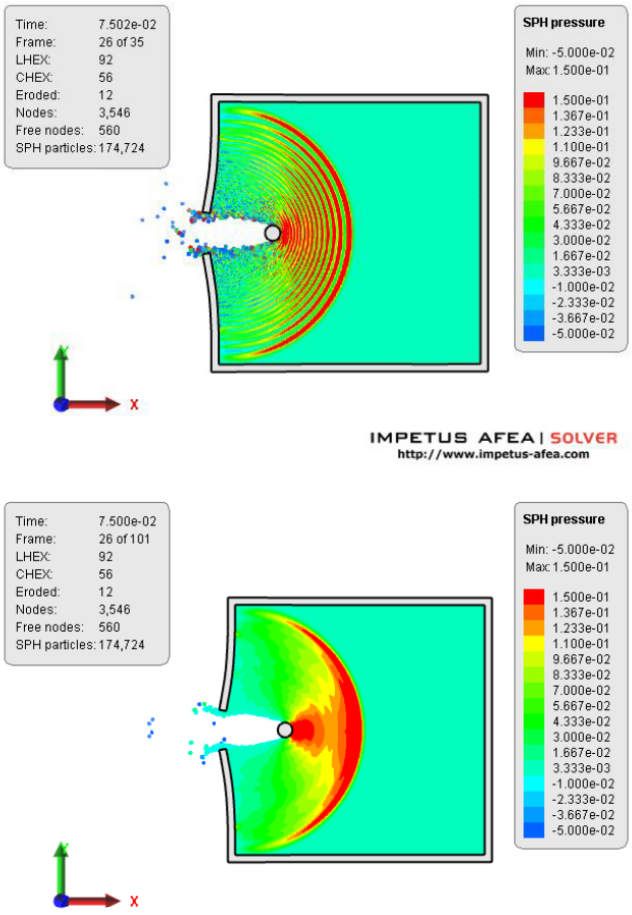

Figure 1.39: Pressure propagation in a fluid filled tank with (bottom) and without (top) the stabilization term used by the Gamma-SPH formulation in Impetus AFEA, as presented by Limido in [58]

1.5.3 Numerical simulation of fluid structure coupling

For the interaction between a structure and a fluid, different methods of simulating the fluid can be used, some of which are the previously presented Arbitrary Lagrangian Eulerian (ALE) element formulation or the meshless Smooth Particle Hydrodynamics method (SPH).

1.5.3.1 Arbitrary Lagrangian Eulerian (ALE)

Different numerical choices could be made to describe the fluid structure coupling using an ALE element formulation in a code such as LS-Dyna. Literature results can give an indication regarding the most accurate coupling solution. A study by Kozak [59] aimed at determining the effect of the fluid structure coupling end material formulation in LS-DYNA by comparing numerically obtained data to experimental data for a sloshing tank experiment, a water filled tank under harmonic excitation.

The experimental data for the sloshing tank used in this study were established by Faltinsen and Rognebakke [60].

This study investigates both fluid-structure coupling solutions and material formulations:

- ALE coupling: tank shares nodes with the fluid
- ALE coupling: tank is defined as constrained Lagrange in solid
- ALE formulation: multi-material (air is a separate material)
- ALE formulation: single-material (air is a void space)

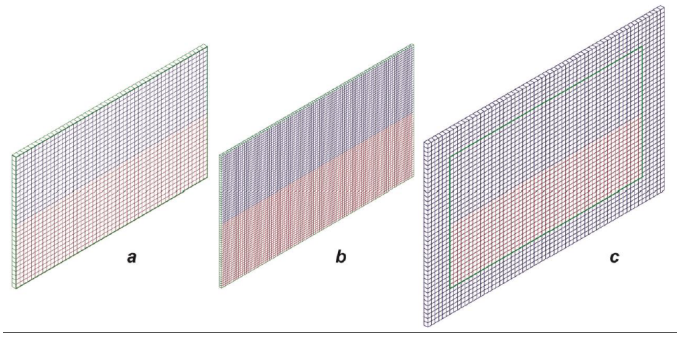

Figure 1.40: Finite element meshed used by Kozak [59] to investigate the fluid-structure coupling solutions available in LS-DYNA. In versions a and b the fluid shares nodes with tank, in version c the Lagrangian elements of the tank are constrained within the ALE domain

The study was divided into 4 investigations:

- Comparison between different fluid modelings when the tank shares nodes with the fluid (basic mesh and refined mesh) for an open tank.

- Comparison between different fluid modelings when the tank shares nodes with the fluid (basic mesh and refined mesh) for a closed tank, thus making the water waves interact with the roof of the tank.
- Comparison between different fluid structure coupling methods (tank shares nodes with fluid and tank defined as constrained Lagrange in solid). For a tank defined with Lagrangian elements, the tank was defined as rigid and elastic for comparison.
- Comparison between fluid modeling using ALE elements and using purely Lagrangian elements (with a higher and lower wave amplitude).

For the comparison of different fluid modelings, 3 different models were established.

- The first model used multi-material elements: elastic fluid material for water and NULL material and a linear polynomial EOS for air.
- The second model used single-material and void elements: NULL material and EOS Gruneisen for water, void material for air.
- The third model used multi-material elements: NULL material and EOS Gruneisen for water, NULL material and linear polynomial EOS for air.

The accuracy of a numerical simulation was determined by comparison of the sloshing frequency and the wave height with the experimental results.

For an open tank, the different fluid modelings has a negligible effect on accuracy of the simulation. However, with mesh refinement, the single material modeling provided a better correlation with experimental results as it obtained higher wave peaks.

When adding a roof to the tank, the single material modeling provided better results as the contact with the roof was modeled more accurately (reaching the roof, duration of the contact with the roof, depth of the troughs). When refining the mesh for this simulation, the single material solution performed slightly better when comparing the results to a simulation with the basic mesh.

When comparing the two fluid-structure coupling methods (shared nodes and Lagrange in solid), it appears that the choice of fluid-structure interaction modeling option has negligible effects on the results. When using either a rigid or elastic material definition for the Lagrangian tank, the effects on the accuracy of the numerical simulation appear to be negligible.

The last comparison was performed between different fluid modeling methods: water modeled with the ALE method and water modeled as a purely Lagrangian element. In the Lagrangian solution, the mesh must deform to simulate the sloshing wave, so the elements would become very much distorted with these large wave heights. Such large deformations cannot be accommodated by a Lagrangian fluid. Also, as the Lagrangian fluid separates

from the tank wall, it retains the shape of the tank rather than flowing into a natural fluid shape. The mesh smoothing formulated in the ALE solution steps allows the fluid material to move through the mesh, which keeps the mesh from distorting. With a lower wave amplitude generated by a higher frequency excitation, these distortions will be smaller. With this scenario, the Lagrangian fluid performed slightly better but its accuracy was still much lower than that of the ALE fluid.

1.5.3.2 Smooth Particle Hydrodynamics (SPH)

Another way of solving fluid-structure interaction problems is to use the SPH computational method. As the Gamma-SPH is relatively new, it was first tested in the classical case of a dam break and compared to experimental and numerical results from the literature. A three dimensional dam-break simulation with a rectangular column was set up by Silvester and Cleary [61], shown in Figure 1.41. Both the experimental results obtained with SPH in the work done by Silvester and Cleary and experimental results obtained by Yeh and Petroff [62] were compared to results obtained with a dam break simulation using Gamma-SPH.

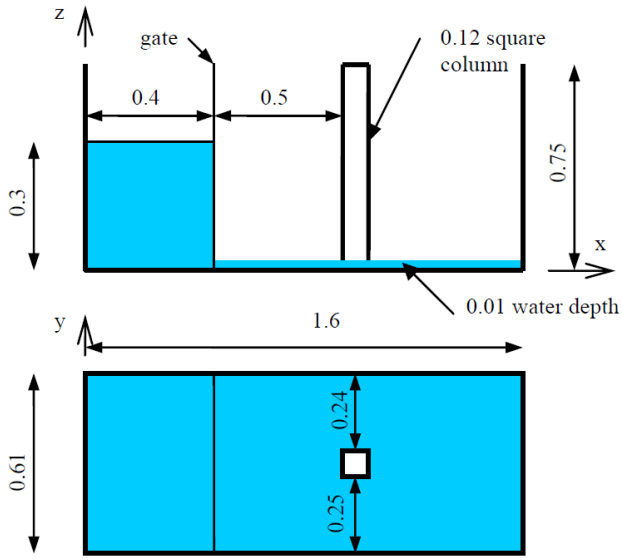

Figure 1.41: Geometry of the numerical model used in [61] and reproduced in Impetus AFEA using Gamma-SPH

Simulations were carried out in this work with Impetus AFEA for different SPH particle spacings. A distance of 2, 5 and 10 mm between two SPH particles was chosen, resulting in an SPH count of 9835440, 643008 and 79068 respectively. For the SPH particle spacing of 10 and 5 mm, 3 seconds of the phenomena were simulated for a calculation duration of 1h14 and 11h47. For the particle spacing of 2 mm, only one second of the phenomena was simulated which took 121h44 to complete. A comparison between numerical and experimental results from the literature and the results obtained from the numerical model in Impetus AFEA are shown in Figure 1.42. Whilst the net force acting on the column is adequately reproduced for a particle spacing of 2 and 5 mm in Impetus AFEA,

particle spacing of 10 mm produces an inaccurate high first force peak. Moreover, the time force signal appears to be perpetuated by more smaller force peaks of short duration. As these peaks do not correspond to a physical phenomenon, a smoothing function can be applied to the results obtained with Impetus AFEA, as shown in Figure 1.43. In that case, the measurement of the force acting on the net column simulated by Gamma-SPH accurately reproduced results from the literature, a particle spacing of 5 mm appeared to provide sufficient accuracy whilst keeping a reasonable simulation time. The cumulative impulse seen by the column is shown in Figure 1.44. It can be seen that in both numerical simulations (using SPH and Gamma-SPH), the cumulative impulse is overestimated when comparing to the experimental results. This can be explained by the fact that, numerically, the column is perfectly rigid and thus sees the entirety of the force being applied to it, which is not the case experimentally. Moreover, experimental measurements are made by a finite number of sensors along the column, thus minimizing the actual total force being applied to it. However, it has to be noted that whilst both codes overestimate the maximal impulse, results with Gamma-SPH with a spacing of 5 mm between particles seem to more accurately reproduce experimental results after 1.5 ms. Overall, it can be said that the Gamma-SPH element formulation has been successfully tested against a common test case, the damn break.

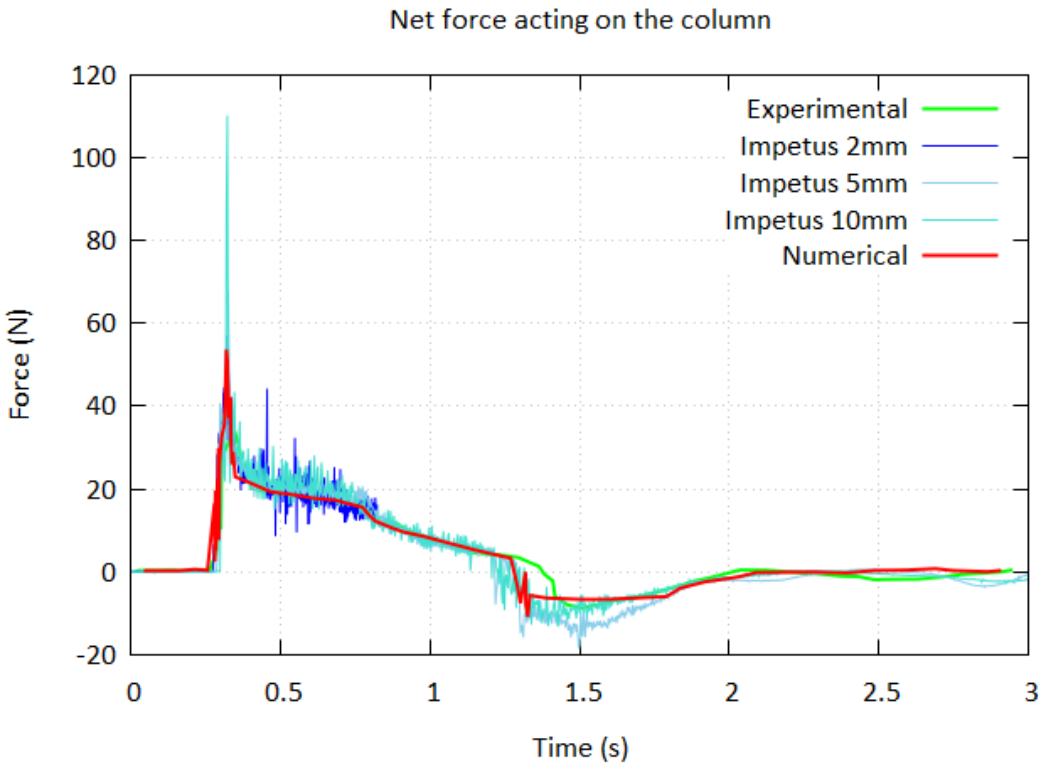

Figure 1.42: Net force acting on the column. Comparison between experimental results [62], numerical results using SPH [61] and numerical results using Gamma-SPH with different particle spacings

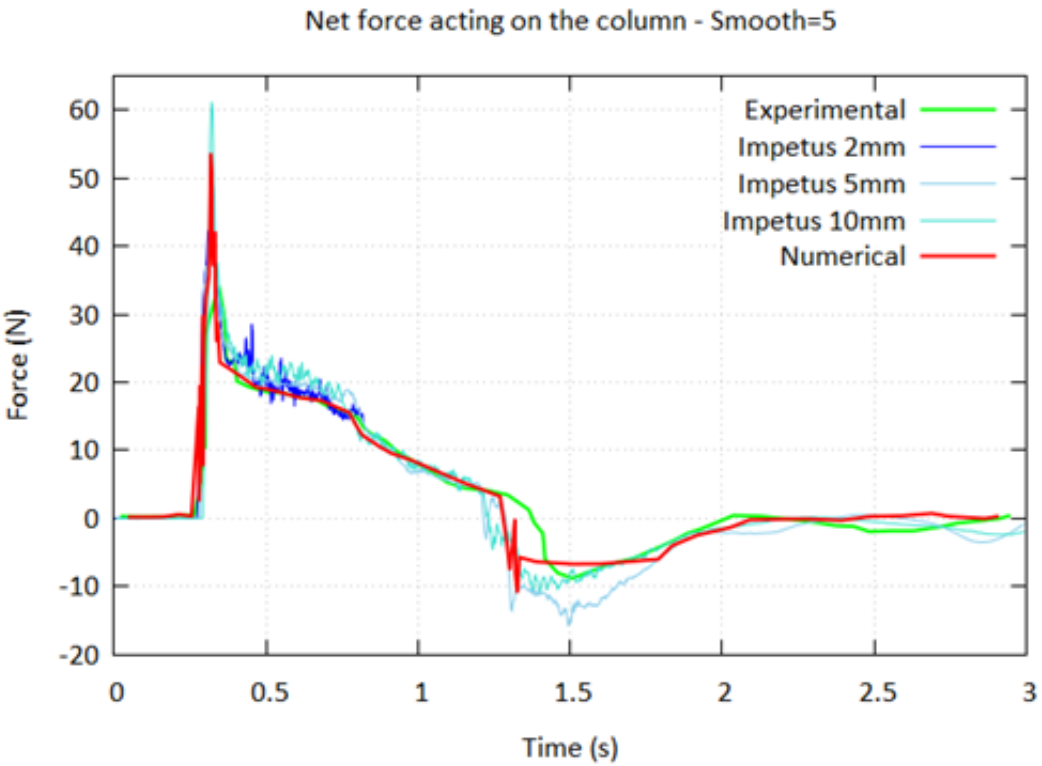

Figure 1.43: Net force acting on the column, smoothing function SMOOTH = 5 applied. Comparison between experimental results [62], numerical results using SPH [61] and numerical results using Gamma-SPH with different particle spacings

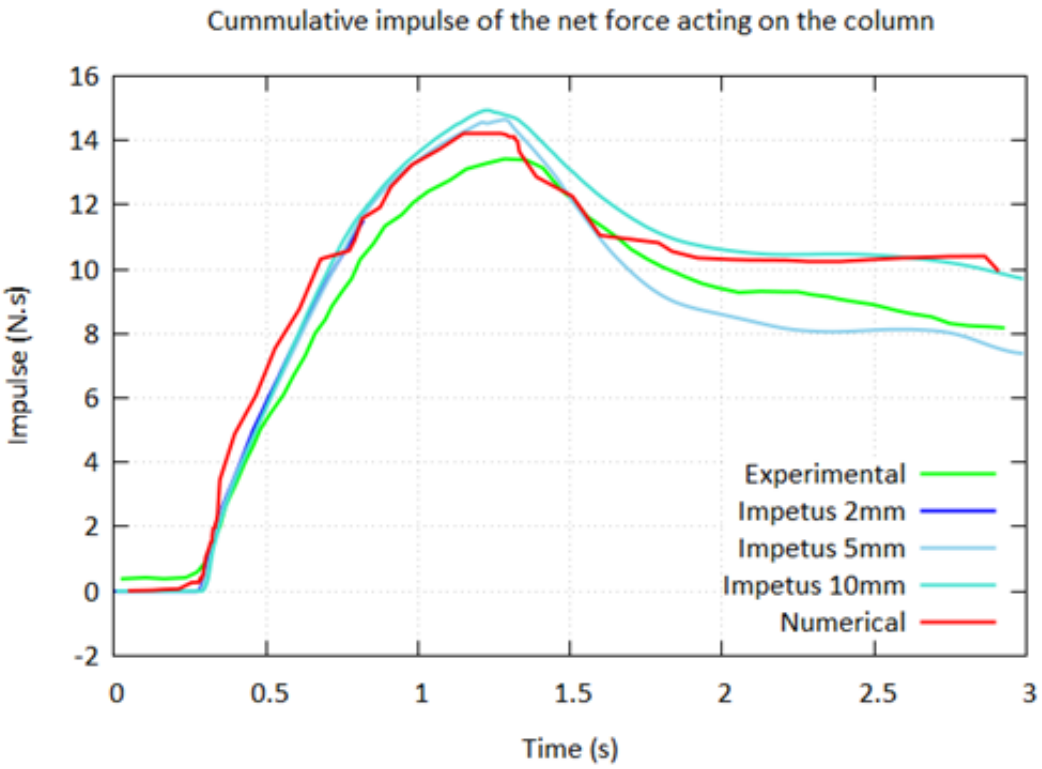

Figure 1.44: Cumulative impulse of the net force acting on the column. Comparison between experimental results [62], numerical results using SPH [61] and numerical results using Gamma-SPH with different particle spacings

In this Section, numerical methods for blast generation and different element formulations were presented. To make a choice regarding the blast generation, both the simulation of the ideal detonation and the simulation of corpuscles will be assessed in the next section, respectively with the commercial codes LS-DYNA and Impetus AFEA. It must be noted that, in the case of this work, data regarding the blast load generated by the experimental setup is numerous and available. Therefore, it becomes possible to apply the loading directly to the structure, which is also the method with the smallest computational cost and could be an alternative to the other blast generation methods. Both the ALE element formulation and the Gamma-SPH formulation were presented as possible solutions for the simulation of fluids. It was chosen to use the ALE element formulation as, at the beginning of this research work, the Gamma-SPH formulation was still relatively new. Its accuracy could be verified for a classical case such as a dam break but the simulation code LS-Dyna was a more established choice for the investigation of fluids under blast loading.

Chapter 2

Impulse spreading

This chapter presents an experimental and numerical investigation of the phenomenon of impulse spreading when a blast load is applied to a fluid with the goal of understanding the key parameters influencing impulse spreading. The experimental setup, comprising a vertical explosive driven shock tube and a fluid filled container, is presented, including the experimental difficulties that were encountered, and resolved, when first using this novel experimental setup. A numerical model of the setup is used to overcome the limitations of what is experimentally feasible and further investigate the levers acting on the parameters having an influence on impulse spreading.

Part of this chapter was submitted as a publication to the International Journal of Impact Engineering.

Contents

2.1 Experimental setup

2.1.1 Vertical explosive driven shock tube and fluid filled container

2.1.1.1 Geometry of the experimental setup

An experimental setup was designed to investigate the protecting capabilities of fluids under blast loading, in particular for the investigation of the phenomenon of impulse spreading.

A 200 by 200 mm wide and 50 mm (or 100 mm) deep cubic container, filled with water and open at the top, was made out of S235 steel. This container was installed underneath a 1750 mm long vertically placed explosive driven shock tube with an internal section of 80 by 80 mm, generating a reproducible planar blast wave, used to project a plate held into place at the lower extremity of the shock tube, into the fluid filled container as shown in Figure 2.1. This EDST has the same design geometry as the EDST presented in Section 1.4.1.5, but was placed vertically to allow the placement of an open fluid filled container. The plates projected into the water had a dimension of 100 by 100 mm (corresponding to a quarter of the free water surface of the container) and varying thicknesses of 1, 3 and 5 mm. The explosive charge used with the explosive driven shock tube during an experiment was of 15 or 30 g of C4 placed at a standoff distance of 50 mm from the entrance of the tube.

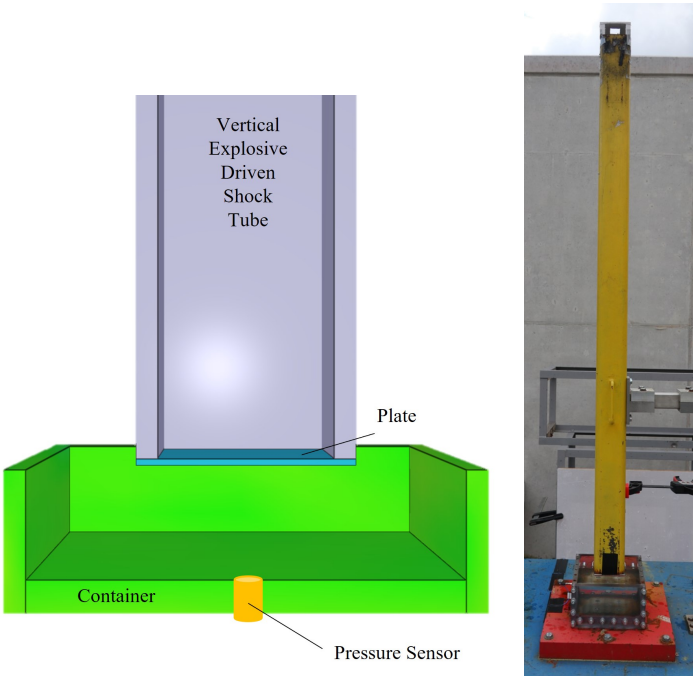

Figure 2.1: Experimental setup

This initial experimental setup was expanded to allow different levels of water confinement, where 0, 50 or 100% of the free water surface could be covered by a lid as shown in Figure 2.2.

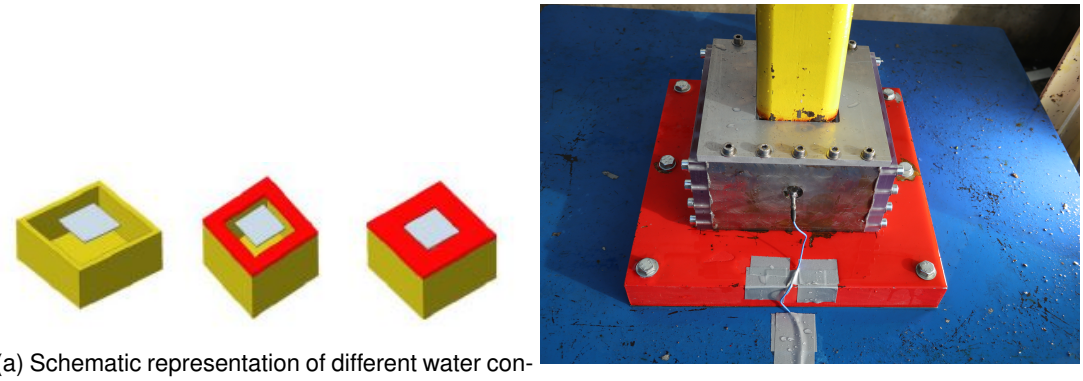

(a) Schematic representation of different water confinement levels. From left to right 0, 50 and 100%.

(b) Illustration of 100% water confinement.

Figure 2.2: Expansion of the experimental setup allowing the study of the influence of water confinement.

2.1.1.2 Measurement of the blast load transmitted to the container bottom

The blast wave generated by the EDST is transmitted to the fluid as a compression wave, which will transmit impulse to the bottom of the container. Measuring this impulse allows to quantify the protection capabilities granted by the presence of water.

Pressure transducers are used to make local measurements at different locations of the container, namely at the center of the bottom of the container (Figure 2.3a), at the center of the side wall of the container (Figure 2.3b) and at the top of the container when when a lid for 100 % confinement is used (Figure 2.3c). The data obtained from the pressure sensor located in the lid was not usable as the vibrations of the tube against the lid during an experiment lead to high perturbations of the signal. As such, the main sensor location used for the analysis of the efficiency of a water filled protective structure was the location at the center of the bottom of the container. As measurements are made in a fluid, the transducer has to be usable in such an environment. Therefore, a stainless steel PCB pressure sensor, model number S113B22, is used to avoid corrosion. The characteristics of the specific pressure transducer used for this study are given in Table 2.1. An exploder from Teledyne Reynolds is used to trigger the data acquisition of the camera, the flash and the pressure sensor simultaneously.

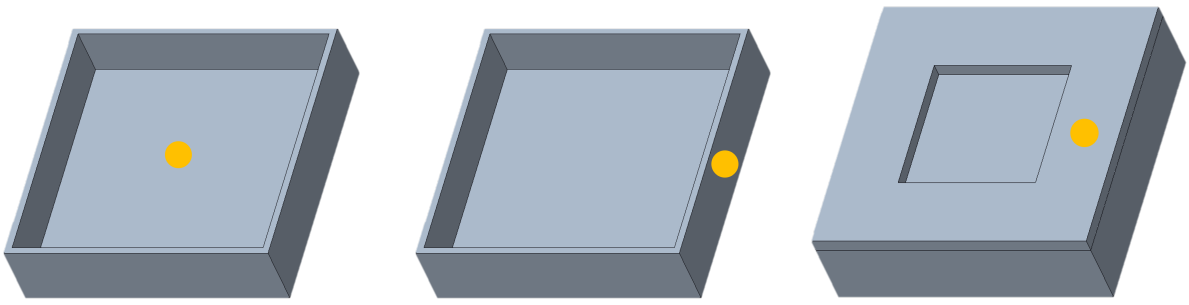

(a) Center of container bottom

(b) Center of container side wall

(c) Container top

Figure 2.3: Sensor locations for localized pressure measurements in the fluid filled container

Table 2.1: Characterisitc of the pressure transducer S113B22

Model Number	Serial Number	Voltage sensitivity		Bias voltage
S11B22	49581	0.9988 mV/PSI	144.9 mV/MPa	10.44 V

2.1.1.3 Visualization of the compression wave and the plate displacement

The visualization of the compression wave inside the fluid was done through a high speed imaging camera (Phantom V310). This was possible as two opposing walls of the container were made out of plexiglas panels. During a given experiment, two phenomena occur at different times. First, the blast wave generated by the explosive driven shock tube is transmitted to the fluid through the plate, generating a compression wave. Then, the plate is set into motion as a result of its interaction with the blast wave. Different lighting techniques were used to visualize both phenomena. The compression wave was shown thanks to a high LED intensity light source placed in alignment with the camera axis and the plate displacement was shown with a high intensity flash (Figure 2.4). The visualization of the path of the compression waves in the fluid could be further enhanced by treating the images with consecutive image subtraction, as shown in Figure 2.5. However, the correct visualization of both phenomena proved to be difficult due to a number of reasons:

- As the experiments were designed to be non destructive, the panel allowing visualization was made out of Plexiglas, which does not offer ideal optical conditions. The camera itself was protected by a further Plexiglas panel.
- During a given experiment, the Plexiglas panel in the container did undergo elastic deformation, creating light reflections.
- The experiment taking place outside, weather conditions could influence lighting.

During the time of this work, visualization techniques of the propagation of the compression wave in water have been greatly improved through the acquisition of new lights and cameras, so much so that processing the images for a more distinct visualization of the compression wave is no longer necessary in some cases (Figure 2.6).

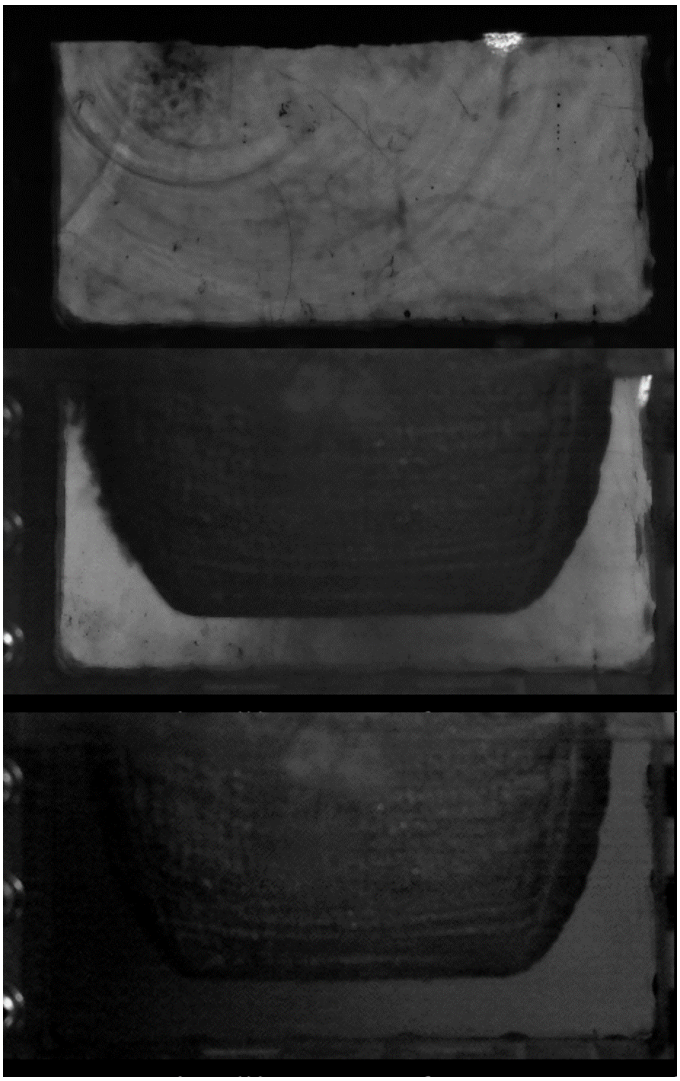

Figure 2.4: Illustration of different lighting techniques used during an experiment. From top to bottom: use of diode for the visualization of the path of the compression wave, with the diode the path of the plate appears dark, with a change of lighting to the flash, water is sufficiently lit and the path of the plate can be followed more clearly.

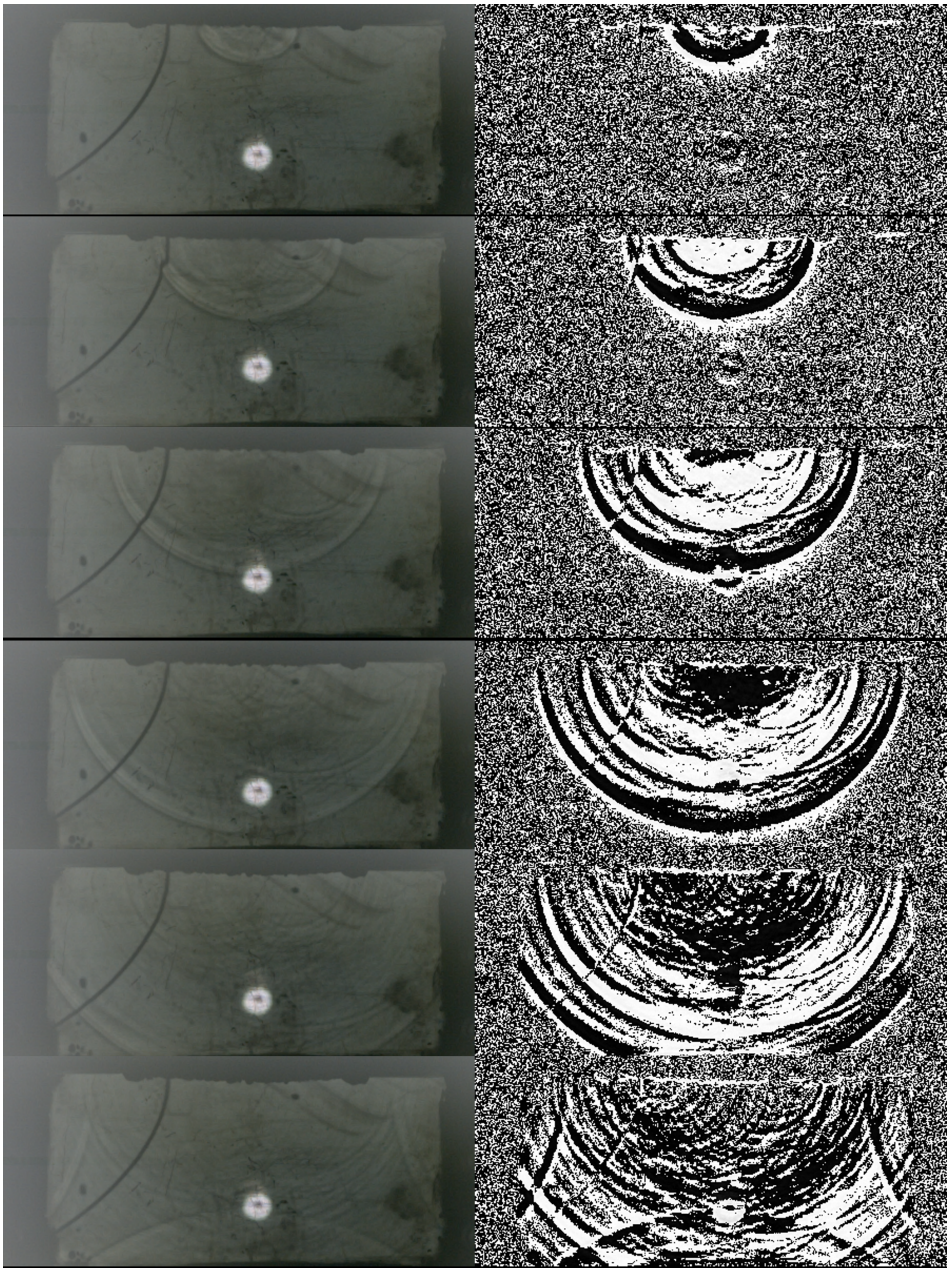

Figure 2.5: Experimental images of the path of the compression wave in the fluid for 15 g of C4, a plate thickness of 1.5 mm and a container depth of 100 mm. Unprocessed images (left) and images having undergone consecutive image subtraction to highlight the compression wave (right).

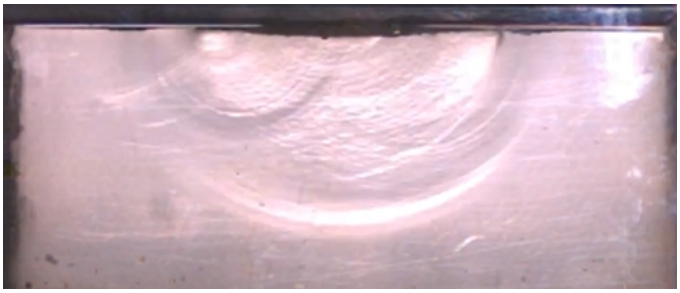

Figure 2.6: Improved visulatization of the compression wave in the fluid during an experiment

2.1.2 Reference values

2.1.2.1 Load applied to the plate

A reference value describing the load applied to the plate was experimentally acquired. This was done experimentally by placing the end of the explosive driven shock tube directly in contact with the pressure sensor, thus determining the pressure profile under perfect reflection conditions. During the projection, fluid structure interaction (FSI) as described in Section 1.3.1 occurs between the plate and the blast wave. Based on the literature [28, 25] and on the different values of the plate velocity observed, these can be safely neglected. Consequently, the signal applied on the plate is almost equivalent to the reference signal.

For a charge of 30 grams of C4, the experiment was repeated 6 times, the variance on the reproducibility being shown in Figure 2.7a. As such, in order to calculate the mean value, the pressure-time curves for the different experiments had to be adjusted in order for the peak overpressures to coincide (Figure 2.7b). By doing this transformation, the information of the arrival time of the peak overpressure was lost. However, the arrival time of a blast wave is directly linked to its peak overpressure so it could be retrieved from this information. Finally, the mean value of the pressure signal for a perfectly reflected blast wave at the end of the tube, which will be used as a reference value for future comparisons to other experimental setups, was obtained (Figure 2.8). The mean impulse signal was calculated in a similar fashion. The impulse signals with time adjustment are shown in Figure 2.9a and the resulting mean impulse signal for the perfectly reflected shock wave at the exit of the tube is shown in Figure 2.9b. This same methodology is to be applied to the calculation of all mean values from experimentally obtained signals.

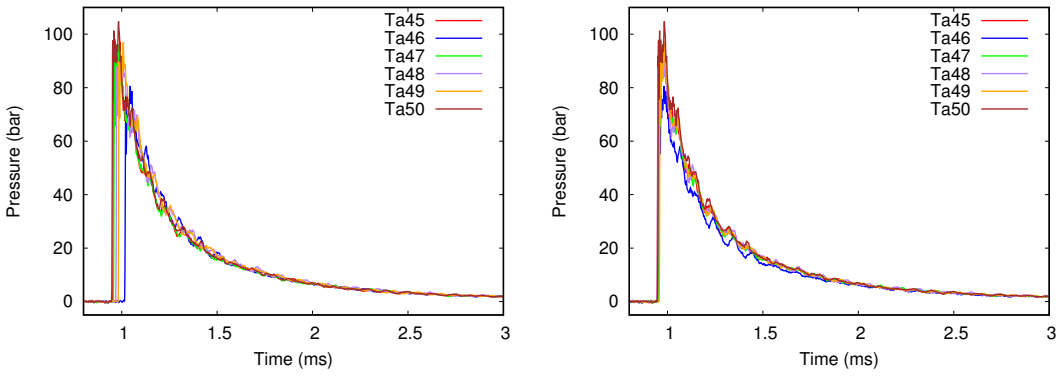

(a) Unedited signals

(b) Time adjusted signals

Figure 2.7: Pressure signal of the perfectly reflected blast wave, experiments 45 through 50. Charge of 30 g of C4

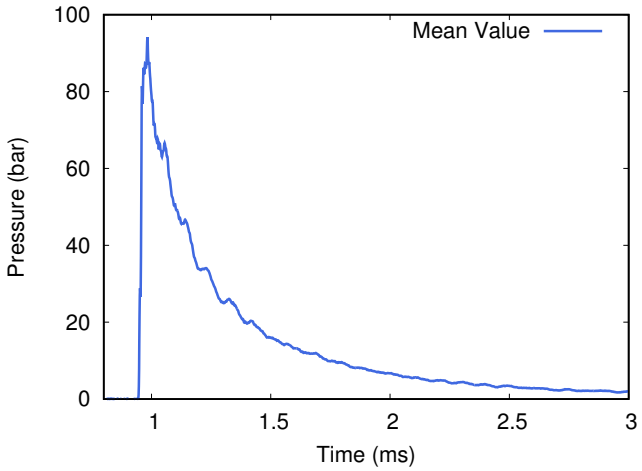

Figure 2.8: Calculated mean value of the pressure profile of the blast wave under perfect reflection conditions for a charge of 30 g of C4

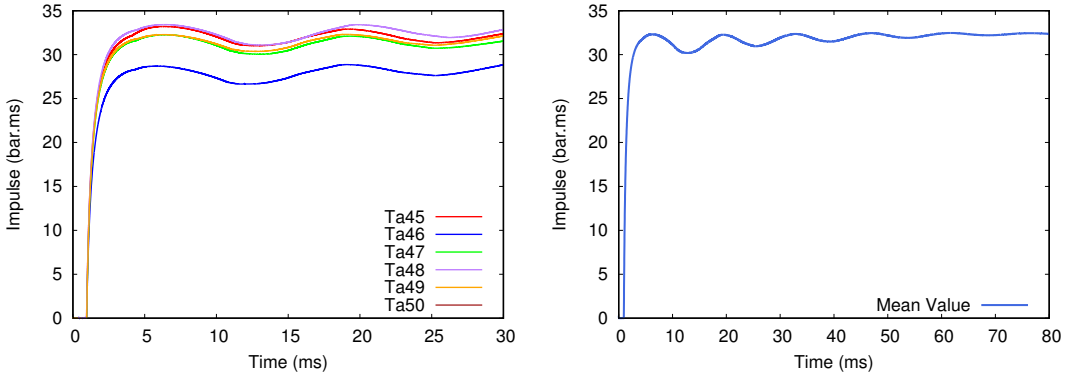

(a) Time adjusted signals

(b) Mean value

Figure 2.9: Impulse signal of the perfectly reflected blast wave. Charge of 30 g of C4

The reference pressure profiles for a charge mass of 15 and 30 grams are shown in Figure 2.10, with their corresponding maximal values stated in Table 2.2 with their relative standard deviation. The associated impulse-time curves result from the integration of the pressure signal over time, done directly through the acquisition system.

Table 2.2: Reference values for the blast wave at the exit of the tube for different charge masses

Charge mass (g)	Overpressure (bar)	Impulse (bar.ms)	Positive phase duration (ms)
15	42 $\pm 6.84\%$	18 $\pm 11.1\%$	2.81 $\pm 2.53\%$
30	87 $\pm 8.66\%$	32 $\pm 5.71\%$	4.6 $\pm 5.61\%$

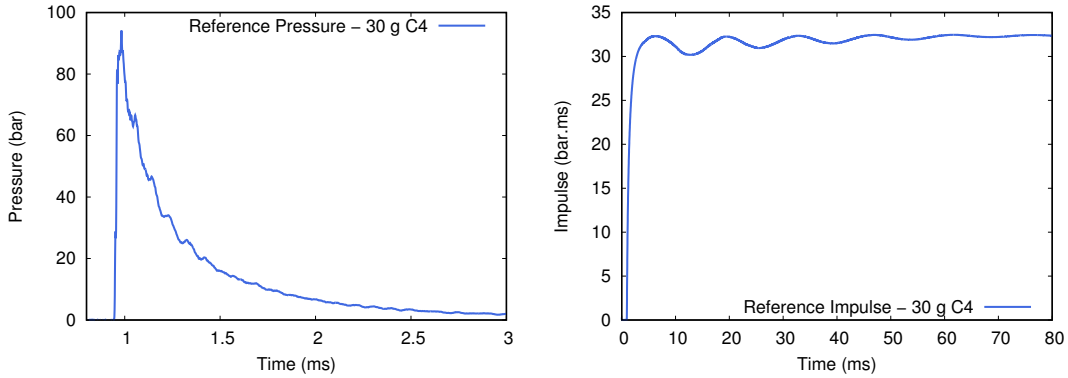

(a) Reference Pressure - 30 g C4

(b) Reference Impulse - 30 g C4

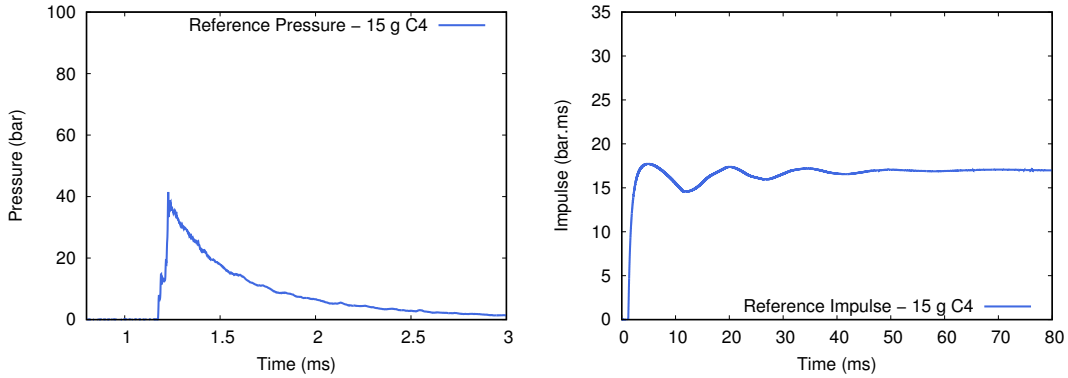

(c) Reference Pressure - 15 g C4

(d) Reference Impulse - 15 g C4

Figure 2.10: Blast loads applied to the plate by the explosive driven shock tube serving as reference values, 15 and 30 g of C4

2.1.2.2 Load transmitted to the bottom of the container

Local pressure measurements are made during the experiments, the main point of measurement being the center of the bottom of the container. A typical pressure signal obtained by the pressure sensor in water is given in Figure 2.11, in this case for 15 grams of C4, an unconfined water height of 50 mm and a plate thickness being projected into the fluid of 3 mm.

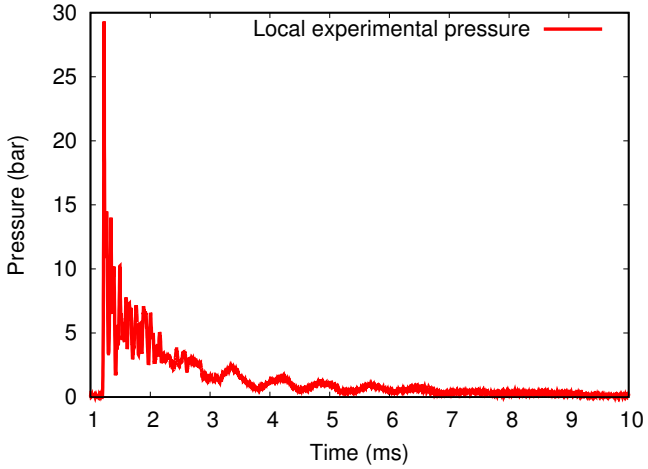

Figure 2.11: Local pressure signal at the center of the bottom of the container for a charge of 15 g of C4, a plate thickness of 3 mm and a water height of 50 mm for an unconfined fluid

2.1.2.3 Wave velocity

It is possible to correlate the pressure signal measured at the center of the container bottom with the images recorded by the high speed camera to determine the velocity of the wave in the water. For the pressure-time curve of experiment TA 66, three notable events could be correlated with the images taken by the high speed camera:

- first, the wave travels through the water filled container, as highlighted in Figure 2.13. This first wave was visible between 0.987 and 1.02 ms on the high speed camera images. On the pressure signal recorded by the sensor at the center of the container bottom, this time of arrival corresponds to the first overpressure peak (Figure 2.12). Knowing the depth of the water (50 mm) and the time of arrival of the wave thanks to the pressure signal and the high speed camera images, the wave velocity can be calculated as $v = \frac{d}{t_0 - t_1}$ with t_0 being the time at which the wave is initiated in the water filled container and t_1 the time at which it reaches the bottom of the container. In the case of experiment Ta66, a wave velocity of $1538 m/s$ can be calculated, which is very close to the speed of sound in water of $1500 m/s$. The difference in these two values can be explained by the fact that the accuracy of the calculation depends on the frame rate of the camera (here 110000 images per second);
- then, a reflection from the bottom of the container back onto the plate of this wave is visible on the high speed camera (Figure 2.14);
- finally, the wave is reflected off of the plate once again after this round trip through the container (Figure 2.15). After some time, the reflections of the wave between container bottom and plate as well as on the sides of the container do not allow to follow the path of the wave further.

When analyzing the pressure profile shown in Figure 2.12, the arrival time of the peaks subsequent to the first pressure peak can be calculated knowing the distance and speed of the wave in water. The arrival times of the

analytically determined pressure peaks are shown in Figure 2.12 by the blue vertical lines. It can be seen that there is a good agreement between the analytically predicted arrival times and the experimentally measures arrival time, comforting the fact that the peaks are due to the round trips of the wave in the between plate and container bottom.

However, several other peaks shown in red are located in between two blue peaks predicted by the round trip of the first incident pressure peak. It is notable that these peaks are at a time distance corresponding to a round trip from the bottom of the container and back. It is assumed that these peaks are due to other reflections of the wave in the container.

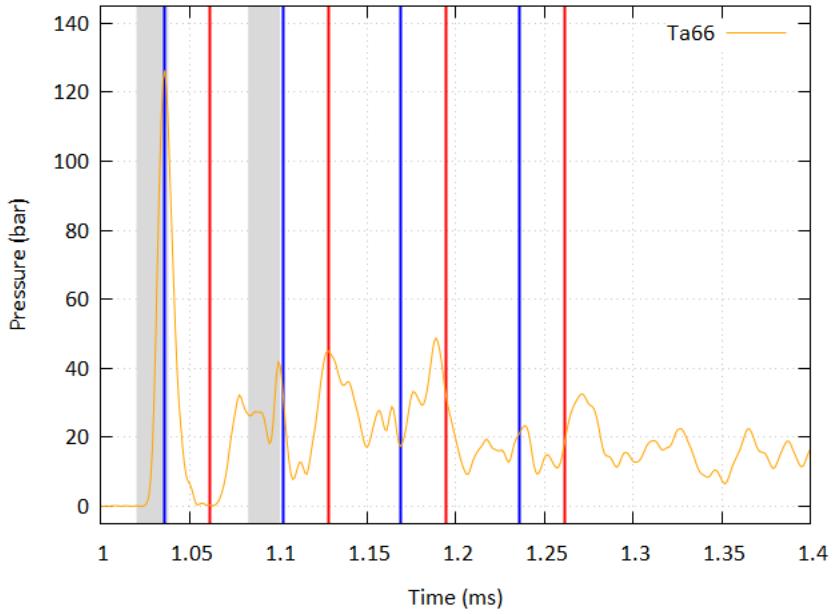

Figure 2.12: Analysis of experiment TA66, grey zones corresponding to the high speed imaging correlation, blue and red lines corresponding to the analytically predicted arrival time of overpressure peaks

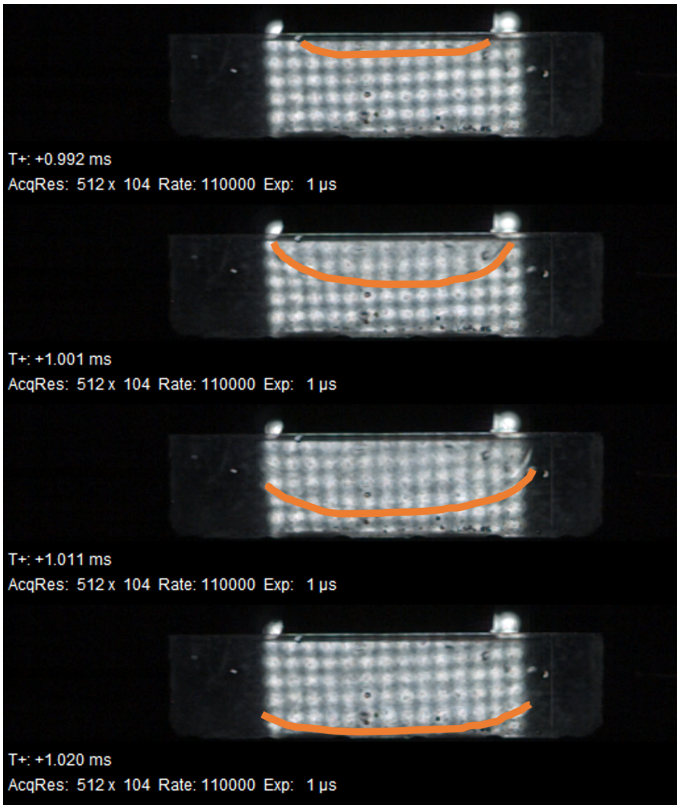

Figure 2.13: High speed camera images for experiment TA 66, first incident wave

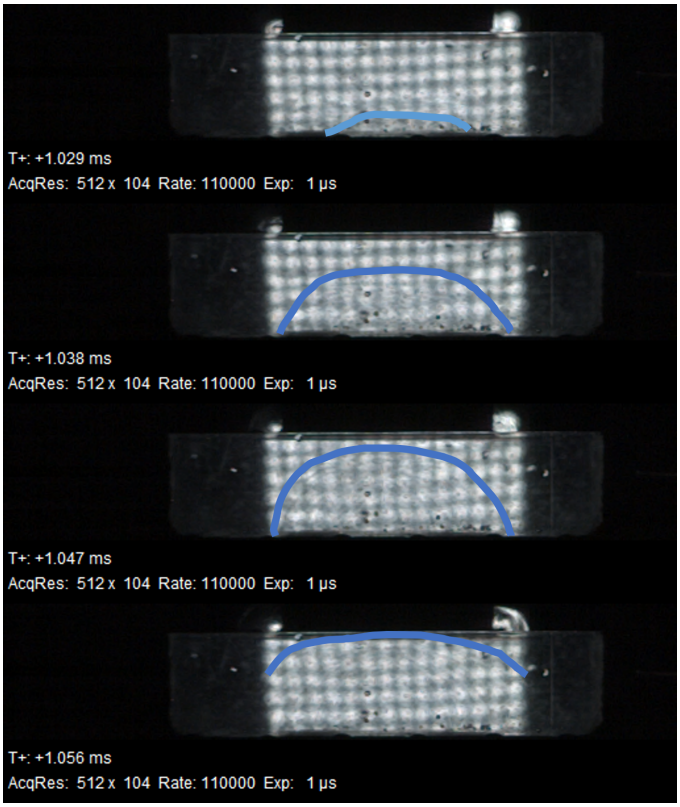

Figure 2.14: High speed camera images for experiment TA 66, reflection of the first incident wave on the container bottom

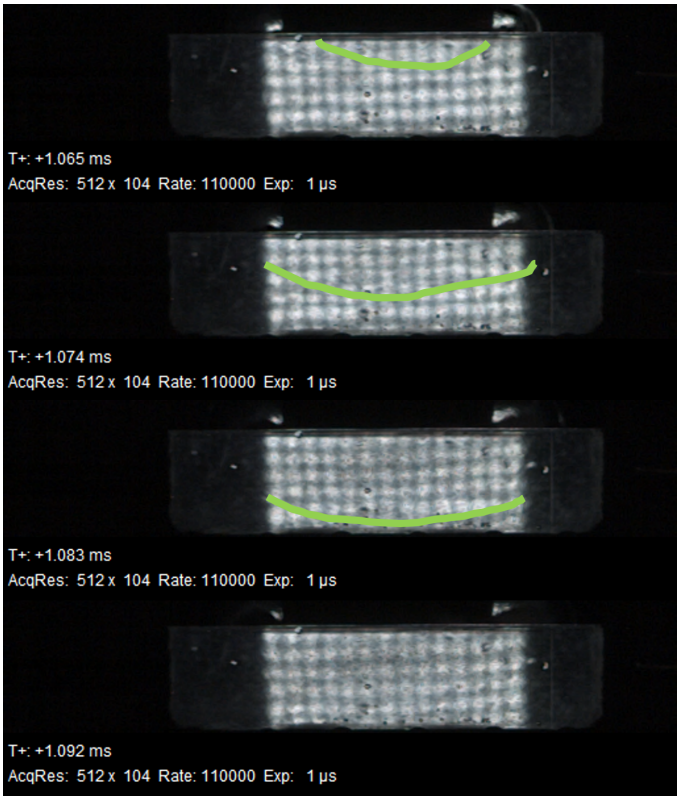

Figure 2.15: High speed camera images for experiment TA 66, reflection of the first incident wave on the plate after one round trip in the container

2.1.3 Experimental difficulties

2.1.3.1 Explosive charge placement

Experimental difficulties were encountered to determine the maximal overpressure and impulse for the reflected shock wave at the end of the tube, used as a reference value. As an explosive driven shock tube of the same geometry had previously been used at ISL, the reflected blast load measurement when rotating the tube by 90 degrees for a vertical placement were expected to be similar. However, initially a significant discrepancy was observed, the maximal overpressure being higher for the vertically placed tube. It was found that this was due to the positioning of the charge.

Detonator placement For the horizontally placed tube, detonator and tube axis were perpendicular (Figure 2.16). The detonator is placed to ensure minimal movement due to the weight of the cable for example, which is especially important for charges with a small diameter as is the case for spheres of 15 or 30 g of C4. The same placement method (detonator perpendicular to the ground) was used for the vertically placed EDST, resulting in the detonator and tube axis being parallel to each other (Figure 2.17a). For a detonator axis placed in the same manner as for the horizontal tube, the placement should be made as shown in Figure 2.17b. The reflected blast wave was measured for both positions of the detonator for the vertical EDST (Figure 2.18) with 5 repetitions of each experiment with a charge of 15 g of C4. Comparing the mean value calculated from these experiments (Figure 2.19), it was found that the different placements mostly had an influence of the repeatability of the experiment, a much higher dispersion in the value of the overpressure peak occurring for the detonator and tube axis with parallel placement. Therefore, detonator and tube axis will be placed perpendicular to each other in the experiments of this study.

Figure 2.16: Placement of the detonator for the horizontal EDST. Detonator and tube axis perpendicular

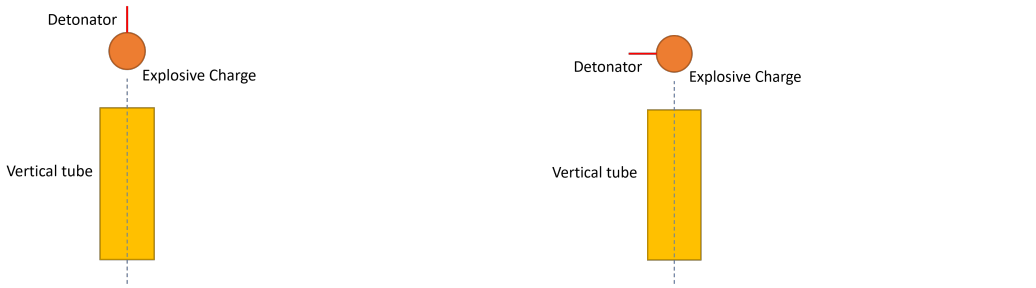

(a) Detonator and tube axis parallel (b) Detonator and tube axis perpendicular

Figure 2.17: Placement of the detonator for the vertical EDST

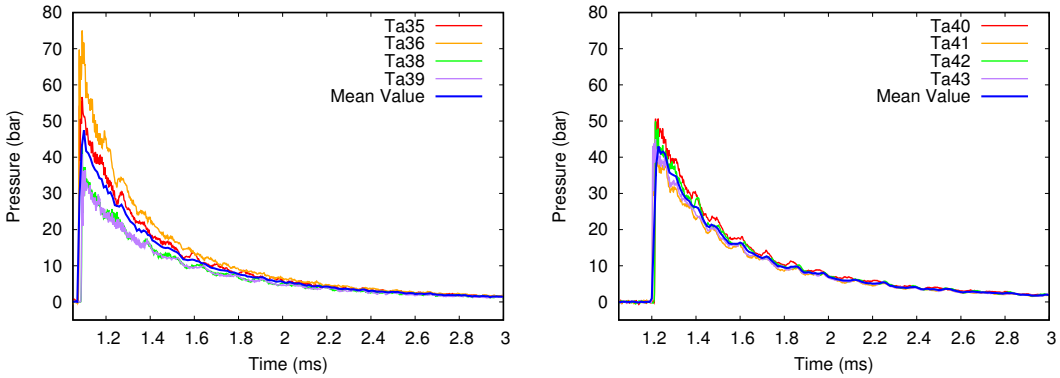

(a) Detonator and tube axis parallel (b) Detonator and tube axis perpendicular

Figure 2.18: Overpressure values of the reflected blast wave for different detonator positions. Charge of 15 g of C4

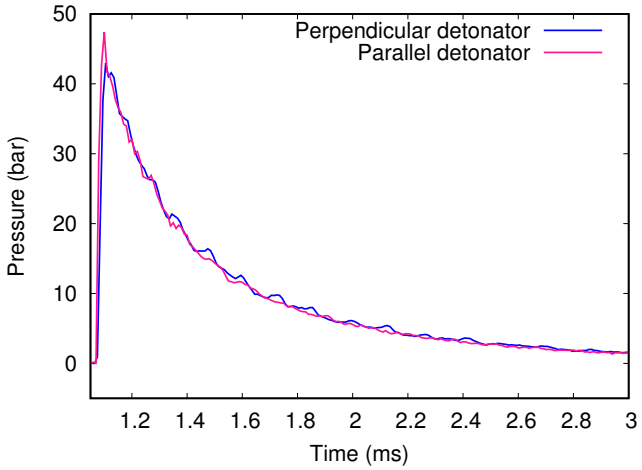

Figure 2.19: Comparison of the mean overpressure values for different detonator positions. Charge of 15 g of C4

Charge placement On the horizontal tube setup, the explosive sphere is placed inside a carved polystyrene bloc as shown in Figure 2.20. However, for the vertical tube, the explosive sphere is placed inside a carved polystyrene table as shown in Figure 2.21, thus changing the contact surface between the polystyrene and explosive charge which could hinder the propagation of the blast wave at the start of the phenomena and thus reduce the measured peak overpressure at the exit of the tube.

Figure 2.20: Positioning of the charge for the horizontal tube

It was found that by increasing the surface area in contact with the charge, the peak overpressure was lowered (2.22). In order to minimize the influence of the charge placement on the energy released during the detonation, the charge positioning with a polystyrene table was chosen.

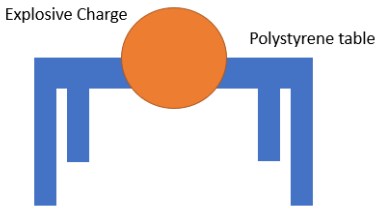

Figure 2.21: Positioning of the charge for the vertical tube

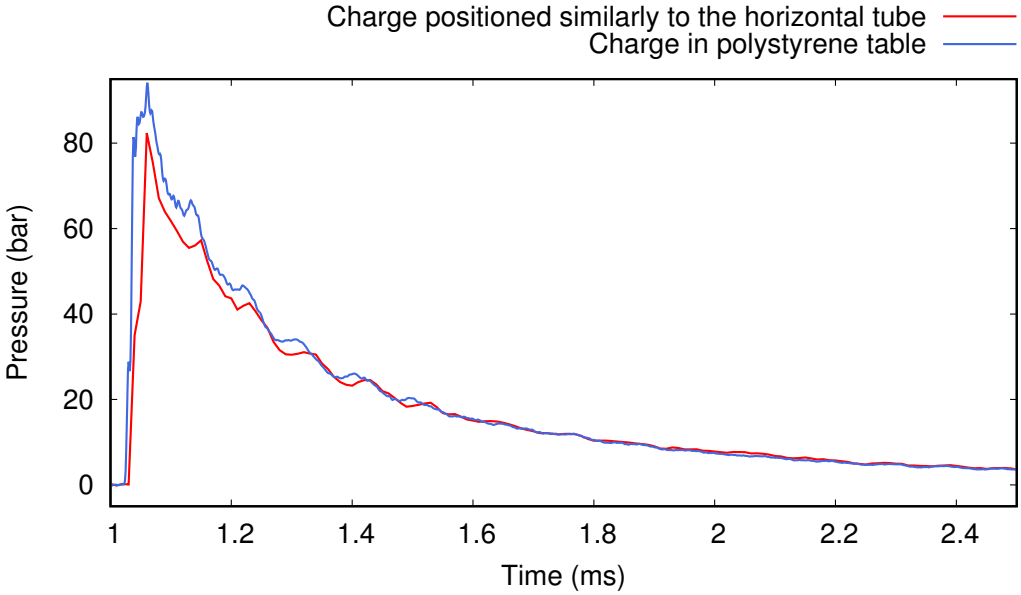

Figure 2.22: Influence of the positioning of the charge

2.1.3.2 Plate placement

A difficulty of the experimental setup was the positioning of the plate at the lower end of the shock tube. If the plate was positioned with a slight angle, the compression wave did not originate at the center of the container, thus arriving differently on the pressure sensor and causing different reflections on the container walls (Figure 2.23). Moreover, it was found that in the case of an inclined plate placement, not one but several compression waves can be initiated in the water, thus leading to not one but several first overpressure peaks being measured at the center of the container, as is the case with the signal shown in Figure 2.24.

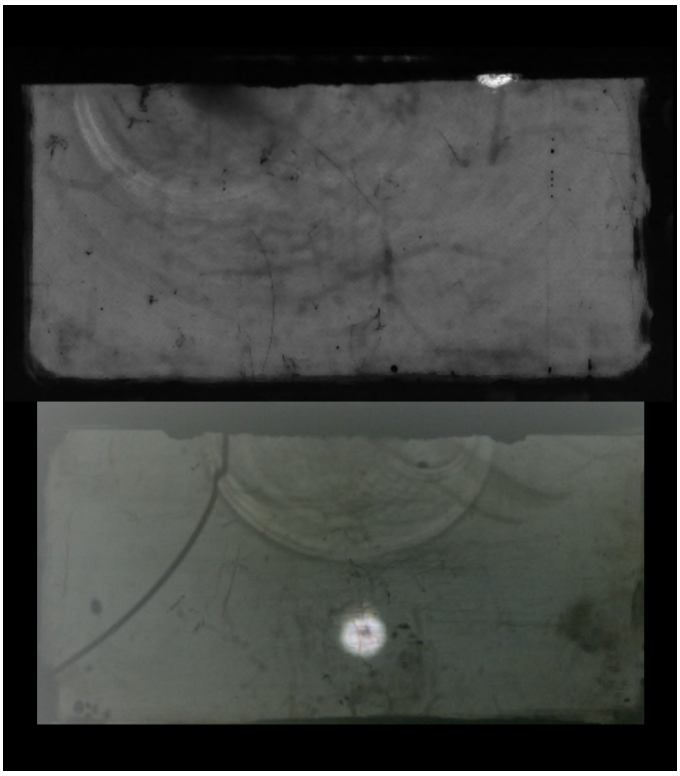

Figure 2.23: Images of a plate placed with a slight angle (top) and a plate placed horizontally (bottom). In the top image the origin of propagation of the compression wave is not centered.

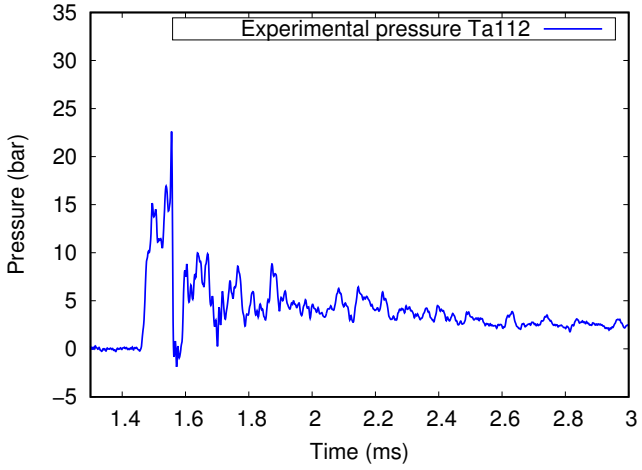

Figure 2.24: Two initial peaks created by the arrival of two compression waves due to an inclined placement of the plate

The numerical model described in Section 2.2 was used to better evaluate the significance of a skewed plate placement on the pressure signal measured locally at the center of the bottom of the container (Figure 2.25). Figure 2.26 shows that for an inclined plate placement, the compression wave does not arrive centered at the bottom of the container, which corresponds to the location of the pressure sensor for experimental measurements.

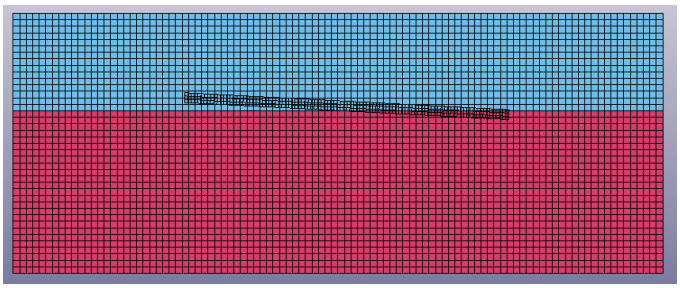

Figure 2.25: Numerical model of a skewed plate placement

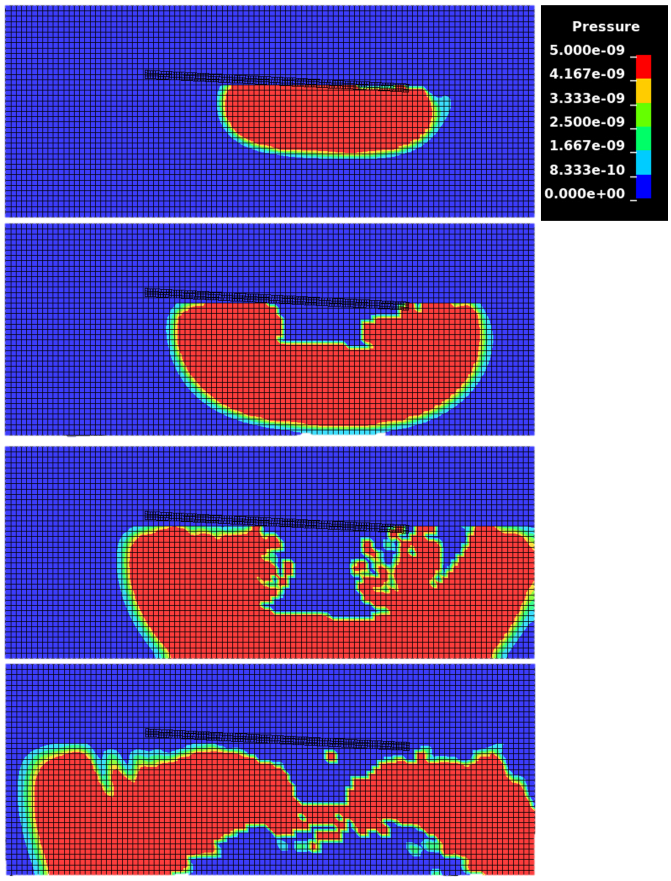

Figure 2.26: Numerical model of a skewed plate placement, propagation of the compression wave not centered, here for 15 g of C4, 3 mm plate and a 50 mm unconfined water depth

The results gained from this imperfection are however of interest, as in practical application, a perfect planar blast wave is unthinkable. Moreover, the quantity of interest being impulse for this work, using the integral of the pressure-time signal allows to smooth out these imperfections of the pressure signal for this experimental difficulty.

2.1.4 Performed experiments

Overall, 168 experiments were performed with the vertical explosive driven shock tube. As this is a novel experimental setup, a definite experimental matrix is hard to determine as a number of experiments also aided the better understanding of tools such as the camera and the lighting. Overall, experiments were performed for:

- the establishment of reference values: 19 experiments
- the variation of the plate velocity: 34 experiments
- the variation of the water height (use of a deeper container): 21 experiments
- the variation of the fluid confinement: 55 experiments
- the calibration of the experimental methodology: 39 experiments

The results of all these experiments will be given in the next Sections.

2.2 Numerical model

The experimental setup described in the previous section makes use of pressure sensors inside the fluid filled container to make local measurements. This can be limiting when a broader understanding of the pressure distribution in the entirety of the container is needed. Therefore, the experimental setup was reproduced numerically.

2.2.1 Modeling of the blast wave in the explosive driven shock tube

In in literature review, different approaches to blast generation were mentioned. Therefore, the next section will present a comparison between the numerical model of the explosive driven shock tube used in this work for both the simulation of an ideal detonation with LS-Dyna and the simulation of corpuscles with Impetus AFEA. A comparison between the reflected and free field pressure and impulse for both codes to experimental results was made.

2.2.1.1 Modeling of the tube

For both codes, the tube was described by Lagrangian elements with a size of 10 mm. As the deformation of the tube was not of interest in this study, the tube was defined as rigid with the density of steel $\rho_{steel} = 7850kg/m^3$.

2.2.1.2 Modeling of air

In LS-DYNA, air was modeled using the *Ideal Gas* equation of state, where the pressure in the ideal gas is defined as shown in Equation 2.1, where C_p and C_v are the specific heat capacities at constant pressure and constant volume respectively. The parameter for air are given in Table 2.3. The element size was taken as 2 mm for this first set of simulations.

$$P = \rho(C_p - C_v)T \tag{2.1}$$

Table 2.3: Material parameters used in the ideal gas equation of state for air

Material	$C_v(J/Kg.K)$	$C_p(J/Kg.K)$	T(K)	$\rho\ (kg/m^3)$
Air	718	1005	300	1.204

In Impetus AFEA, air was modeled by defining an air domain, which is an option directly provided by the code software. This air domain is then filled by corpuscles following Newtonian physics, described in Section 1.5.1.

2.2.1.3 Modeling of the explosive charge

In LS-Dyna, the ALE element formulation was used for the explosive charge. The John-Wilkins Lee equation of state, presented in Section 1.5.1 was used for C4. For this study, the parameters for C4 were set accordingly to the

Table 2.4: JWL parameters for C4

A (Pa)	B (Pa)	R_1	R_2	ω	e_0 (Pa)
6.10e+11	1.30e+10	4.5	1.4	0.25	9.00e+9

work of Dobratz [63] as detailed in Table 2.4.

In Impetus AFEA, the explosive charge is simulated with corpuscles. The Chapman-Jouget parameters of C4, defined internally by Impetus AFEA, are used to initiate the particle velocity.

2.2.1.4 Geometry of the numerical model

Figure 2.27 shows the geometry of the numerical model of the tube. For the model both in LS-Dyna and Impetus AFEA, symmetries are taken advantage of to reduce the size of the domain that has to be simulated and thus the simulation time. Therefore, only a quarter of the air domain is simulated and boundary conditions are applied to represent the symmetry planes (in this case the XZ and XY planes). Non reflecting boundary conditions were applied to the air domain in LS-Dyna to simulate an infinite air domain.

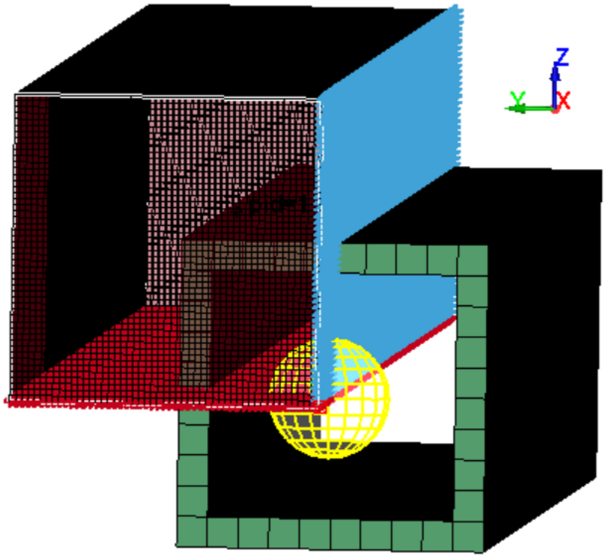

(a) LS-DYNA: in green the tube, in red the air domain defined using the ALE element formulation, in yellow the geometry defined for the explosive charge in the air domain, nodes highlighted in blue and red define the symmetries to simulate a quarter model

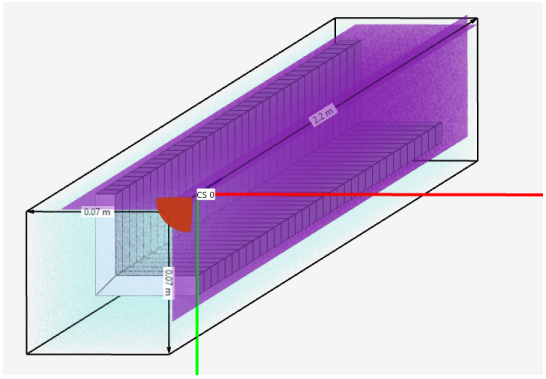

(b) Impetus AFEA: in grey the tube, the black box defines the air domain in which air (blue) and explosive (red) particles defined by corpuscles are located, in purple the symmetries for the simulation of a quarter model

Figure 2.27: Geometry of the numerical simulation of the vertical explosive driven shock tube

This numerical model was used to compare the generation of a blast wave through the simulation of an ideal detonation process with LS-Dyna and through the use of corpuscles in Impetus AFEA. In particular, two cases were simulated:

- the simulation of a reflected blast wave, presented as the reference values for this work (Section 2.1.2). In this case, the end of the tube was closed by a rigid plate in Impetus AFEA and by a boundary condition in the form of the *Rigidwall* command in LS-DYNA.
- the simulation of the blast wave in free field at the exit of the tube. The experimental data in this case was obtained for the tube of the same geometry by Blanc [25] with a pressure sensor mounted on a pen.

Numerically, the pressure was measured by a sensor placed at the center of the exit of the tube. However, as the blast wave generated in the tube is planar, a uniform pressure distribution is assumed for the entire section at the exit of the tube.

2.2.1.5 Comparison between numerical and experimental results for free field and reflected blast

Comparisons were made between experimental and numerical results for the free field and reflected experiments for a charge of 50 grams of C4. Figure 2.28 shows the pressure-time curve for the reflected blast wave at the exit of the explosive driven shock tube. In Figure 2.28a, it can be seen that the peak overpressure obtained with Impetus AFEA is significantly higher than the experimental value. On the contrary, the overpressure and impulse obtained with LS-DYNA seems to be in good agreement with the experimental value. This is due to the fact that, in Impetus AFEA, a particle deactivation time has to be set to remove the corpuscles from the calculation at a user defined time. Otherwise, the energy provided by the explosive charge simulated using corpuscles is too high. Figure 2.28 shows the comparison between the experimental and numerical results when such a particle deactivation time is set in Impetus AFEA. As the peak overpressure has been adjusted by the user, the value obtained with Impetus AFEA is very close to the experimental value (see Table 2.5 for the values). However, the effect of the time adjustment on impulse also has to be considered. When a deactivation time is defined, the discrepancy between the experimental and numerical value obtained with Impetus AFEA drastically increases.

-	Peak Overpressure (bar)	Time of arrival (ms)	Impulse (bar.ms)
Experimental	131	0.84	40
Numerical LS-DYNA	123 (6%)	0.89 (6%)	43.06 (10%)
Numerical IMPETUS Afea no particle deactivation	222 (70%)	0.66 (22.7%)	45.23 (15.5%)
Numerical IMPETUS Afea with particle deactivation	129 (1%)	0.74 (12%)	25.22 (36%)

Table 2.5: Peak overpressure and impulse value comparison for the reflection experiment

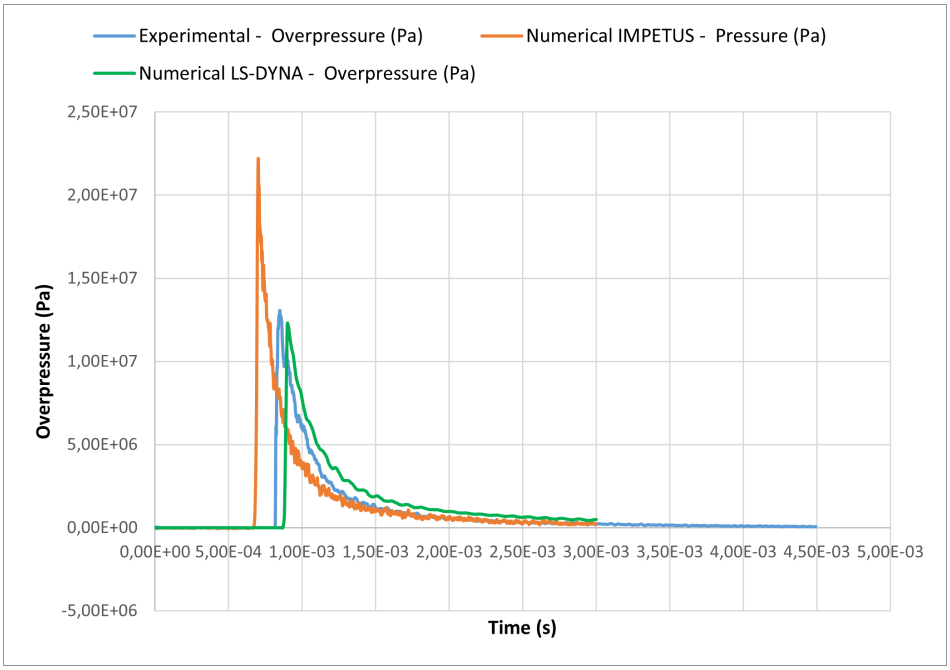

(a) No deactivation time set for the corpuscles in Impetus AFEA

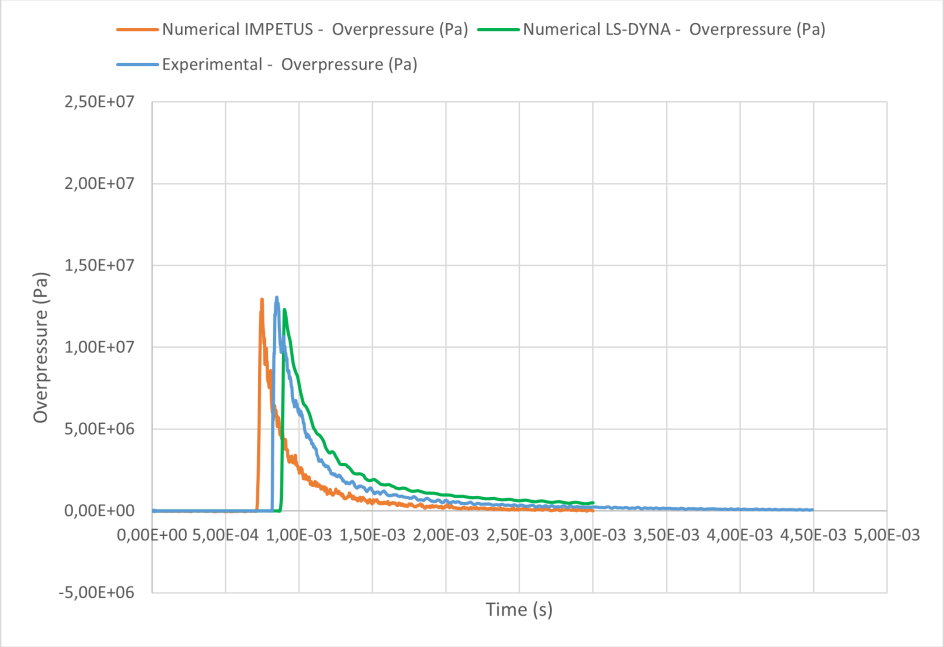

(b) Deactivation time set for the corpuscles in Impetus AFEA using the knowledge from the experimental results

Figure 2.28: Comparison between numerical and experimental results for the reflected blast wave at the exit of the explosive driven shock tube

For the free field experiments, the comparison between numerical and experimental results is shown in Figure 2.29. The particle deactivation time is defined for Impetus AFEA to match the experimentally obtained overpressure peak. However, the effect on impulse can again be observed, a high discrepancy between numerical and experimental values being present. On the other hand, numerical values obtained with LS-DYNA are again in good

-	Peak Overpressure (bar)	Time of arrival (ms)	Impulse (bar.ms)
Experimental	22	0.84	7.15
Numerical LS-DYNA	20.7 (7%)	0.86 (1%)	7.35 (3%)
Numerical IMPETUS Afea	21 (5%)	0.73 (17%)	5.33 (25%)

Table 2.6: Peak over pressure and impulse value comparison for the free field experiment

agreement with experimental data.

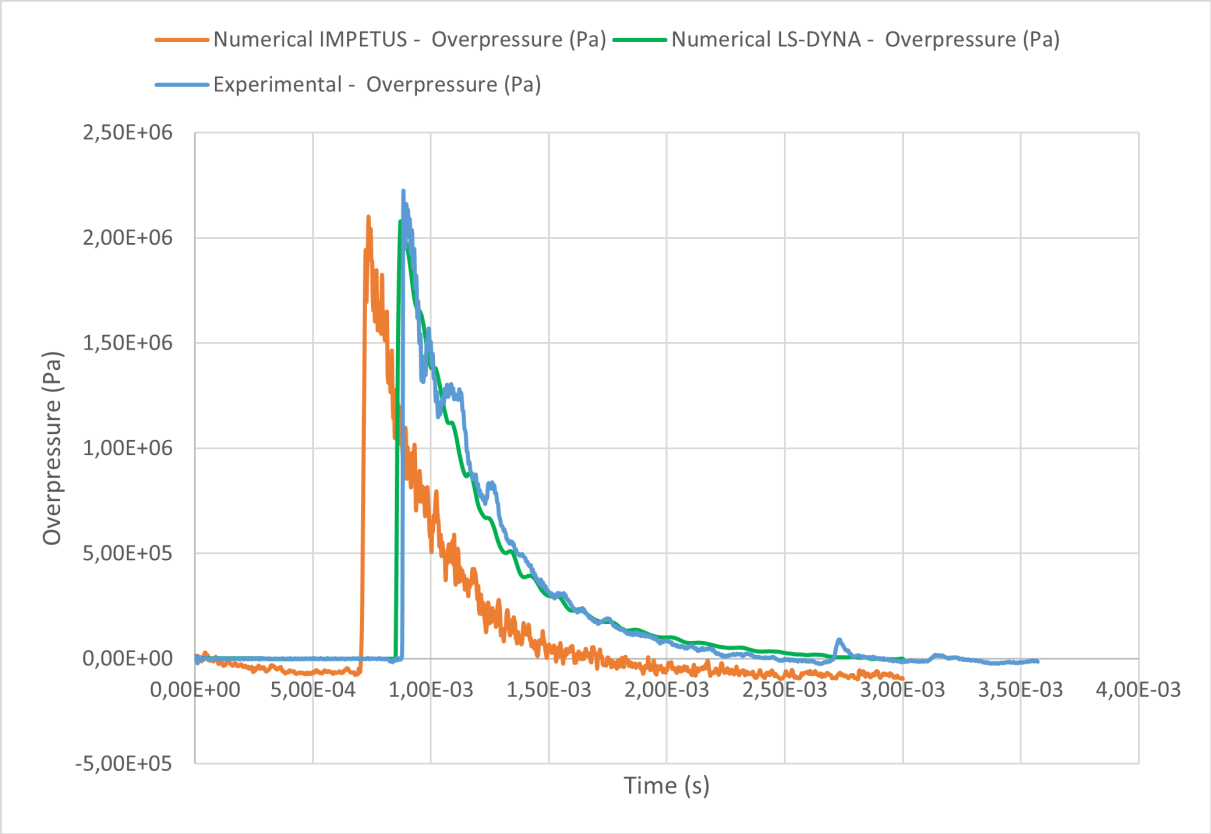

Figure 2.29: Comparison of numerical and experimental results for the free field

To conclude this comparison, when using Impetus AFEA, a relatively good knowledge of the expected overpressure and impulse has to be known in order to adjust the deactivation time. However, it is not possible to account for an accurate overpressure and impulse value at the same time, at the adjustment of the deactivation time only affects peak overpressure and not the exponential decrease of the pressure, and thus the impulse value. However, the simulation time is drastically different between the use of both codes, with a simulation time of 39 minutes for the simulation in Impetus Afea and a simulation time of 18 hours for a mesh size of 2 mm for the ALE elements for the fluid domain in LS-DYNA. Therefore, it could be interesting to perform a study on the mesh refinement for the simulation in LS-DYNA.

Mesh size (mm)	Calculation time (s)
10	145
8	253
6	578
4	2748
2.5	17573
1.5	77097

Table 2.7: Mesh sized and corresponding calculation time

2.2.1.6 Study of the mesh refinement

When performing numerical simulations, a compromise has to be found between mesh refinement and calculation time. Indeed, the finer the mesh the more accurate the result. However, a finer mesh also implies a higher calculation time. A mesh refinement study was performed to identify a suitable approach to resolve the blast wave propagation. This study was performed in the tube at various distances from the detonation point (ranging from 0 mm, being the entrance of the tube, to 1750 mm, the exit of the tube. For the assessment of the mesh refinement, a curve giving the calculation accuracy as a function of mesh size was traced. The accuracy was determined by doing the ratio of the peak overpressure and impulse for a given mesh refinement and the peak overpressure and impulse for the finest mesh possible (1.5 mm). The assessed mesh sizes were 10, 8, 4, 6, 2.5 and 1.5 mm. The simulation times for these mesh sizes are given in Table 2.7.

In Figure 2.30, it can be seen that at the entrance of the tube (0 mm), a convergence behavior can be observed rapidly when the mesh size decreases. The overestimation of the numerical pressure at this location for larger mesh sizes is due to fact that the sphere of explosive is approximated by larger elements, thus overestimating the quantity of explosive in the numerical model. It is generally recommended to have at least 10 elements in the radius of the explosive sphere. When approaching the exit of the tube at $x = 1750mm$, the blast wave becomes planar and shows a beginning of convergence.

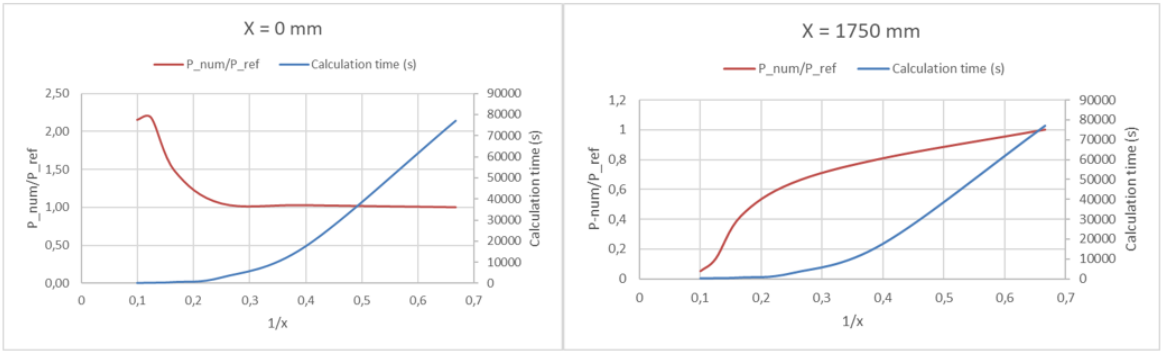

Figure 2.30: Mesh refinement study, convergence of the peak overpressure

In Figure 2.31, the convergence is studied for the value of impulse. At a distance of 1750 mm, a convergence behavior can be observed.

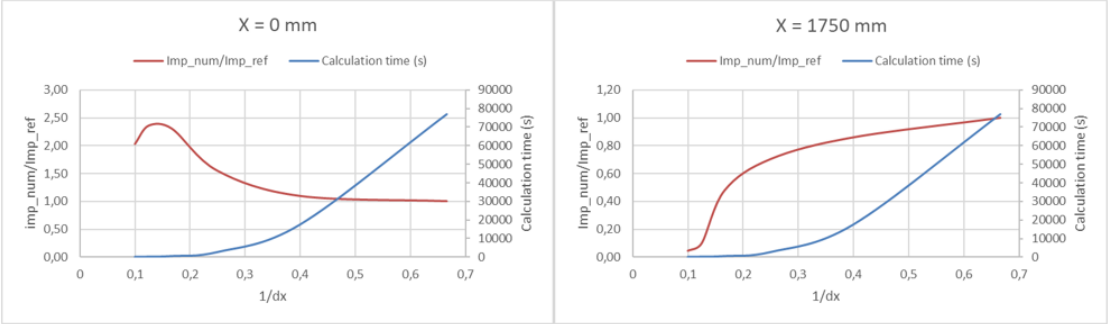

Figure 2.31: Mesh refinement study, convergence of the impulse value

To fully asses the convergence to a value beyond which a mesh refinement would no longer increase accuracy, smaller mesh sizes would have to be studied, which would exceed the current material capabilities of ISL.

Finally, with the description of several means of numerically generating a blast in Section 1.5.1, the generation of an ideal detonation with LS-DYNA and the use or corpuscles with Impetus AFEA have been compared. It was found that setting a deactivation time in Impetus AFEA was necessary. However, with this deactivation time, impulse and overpressure values cannot both be in good agreement with experimental values. Whilst having a much longer simulation time, a good agreement between experimental and numerical values was found with LS-DYNA. However, the mesh refinement study for the size of the ALE elements needed for the accurate description of the propagation of a blast wave in LS-Dyna showed that a very small element size is needed to reach convergence. As the simulation times are already very high, adding the water filled container would ever further increase calculation times. Therefore, simulating both the tube and the container in the same model is not possible, and it will be chosen to perform only a partial simulation of the experimental setup (the container alone) in this work. As the characteristics of the explosive driven shock tube could be extensively studied experimentally in this study, the direct application of an experimental blast load measurement on the nodes of the structure (the plate) was chosen.

2.2.2 Model of the experimental setup of the fluid filled container

With a choice regarding the best suited approach to the numerical model of the experimental setup being made, a model reproducing the experimental setup was simulated using the finite-element code LS-DYNA R12 [64]. The combination of an Arbitrary Lagrangian Eulerian (ALE) element formulation for water and air and Lagrangian elements for the plate is particularly well suited to this study. The ALE mesh will allow an accurate simulation of the fluid domains as they are expected to undergo deformations too large to consider a pure Lagrangian description as an appropriate option.

2.2.2.1 Modeling of the plate

The plate was discretized by means of eight-node solid hexahedron Lagrangian elements of 1 mm in size. The plate was modeled using a hypoelastic material definition, *Material Elastic*, as the deformation of the plate during an experiment is small and in the elastic domain. The parameters used are given in Table 2.8.

Table 2.8: Material parameters for the plate

Material	$\rho(kg/m^3)$	E(GPa)	ν
S235 Steel	7850	210	0.33

2.2.2.2 Modeling of the container

The deformation of the container was not of interest in this study. Therefore, it was simulated as being a boundary condition at the edges of the fluid domain. Translations and rotations were fully constrained on the nodes at the edge of the water domain.

2.2.2.3 Modeling of the fluid

The fluid domain was modeled with a size of 100 x 100 x 50 mm and was discretized by means of eight-node solid hexahedron elements with the ALE formulation. The element size considered by the fluid was of 2 by 2 by 2 mm. This element size was accurate enough to reproduce experimental local impulse measurements while still providing reasonable simulations times of about 8 hours. The water was modeled using the constitutive equation *Material Null* as defined by LS-DYNA and a linear polynomial equation of state. This linear polynomial equation of state is linear in internal energy and the pressure is given by Equation 2.2, where C_i are the polynomial equation coefficients, E is the internal energy and μ is a volumetric parameter defined in Equation 2.3.

$$P = C_0 + C_1\mu + C_2\mu^2 + C_3\mu^3 + (C_4 + C_5\mu + C_6\mu^2)E \tag{2.2}$$

$$\mu = \frac{\rho}{\rho_0} - 1 \tag{2.3}$$

Material parameters for water were taken from [65, 66] and are given in Table 2.9.

Table 2.9: Material parameters used in the linear polynomial equation of state for water [65, 66]

Material	C_0(GPa)	C_1(GPa)	C_2(GPa)	C_3(GPa)	C_4	C_5	C_6	E(GPa)
Water	0	2.002	7.727	8.436	0	0	0	$2.068e^{-4}$

The air above the fluid domain was modeled using the same element formulation as the water. Modeling the air region is essential as it allows the water to flow into it. Nodes are shared at the interface between the two domains.

The parameters for the simulation of air used in this model are the same that those used for the air surrounding the explosive driven shock tube described in Section 2.2.1.

2.2.2.4 Geometry of the numerical model

The numerical setup was able to take advantage of the symmetry of the problem by modeling only a quarter of the setup and applying boundary conditions to the plate and fluid domains.

- Symmetry conditions on two planes for the simulation of a quarter model for both fluid domains (air and water) and the plate
- Non reflecting boundary conditions for the fluid domain containing air for the simulation of a semi-infinite domain above the initial water surface

To further reduce the calculation time, it was chosen to perform only a partial simulation and apply the pressure profile delivered by the explosive driven shock tube directly to the nodes of the plate, thus not including the shock tube as well as the explosive charge in the numerical setup.

Database tracer sensors were placed on the entirety of the bottom of the container as shown in Figure 2.32, allowing to overcome the experimental limitation of having a restricted number of measurement points for the pressure history.

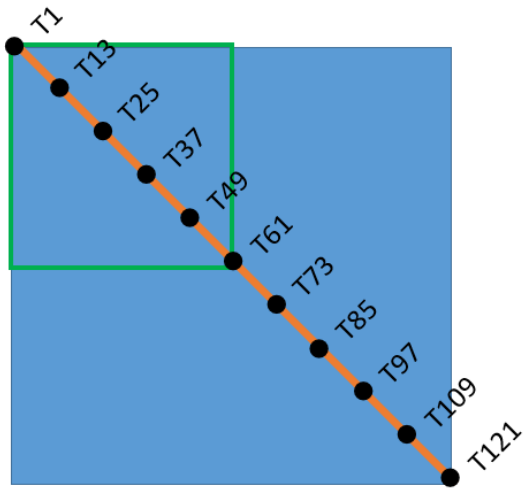

Figure 2.32: Database tracer placement along the diagonal of the container bottom in the numerical model

To consider the different levels of water confinement studied experimentally, additional boundary conditions removing all possible rotations and translations of the nodes making up the confined water surface were applied to the top of the water domain. Figure 2.33 shows the water ejection out of the container for an unconfined case both numerically and experimentally.

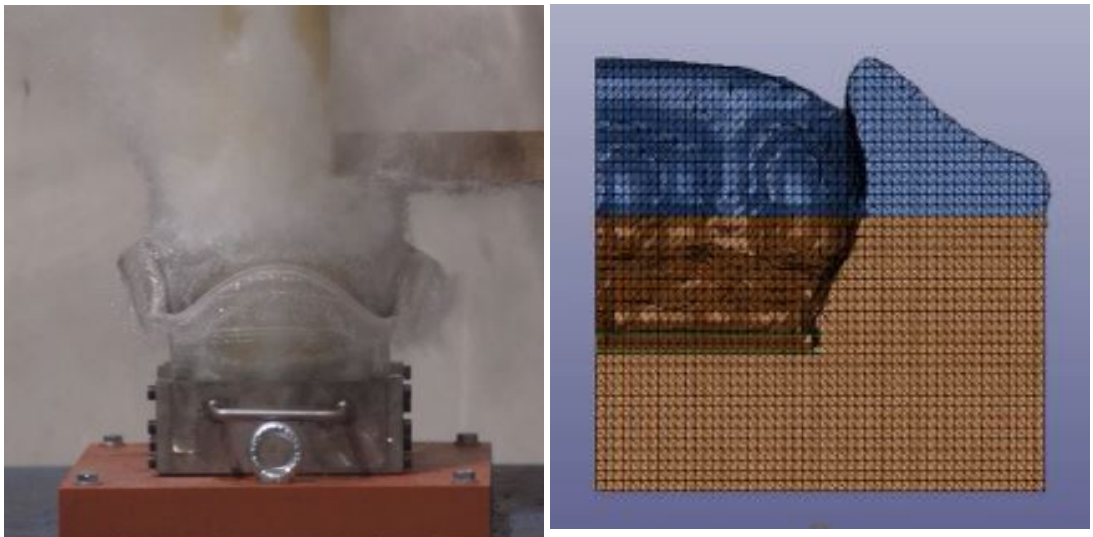

(a) Fluid ejection during an experiment

(b) Transfer of the water material between the ALE multi-material group located inside and outside of the container

Figure 2.33: Numerical simulation and experiment of a plate being projected into a water filled container

2.2.3 Validation of the numerical model

The accuracy of the aforementioned numerical model had to be verified in order to allow its use for further investigation of impulse spreading on the entirety of the container bottom. This was done through the verification of certain physical quantities and the comparison between numerically and experimentally obtained pressure signals.

The validation was done by comparison to the experimental data for a plate thickness of 3 mm, a charge mass of 15 g of C4, 0% confinement of the free water surface and a water depth of 50 mm.

2.2.3.1 Validation of physical parameters

The velocity of propagation of the compression wave in the fluid medium could be computed in the simulation and was of 1563 m/s, which is comparable to the theoretical value of the 1500 m/s for water as well as to the experimentally observed one of 1538 m/s. The difference between these two values can be explained by the numerical determination of the arrival time of the compression wave as it is dependent on the time step size chosen as an output for plots and sensor data. Figure 2.38 shows the propagation of the compression wave in the fluid filled container at its corresponding time stamps.

The numerical simulation allowed the investigation of energy quantities. Numerical results show that potential energy is negligible, thus mainly kinetic energy was examined. The kinetic energy of the fluid inside the container and the fluid already having been ejected out of the container was computed for each time step, as shown in Figure 2.35 by defining a an initially empty material group and a set of segments representing the limit of the container. The fluid material was then transferred from one material group to the other by using the ALE_FSI_SWITCH_MMG

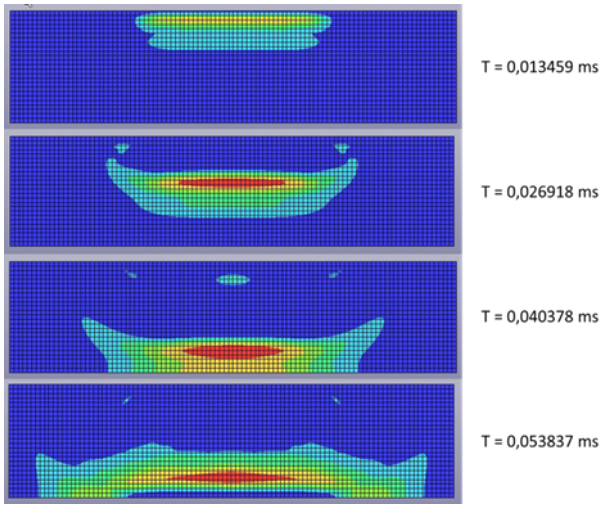

Figure 2.34: Propagation of the compression wave in the water filled container.

keyword as defined in LS-DYNA. This shows that in the given configuration, almost half of the kinetic energy is transferred outside of the container i.e. extracted from the system. This conclusion shows some similarities with the Kinetic Energy Defeat Device presented in the introduction [32].

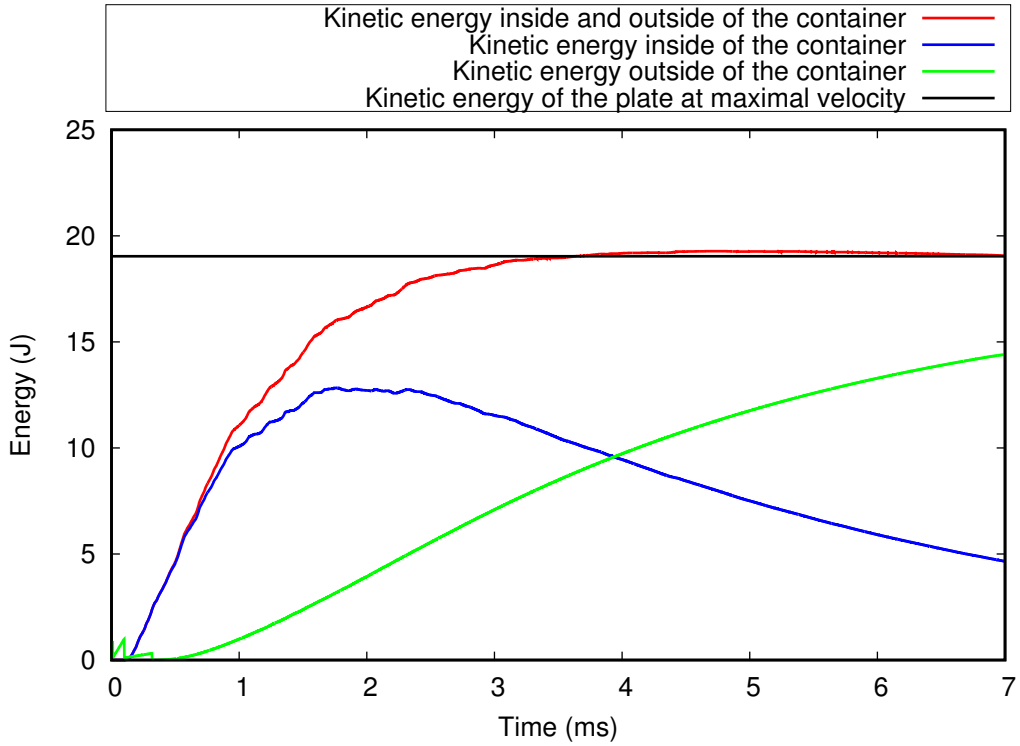

Figure 2.35: Conservation of energy in the numerical model, here illustrated for a confinement level of 0%. Transfer of the kinetic energy from the container to the outside.

The plate velocity between the numerical and experimental models could also be compared. However, establishing the experimental plate velocity thanks to the high speed camera images proved to be difficult due to experimental

conditions, as described in the previous section. The methodology used for the calculation of the experimental plate velocity was to track the coordinated of the edge of the plate with an image correlation software. This analysis had to be performed manually due to the quality of the experimentally obtained images. With that knowledge, Figure 2.36 shows that numerical and experimental plate velocities are in relatively good agreement.

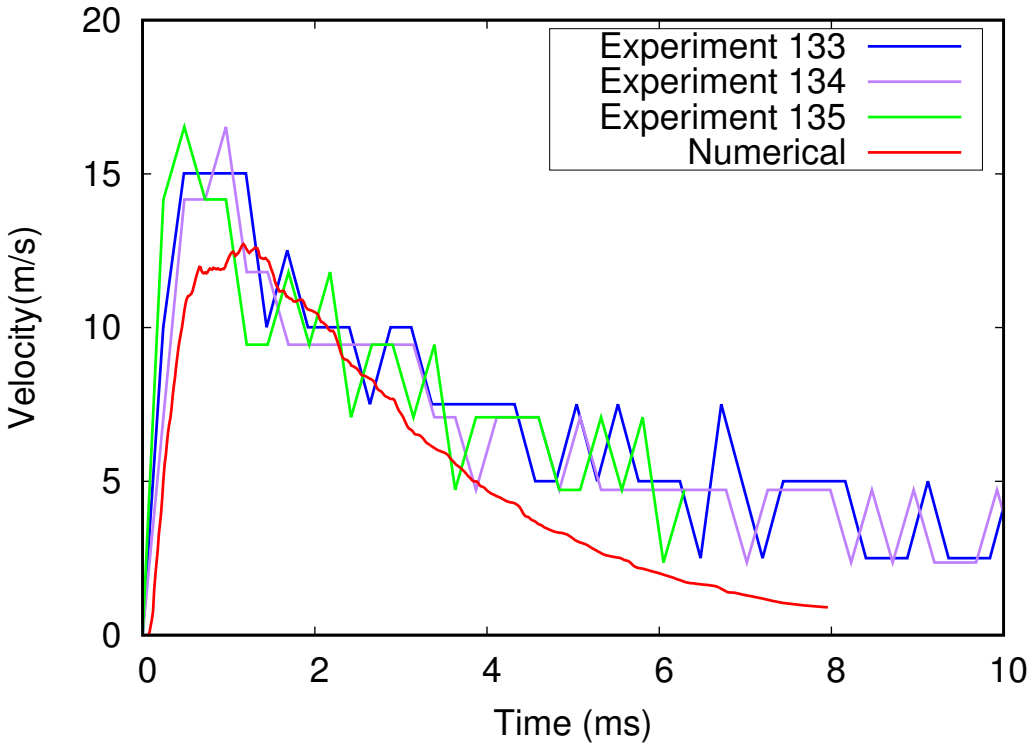

Figure 2.36: Comparison between numerical and experimental plate velocities - 15 g C4, 3 mm plate, 50 mm fluid depth and 0% confinement.

2.2.3.2 Comparison to experimental signals

Local experimental pressure signals and their numerical counterparts at the same location were compared for different levels of confinement. Figure 2.37 shows the comparison between the numerically and experimentally obtained pressure-time histories at the center of the bottom of the container for an unconfined and a fully confined case and a container depth of 50 mm for a charge of 15 g of C4 and a plate thickness of 3 mm. The experimental and numerical signals were aligned taking into consideration the known experimental time necessary between detonation and arrival of the blast wave at the exit of the explosive driven shock tube. Figure 2.38 shows the comparison between experimental and numerical impulse values at sensor location for different levels of water confinement. Whilst no direct comparison between experimental and numerical pressure signals could be made, impulse values are in good agreement for all levels of water confinement. The discrepancy between numerical and experimental pressure signals can be explained by the high sensitivity of pressure signal to mesh refinement: a

balance between accuracy and reasonable simulation times had to be found. Furthermore, the numerical boundary conditions offer a perfectly rigid container wall, whereas experimentally the walls are subject to elastic deformation, which is especially the case for the two Plexiglas panels. Thus the wave combinations will present slight differences between the numerical and experimental model, especially in the second peak due to the combination of four waves reflected on the container sides.

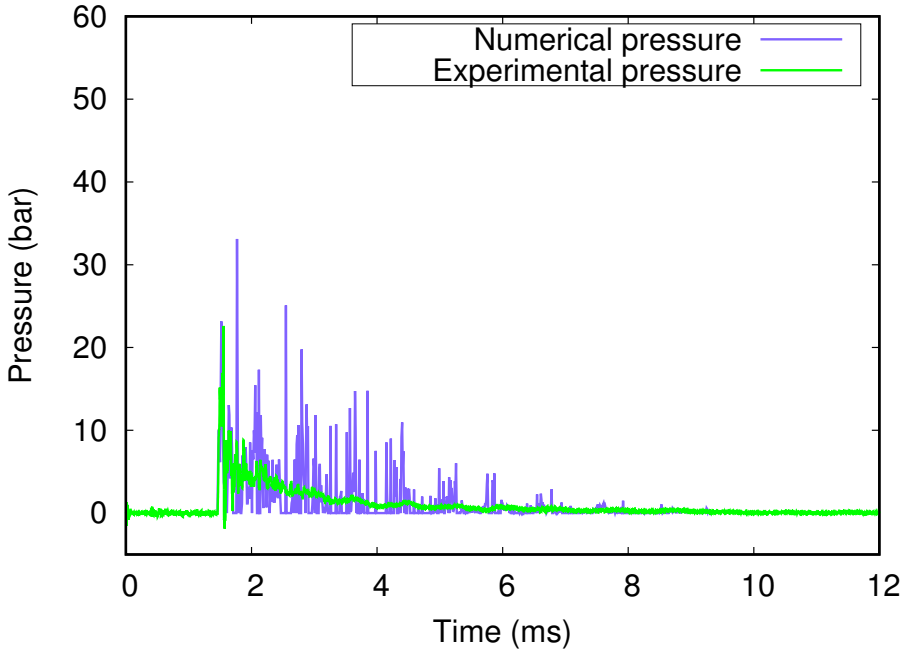

(a) 0% fluid confinement

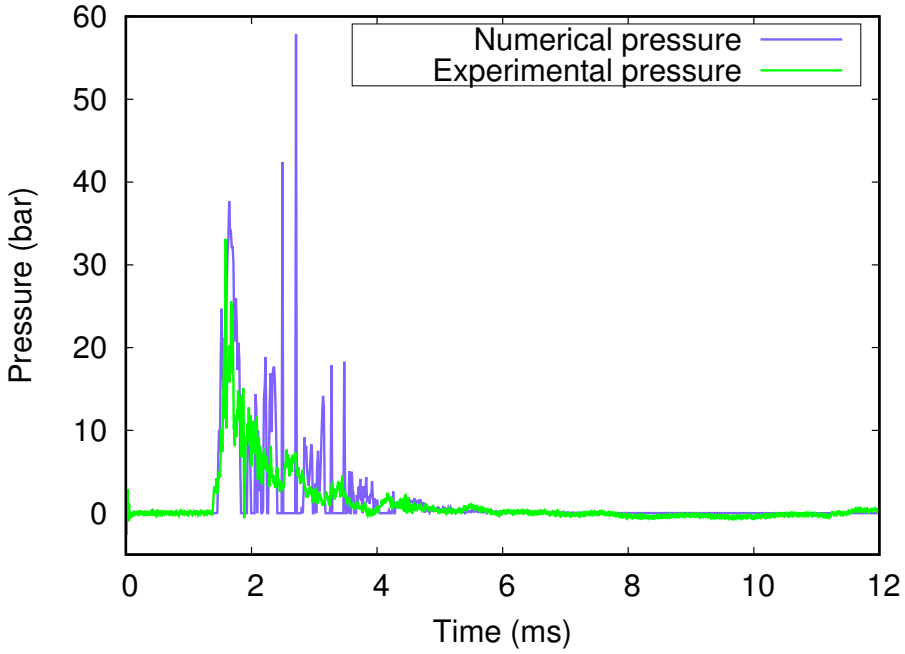

(b) 100% fluid confinement

Figure 2.37: Comparison between the numerical and experimental pressure signal for different levels of confinement - 15 g of C4, 3 mm plate, 50 mm fluid depth

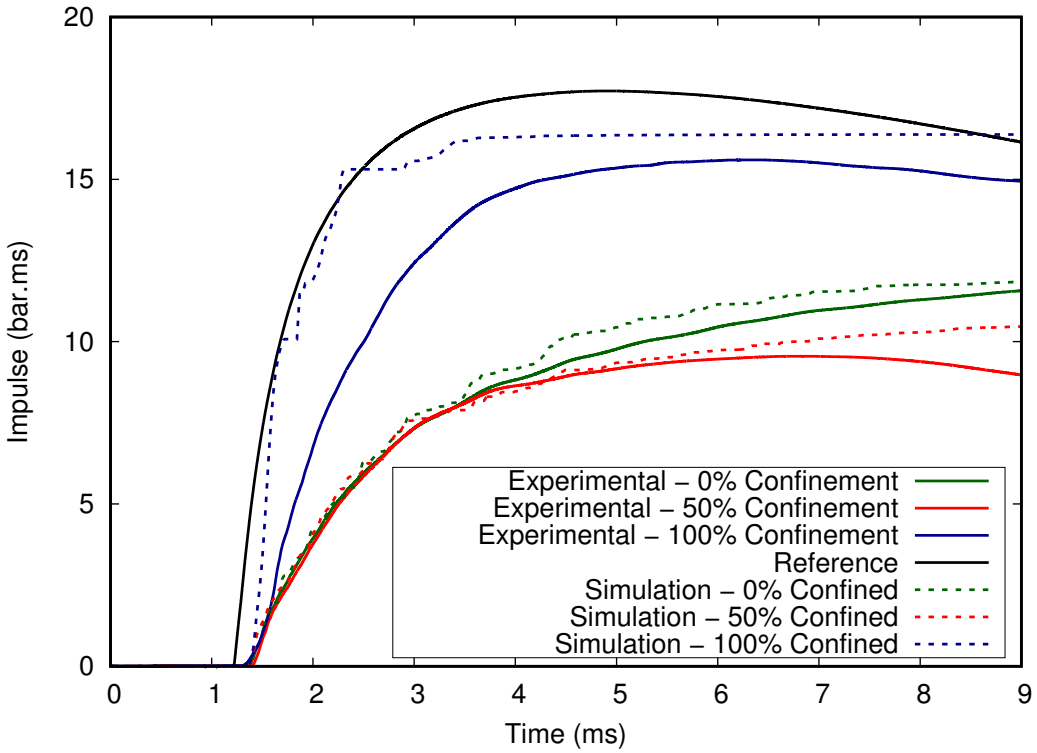

Figure 2.38: Comparison between experimental and numerical impulse values at the center of the bottom of the container for three levels of water confinement - 15 g of C4, 3 mm plate, 50 mm fluid depth.

2.3 Variation of the plate velocity

In order to investigate the capabilities of water to act on the impulse distribution on a target, in this case the bottom of the container, it was chosen to vary the intensity of the compression wave by varying the velocity at which the plate was projected into the water. Firstly, local observations were made through experimental pressure measurements at the sensor location (center of the container bottom) for different ways of changing the plate velocity. The plate velocity was changed through:

- variation of the plate thickness by using steel plates of 1.5, 3 and 5 mm thickness
- variation of the plate weight by using a steel and aluminum plate of same dimensions
- variation of the initial acceleration of the plate by leaving a layer of air between the water surface and the bottom of the plate, thus allowing it to freely accelerate without the resistance of the fluid, instead of placing the plate directly in contact with the water

Then, these experimental measurements were completed by numerical results, allowing to compute the impulse distribution on the entirety of the container bottom.

2.3.1 Local experimental pressure measurements: effect of the plate thickness

2.3.1.1 Plate thickness of 1.5 mm

Similarly to the establishment of the reference value, several experiments were performed for each configuration in order to calculate a mean value (Figure 2.39).

When comparing the reference pressure, in the case of a perfectly reflected blast load, and the pressure time curve obtained for this experiment, the difference in arrival time between the two cases had to be taken into consideration.

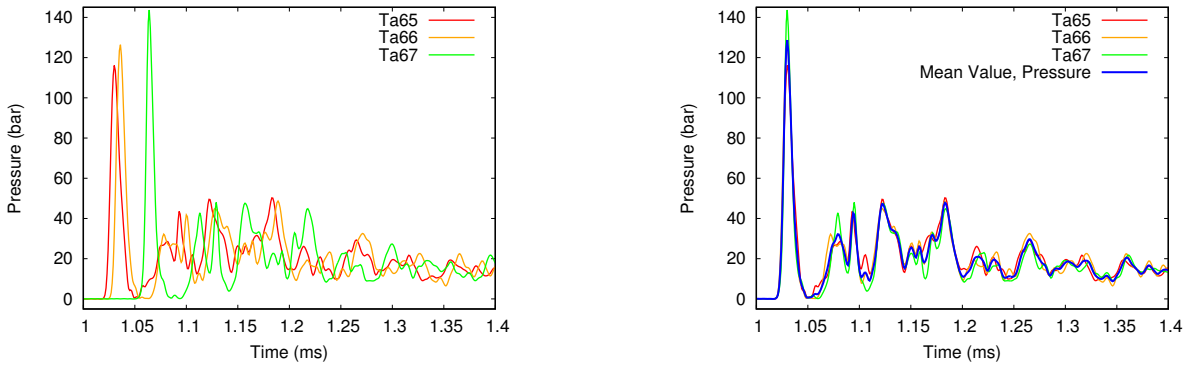

(a) Experimental results with no time adjustment

(b) Experimental results with time adjustment and mean value

Figure 2.39: Experimental results for the 1.5 mm thick plate

Indeed, in the case of the perfectly reflected blast load, the exit of the tube is directly level to the pressure sensor. However, in the experimental setup with the plate and the water container, the compression wave first has to travel through the 1.5 mm thick steel plate and the 50 mm thick water mass.

In a given material, a compression wave travels at the speed of sound of that material. As such, the shift between the arrival time of the blast wave in the two setups depends on the thickness of the two mediums and the celerity in the given medium as shown in Equation 2.4.

$$t = \frac{d}{c} \tag{2.4}$$

The numerical application in this case is given in Equation 2.5

$$t_{shift} = \frac{d_{plate}}{c_{plate}} + \frac{d_{water}}{c_{water}} = \frac{0.003}{5900} + \frac{0.05}{1500} = 3.38e^{-5}s \tag{2.5}$$

When shifting the arrival time of the reference value accordingly, a comparison between the experimental curve for the projection of a plate and the reference curve becomes possible as shown in Figure 2.40. It can be seen that the first overpressure peak is higher than the maximal overpressure of the reference. This could be explained by the rapid change of velocity in the fluid.

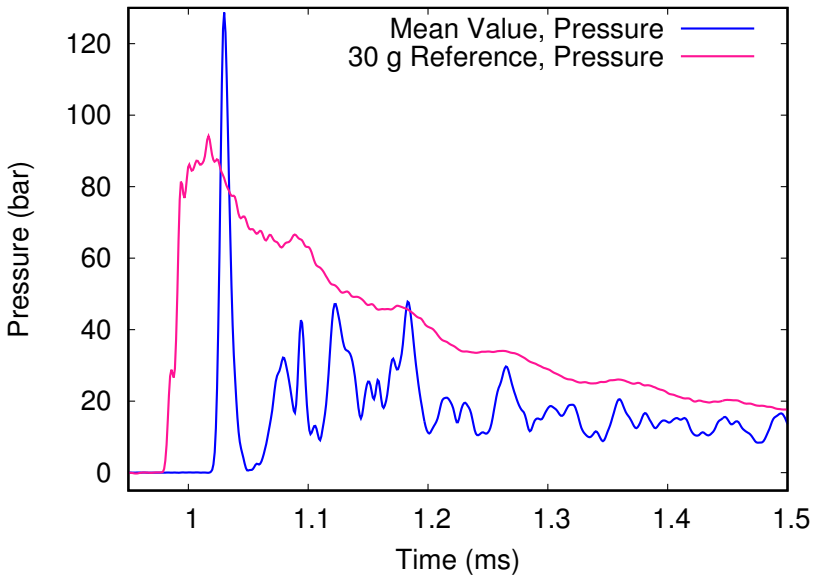

Figure 2.40: Comparison of the locally measured pressure for a plate thickness of 1.5 mm

Figure 2.41 shows the transmitted impulse to the bottom of the container for all 3 experiments and the calculated mean value.

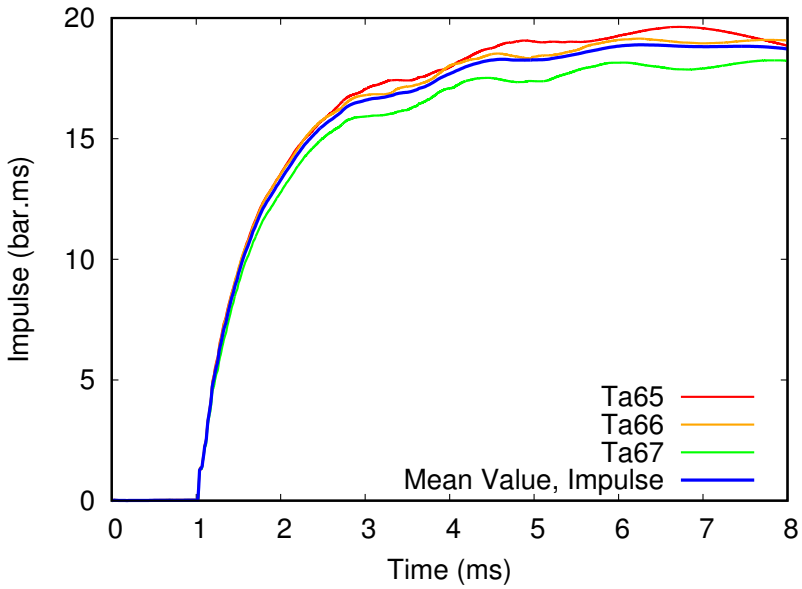

Figure 2.41: Impulse values for a plate thickness of 1.5 mm

As shown in figure 2.42, when comparing these experimental results to the reference results in the case of a perfectly reflected blast wave, the value of the local impulse measured at the center of the bottom of the container was greatly reduced.

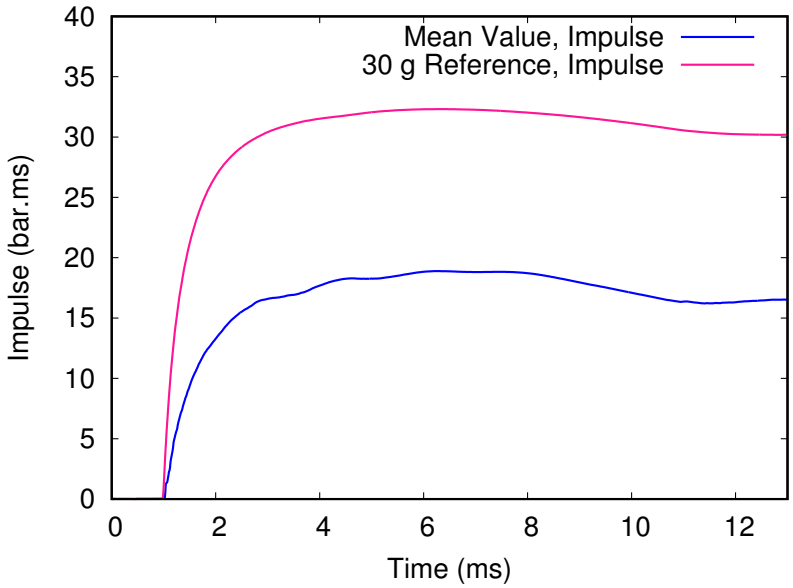

Figure 2.42: Comparison of the impulse value for a plate thickness of 1.5 mm to the reference value

2.3.1.2 Plate thickness of 3 and 5 mm

In the cases of 3 mm and 5 mm thick plates, the experiments were not analyzed separately as the images provided by the high speed camera were quickly disturbed and did not enable the establishment of correlations between

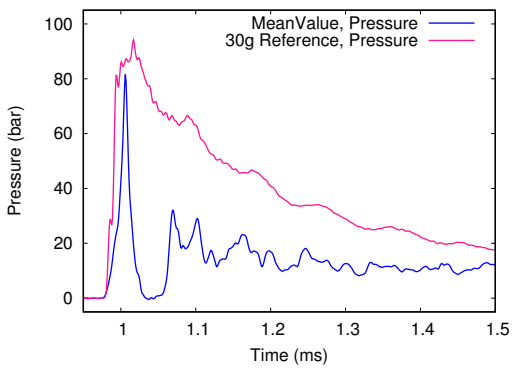

(a) Pressure comparison

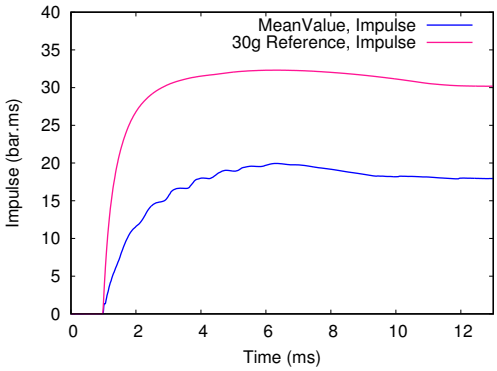

(b) Impulse comparison

Figure 2.43: Comparison of the experimental results for the 3 mm thick plate to the reference value

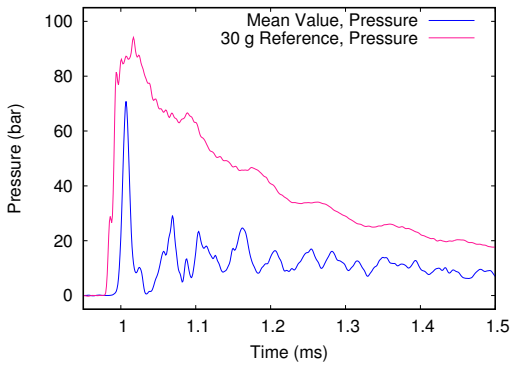

(a) Pressure comparison

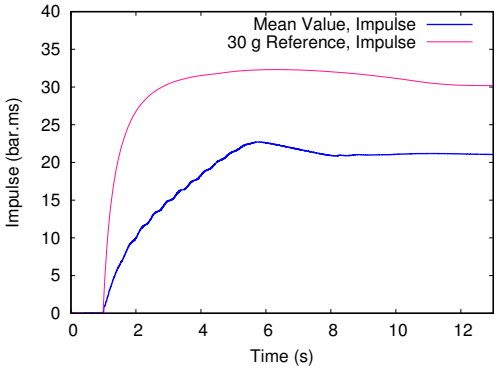

(b) Impulse comparison

Figure 2.44: Comparison of the experimental results for the 5 mm thick plate to the reference value

images and pressure-time curves. Comparisons of pressure- and impulse-time curves could still be carried out.

Figures 2.43a and 2.43b show the comparison of peak overpressure and impulse value comparisons to the reference value for a 3 mm plate. Figure 2.44a and 2.46 show the same values for a 5mm plate. In both cases, the measured peak overpressure at the bottom of the container matches the peak overpressure of the reference signal but the measured impulse value has decreased when comparing to the reference value.

2.3.1.3 Comparison of different plate thicknesses

Finally, a comparison between the experimentally measured impulse and pressure time curves for all plate velocities to the reference values can be made. The comparison of the pressure-time curves (Figure 2.45) shows that, at the center of the container bottom, a first overpressure peak is either higher of matches the maximal overpressure of the reference signal, however when considering impulse, Figure 2.46 shows that a local impulse reduction could be achieved for all plate velocities. Whilst the 1.5 mm and 3 mm plates offer an equivalent level of impulse reduction, the slower plate of 5 mm appears to provide a higher level of local impulse.

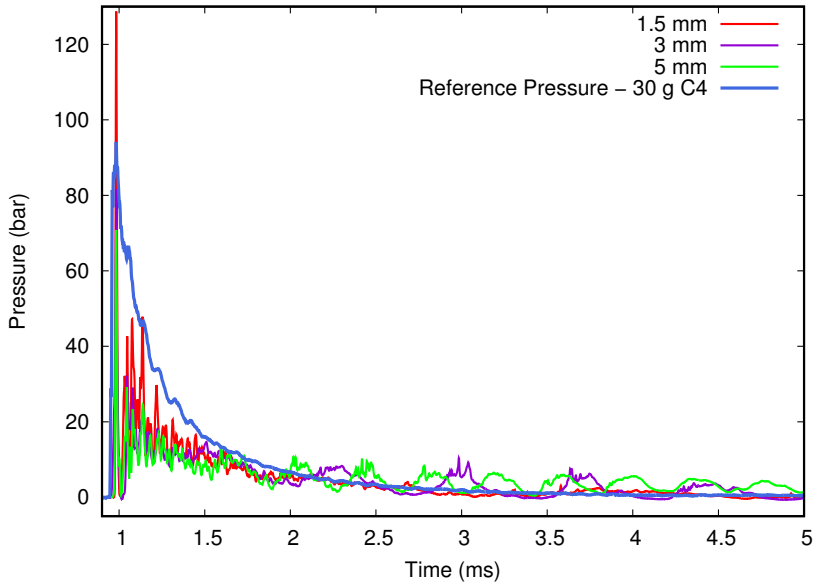

Figure 2.45: Comparison of the locally measured pressure at the center of the container bottom for three different plate velocities and comparison to the reference value for 30 g of C4

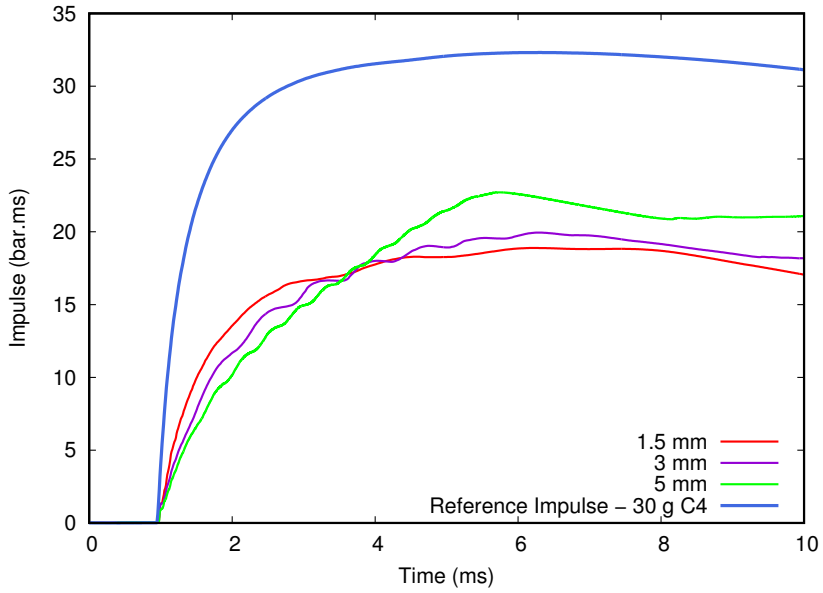

Figure 2.46: Comparison of the locally measured impulse at the center of the container bottom for three different plate velocities and comparison to the reference value for 30 g of C4

2.3.1.4 Exploitation of the numerical model

As local results between numerical and experimental data presented in Section 2.2.3 were in good agreement, it was possible to use the numerical tool for a finer investigation of the fluid domain under blast loading. Most notably, the impulse could be numerically investigated using the database tracers located on the entire surface of the container bottom, in contrary to the experimental setup where information was restricted to the location of the pressure sensor at the center of the container. A parametric study was performed, investigating impulse distribution

on the bottom of the container for different charge masses (15 and 30 g of C4) and plate thicknesses (1.5, 3 and 5 mm). Therefore, the influence of the plate velocity on impulse distribution was investigated numerically. Figure 2.47 shows the different plate velocities obtained numerically for both charge masses.

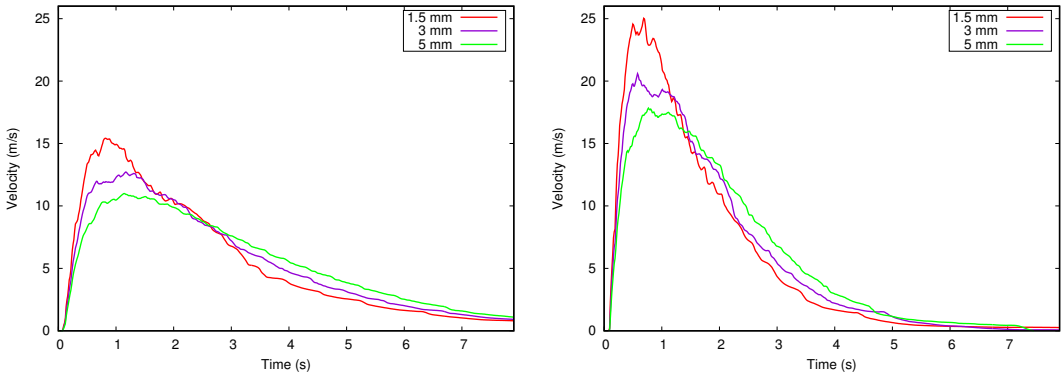

(a) Charge of 15 g of C4

(b) Charge of 30 g of C4

Figure 2.47: Numerical plate velocities for different plate thicknesses and charge masses - 0% confinement

Figure 2.48 shows a 3D mapping of the impulse on the container bottom once the blast loading has been fully transmitted to the fluid for a container depth of 50 mm. A spreading of impulse occurs along the diagonal of the container, with the highest impulse measured at the center of the container and a gradual decrease when moving towards the edges of the container. A comparison can be made for a given plate thickness and varying charge. Figure 2.49 shows impulse along the diagonal of the container. The numerical results show that plate velocity does not have a significant influence on the shape of the spreading phenomenon along the bottom of the container. As described in Section 1.5.1, only the effect of the free boundary condition and the shape of the wave propagation are simulated with the ALE element formulation chosen here. Therefore, the effect of the diffusion of momentum [67] linked to fluid density and compressibility as well as viscosity does not appear numerically as they are not solved by Euler equations. Only the effect of the free surface boundary condition was numerically investigated through water confinement.

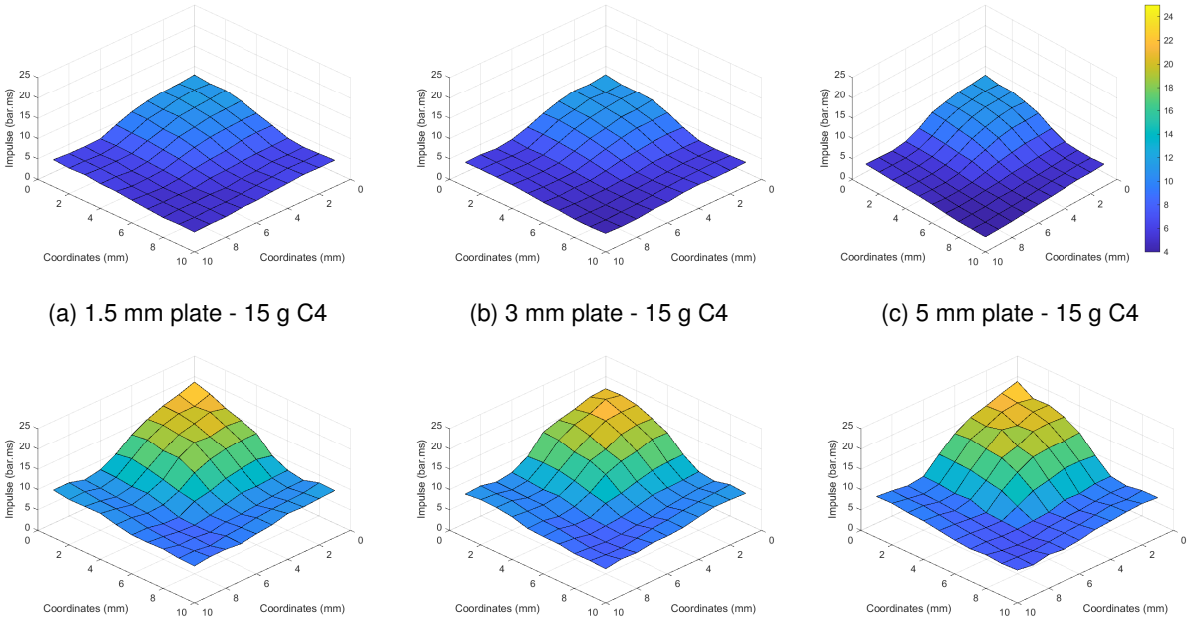

(a) 1.5 mm plate - 15 g C4 (b) 3 mm plate - 15 g C4 (c) 5 mm plate - 15 g C4

(d) 1.5 mm plate - 30 g C4 (e) 3 mm plate - 30 g C4 (f) 5 mm plate - 30 g C4

Figure 2.48: Impulse distribution on the bottom of the container for different charge masses and plate thicknesses, time = 8 ms - 0% confinement, 50 mm fluid depth

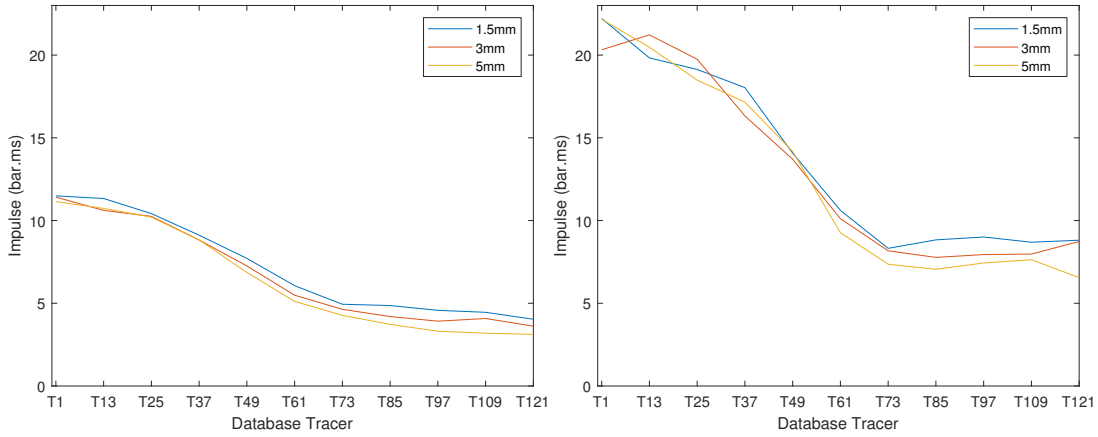

(a) 15 g C4 (b) 30 g C4

Figure 2.49: Impulse distribution along the diagonal of the container for a given charge and varying plate thickness - 0% confinement, 50 mm fluid depth.

2.3.2 Local experimental pressure measurements: effect of the plate weight

In order to achieve a velocity variation of the plate being projected into the water, the plate thickness was varied in Section 2.3.1. It had the be verified that this reduction was not only due to the thickness of the plate used. Therefore, in this section, the weight variation of the plate was achieved by varying the plate material. A comparison was made between a 5 mm thick steel plate of density $7800kg/m^3$ and a lighter 5 mm thick aluminum plate of density $2700kg/m^3$ with a charge of 30 g of C4.

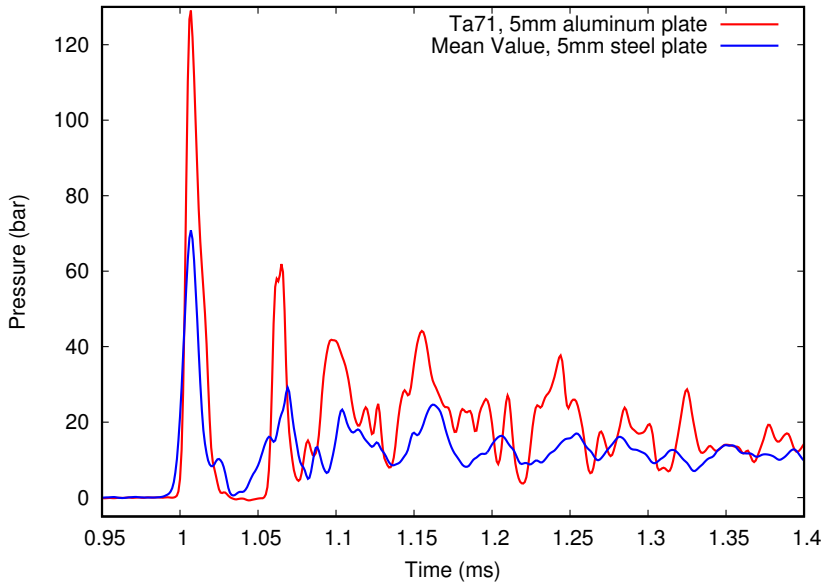

Figure 2.50: Pressure time curve for different plate densities

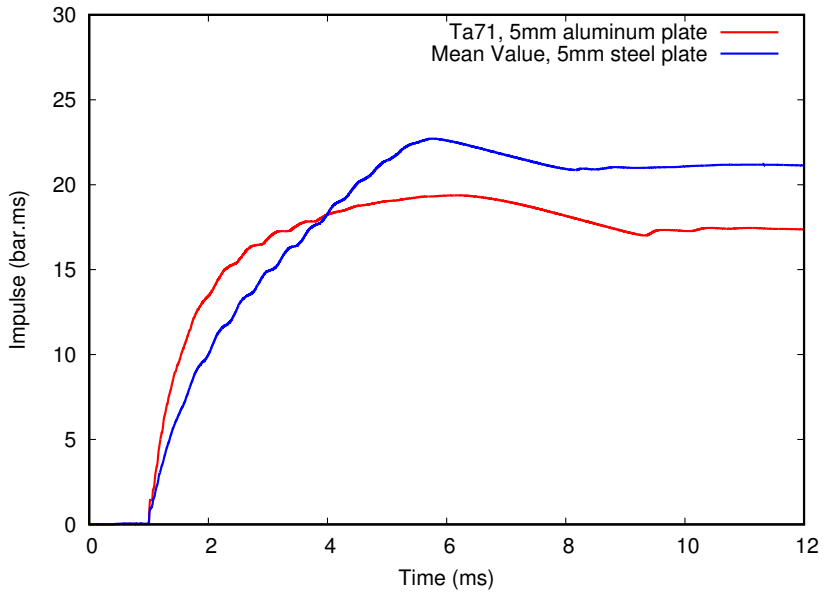

Figure 2.51: Impulse time curve for different plate densities

For the faster plate, local measurements show a higher first overpressure peak but a lower local impulse mea-

surement. However, these results have to be carefully interpreted as the impedance of the plate is also changed in this case, with a factor of 2.5 between the impedances of the two materials. This will change the shock transmission from the blast wave generated by the tube to the plate. Therefore, another way of varying plate velocity whilst sill having a constant plate thickness should be found.

2.3.3 Local experimental pressure measurements: effect of the initial acceleration of the plate

A way of achieving a variation in the plate velocity is to let the plate freely accelerate in air before encountering the resistance provided by the water as illustrated in Figure 2.52. For this purpose, the container was only filled with 40 mm of water instead of 50mm, creating a 10 mm layer of air between the plate and the water surface. Figure 2.53 and 2.54 show the pressure and impulse-time curves of the local measurements made by the pressure sensor at the center of the container bottom for an experiment with an explosive charge of 30 gr ams of C4 and a plate thickness of 3 mm. It can be observed that the first overpressure peak is much higher for the plate that was able to freely accelerate. However, the local impulse measured is lower for the freely accelerated plate.

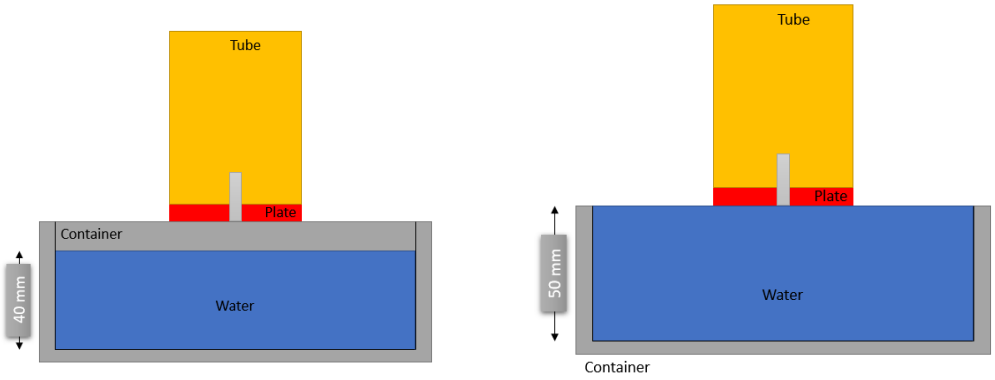

(a) 40 mm (b) 50 mm

Figure 2.52: Different water height to achieve a higher acceleration of the plate

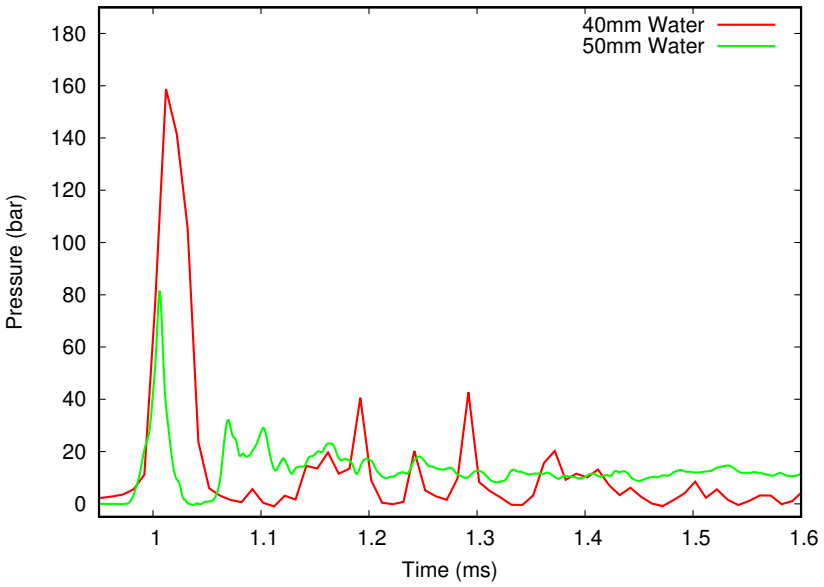

Figure 2.53: Pressure time curve for different water heights

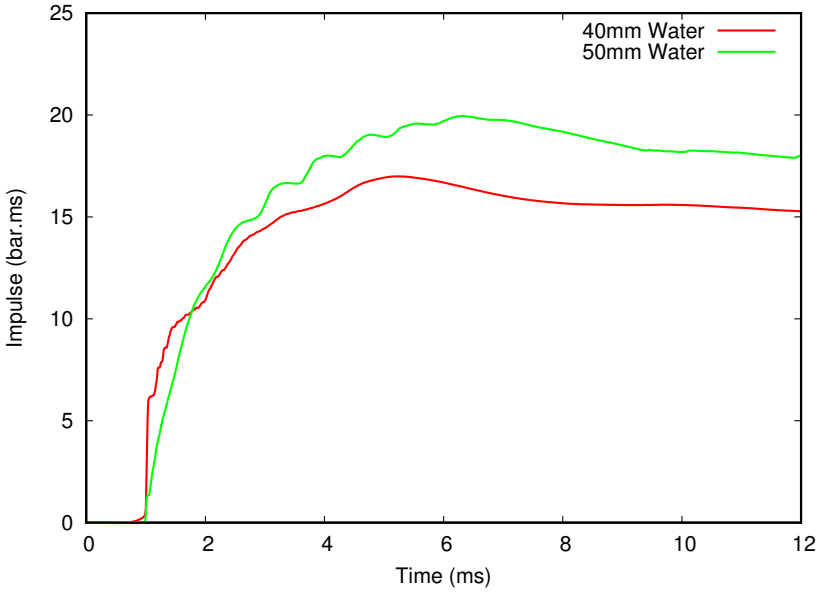

Figure 2.54: Impulse time curve for different water heights

In this case, the plate can be seen as an impactor and the equations described in Section 1.1.1.2 could be applied to predict the pressure at the bottom of the container.

However, this analytical model possesses several limitations. It is a one dimensional acoustic model, neglecting dissipation, and it assumes that the impactor is stopped at the boundary and the pressure/velocity is transferred instantaneously. As observed previously, none of these assumptions are met experimentally. Nonetheless, this analytical model has been applied in this configuration. Whilst the effect of fluid structure interaction could be neglected previously as the plate encountered immediate resistance, it has to be taken into account in this case. For a plate of 3 mm and 30 grams of C4, Blanc [25] calculates the velocity of the plate taking the effect of FSI into account. Therefore, the velocity of the plate after 10 mm of acceleration would be $46.8\,m/s$, which was verified experimentally in [25]. Using model presented in Section 1.1.1.2, the pressure of the first peak resulting from the compression wave should be equal to $\sigma = -\frac{2Z_2Z_1}{Z_2+Z_1}v_{impactor}$ where $Z_1 = 45e^6\,kg.m^{-2}.s^{-1}$ and $Z_2 = 1.5e^6\,kg.m^{-2}.s^{-1}$ are the acoustic impedances of steel and water respectively and $v_{impactor}$ is the velocity of the plate after 10 mm of acceleration. The first overpressure peak calculated with this model should have a pressure of 1340 bar, as opposed to the experimental value of 130 bar, confirming that the model is not valid for such experiments.

The influence of the variation of the intensity of the compression wave was investigated experimentally and numerically (in the case of the variation of the plate thickness) through the variation of the plate velocity. Through local measurements, it was found that a higher plate velocity increased the first overpressure peak. Regarding local impulse, there did not seem to be an effect of an increasing plate velocity when the thickness of the plate was varied. In cases where the plate was allowed to freely accelerate in air before coming into contact with the water surface, a difference in the locally measured impulse could be observed. Therefore, the range in plate velocities achieved by the variation of plate thickness may not be sufficient to draw a definite conclusion regarding the influence of the plate velocity on the locally measured pressure signal. The numerical results enabled us to gain additional insight on the impulse distribution in the bottom plate. In particular, the impulse is not homogeneously distributed on the bottom plate, but spreading was observed, with a maximal value at the center and a minimum at the corners of the container.

2.4 Variation of fluid confinement

During the experiments with varying plate velocity, a large quantity of the fluid initially present in the container was ejected due to the free water surface. Thus, the influence of fluid confinement on the measurements made at the bottom of the fluid filled container was investigated. This investigation was made with three different levels of water confinement (0, 50 and 100 %) and two different container depth (50 and 100 mm).

2.4.1 Local experimental measurements

Experimentally, the influence of the confinement level on the global impulse distribution on the bottom of the container was investigated with a charge mass of 15 g, a plate thickness of 3 mm and container depth of 50 and 100 mm (Figure 2.55). It can be observed that a similar local reduction in impulse is achieved when the fluid is fully unconfined or when 50% of the water surface is free. However, for a fully confined fluid there is no reduction in the measured impulse. These very interesting local observations seem to point in the direction of the high importance of the ability of the fluid to be ejected of the container. Similarly to the investigation regarding plate velocity, an interest has to be taken for the impulse distribution on the entirety of the container bottom, which will be done using the numerical model presented in Section 2.2.2.

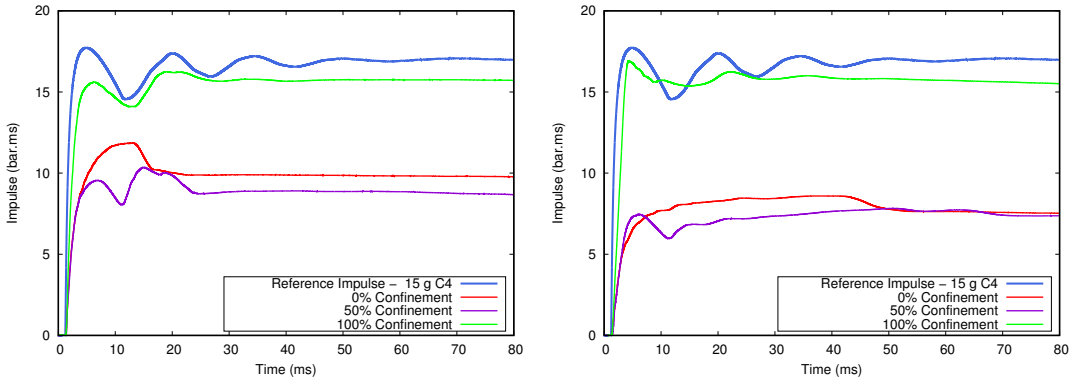

(a) Container with a depth of 50 mm

(b) Container with a depth of 100 mm

Figure 2.55: Experimental local impulse measurements for different degrees of water confinement and two container depth - 15 g C4, 3 mm plate.

2.4.2 Exploitation of the numerical model

Numerically, the investigation was performed with the same charge mass and plate thickness to provide some elements of comparison to experimental results but only the container depth of 50 mm was included in the numerical simulations. Experimentally investigated levels of water confinement of 0, 50 and 100% were expanded numerically with intermediate values of 25 and 75% on confinement.

In the case of an unconfined fluid (Figure 2.56), impulse spreading occurs along the diagonal of the container, with the highest impulse measured at the center of the container and a gradual decrease when moving towards the edge of the container. As the spreading does not occur when the fluid is fully confined, as shown in Figure 2.57, it can be concluded that it is most likely due to the boundary conditions. When considering the incremental increase in fluid confinement (Figures 2.58 and 2.59), the spreading phenomenon can still be observed for 25, 50 and 75% of fluid confinement. However, with increasing confinement levels, the spreading is less pronounced and measured impulse values at the edge of the container are higher, highlighting the role of the free surface condition in impulse spreading.

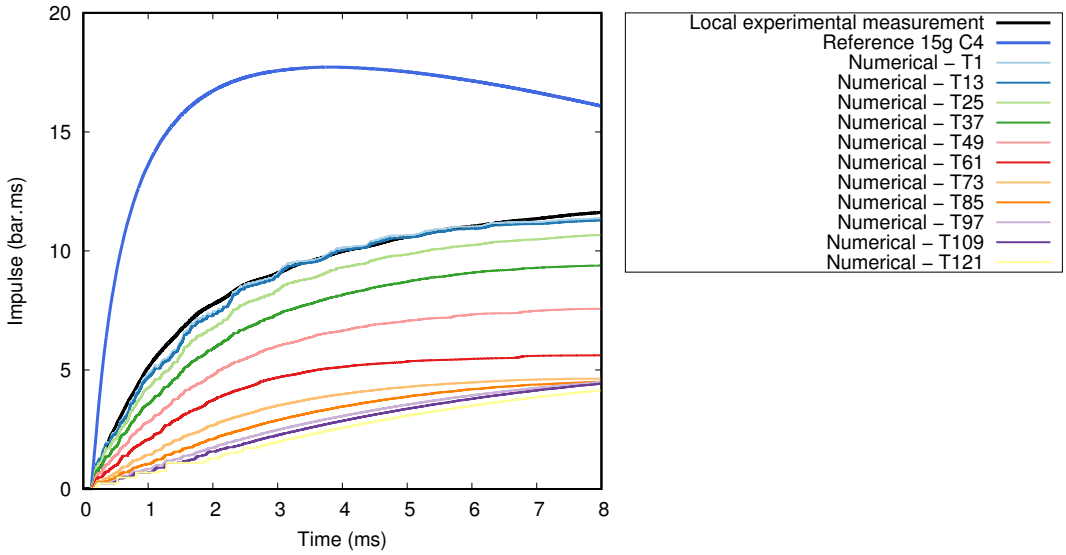

Figure 2.56: Impulse along the diagonal of the container bottom for an unconfined fluid - 15 g C4, 3 mm plate, 50 mm fluid depth.

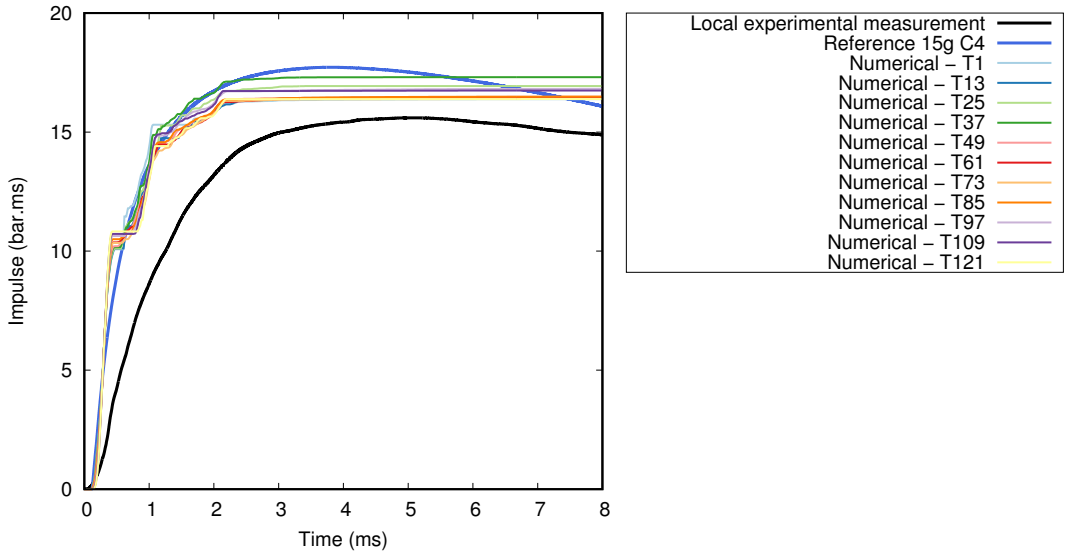

Figure 2.57: Impulse along the diagonal of the container bottom for a fully confined fluid - 15 g C4, 3 mm plate, 50 mm fluid depth.

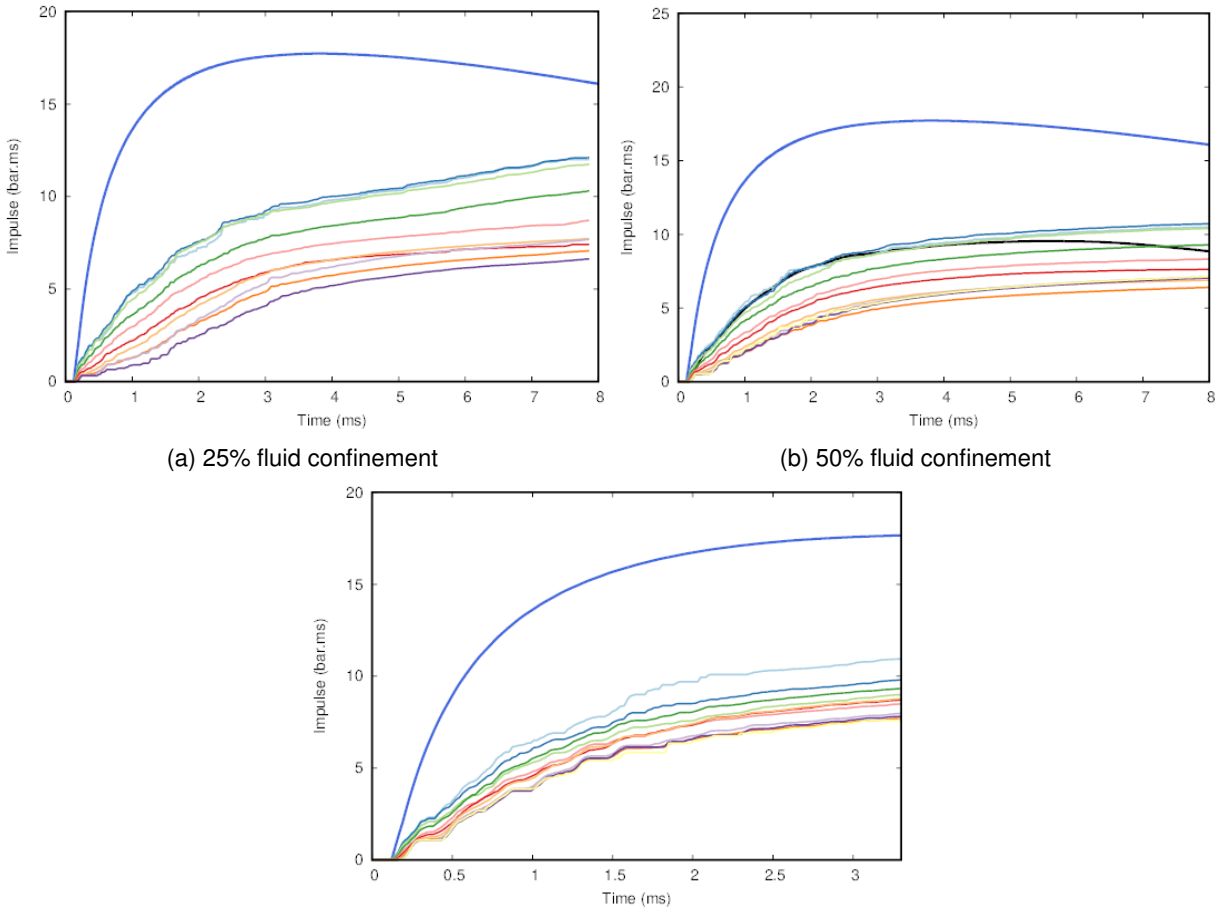

(a) 25% fluid confinement

(b) 50% fluid confinement

(c) 75% fluid confinement

Figure 2.58: Impulse along the diagonal of the container bottom for increasing levels of fluid confinement - 15 g C4, 3 mm plate, 50 mm fluid depth.

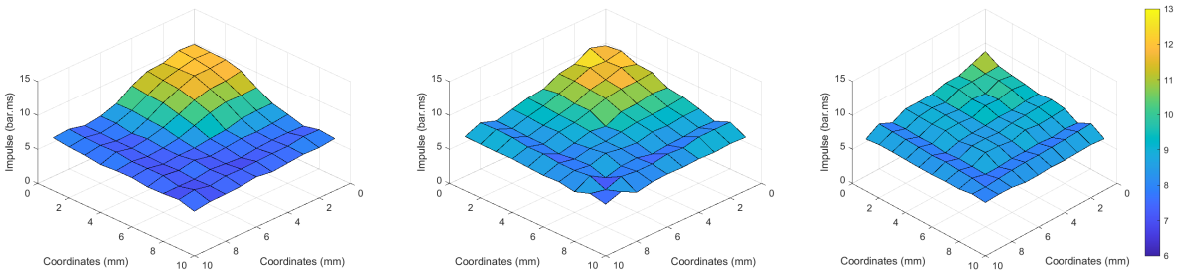

(a) 25% fluid confinement (b) 50% fluid confinement (c) 75% fluid confinement

Figure 2.59: Impulse on the container bottom for increasing levels of fluid confinement at constant plate thickness, charge and fluid depth- 15 g C4, 3 mm plate, 50 mm fluid depth.

Following these observations, novel configurations for the free surface boundary condition were investigated numerically using the model presented in the previous section, the total level of confinement in each configuration was of 50%:

- On the top of the container, confinement around the plate (Figure 2.60a) and around the border (Figure 2.60b)
- On the sides of the container, confinement creating an opening in the middle of the side wall (Figure 2.61a) and on the bottom of the side wall (Figure 2.61b)
- On the bottom of the container, confinement in the middle of the container bottom, under the plate (Figure 2.62a) and around the border of the container bottom (Figure 2.62b)

Of course, practical implementation of such configurations in an experimental setting would require a solution to keep the water in place prior to blast arrival, and to release it once the loading occurs. Such a problem, which will have to be tackled in a future integration context, should the protection solution be retained, is partially investigated in Chapter 3.

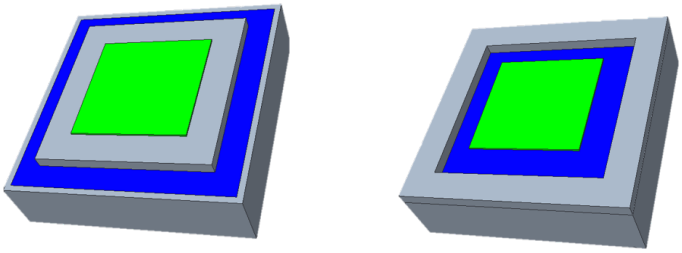

(a) Confinement around the plate

(b) Confinement around the border

Figure 2.60: Confinement configurations on the top of the container with the plate in green, the fluid in blue and the steel container in grey

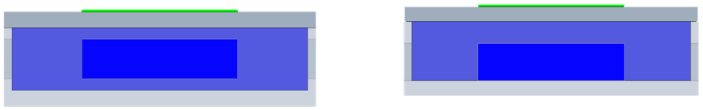

(a) Opening in the middle of the container side

(b) Opening at the bottom of the container side

Figure 2.61: Confinement configurations on the sides of the container with the plate in green, the fluid in blue and the steel container in transparency.

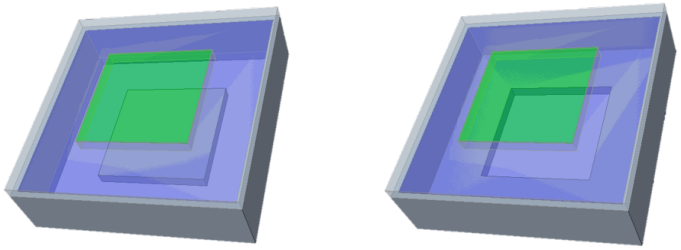

(a) Confinement at the center of the container bottom

(b) Confinement around the sides of the container bottom

Figure 2.62: Confinement configurations on the bottom of the container with the plate in green, the fluid in transparent blue and the steel container in transparent grey

Figure 2.63 shows the impulse spreading along the diagonal of the container for a free surface on the top of the container. Impulse spreading is more pronounced in the case where the confinement is located around the plate and the free boundary surface is close to the edge of the container, as shown in the direct comparison in Figure 2.64.

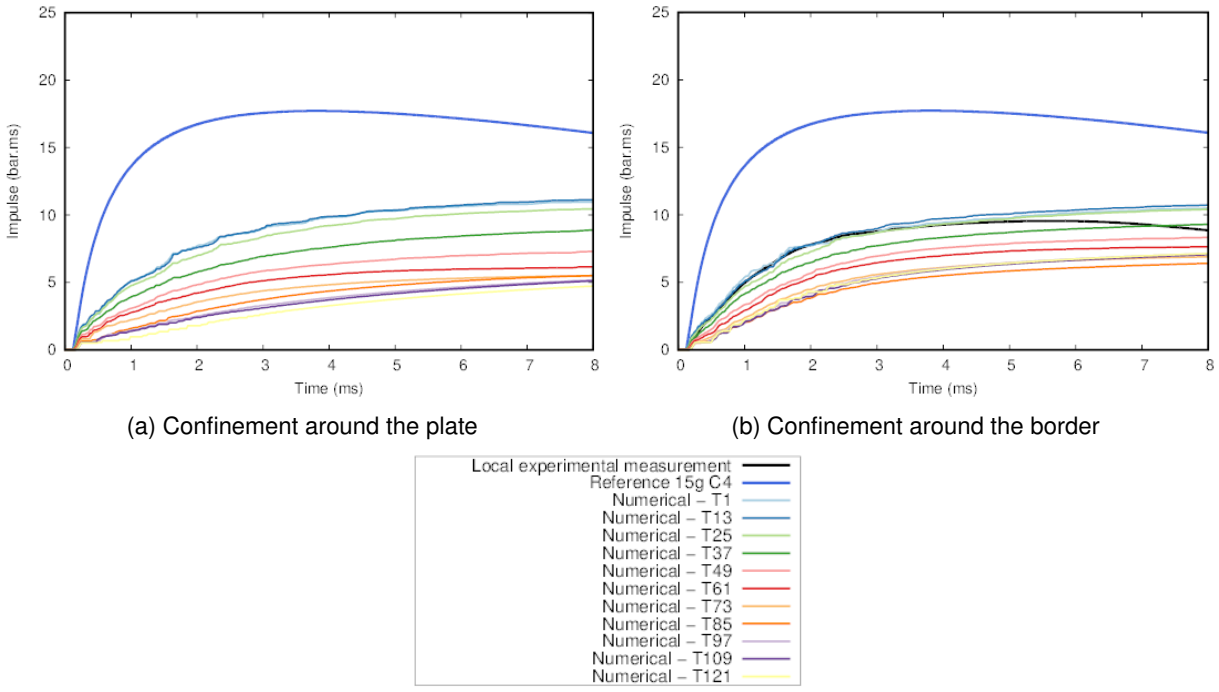

(a) Confinement around the plate

(b) Confinement around the border

Figure 2.63: Impulse along the diagonal of the container bottom when the free surface is located on the top of the container with comparison to the experimental value when available

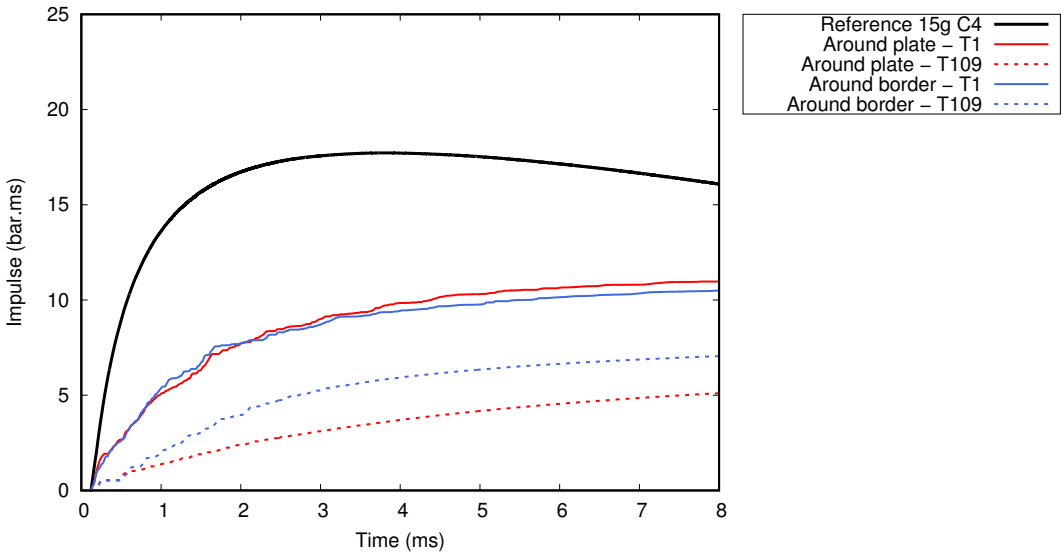

Figure 2.64: Comparison of two placements for the free surface on the top of the container

Figure 2.65 shows the numerical velocity vectors inside the fluid for the two opening locations at the top of the container. It can be seen that for an opening located around the border of the container (Figure 2.65b), the path of the velocity vectors causing the fluid to be ejected out of the container is more direct.

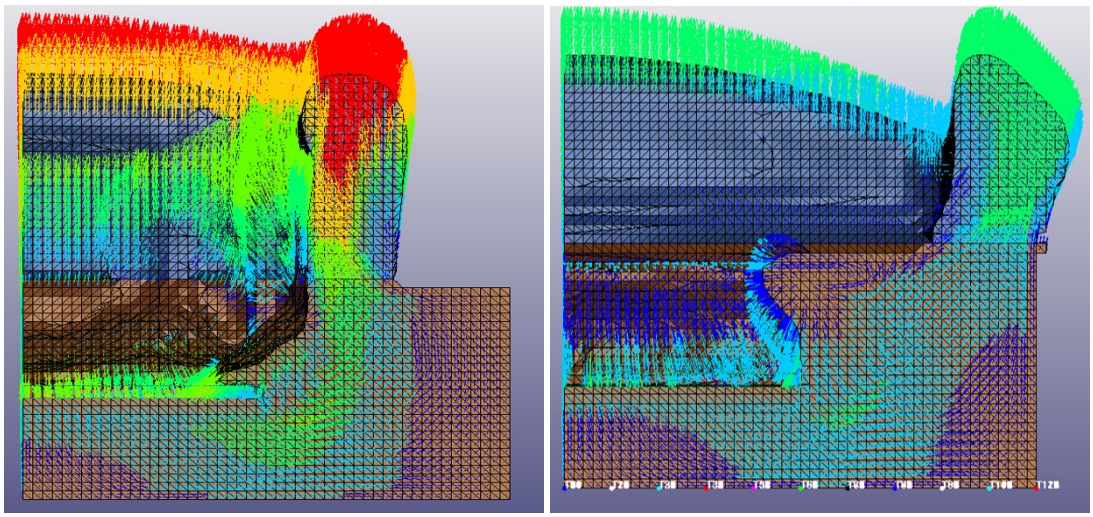

(a) Confinement around the border of the container (b) Confinement arount the plate

Figure 2.65: Numerically obtained vectors inside the fluid for different openings on the top of the container

Figure 2.66 shows the impulse along the diagonal of the container when the free surface is located on the sides of the container; both for an opening in the middle and on the lower end of the side wall. The direct comparison between the two locations shown in Figure 2.67 shows that the location of the opening does not influence the impulse spreading.

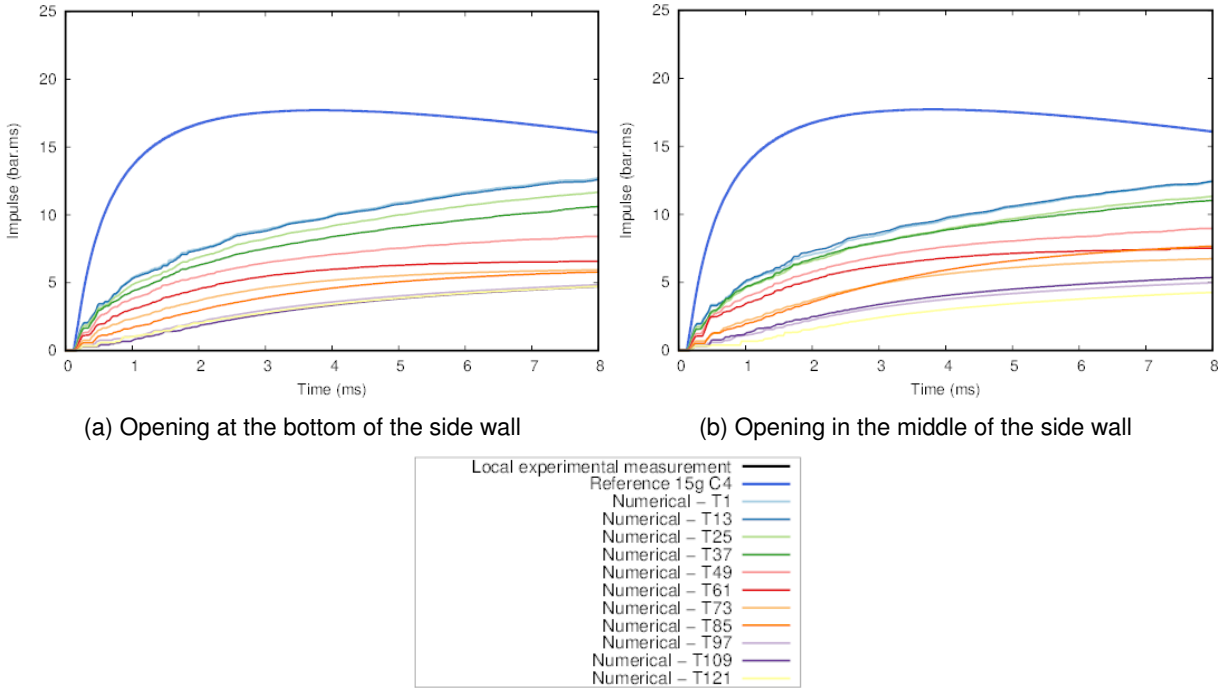

(a) Opening at the bottom of the side wall

(b) Opening in the middle of the side wall

Figure 2.66: Impulse along the diagonal of the container bottom when the free surface is located on the sides of the container

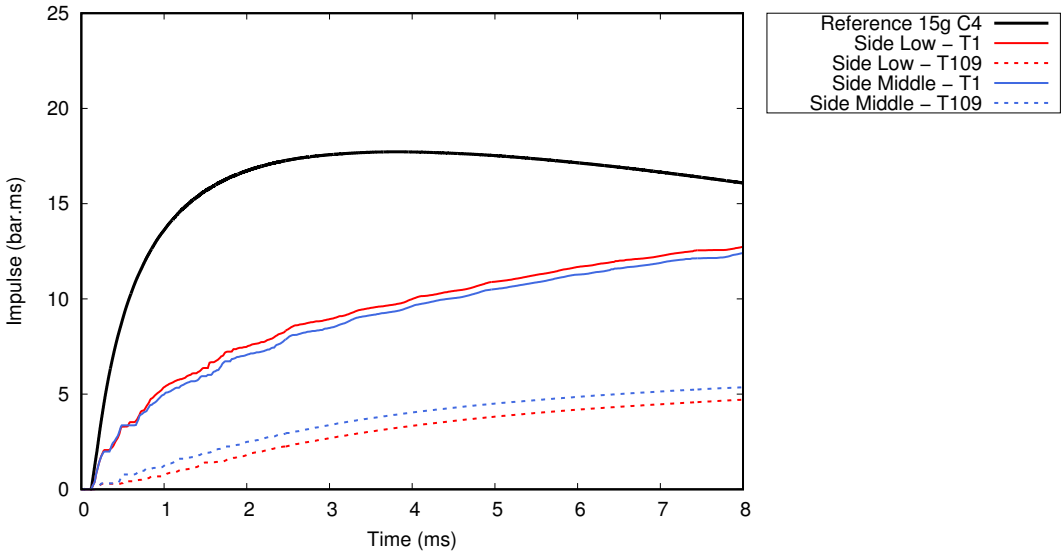

Figure 2.67: Comparison of two placements for the free surface on the sides of the container

In the case where the free surface was located at the bottom of the container, a direct comparison between impulse values for both variations was not possible, as part of the sensors are located in the free boundary condition in both cases. In particular, sensor T1 is located in the free boundary for an opening under the plate. Therefore, a comparison was made to the configuration most favorable to impulse spreading for free boundaries located on the sides and the top of the container, as shown in Figure 2.68 to the case where the container is opened along the

sides of the bottom of the container (as shown in Figure 2.62a). It can be seen that impulse spreading as well as the local impulse at the center of the container (numerical sensor T1) corresponding to the highest impulse transmitted to the bottom of the container, is achieved when the fluid can take to most direct path to the free surface boundary, more specifically in the case of the opening location being on the top of the container, with a confinement around the plate.

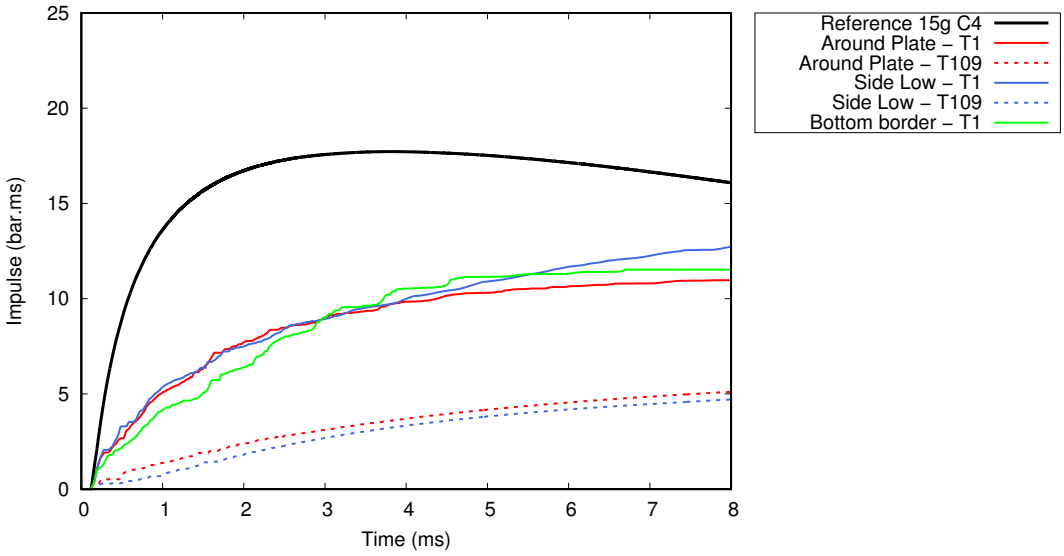

Figure 2.68: Comparison of a free surface location on the top of the container with confinement around the plate, the side of the container creating a lower opening and on the bottom of the container with confinement under the plate

In this Section, the ejection of water was investigated experimentally with three different levels of confinement. Local measurement at the center of the bottom of the container showed that, when comparing to the reference value, impulse reduction can be observed only when a certain free water surface allows to fluid to move out of the container. This reduction was comparable for a free water surface of 50% or 100% (a larger opening did not improve impulse reduction). When the fluid is fully confined, no impulse reduction occurs. The numerical model allowed to compute impulse on the entirety of the container bottom and to add further confinement levels that were not investigated experimentally. Here, it could be shown that impulse spreading occurred, meaning that the impulse decreased with increasing distance from the center of the container bottom, location of the highest impulse measurement. Whilst local reduction in the center of the container was comparable for different levels on confinement experimentally and numerically, the range in the impulse spreading increased with the degree of opening present. Meaning that impulse spreading is more pronounced the larger the free surface is. Furthermore, different locations for these openings could be investigated numerically (with a free water surface of 50% chosen for this study) where it was shown that impulse spreading is optimized when the water can take the most direct path towards the opening making up the free water surface.

2.5 Variation of the water height

Impulse spreading on the bottom of the container was investigated for water depth of 50 and 100 mm experimentally (Figure 2.69) and numerically (Figure 2.71 and 2.70).

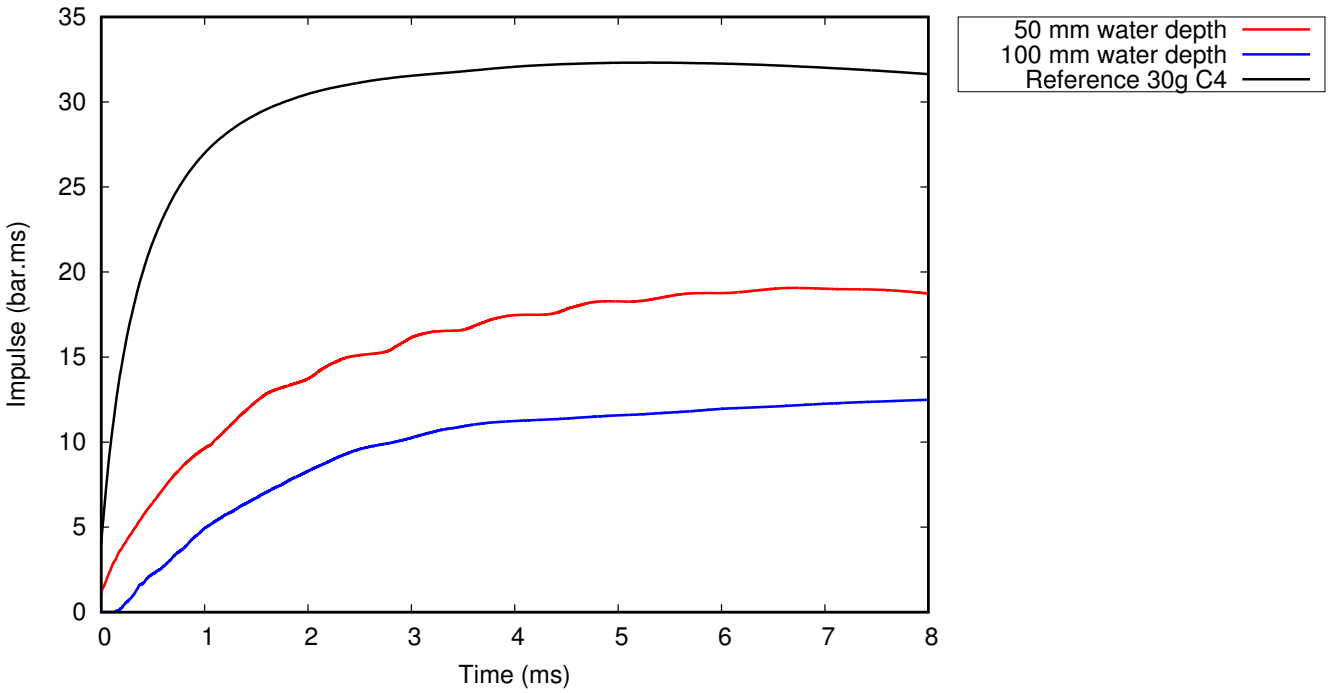

Figure 2.69: Local impulse at the center of the container bottom for wather depth of 50 and 100 mm - 30 g C4, 3 mm plate, 0% confinement.

It can be seen in Figures 2.71 and 2.70 that for a greater fluid depth, the difference in spreading between the center of the container and the edges is less pronounced. As the compression wave inside the fluid is of spherical shape, the additional water height allows time for this spherical shape to reach a larger radius, thus smoothing the local variations observed at the bottom of the container. Even though the shape of the impulse distribution at the bottom of the container is less pronounced, local reduction in impulse are still measured as shown in Figure 2.69.

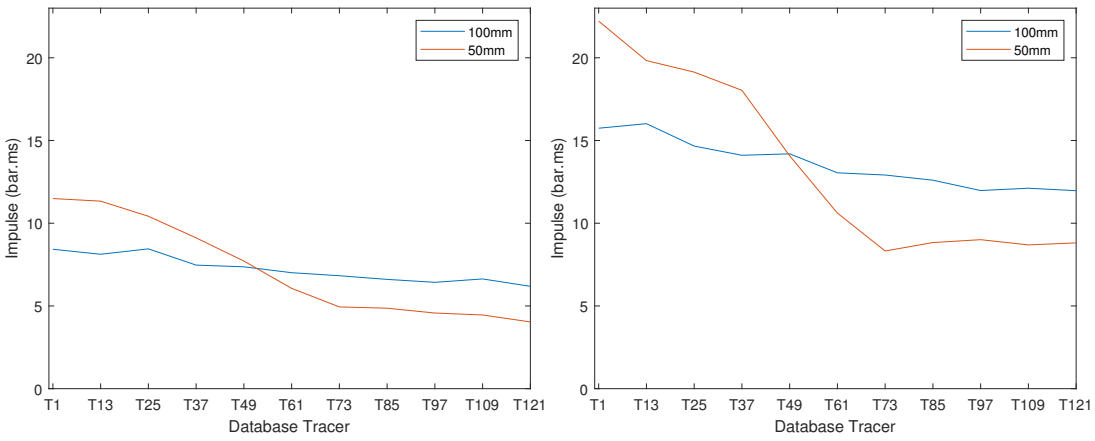

(a) 1.5 mm plate - 15 g C4

(b) 1.5 mm plate - 30 g C4

(c) 3 mm plate - 15 g C4

(d) 3 mm plate - 30 g C4

Figure 2.70: Comparison of the impulse distribution along the diagonal of the bottom of the container for two different water heights - 15 g C4, 3 mm plate, 0% confinement.

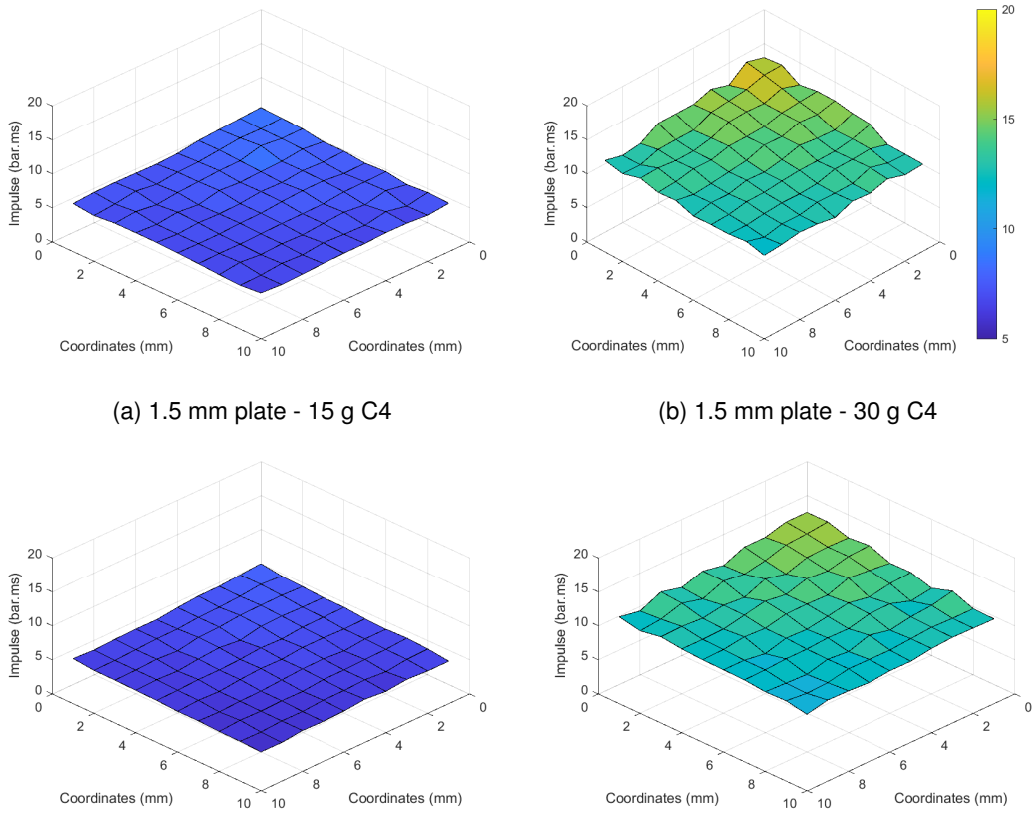

(a) 1.5 mm plate - 15 g C4

(b) 1.5 mm plate - 30 g C4

(c) 3 mm plate - 15 g C4

(d) 3 mm plate - 30 g C4

Figure 2.71: Impulse distribution on the bottom of the container for different charge masses and plate thicknesses - 0% confinement, 100 mm fluid depth

2.6 Discussion on the limits of the experimental setup and conclusion

2.6.1 Experimental influence of the container geometry

The geometry of the container in the experimental investigation has to be taken into account as the lateral container walls lead to reflections of the compression wave. These reflections are not representative of a real protection response, as the integration of a water filled protective solution on a platform will not have the dimensions of the container used in this experimental setup. Whilst an infinite water container can not be studied experimentally, the numerical simulation allows to extend the water domain by applying non reflecting boundary conditions. The difference in the propagation of the compression wave is shown in Figure 2.72, while the pressure and impulse signals are given in Figure 2.73. The impulse measurements at the center of the bottom of the container are quite similar for the two configurations. In an integration context, numerical simulations accounting for the real geometry of the protective solution could enable the prediction of the actual response and impulse distribution more closely.

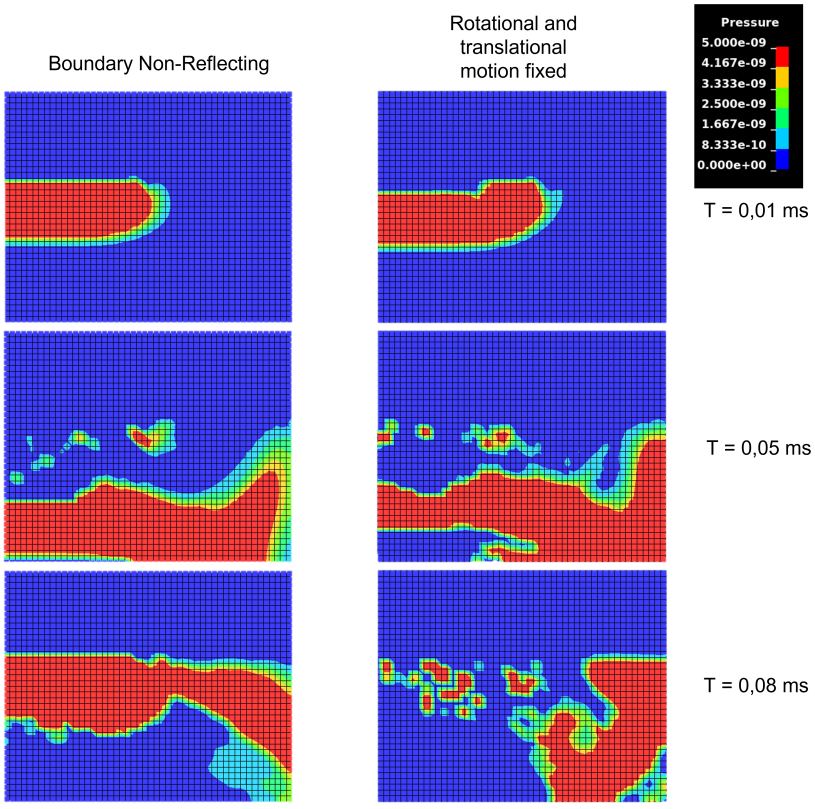

Figure 2.72: Path of the compression wave in the fluid for an infinite water domain (left) and a water domain limited by the container walls (right)

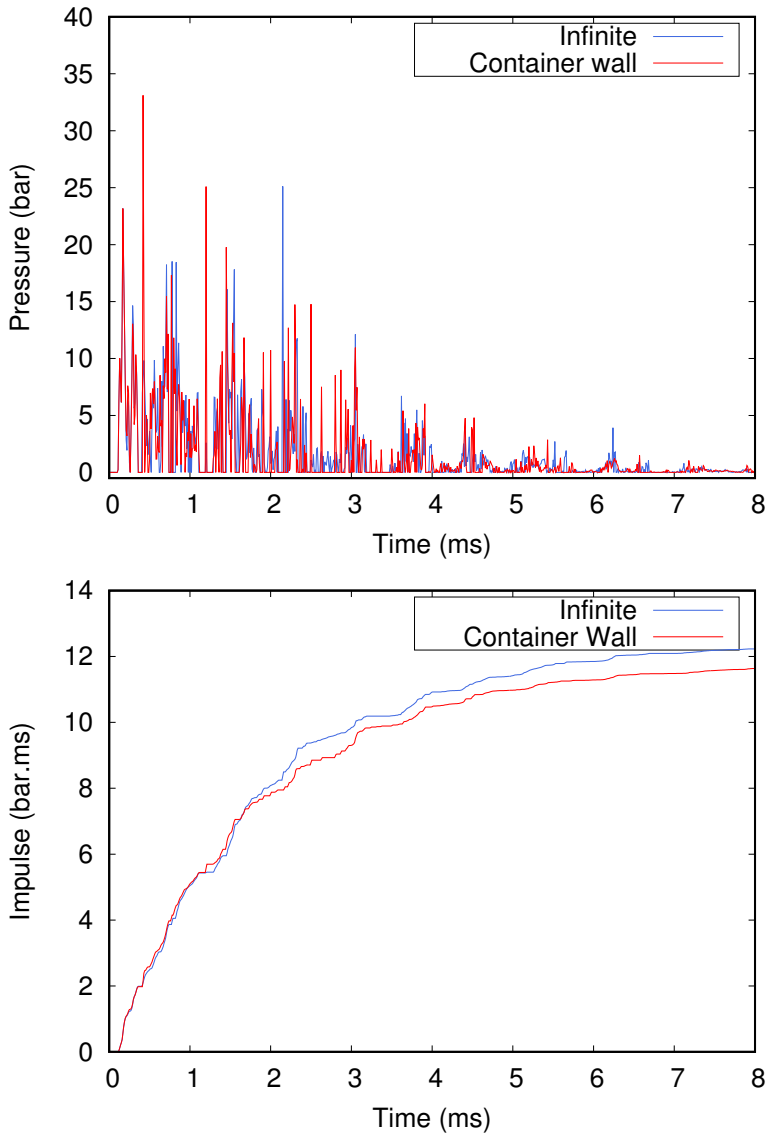

Figure 2.73: Numerically measured local pressure and impulse time curves at the center of the bottom of the container

2.6.2 Natural decay

When protecting a structure from a blast wave, two approaches can be taken:

- the protection can be an over-protection. In this case the protection is added on top of the existing vehicle floor and the overall ground clearance is reduced. That implies that the distance from the explosive device and the vehicle is reduced (Figure 2.74b).
- or the protection is directly integrated in the design of the vehicle. In this case the distance between the explosive device and the vehicle stays the same (Figure 2.74c).

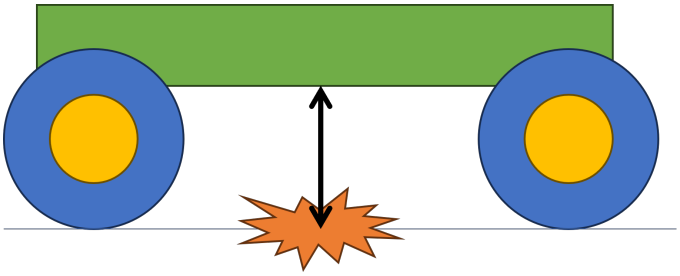

(a) Initial ground clearance of a vehicle before addition of a protective solution

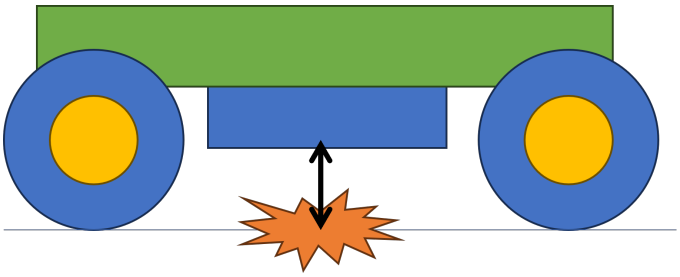

(b) Integration of a protective solution as an over-protection. The overall ground clearance is reduced

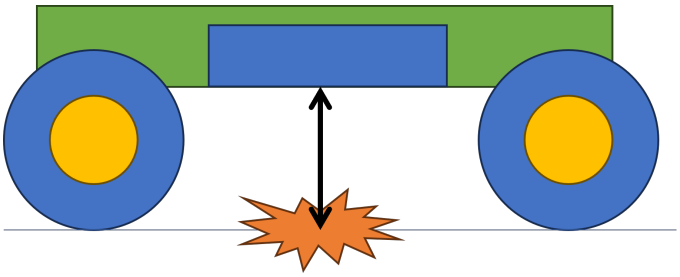

(c) Integration of a protective solution in the design of the vehicle. The ground clearance stays the equal to that of the vehicle before integration of the protection.

Figure 2.74: Different integration possibilities of a protective solution

In the case of an over-protection, it has to be assessed whether the natural decay of the shock wave in air (i.e. if no protection was added) offers comparable beneficial effects to the protection. Therefore, the natural decay of the shock wave in air was measured experimentally by placing the tube over the empty container and measuring the pressure at the center of the bottom of the container (i.e. 50 and 100 mm of air between the exit of the tube and the pressure sensor). Figures 2.75 and 2.76 show the comparison between the pressure signal measured locally at the center of the bottom of the container in the case of a fluid filled protection and an empty container to allow for the natural decay of the shock wave in air. In can be seen that the natural decay regarding the over-pressure is more important over the distance of 100 mm as the shock wave propagates overs a greater distance and has the time to obtain a more spherical shape, as can be seen on Figure 2.79.

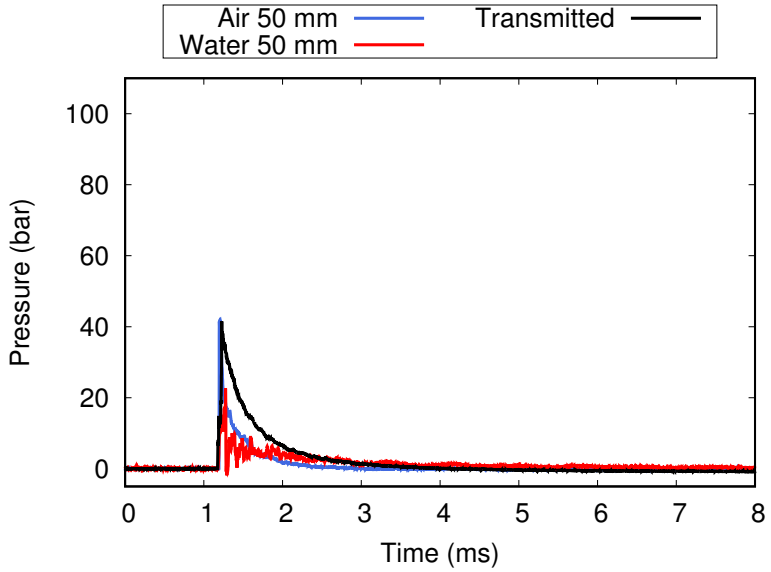

(a) 50 mm distance

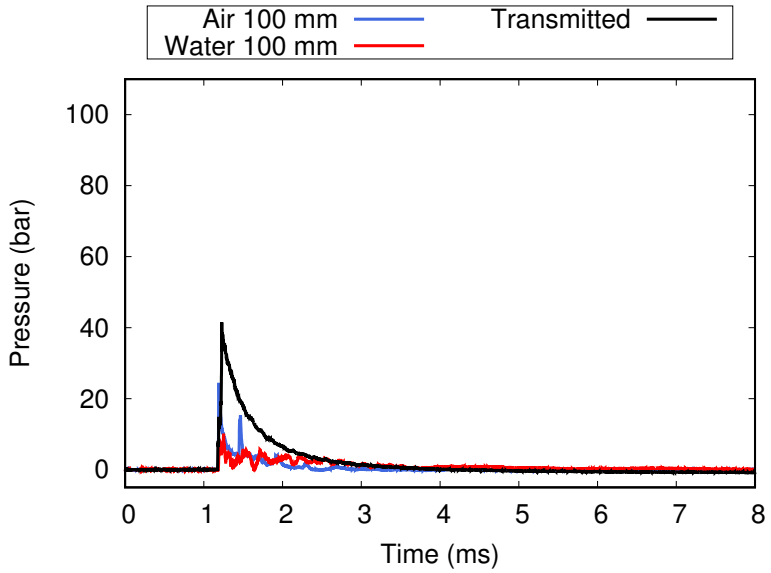

(b) 100 mm Distance

Figure 2.75: Comparison of the local pressure measurement on the vehicle floor with presence of the protective solution and for the natural decay of the shock wave in air for 15 g of C4

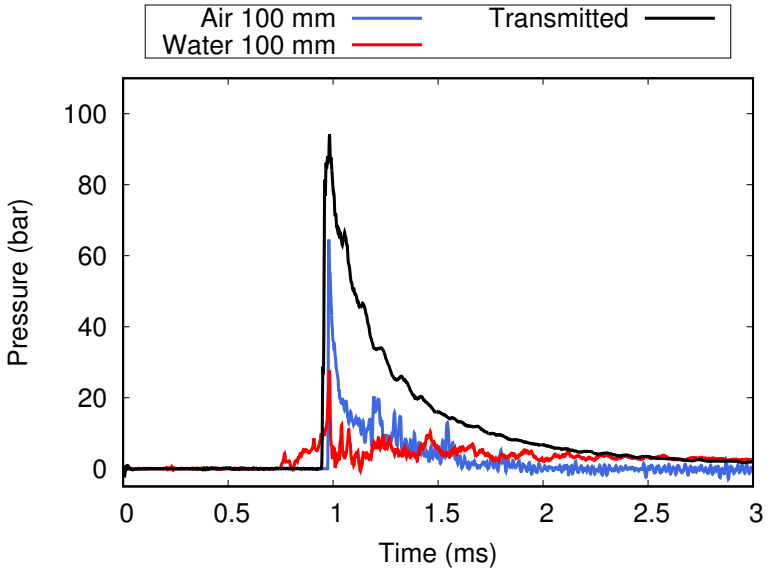

(a) 50 mm Distance

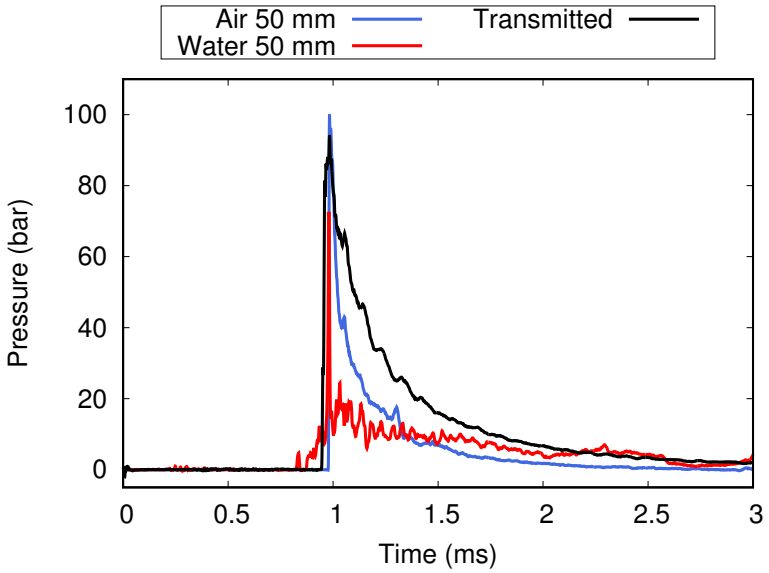

(b) 100 mm Distance

Figure 2.76: Comparison of the local pressure measurement on the vehicle floor with presence of the protective solution and for the natural decay of the shock wave in air for 30 g of C4

Looking at the local impulse value (Figures 2.77 and 2.76), for a given distance, the local impulse measurement for the water filled protective structure is more beneficial than the natural decay in air up to about 3 ms. After this point in time, the water filled protective structure does not appear to have a more beneficial impact than the natural decay of the shock wave over the same distance. This is explained by the difference in pressure-time history in both cases. For a blast wave propagating in air, the typical Friedlander pressure profile can be observed, thus creating a rapid increase of the impulse curve as the area of the pressure-time curve is highest at the beginning of the signal with a rapid decrease to the ambient pressure. On the contrary, the typical pressure-time signal measured at the bottom of the container in water shows narrow overpressure peaks over a longer duration of time, thus a slower increase of impulse will occur. However, it has to be noted that this local measurement does not allow to draw conclusions regarding the other beneficial aspects of the fluid filled protection, namely energy redirection and impulse spreading. Moreover, for this experimental setup the measurement of the natural decay of the shock wave was possible only with the sensor still mounted on the container bottom. Therefore, the impulse results for the natural decay are not free of reflections on the container walls that might be recorded by the pressure sensor and increase the measured impulse.

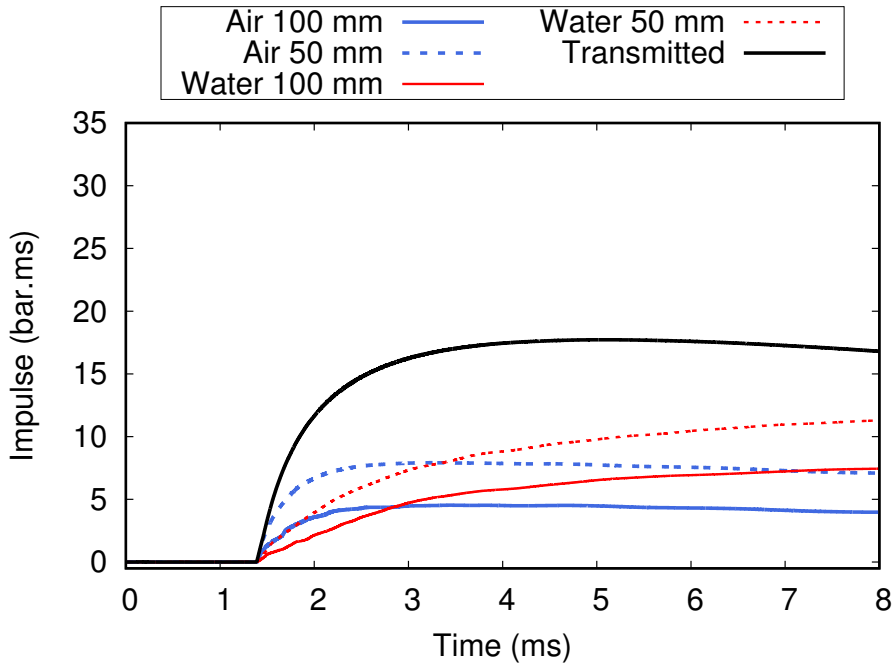

Figure 2.77: Comparison of the local impulse measurement on the vehicle floor with presence of the protective solution and for the natural decay of the shock wave in air for 15 g of C4

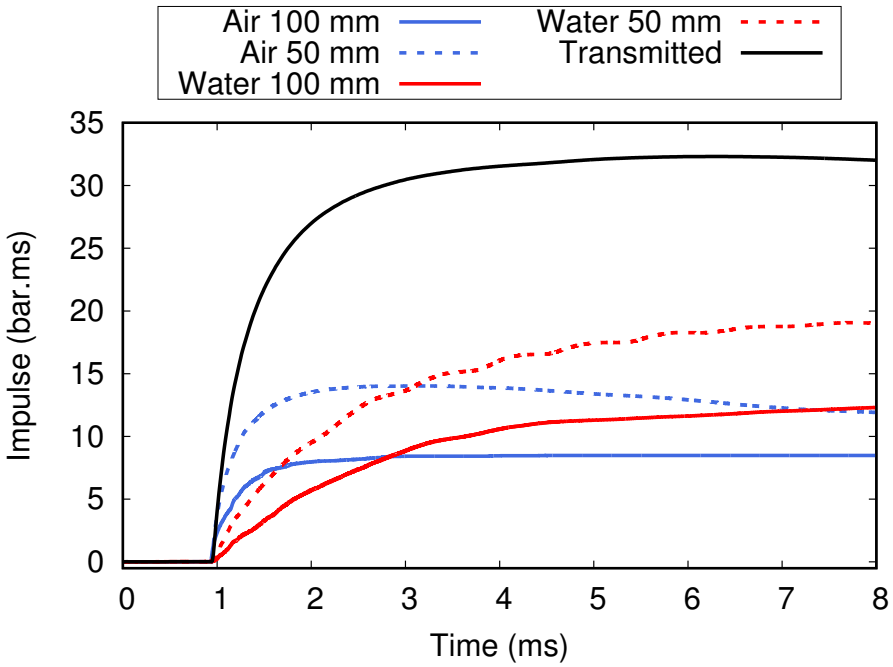

Figure 2.78: Comparison of the local impulse measurement on the vehicle floor with presence of the protective solution and for the natural decay of the shock wave in air for 30 g of C4

With these observations being made, a water filled structure would prove more efficient if integrated in the design phase of the vehicle rather than as an add-on protection.

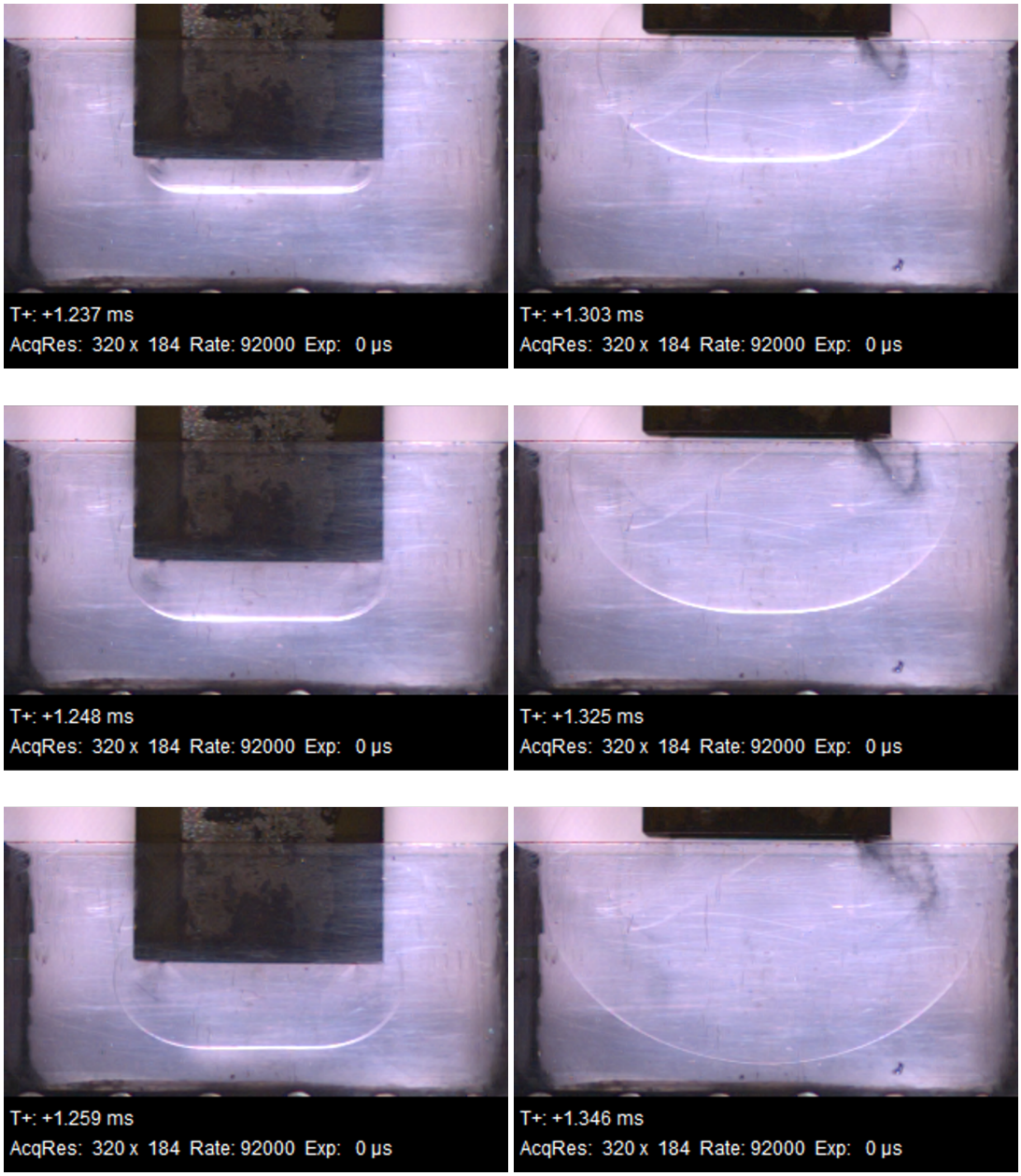

(a) 50 mm distance from the sensor (b) 100 mm from the sensor

Figure 2.79: High speed camera images for the propagation of the shock wave in air

2.6.3 Conclusion regarding parameters influencing impulse spreading

The purpose of this work was to look at the phenomena occurring in the fluid itself that could be a lever on which to act on in order to design a protective structure acting on momentum transmission to a vehicle.

It was identified that the presence of fluid allows for the spreading of impulse over a larger surface. This spreading is possible when the area of application of the blast load is smaller than the area made up of fluid. The spreading phenomenon is also linked to the free boundary of the fluid. Indeed, the study on fluid confinement revealed that no impulse spreading occurred when the water was unable to flow out of the container. This experimental result was

completed by a numerical study investigating a range of confinement levels, and showed that impulse spreading increases with the surface area of the free boundary condition. The location of this boundary condition was also investigated numerically. It was shown that impulse spreading is increased when the fluid has the most direct path towards the openings making up the free boundary condition.

The fluid investigated in this study being water, the influence of the momentum diffusion by shear waves was not investigated. Indeed, the effect of viscosity was not included in the numerical simulations and good accordance to experimental values was still found. Therefore, it can be assumed that the effect of viscosity is small compared to the effect of the free boundary condition. A perspective of this study could be to investigate, experimentally and numerically, the use of different fluids, eventually more viscous, to investigate the role of the fluid material properties on impulse spreading.

With this experimental setup, the impulse is fully being transmitted to the bottom of the container as it is rigid and fixed in space. This allowed to make observations on the influence of a fluid on impulse spreading. To gain understanding regarding global momentum transmission, a fluid filled structure that can be set into motion has to be tested. The blast pendulum was identified in Chapter 1 as being an experimental way of observing momentum transmission to a structure. Therefore, the next Chapter will make use of a new experimental setup including a blast pendulum for the understanding of momentum transmission.

Chapter 3

Global momentum transmission

For the investigation of global momentum transmission, an experimental setup allowing a fluid filled structure to be set into motion following an interaction with a blast wave had to be used. One approach consists in the use of a blast pendulum. The maximal angle reached by the pendulum could be compared for a water filled structure and a reference value of equivalent mass established using steel plates. Different experimental configurations were tested to address a number of requirements related to the containment of water prior to the blast, as well as its ejection time and direction once the blast interacts with the structure. Preliminary results show that this concept has good potential for reduction of the global momentum transferred by the blast to the structure.

Contents

3.1 Experimental setup

This chapter was driven by the analysis made of the KEDD results in Chapter 1 and the impulse spreading observed in Chapter 2. Based on the KEDD analysis, it is expected that the water mass spreads out on the side when pushed by a front plate. In parallel, water allows an attenuation of local impulse transmission to the rear plate. Consequently, the first design described in this chapter aims to combine these two effects.

3.1.1 Description

The blast pendulum described in Section 1.4.3 was used in this experimental study with some modifications to allow the placement of water on the body of the pendulum. In particular, different experimental configurations were designed and tested to handle water containment prior to the blast, as well as its time and direction of ejection. For this purpose, the square load impact area was replaced by a water bag sandwiched in between two steel plates (a front plate and a back plate) placed in front of the body of the pendulum as shown in Figure 3.1a. By not restricting the water in a closed architecture, this design should allows the water to spread on the side as it is pushed by the front plate during its deformation. To ensure that the center of mass of the entire setup is positioned in the center of the pendulum body, steel plates were placed on the opposite side for weight compensation (Figure 3.1b).

(a) Front plate, water filled bag and back plate

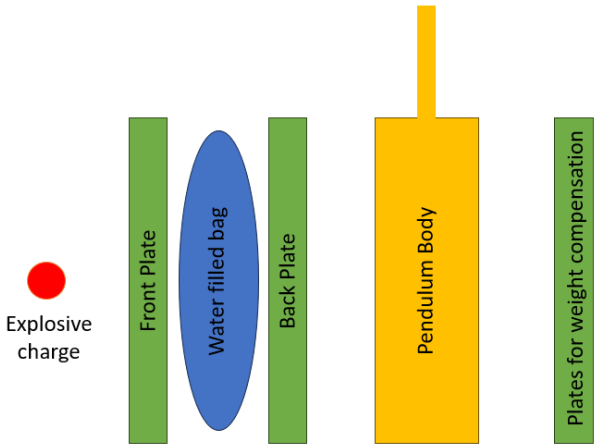

(b) Schematic representation of the experimental setup

Figure 3.1: Placement of water bags on the blast pendulum

The front and back plates placed around the water bag were steel plates with a thickness ranging from 1 to 4 mm. The explosive charge used was of 840 grams of C4 (equivalent to 1 kg of TNT) placed centered with the pendulum structure at a stand-off distance of 1 meter from the front plate. The motion of the blast pendulum was recorded with a high speed imaging camera (Figure 3.2), a rotation sensor placed in the axis of the pendulum and a mechanical indicator (Figure 3.3) giving the maximal angle reached by the pendulum during an experiment.

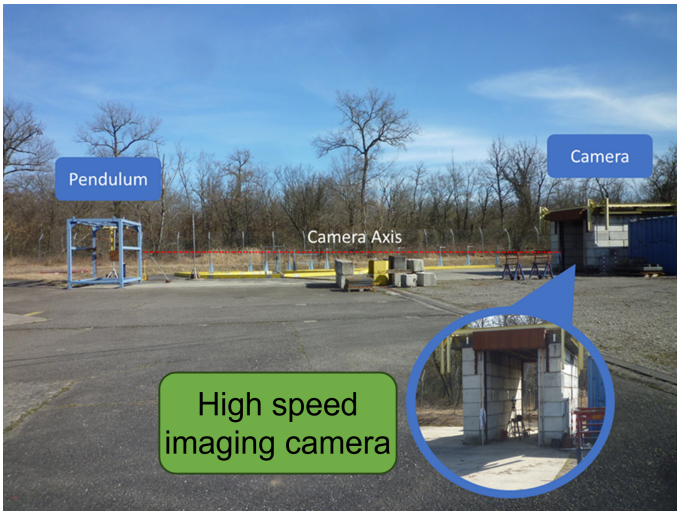

Figure 3.2: Placement of the high speed camera

Figure 3.3: Mechanical indicator giving the maximal angle of the pendulum

Overall, 39 experiments were performed with the blast pendulum.

- 10 experiments for the establishment of reference values
- 10 experiments with both a front and a back plate
- 6 experiments without a front plate
- 13 experiments with a confined fluid and tubes for fluid ejection

3.1.2 Reference values

In order to asses the effect of a water filled structure on the motion of the pendulum, a reference value needs to be established for a given weight and distance between the explosive charge and the load impact area of the pendulum

when no fluid is used.

3.1.2.1 Reference values for different charge distances

As the pendulum had previously been used at ISL by Reck [53], reference values were established for a pendulum equipped with 8 mm thick steel plates on either side of the pendulum body and stand-off distances of 0.5 m and 1 m from the square load impact plate for the explosive charge of 840 grams of C4, which is equivalent to 1 kg of TNT. As a first step, these experiments were reproduced and an additional intermediate stand-off distance of 0.66 m was added. The angle as a function of time for the different stand-off distances is shown in Figure 3.4 with a comparison to the experimental results previously obtained by Reck. Under identical conditions, the previously established experimental results could be accurately reproduced.

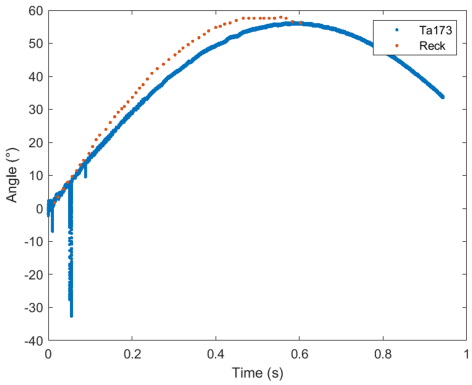

(a) Stand-off distance 0,5 m

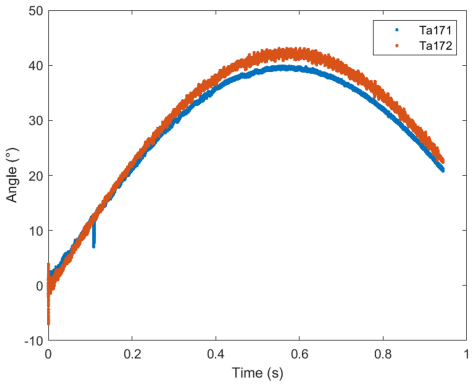

(b) Stand-off distance 0,66 m

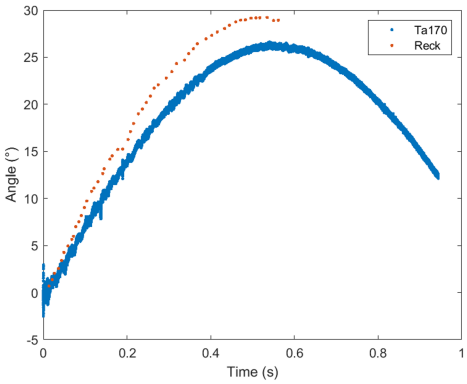

(c) Stand-off distance 1 m

Figure 3.4: Pendulum motion for different stand-off distance of the charge of C4, comparison to previous results by Reck [53]

3.1.2.2 Reference values for a different pendulum weight

To prevent the deformation of the steel rods used to assemble the structure described in the previous Section, a steel frame was added (Figure 3.5), the total weight of the pendulum for this reference being 215 kg. A new reference

had to be established in order to take into account the weight of 13.5 kg added by the frame. This reference was made for a charge of 840 g of C4 (equivalent to 1 kg of TNT) at a standoff distance of 1 m from the front plate. This reference will be used as a point of comparison for the investigation presented in this Chapter, where the maximal angle reached during the first oscillation of the pendulum at equal weight for fluid filled structures will be compared to the reference. The mean value, calculated for the two experiments of the pendulum at the new weight, is shown in Figure 3.6.

Figure 3.5: Frame for structure rigidity

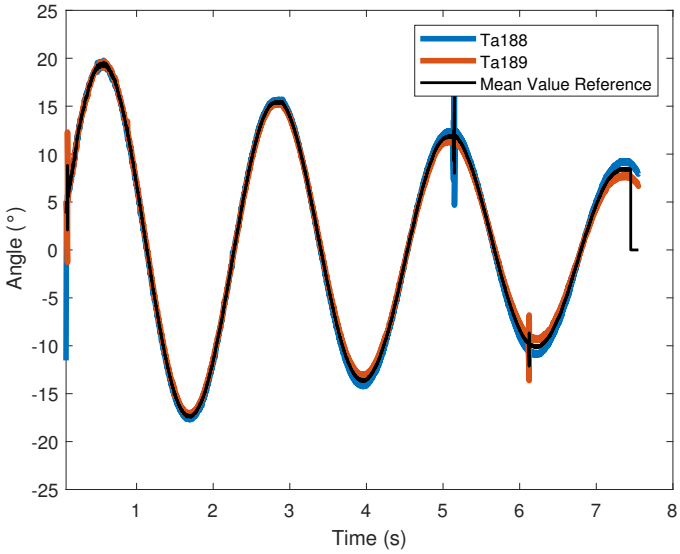

Figure 3.6: New reference with the addition of the stabilization frame, calculation of the mean value

In the case of this investigation, only the first oscillation of the pendulum is of interest. Figure 3.7 shows the first oscillation, where it can be seen that the signal is disturbed during the first 0.08 seconds of the experiment when the pendulum is first set into motion. Therefore, for the sake of clarity of the curves shown later in this investigation, the signal will be shown starting at 0.08 s as shown in Figure 3.8. The maximal angle and impulse values, calculated

with Equation 1.42 presented in Section 1.4.3.3, are presented in Table 3.1.

Table 3.1: Maximal angle and calculated impulse for the new reference including the stabilization frame

Experiment	Maximal Angle	Calculated Impulse (kg.m/s)
Ta188	$20.79°$	72.4
Ta189	$19.72°$	68.71
Mean Value	$20.26°$	70.55

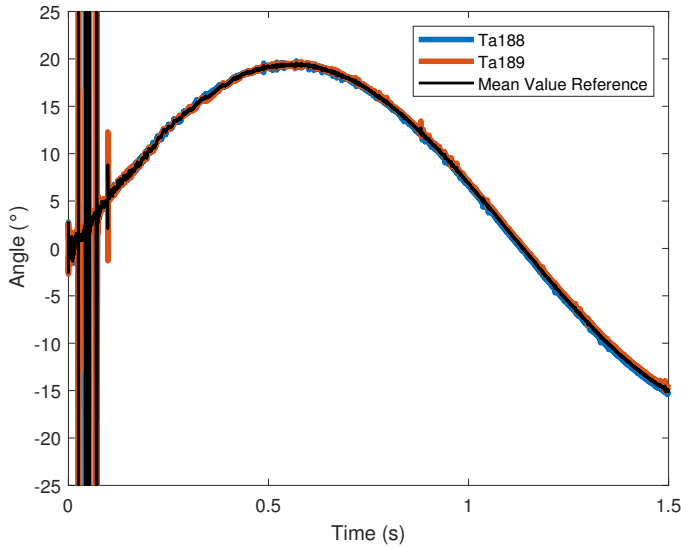

Figure 3.7: First oscillation of the pendulum for the new reference value, disturbed signal for the first 0.8 seconds of the experiment

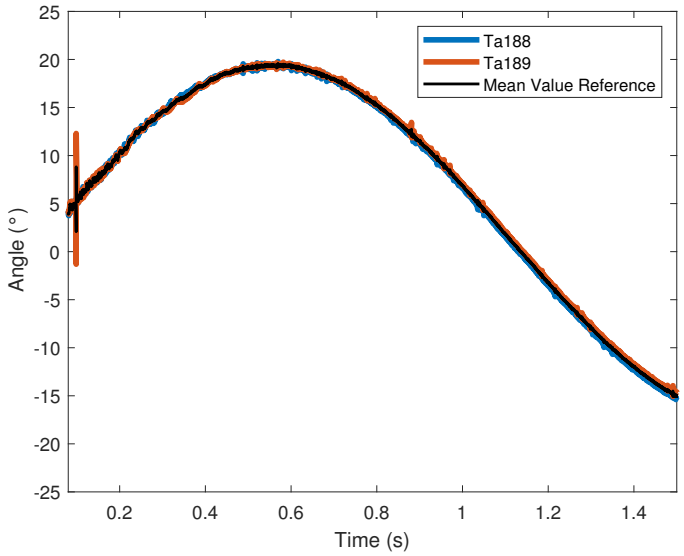

Figure 3.8: First oscillation of the pendulum for the new reference value

The experimental setup of the blast pendulum was adapted for the installation of a water filled bag placed in between two steel plates. A reference value was established for a charge of 840 g of C4 placed at a stand-off distance of 1 m of the impact plate. In this experimental investigation, the maximal angle of elevation of the pendulum (occurring during the first oscillation) can be assimilated to the maximum vertical displacement of a target following the detonation of an explosive charge below a vehicle. Thus, the maximal angle of elevation of fluid filled structures will be compared to the reference value where the pendulum has an equal weight without fluid.

3.2 First experimental configuration: variation of the water mass

3.2.1 Experimental configurations

In order to investigate the quantity of water needed for a reduction in the angle of elevation of the pendulum, the water mass present in the fluid filled bag, placed in between a front and a back plate was varied. This increase in water mass translates into a larger water height, which allows the improvement of impulse spreading as described in Section 2.5. Figure 3.9 shows a schematic illustration of the three experimental configurations used to investigate the variation of the water mass. For all three configurations, the total weight of the pendulum was kept constant and equal to the weight of the pendulum of the reference value. To account for an increased or decrease water mass, the thickness of the front and back plates surrounding the water bag were adjusted accordingly.

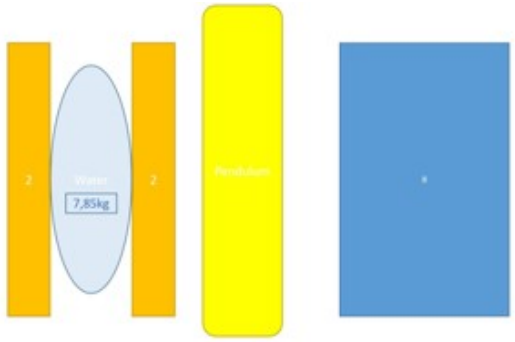

(a) 7.85 kg of water, 2 mm front plate, 2 mm back plate. The water mass represents 4.9% of the total pendulum weight.

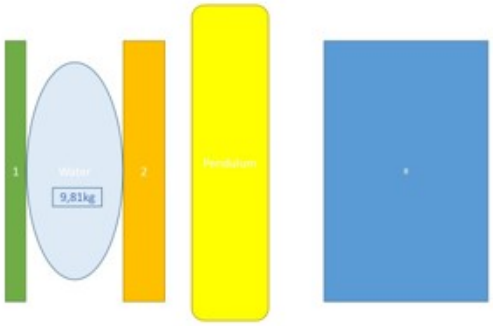

(b) 9.81 kg of water, 1 mm front plate, 2 mm back plate. The water mass represents 6% of the total pendulum weight.

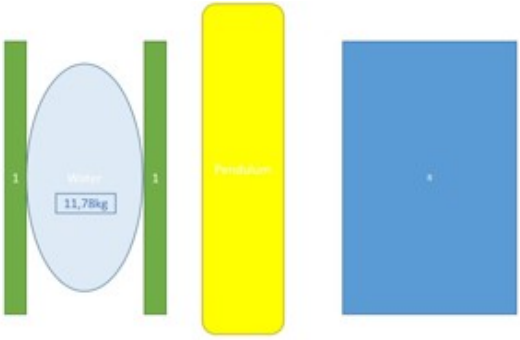

(c) 11.78 kg of water, 1 mm front plate, 1 mm back plate. The water mass represents 7.3% of the total pendulum weight.

Figure 3.9: Water filled bag surrounded by a front plate and a back plate. In blue the counterweight, in yellow the body of the pendulum, in orange the 2 mm thick plates and in green the 1 mm thick plates.

3.2.2 Comparison of the maximal angle of elevation

Figures 3.10, 3.11 and 3.12 show a comparison between the maximal angle reached by the pendulum for two repetitions for each experiment and the reference value for different water masses as recorded by the rotation sensor. For the water mass of 11.78 kg, the sensor did not work for the second experiment, however it was possible to determine the maximal angle reached by the pendulum during the experiment with the images taken by the camera. The values for all maximal angles are given in Table 3.2.

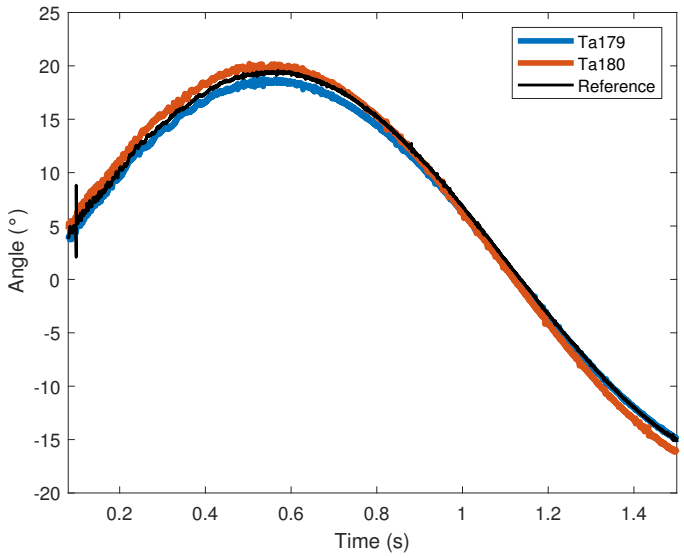

Figure 3.10: Angular elevation of the pendulum for a water mass of 7.85 kg, comparison to the reference value

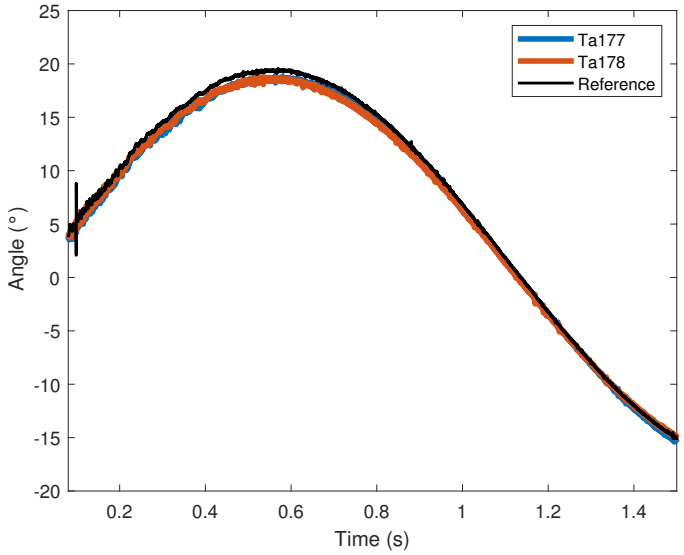

Figure 3.11: Angular elevation of the pendulum for a water mass of 9.81 kg, comparison to the reference value

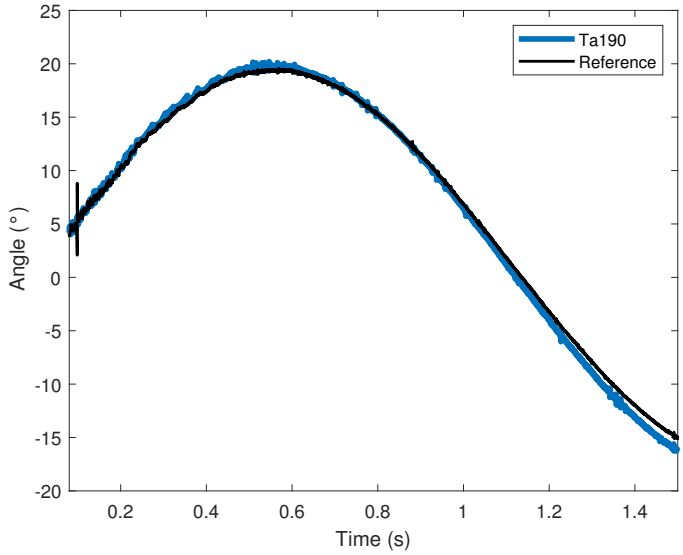

Figure 3.12: Angular elevation of the pendulum for a water mass of 11.78 kg, comparison to the reference value

Table 3.2: Maximal angle for different water masses

Reference	Water mass 7.85 kg		Water mass 9.81 kg		Water mass 11.78 kg	
Mean Value	Ta 179	Ta 180	Ta 177	Ta 178	Ta 187	Ta 190
$20.26°$	$18.84°$	$20.22°$	$18.92°$	$18.84°$	$18.81°$	$19.8°$

The use of water in the pendulum does not achieve a reduction in elevation. Figure 3.13 shows the first oscillation for an experiment with a water mass of 9.81 kg of water. It can be seen that water ejection occurs only after the pendulum has already been set into motion, when the entire momentum has already been transmitted to the pendulum structure. Therefore, it could be established with these experiments that the mass ejection can not occur too late after the detonation of the explosive charge as there is no benefit of the presence of fluid in that case. During the analysis of these results it has to be noted that the water mass represents only 5 to 7% of the total weight of the pendulum due to the difficulty of installing the water filled bag on the pendulum and the high weight of the pendulum body (with arms) of 130 kg. This might not be sufficient to observe notable reductions in angular elevation. Consequently, spreading water on the side following the observations made on the KEDD was unconclusive, mainly due to the large inertia of the water. The deformation of the rear plate was also negligeable, hence no effect of the wave attenuation due to the mechanical spreading were observed.

These results lead to the modification of the experimental target. In the work of Denefeld [31] on the dynamic impulse compensation concept (DIC) presented in Section 1.3.3.2, the ejection of the mass occurs at the moment of the detonation underneath the scaled model of the vehicle. One difficulty of this concept was the timing of such an ejection in a real case scenario when the moment of detonation is unknown. the advantage of a system with fluid ejection is that fluid is inherently movable without the necessity of an external trigger. It was consequently necessary to work on the direction of the water ejection, preferably on the direction of the pendulum rotation.

(a) t=0 ms, position of the pendulum at the start of the experiment

(b) t=1.643 ms, the luminosity of the fireball does not allow to visualize pendulum motion at the start of the experiment

(c) t=75.643 ms, when visualization becomes possible the pendulum has already been set into motion but the water is still situated in between the front and back plate

(d) t=160.643 ms, at this time the water ejection becomes notable (circled in red) but the pendulum has already been set into motion before the water ejection can occur

Figure 3.13: High speed camera images of the first oscillation of the pendulum for experiment Ta179

With these experiments, the importance of the timing of the water ejection with regards to the global motion of the structure could be highlighted. The pendulum is set into motion by the explosion long before the first water ejection occurs, thus no reduction in the angular elevation when comparing to the reference value could be observed. It is also worth noting that due to the difficulty of fastening the water filled bag between the front and back plates of the fluid filled structure, the water mass is small when compared to the total weight of the pendulum. Lastly, the direction of water ejection may not be appropriate as the front plate displacement is insufficient to push water on the side of the pendulum structure, as is the case for the KEDD device.

3.3 Second experimental configuration: variation of the water filled structure, influence of the front plate

3.3.1 Experimental configurations

As in the previous experimental configuration the water was trapped in between the front plate and back plate of the water filled structure and could therefore not be ejected before the pendulum was set into motion, it was chosen to repeat the previous configurations in terms of the water masses used but to remove the front plate to allow more freedom of motion to the fluid as depicted in Figure 3.14. To ensure a constant total weight of the water filled structure, the thickness of the back plate was increased.

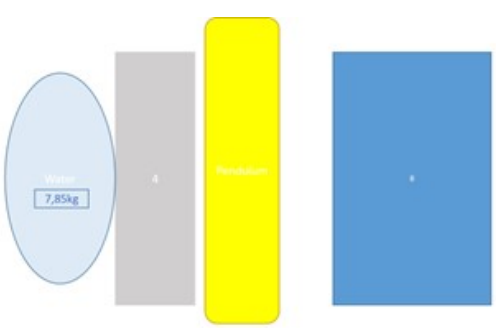

(a) 7.85 kg of water, 4 mm back plate

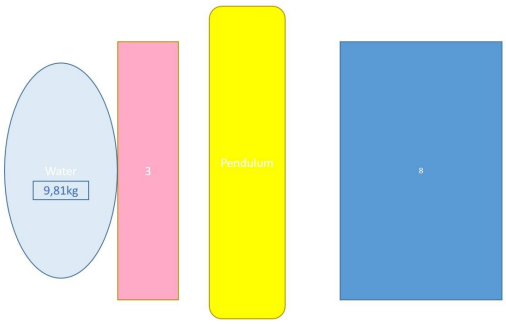

(b) 7.85 kg of water, 3 mm back plate

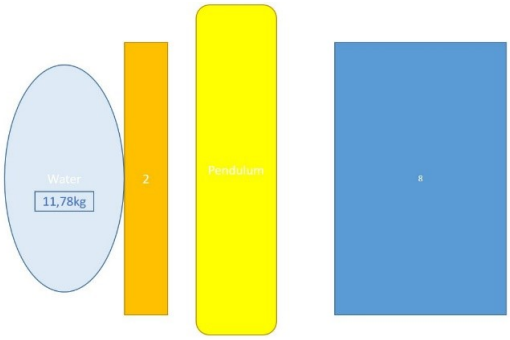

(c) 7.85 kg of water, 2 mm back plate

Figure 3.14: Water bag and back plate. In blue the counterweight, in yellow the body of the pendulum, in orange the 2 mm thick plates, in pink the 3 mm thick plates and in grey the 4 mm thick plates.

3.3.2 Comparison of the maximal angle of elevation

Figures 3.15 and 3.16 show the experimental results for a structure without front plate and the comparison to the reference value for a pendulum of equal weight but without fluid. For the experiments with a water mass of 9.81 kg of water, the sensor malfunctioned. Therefore, the maximal angle reached by the pendulum was observed with the images provided by the high speed camera. The values for all maximal angles are given in Table 3.3. It can be observed for this experimental configuration that a reduction of the maximal angle of elevation of the pendulum

occurs for the higher water masses of 9.81 and 11.78 kg. However, for the interpretation of these results it has to be noted that, as no front plate is present, the water ejection following the detonation can be directly projected towards the explosive charge, thus possibly mitigating the fire ball with the water droplets and therefore reducing the total impulse being transmitted to the pendulum.

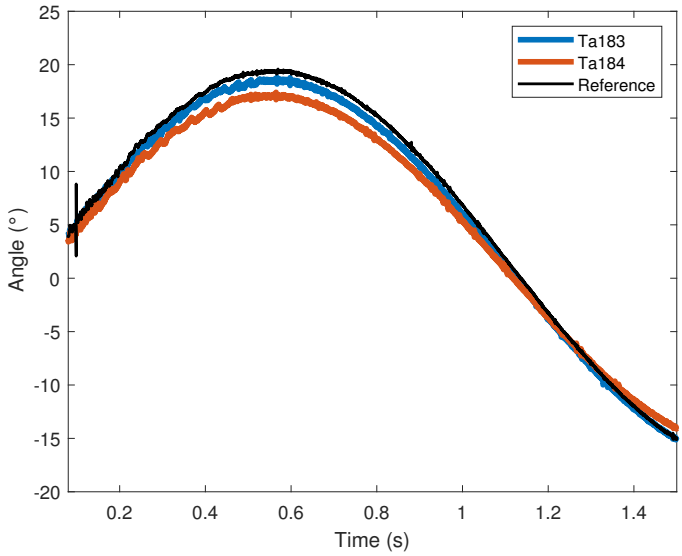

Figure 3.15: Angular elevation of the pendulum for a water mass of 7.85 kg, comparison to the reference value

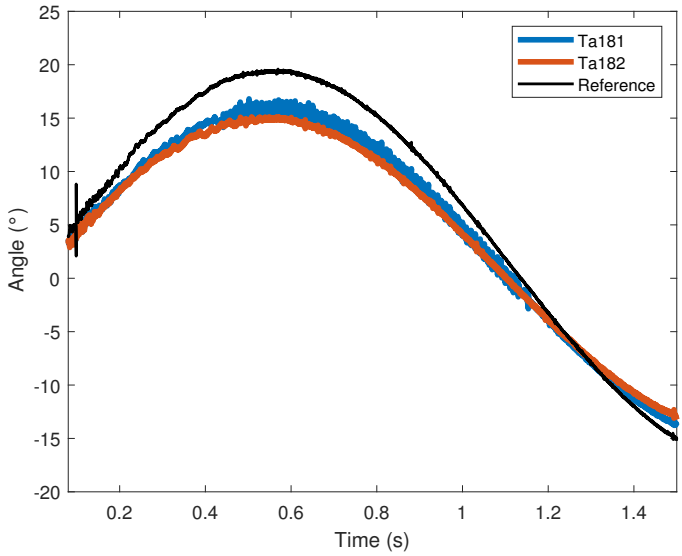

Figure 3.16: Angular elevation of the pendulum for a water mass of 11.78 kg, comparison to the reference value

Table 3.3: Maximal angle for different water masses

Reference	Water mass 7.85 kg		Water mass 9.81 kg		Water mass 11.78 kg	
Mean Value	Ta 183	Ta 184	Ta 185	Ta 186	Ta 181	Ta 182
$20.26°$	$18.82°$	$17.41°$	$17.8°$	$17.41°$	$15.82°$	$15.11°$

Through this alternative experimental configuration, it could be observed that without a front plate the fluid does not get trapped between both plates and can more freely choose its path of evacuation. Results of the numerical investigation of the location of the opening in a fluid filled container presented in Section 2.4.2 already discussed the influence of the opening allowing fluid ejection, highlighting that the path taken by the water towards the opening had to be as direct as possible. Whilst these results regarded local impulse, the experiments with the blast pendulum indicate that the location of the opening for fluid ejection is also of importance for the global momentum transmission. In this particular case, water could be ejected in the direction of the explosive, the expansion of the fireball could be limited thus reducing the impulse transmitted to the pendulum. However, when considering vehicle integration the fluid still has to be contained in an enclosed structure. Therefore, a filled structure with tubes serving as openings will be considered in the next Section.

3.4 Third experimental configuration: direction of water ejection

In the previous experimental investigations, the pendulum was set into motion before the water could be ejected. Therefore, no influence on the angle of elevation of the pendulum could be observed. Then it was observed that, by removing the front plate and allowing the water to mitigate the fireball, a reduction of the angle of elevation was seen. In this section, the direction of water ejection will once again be changed, based on the the study by Denefeld [31] of the dynamic impulse compensation concept (DIC) presented in Section 1.3.3.2. This study shows that the direction of ejection of the compensating mass needs to be in the same direction as the blast loading in order for the velocity vector generated by the vertical acceleration of the vehicle to be counteracted by the velocity vector generated by the ejection of the mass accordingly to Newton's third law of motion. This observation, completed by the previous results on impulse spreading showing that fluid needs to be able to follow the most direct path towards the free surface boundary, lead to the need to modify the experimental setup by controlling the direction of water ejection.

3.4.1 Modification of the experimental setup

The previously presented pendulum had to be modified to allow the passage of a tube serving for water ejection through the body of the pendulum. Figure 3.17 illustrates the placement of the tube forcing the direction of water ejection, requiring holes to be made in the back plate and the body of the pendulum. For the side confinement of the fluid, a frame was added in between the front and back plate, allowing for a closed fluid filled structure where the only openings are provided by the tubes. In this particular case, the front plate had a thickness of 2 mm and the back plate had a thickness of 1 mm. During a given experiment, the tube has to be fastened to the body of the pendulum. As welding the tube directly to the back plate of the fluid filled structure would increase the preparation time in between each experiment, it was chosen to weld a stopper ring on one side of the tube (the side towards the explosive charge) and to use a clamped ring to stop the translation movement of the tube (Figure 3.18).

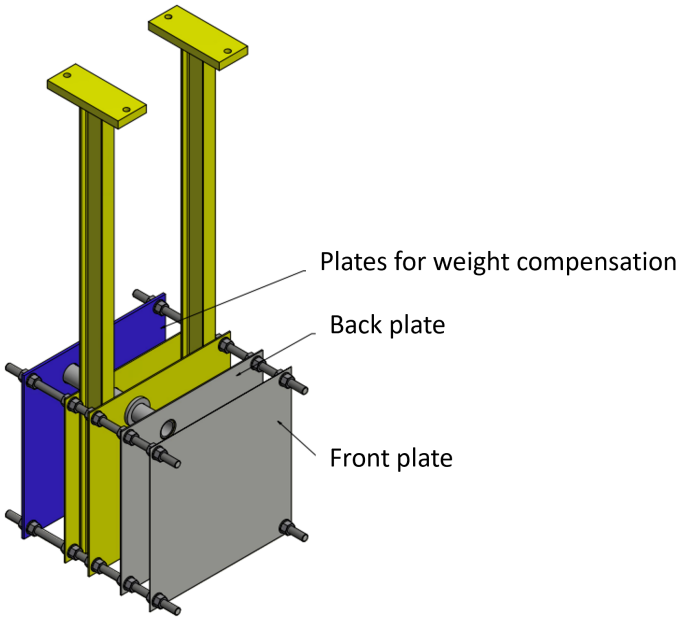

(a) New configuration of the pendulum with holes in the pendulum body for the insertion of a tube to guide the direction of water ejection. The confinement frame inserted between front and back plate is not shown in this schematic

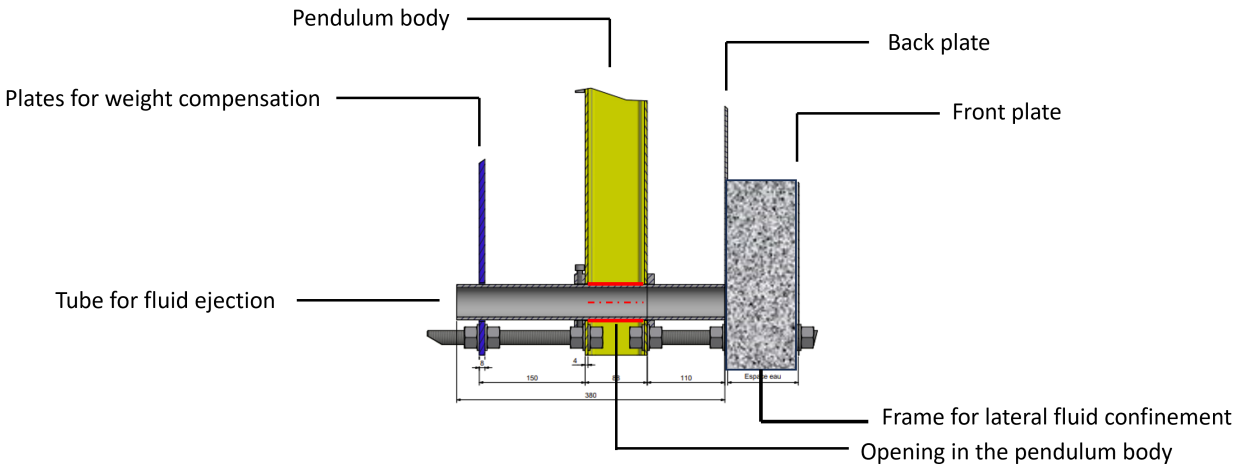

(b) Detail of the modification of the body of the pendulum allowing the passage of a tube

Figure 3.17: Schematic representation of experimental setup allowing the evacuation of the fluid through tubes at the back of the pendulum

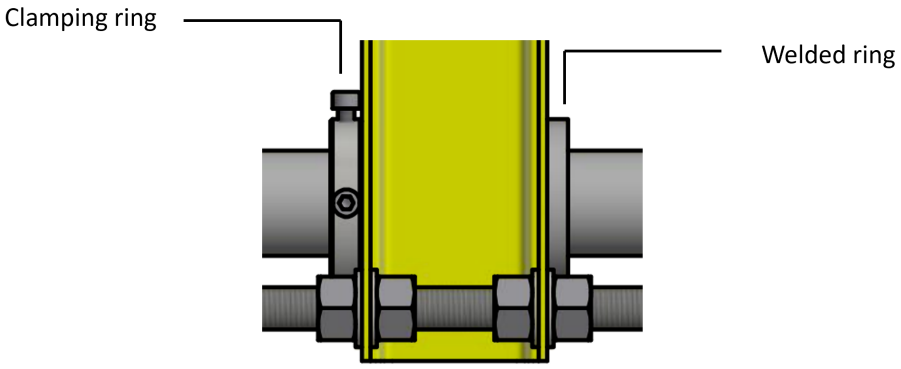

Figure 3.18: Welded ring and clamped ring holding the tube into place during an experiment whilst allowing an easy removal

3.4.2 Experimental difficulties: sealing of the water filled structure

Several experimental difficulties, mainly regarding the sealing of the water filled structure were encountered during this investigation. In this Section, these difficulties and the applied solutions will be described in chronological order, as the solution to one difficulty often revealed the next. It should be noted that for each difficulty encountered, several tests were carried out to better understand how to improve the architecture. It should also be reminded that between the possible improvements available at the time, most choices were also conditioned by the time available to develop and test the solutions. Some of the solutions developed here could serve as a guide to tackle similar issues in the integration phase, should this kind of protective structure be implemented onto a vehicle.

3.4.2.1 Seal of the water filled structure

The first approach to containing the water was to use the same bags as used in the previous experiments to contain the water before the experiment and to use frame made out of polystyrene foam for the confinement during the experiment (Figure 3.20b). However, after a first experiment, it was found that the water bag would rupture towards the front plate and thus covering the openings on the back plate in which the tubes are inserted, preventing the fluid from being ejected out of the structure (Figure 3.19).

Figure 3.19: Image taken after the experiment. Use of the previously used bags to contain the water. The water bag ruptures towards the front plate, thus covering the entrance of the tubes and preventing water ejection.

It was therefore chosen to completely fill the polystyrene structure without other means of containing the water. In that case the openings of the tube had to be sealed, which was done by using adhesive tape and aluminum foil (Figure 3.20a) applied to the back plate of the structure and covering the opening of the tube. Whilst some water leaking next to the polystyrene framing could be observed, the amount of water leaking from the fluid filled structure was reasonable if the time between setup and completion of the experiment was short by filling the structure at the last moment.

(a) Aluminum foil and tape to seal the tube openings (b) Polystyrene frame for lateral confinement

Figure 3.20: Sealing of the water filled structure

After experiments with this new solution for containing the water, it could be observed that no water ejection through the tube occurred and that the front plate presented no deformation, thus not pushing the water for its ejection. On the contrary, for an experiment where the leak of the polystyrene confinement was more important and the structure was not fully filled towards the top, a deformation of the plate could be observed only towards the top. Therefore, one hypothesis was that the front plate needs to deform inwards of the water filled structure to allow its ejection and overcome the inertia of the water.

3.4.2.2 Preliminary cutting of the front plate

Thus, a preliminary cut was made in the front plate before an experiment to allow its acceleration into the water following the detonation of the explosive charge. Figure 3.21 shows this cut, where a 1 mm gap was left between each cut to hold the center of the plate in place before the experiment.

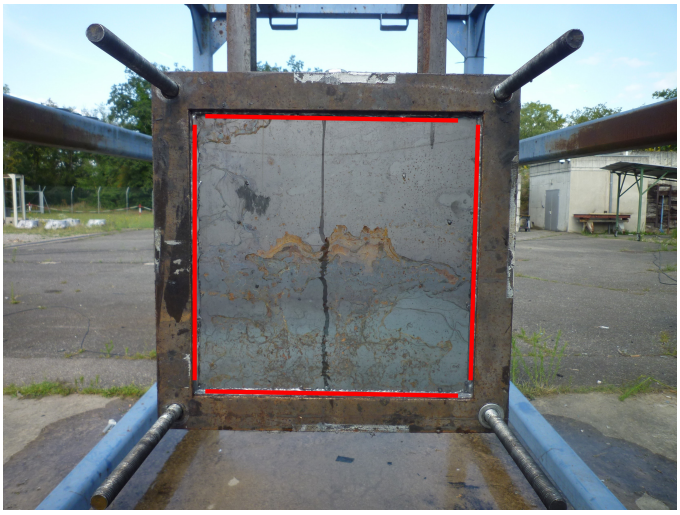

Figure 3.21: Preliminary cutting of the front plate to allow the projection of the front plate into the water filled structure. Cuts are highlighted in red

In this case, it was observed that the plate was fully projected into the fluid filled structure and caused the displacement of the water. However, due this projection, the polystyrene framing did rupture and therefore the confinement (and direction of ejection) could not be sufficiently controlled with this experimental configuration.

3.4.2.3 Addition of a rigid frame

To ensure the lateral confinement of the fluid during an experiment, the rigidity of the frame had to be increased. This was done by manufacturing an aluminum frame to replace the previously used polystyrene frame. The structure could be filled through two openings in the top of the aluminum frame that could be closed during the experiment (Figure 3.22).

Figure 3.22: Aluminum frame for lateral water confinement

Finally, a correct water confinement was ensured with this experimental configuration. Therefore, future investigations will be made with fluid filled directly into a structure made of a pre-cut front plate, an aluminum frame for lateral confinement and a back plate where openings are covered with aluminum foil and adhesive tape. For this setup, the water mass used corresponds to the volume allowed by the aluminum frame and is of 16 kg, which is 7% of the total pendulum mass. Similarly to Section 3.1.2.2, the total mass of the pendulum was changed through the addition of the aluminum frame and the different water mass and is now of 231 kg. A new reference value has to be established for future comparisons between the maximal angular elevation of a fluid filled structure and a pendulum of equal weight without water.

3.4.3 Comparison of the maximal angle of elevation

The experimental investigations for this particular configuration are ongoing. A first result with four openings of a diameter of 100 mm as illustrated in Figure 3.23 can be shown. The images provided by the high speed camera

shows that in this case, water ejection occurs before pendulum motion (Figure 3.24). Figure 3.25 shows the comparison of the angular elevation of the pendulum for the aforementioned fluid filled structure and a reference value. A reduction of the maximal angular elevation of around $4°$ can be observed, corresponding to 35% of the reference maximal angle.

Figure 3.23: Experimental setup with four openings with a diameter of 100 mm for water ejection (front plate not shown)

(a) t=41.317 ms, start of the water ejection before pendulum motion

(b) t=60.317 ms, water ejection before pendulum motion

(c) t=91.317 ms, directed water ejection

(d) t=245.317 ms, pendulum motion once the majority of the fluid is ejected

Figure 3.24: High speed camera images of the first oscillation of the pendulum for experiment Ta265

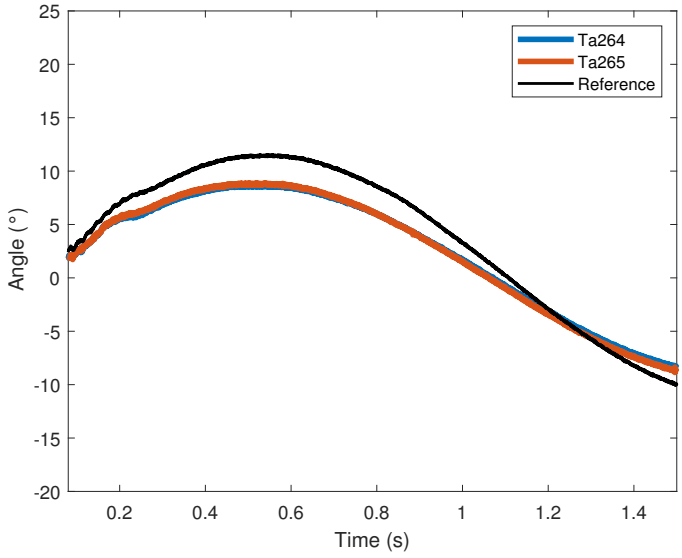

Figure 3.25: Angular elevation of the pendulum for a fluid filled structure with 4 openings of diameter 100 mm

The third experimental setup represents a first step towards integration of a fluid filled structure in a vehicle with an intentional path for fluid ejection through tubes. A first phase of this investigation consisted in establishing a working experimental setup and solving issues mainly related to the sealing of a fluid filled structure installed on a blast pendulum. First experimental results show a reduction of the angular elevation of the pendulum when equipped with a fluid filled structure and show the potential of such a solution for global momentum reduction.

Conclusions and perspectives

This work aimed at investigating the transmission of a blast wave through a fluid filled structure, identifying the levers on which to act on in order to design a protective structure acting on momentum transmission to a vehicle. Impulse spreading and global momentum transfer were investigated in particular.

The investigation of impulse spreading (Chapter 2) made use of a novel experimental setup where a water filled container was subjected to blast loading. Measurements were provided through a pressure sensor at the bottom of the container and high speed camera images allowing the visualization of the compression wave in the water. Experimental results revealed that a local reduction in impulse could be achieved through the presence of fluid. This experimental observation could only be made locally at the sensor location. Impulse distribution on the entirety of the container bottom was investigated with a numerical model. Numerical results showed that the presence of a fluid allows for the spreading of impulse over a larger area at a lower intensity. Several parameters were varied experimentally and numerically to identify their influence on impulse spreading. To allow a spherical propagation of the compression wave in the fluid container, the area of application of the blast loading needs to be smaller than the area made up of fluid. In that case, impulse spreading can be observed as the difference between the highest measured impulse (occurring at the center of the container) and the lowest impulse measurement (occurring at the border of the container). By varying the container depth, it was shown that for a deeper container the radius of the spherical compression wave is larger and the difference between the impulse at the center of the target and its border is less pronounced, increasing impulse spreading. The addition of a lid on the container allowed to vary its degree of confinement, with fluid confinements of 0, 50 and 100% being studied experimentally and additional confinement levels of 25 and 75% being studied numerically. For a fully confined fluid, no local impulse reduction or impulse spreading occurs. When the fluid is able to be ejected out of the protective structure, local impulse reduction at the center of the target can be measured. Impulse spreading increases with the size of the surface area where fluid is able to move out of the container. The location of the free surface area was investigated numerically by placing the opening corresponding to 50% fluid confinement on the top, side and bottom of the container. Here it was shown that providing the most direct path for the fluid to be ejected out of the structure increases impulse spreading. As the structure of the container could be considered fully rigid, the entirety of the impulse from the blast loading was transmitted to the bottom of the container, which allowed the study of impulse spreading but not

of momentum transfer.

Therefore, in Chapter 3, an experimental setup that allowed a fluid filled structure to be set in motion following its interaction with a blast wave was used, a blast pendulum. This allows the study of the effects of fluid on global momentum transmission. The main work done in this Chapter focused on the design of such a structure, mainly to provide sufficient sealing of the water. As such, the experimental difficulties encountered during this design process reflect the design challenges of the future integration of fluid filled structures on vehicles. Preliminary results show the potential of a fluid filled protection for the reduction of global momentum transmission.

With regards to the conclusions drawn from this study, different perspectives for future investigations can be explored.

A further academic study on the type of fluid used in the protective structure could be of interest. Mainly, fluids already present in a vehicle such as cooling fluid or oil should be investigated as their use would have a less significant impact on the overall added weight due to the protective solution. This could be done experimentally, keeping in mind the difficulties of the ejection of such types of fluids in respects to environmental norms. The numerical models prepared in this work could in this case be a good compromise as a modification of the material laws and equation of state assigned to the fluid could give interesting first numerical results. Furthermore, the fluid filled structure equipped with tubes for fluid ejection used on the blat pendulum described in Chapter 3 provided interesting preliminary experimental results. Experiments with a different number of tubes and different tube diameters are ongoing and hope to improve current knowledge. However, the design of this structure still proves to be difficult to implement experimentally. With fluids being rarely used on a blast pendulum, the novelty of this experimental setup requires several iterations in the design of the water filled structure before providing usable results. In this context, a numerical model of the blast pendulum and the fluid filled structure should be established to aid the design process at a lower cost. Further steps from the academic study of wave propagation in a structure towards vehicle integration could be taken, with the use of experimental setups closer to the actual final use to the protective solution. For example, a fluid filled structure could be tested in an underbelly configuration with the use of steel pots. Such an investigation could be carried out with the experimental means of ISL.

In the case of an integration of a fluid filled structure for protection purposes on a vehicle, the influence of the particular geometry of the structure on the wave propagation inside the fluid will have to be reviewed. As with the experimental setup, the fluid filled structure will be finite and therefore reflections of the compression wave in water on the borders of the structure will have to be checked, as well as the effects of overpressure peaks. With these design guidelines, limitations in vehicle integration have to be kept in mind. Similarly to the integration of tubes for fluid ejection on the blast pendulum, technical solutions for fluid confinement and release in accordance to the existing vehicle space requirements have to be found.

Appendix A

Extended abstract

This thesis being a French-German collaboration, the main language chosen for communication was English. A condensed version of the main results of the thesis are given in both German and French as well as in English.

A.1 Français

Introduction

Lors de la détonation d'une charge explosive sous le plancher d'un véhicule, telle qu'une mine enterrée ou un engin explosif improvisé, deux effets principaux se produisent : la déformation ou rupture du plancher due à la contrainte transmise par le blast et l'accélération verticale globale du véhicule pouvant mener à son retournement due à l'impulsion qui lui est transmise. Dans un but de protection, de nombreuses études dans la littérature se concentrent sur la transmission du chargement afin de réduire les déformations du plancher mais très peu d'études se concentrent sur la transmission d'impulsion, et donc de variation de quantité de mouvement. L'utilisation de fluides, en particulier l'eau, a été identifié comme pouvant potentiellement permettre d'agir sur cette transmission d'impulsion. Néanmoins, les quelques études présentes dans la littérature se focalisent sur les effets de la présence de l'eau dans la protection. Elles évaluent ainsi la réduction d'impulsion transmise à une cible par la déformation de celle-ci. Ainsi, ces travaux proposent d'identifier les phénomènes ayant lieu dans le fluide en lui-même agissant sur la transmission d'impulsion, se plaçant donc en amont de la cible. Des études expérimentales utilisant un tube à choc explosif permettant de transmettre un blast proche de celui généré par une mine enterrée à un conteneur rempli d'eau ont été réalisées. Ces études expérimentales ont été complétées par des simulations numériques, permettant de surmonter certaines limitations tel que le nombre de points de mesure. Il a été montré que l'utilisation d'un fluide dans une protection contre les effets de souffle permet un étalement de l'impulsion, et donc sa diminution locale. Un lien entre la surface libre permettant au fluide d'être éjecté de la protection et cet étalement d'impulsion a été établi. Pour une compréhension plus globale du phénomène, un pendule à blast a été utilisé pour observer les effets d'un fluide dans une protection sur la quantité de mouvement. Ce second dispositif expérimental a été utilisé afin d'étudier l'effet de la direction d'éjection du fluide par rapport à l'origine du chargement par le blast.

Etude de l'étalement de l'impulsion

Description du dispositif expérimental et du modèle numérique

Un dispositif expérimental a été conçu pour l'étude d'un liquide contenu dans un conteneur soumis à un chargement explosif (Figure A.1). Ce dispositif expérimental comprend un tube à choc alimenté par explosifs générant une onde plane avec une charge de 15 ou 30 grammes de C4 placée à une distance de 50 mm de l'entrée du tube. Ce tube a une dimension interne de 80 par 80 mm et une longueur de 1750 mm. Sur la partie basse du tube, une plaque de dimension 100 par 100 mm ayant une épaisseur de 1.5, 3 ou 5 mm est maintenue par une bande adhésive jusqu'à interaction de l'onde de choc générée par le tube avec la plaque. Suite à cette interaction, la plaque est projetée dans le conteneur rempli d'eau. Ce conteneur a une dimension de 200 par 200 mm et une profondeur de 50 ou 100 mm. Au cours d'une expérience, des mesures peuvent être réalisées par un capteur de pression PCB

placé au centre du fond du conteneur. Une caméra à haute vitesse permet de visualiser la propagation de l'onde de compression dans l'eau au cours de l'expérience.

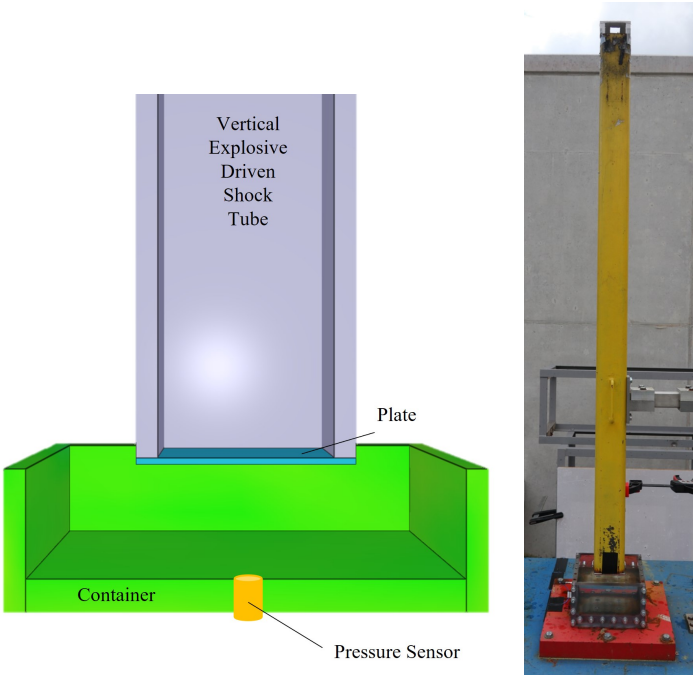

Figure A.1: Dispositif expérimental

Ce dispositif expérimental a été étendu par l'ajout de couvercles sur le conteneur permettant l'étude de différents degrés de confinement du fluide par fermeture de tout ou partie de la surface libre du fluide. Ceci permet de restreindre la capacité du fluide à être éjecté du conteneur (Figure A.2).

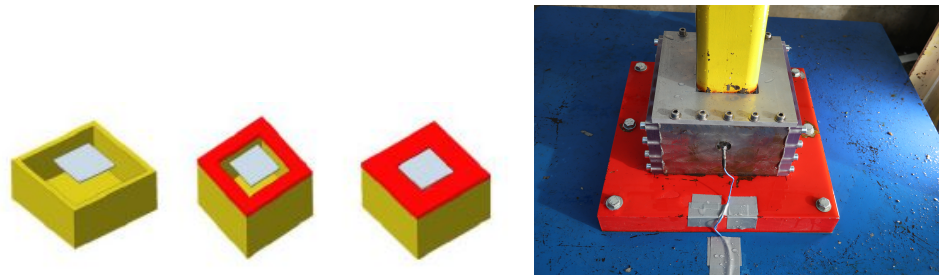

(a) Représentation schématique des nivaux de confinement. De gauche à droite : 0% , 50% et 100 %

(b) Illustration d'un confinement du fluide à 100%

Figure A.2: Dispositif expérimental permettant une variation du degré de confinement

Une valeur de référence décrivant le chargement transmis à la plaque à été acquis expérimentalement. A cette fin, la partie basse du tube à été placée directement en contact avec le capteur de pression, permettant ainsi une mesure du profil de pression lors de conditions de réflexions parfaites. Une comparaison entre le signal mesuré par le capteur de pression au fond du conteneur rempli d'eau et cette référence permettra l'évaluation de l'efficacité de la structure remplie d'eau à des fins de protection. La Figure A.3 montre la courbe pression-temps et impulsion-temps

pour une telle référence lorsque 15 g de C4 sont utilisés.

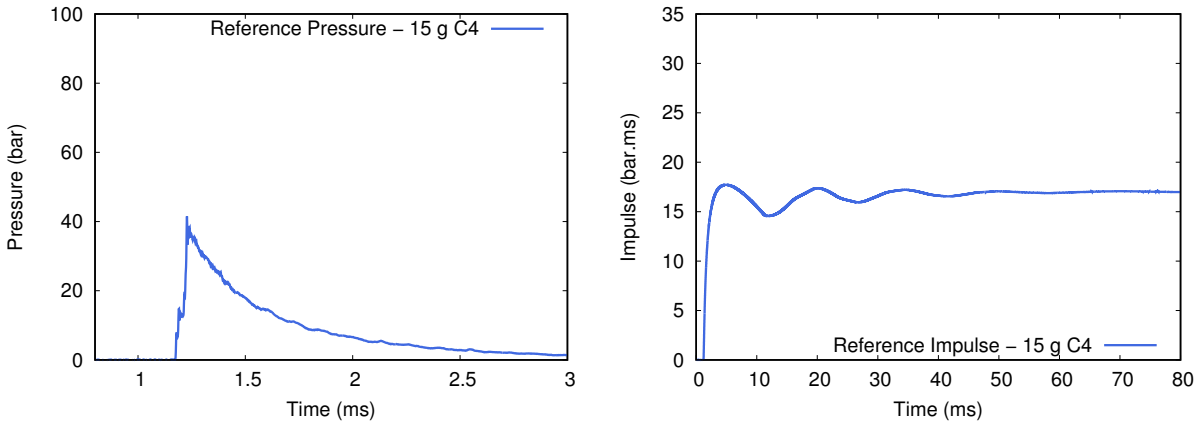

(a) Pression de référence – 15 g de C4

(b) Impulsion de référence – 15 g de C4

Figure A.3: Chargement appliqué à la plaque par le tube de choc alimenté par explosifs servant de valeur de référence, 15 g de C4

Le dispositif expérimental à été reproduit numériquement avec LS-Dyna. L'eau et l'air sont simulés par une formulation d'éléments ALE (arbitrairement lagrangien eulérien) et la plaque est simulée par une formulation d'éléments lagrangienne. Afin d'optimiser le temps de calcul, une simulation partielle du dispositif expérimental est réalisée en n'intégrant pas le tube et la charge explosive au modèle. Plutôt, le chargement de référence ayant été déterminé expérimentalement est directement appliqué aux nœuds supérieurs de la plaque. Afin d'améliorer davantage le temps de calcul, les symétries présentes dans le dispositif expérimental sont exploitées, permettant la simulation d'un quart de modèle. Un ensemble de nœuds contraints pour toutes rotations et translations sont utilisés pour définir les conditions limites correspondant aux parois du conteneur et aux zones de confinement. Le modèle numérique a permis de surmonter la limitation expérimentale liée à l'unique point de mesure sur le fond du conteneur en permettant le placement de points de mesures numériques sur l'entièreté du fond du conteneur. Pour ces travaux, un intérêt particulier est porté aux capteurs sur la diagonale du fond du conteneur (Figure A.4) , T1 correspondant au point de mesure au centre du fond du conteneur et T121 étant le point de mesure le plus éloigné sur la diagonale.

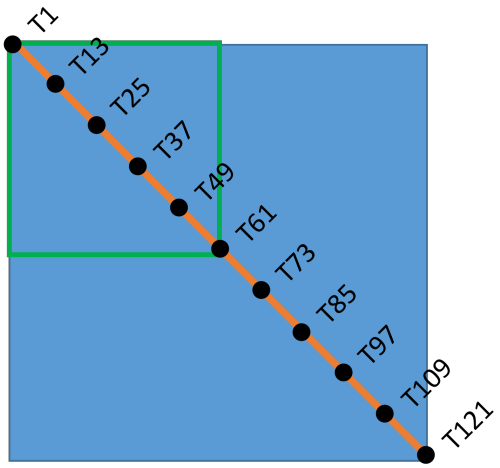

Figure A.4: Points de mesure placés sur la diagonale du fond du conteneur dans le modèle numérique

Etude de la variation de la vitesse de la plaque

Afin d'étudier la capacité de l'eau à agir sur la distribution d'impulsion au fond du conteneur, il a été choisi de faire varier l'intensité de l'onde de compression en variant la vitesse avec laquelle la plaque est projetée dans l'eau.

Cette variation de vitesse a pu être obtenue en utilisant différentes épaisseurs de plaques, ayant donc des masses différentes. La comparaison des courbes pression-temps (Figure A.5a) pour les différentes vitesses de plaque montre que, au centre du fond du conteneur, la mesure du premier pic de surpression est d'intensité comparable ou supérieure à celle de la valeur de référence. Toutefois, si l'on considère l'impulsion, la Figure A.5b montre qu'une réduction d'impulsion locale a pu être atteinte pour toutes les vitesses de plaque. Alors que les plaques de 1.5 mm et de 3 mm offrent un niveau équivalent de réduction de l'impulsion, la plaque plus lente de 5 mm semble fournir un niveau plus élevé d'impulsion locale.

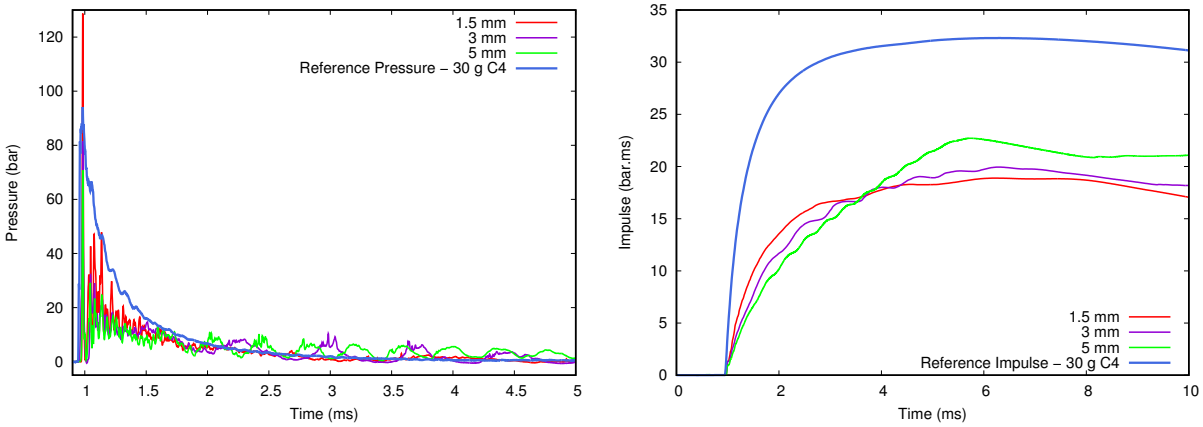

(a) Mesure locale de pression

(b) Mesure locale d'impulsion

Figure A.5: Comparaison de mesures locales au centre du fond du conteneur pour trois différentes vitesses de plaque et comparaison avec la valeur de référence pour l'utilisation de 30 g de C4.

Le modèle numérique permet de tracer l'étalement d'impulsion sur l'ensemble du fond du conteneur (Figure A.6) pour différentes masses d'explosif et d'épaisseurs de plaque. La Figure A.6 montre une cartographie 3D de l'impulsion transmise au fond du conteneur une fois que le chargement appliqué sur la plaque est entièrement transmis au fluide dans le cas d'une profondeur de conteneur de 50 mm. Un étalement de l'impulsion se produit le long de la diagonale sur le fond du conteneur. L'impulsion la plus forte est mesurée au centre du fond du conteneur et diminue progressivement le long de la diagonale. Les résultats numériques montrent que la vitesse de la plaque ne semble pas avoir d'influence significative sur l'allure de l'étalement d'impulsion.

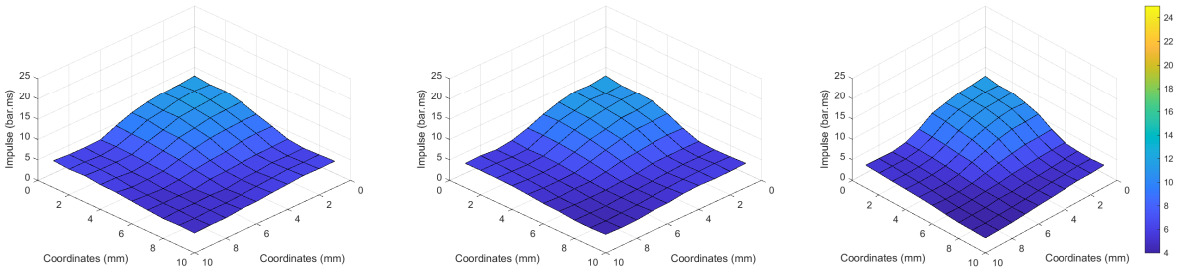

(a) 1.5 mm plate - 15 g C4 (b) 3 mm plate - 15 g C4 (c) 5 mm plate - 15 g C4

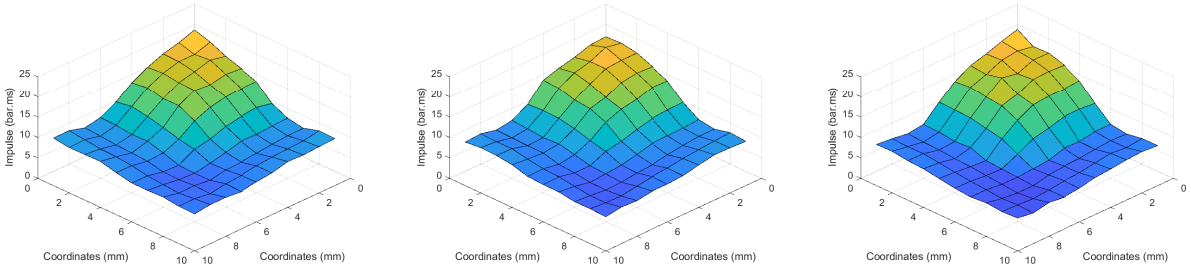

(d) 1.5 mm plate - 30 g C4 (e) 3 mm plate - 30 g C4 (f) 5 mm plate - 30 g C4

Figure A.6: Distribution de l'impulsion sur le fond du conteneur pour différentes masses d'explosif et d'épaisseurs de plaque, t = 8 ms – 0% de confinement, profondeur de conteneur de 50 mm

Étude du confinement du fluide et de la hauteur d'eau

Au cours des expériences étudiant la variation de la vitesse de la plaque, une grande quantité du fluide initialement présent dans le conteneur à été éjecté en raison de la surface libre de l'eau. Ainsi, l'influence du confinement de ce fluide sur les mesures pouvant être réalisées au fond du conteneur a été étudiée. Cette étude à été faite avec trois niveaux de confinement de fluide (0, 50 et 100%).

Expérimentalement, l'influence du niveau de confinement sur la mesure d'impulsion locale au fond du conteneur a été étudiée pour une charge de 15 g de C4, une épaisseur de plaque de 3 mm et une hauteur d'eau de 50 mm (Figure A.7). Il peut être observé qu'une réduction locale d'impulsion similaire est obtenue dans le cas où le fluide n'est pas confiné et le cas où le fluide est confiné a 50%. Au contraire, pour un fluide totalement confiné, aucune réduction d'impulsion locale ne peut être mesurée. Ces observations locales très intéressantes semblent indiquer l'importance de la capacité du fluide à être éjecté du conteneur.

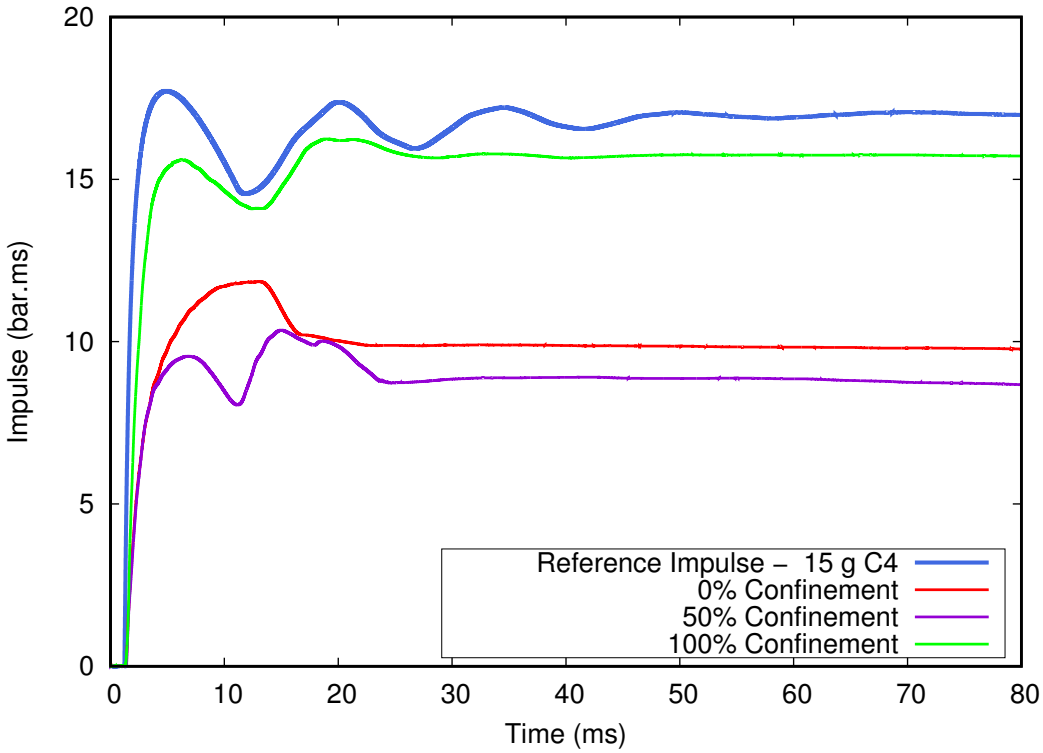

Figure A.7: Mesures expérimentales de l'impulsion locale pour différents niveaux de confinement – 15 g de C4, plaque de 3 mm, hauteur d'eau de 50 mm

Un modèle numérique reproduisant les niveaux de confinement de l'eau étudiés expérimentalement (0, 50 et 100%) permet d'observer l'étalement de l'impulsion le long de la diagonale sur le fond du conteneur (Figure A.8). Dans le cas d'un fluide non confiné (Figure A.8a), un étalement de l'impulsion se produit le long de la diagonale du conteneur, l'impulsion la plus forte étant mesurée au centre du conteneur et diminuant progressivement lorsqu'on se déplace vers le bord du conteneur. Pour un niveau de confinement du fluide de 50% (Figure A.8b), la réduction locale de l'impulsion au centre du conteneur se produit de la même manière que dans le cas d'un fluide non confiné. Cependant, l'étalement de l'impulsion le long de la diagonale sur le fond du conteneur est moins prononcé dans ce cas. Comme aucun étalement d'impulsion ne se produit lorsque le fluide est entièrement confiné (Figure A.8c), il peut être conclu que l'étalement d'impulsion est très probablement dû aux conditions limites.

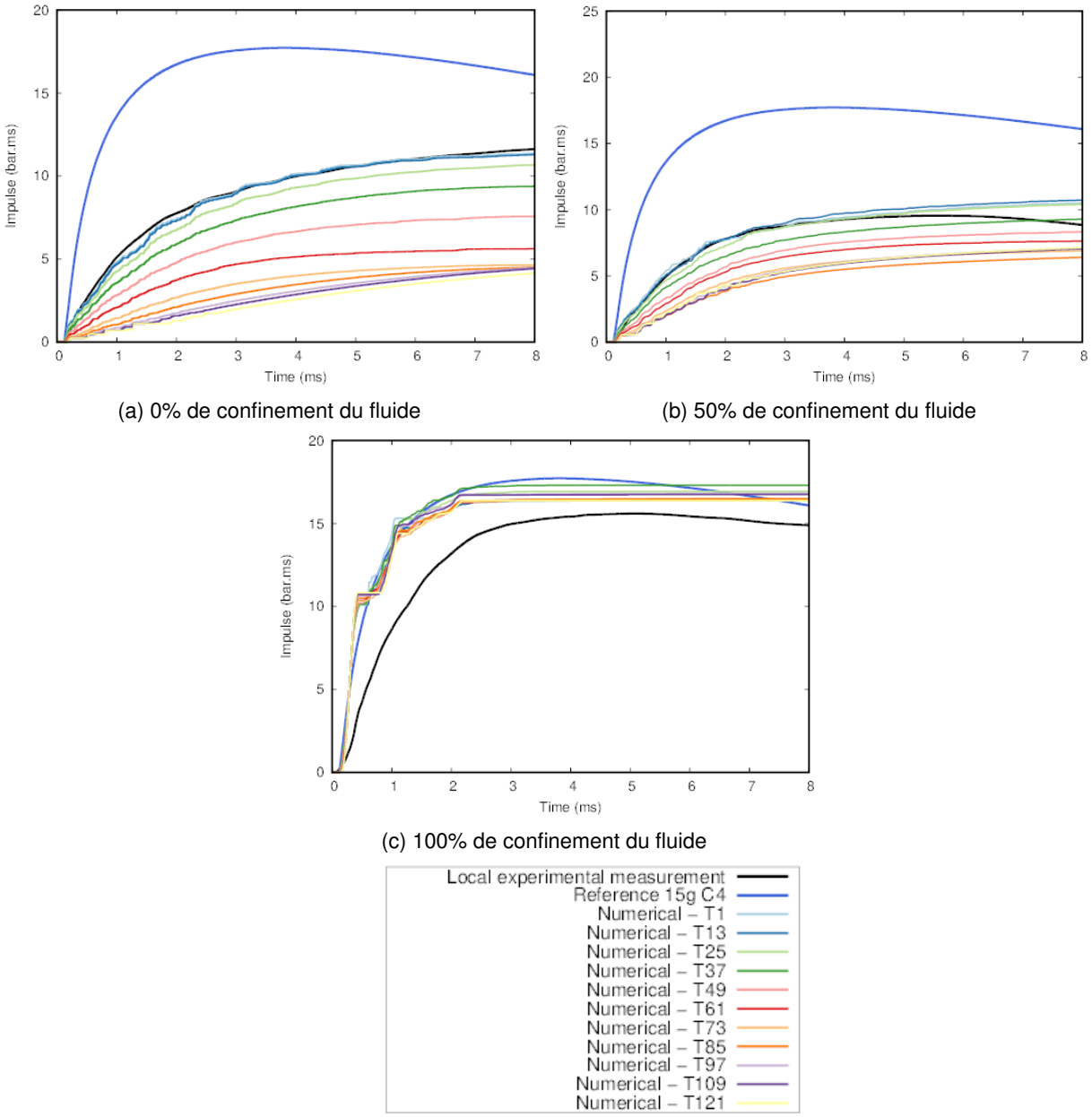

(a) 0% de confinement du fluide

(b) 50% de confinement du fluide

(c) 100% de confinement du fluide

Figure A.8: Impulsion le long de la diagonale sur le fond du conteneur pour différents niveaux de confinement – 15 g de C4, plaque de 3 mm, hauteur d'eau de 50 mm

Un dispositif expérimental avec une hauteur d'eau accrue de 100 mm a également été étudié. Les conclusions précédentes établies avec une hauteur d'eau de 50 mm ont également pu être observées avec une hauteur d'eau plus importante. Cependant, comme l'onde de compression dans le fluide est sphérique, une hauteur d'eau additionnelle laisse le temps au rayon de cette sphère de s'accroitre, lissant ainsi les variations locales observées au fond du conteneur. Même si la forme de la distribution de l'impulsion au fond du conteneur est moins prononcée, des réductions locales de l'impulsion sont encore mesurées.

Des mesures locales ont permis de constater qu'une vitesse de plaque plus élevée augmentait le premier pic de surpression mesuré au centre du fond du bac. En ce qui concerne l'impulsion locale, il ne semble pas y avoir d'effet de l'augmentation de la vitesse de la plaque sur la transmission d'impulsion. Les résultats numériques ont permis de mieux comprendre la distribution de l'impulsion sur l'intégralité du fond du conteneur. En particulier, l'impulsion n'est pas distribuée de manière homogène sur le fond du conteneur, mais un étalement a été observé, avec une valeur maximale au centre et minimale aux bords du conteneur. Avec ce dispositif expérimental, l'impulsion est entièrement transmise au fond du conteneur, qui est rigide et fixe dans l'espace. Cela a permis de faire des observations sur l'influence d'un fluide sur la propagation de l'impulsion. Pour mieux comprendre la transmission globale de la quantité de mouvement, une structure remplie de fluide qui peut être mise en mouvement doit être étudiée. C'est pourquoi un autre dispositif expérimental a été mis au point, comprenant un pendule à blast, afin de comprendre la transmission de la quantité de mouvement.

Transmission de la quantité de mouvement

Dispositif expérimental

Un pendule à blast est un dispositif expérimental permettant d'établir un lien entre le mouvement du pendule et l'impulsion qui lui à été transmise à la suite de la détonation d'une charge explosive. Le pendule utilisé à l'ISL est montre sur la Figure A.9. Dans le cas de cette étude, l'angle maximal d'élévation du pendule (se produisant durant la première oscillation) peut être assimilé au déplacement vertical maximal d'un véhicule après détonation d'une charge explosive sous le plancher de celui-ci. Ainsi, l'angle maximal d'élévation de structures remplies de fluide sera comparé à une valeur de référence pour un pendule à poids égal mais sans fluide. Dans le cas de cette étude, cette valeur de référence correspond à l'oscillation du pendule lorsque 840 g de C4 sont placés à une distance de 1 m d'un pendule pesant 215 kg. Le mouvement du pendule à été enregistré à l'aide d'une caméra à haute vitesse et d'un capteur de rotation placé dans l'axe du pendule.

Figure A.9: Pendule utilisé à l'ISL

Pour ce dispositif expérimental, le fluide a été placé dans une poche d'eau entre une plaque avant et une plaque arrière (Figure A.10a). En ne restreignant pas l'eau dans une architecture fermée, cette conception devrait permettre à celle-ci de se répandre sur le côté lorsqu'elle est poussée par la plaque avant lors de sa déformation. Pour s'assurer que le centre de masse de l'ensemble du dispositif soit placé au centre du corps du pendule, des plaques d'acier ont été placées sur le côté opposé pour compenser le poids de la structure remplie d'eau (Figure A.10b).

(a) Plaque avant, poche d'eau, plaque arrière

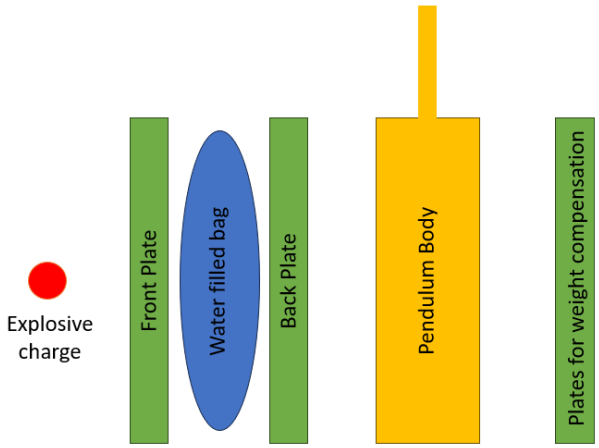

(b) Représentation schématique du dispositif expérimental

Figure A.10: Placement d'une poche d'eau sur le pendule à blast

Variation de la masse d'eau et de la configuration de la structure

Afin d'étudier la quantité d'eau nécessaire pour réduire l'angle d'élévation du pendule, la masse d'eau présente dans la poche placée entre une plaque avant et une plaque arrière, a été modifiée. Des masses d'eau de 7.85 kg, 9.81 kg et 11.78 kg ont été utilisées, correspondant respectivement à 4.9, 6 et 7.3 % de la masse totale du pendule. Pour les trois configurations, le poids total du pendule a été maintenu constant et égal au poids du pendule ayant servi à établir la valeur de référence. Pour tenir compte de l'augmentation ou de la diminution de la masse d'eau, l'épaisseur de la plaque avant et arrière a été ajustée en conséquence. Les résultats expérimentaux pour la configuration avec 11.78 kg d'eau sont montrés sur la Figure A.11. Il peut être observé qu'aucune réduction de l'angle maximal d'élévation atteint par le pendule ne se produit pour cette configuration. Une observation identique a pu être faite pour toutes les masses d'eau étudiées.

En regardant les images fournies par la caméra à haute vitesse, on peut observer que l'éjection du fluide ne se produit qu'après que le pendule a été mis en mouvement par l'onde de souffle générée par la détonation de la charge explosive. En effet, l'eau semble coincée entre la plaque avant et la plaque arrière. C'est pour cela que la plaque avant a été retirée pour l'étude d'une seconde configuration expérimentale afin de donner plus de liberté de mouvement à l'eau. Les mêmes quantités d'eau ont été utilisées dans cette deuxième série d'expériences.

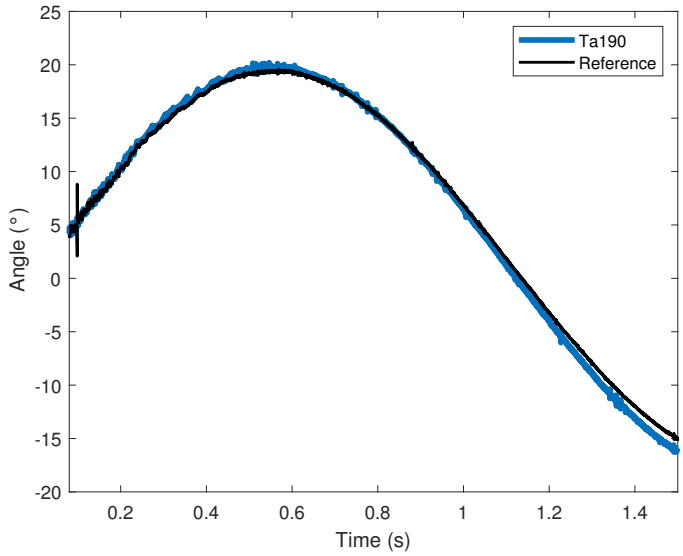

Figure A.11: Elévation angulaire du pendule pour une masse d'eau de 11.78 kg placée entre une plaque avant et une plaque arrière, comparaison à la valeur de référence

Dans cette configuration, une réduction de l'angle maximal d'élévation du pendule se produit (Figure A.12). Cette réduction semble augmenter avec l'augmentation de la masse d'eau utilisée. Cependant, pour l'interprétation de ces résultats, il faut noter que l'absence de plaque avant permet à l'eau éjectée après détonation d'être projetée dans la direction de la charge. Les gouttelettes d'eau pouvant atténuer la boule de feu, l'impulsion transmise au pendule peut être réduite.

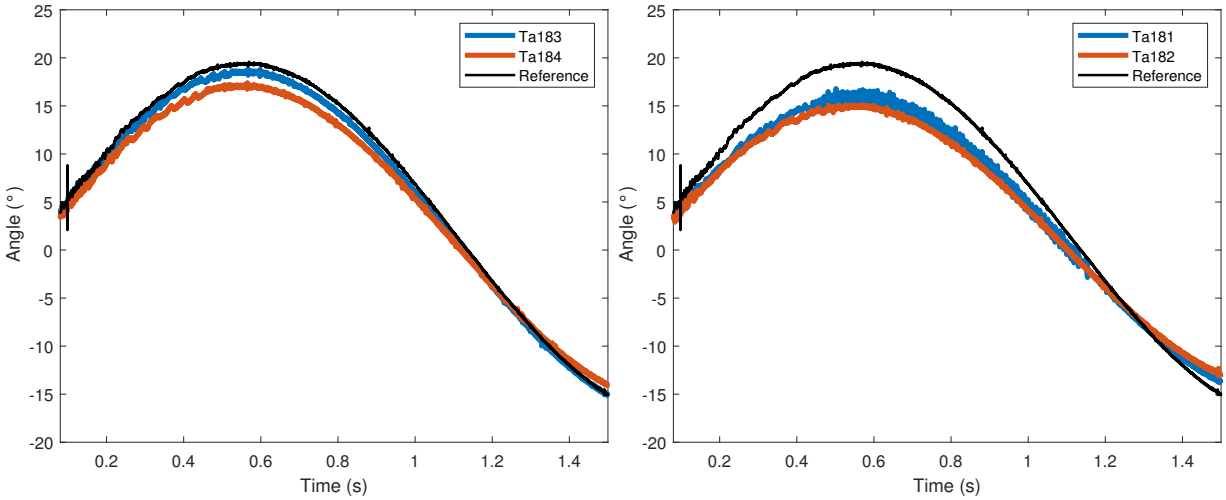

(a) Masse d'eau de 7.85 kg

(b) Masse d'eau de 11.78 kg

Figure A.12: Elévation angulaire du pendule lorsque la plaque avant a été retirée, comparaison à la valeur de référence

Modification du dispositif expérimental

À la suite de ces premières observations expérimentales, le dispositif a été modifié pour améliorer l'éjection du fluide hors d'une structure dotée d'une plaque avant et d'une plaque arrière. Le sens d'éjection de la masse d'eau doit être le même que celui de l'onde de souffle généré par la détonation de la charge explosive pour que le vecteur vitesse généré par l'accélération verticale du véhicule soit contrecarré par le vecteur vitesse généré par l'éjection de la masse d'eau, conformément à la troisième loi du mouvement de Newton.

Le pendule présenté précédemment a dû être modifié pour permettre le passage d'un tube servant à l'éjection de l'eau à travers le corps du pendule. La Figure A.13a illustre l'emplacement du tube forçant la direction d'éjection de l'eau. Ceci nécessitant la réalisation de trous dans la plaque arrière et dans le corps du pendule. Pour le confinement latéral du fluide, un cadre a été ajouté entre la plaque avant et la plaque arrière, ce qui permet d'obtenir une structure fermée remplie de fluide où les seules ouvertures sont fournies par les tubes (Figure A.13b). Dans ce cas, l'eau n'est plus placée dans une poche, mais directement dans la structure par une ouverture dans le cadre en aluminium. La principale difficulté de cette étude consistait à trouver des solutions appropriées pour empêcher les fuites d'eau de la structure. Le dispositif expérimental ayant été modifié, une nouvelle valeur de référence a été établie pour tenir compte de l'augmentation de poids due à l'ajout du cadre en aluminium. Pour cette configuration expérimentale, le poids total du pendule est de 231 kg et la masse d'eau de 16 kg représente 6,92 % de la masse totale du pendule.

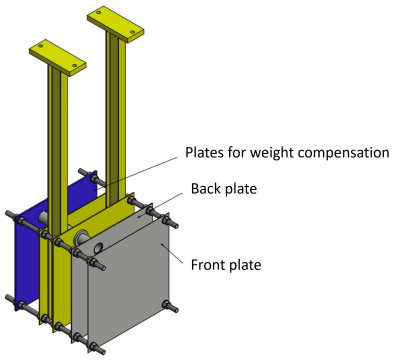

(a) Représentation schématique, le cadre en aluminium n'apparait pas

(b) b. Nouvelle configuration expérimentale avec confinement latéral du fluide avec un cadre en aluminium

Figure A.13: Nouvelle configuration expérimentale permettant l'éjection de l'eau au travers de tubes

Des études expérimentales pour cette configuration sont en cours. Un premier résultat avec quatre ouvertures d'un diamètre de 100 mm a été obtenu. Les images de la caméra haute vitesse montrent que, dans ce cas, l'éjection de l'eau se produit avant la mise en mouvement du pendule (Figure A.15). Une réduction de l'élévation angulaire maximale d'environ 4° peut être observée (Figure A.14), ce qui correspond à 35% de l'angle maximal de référence.

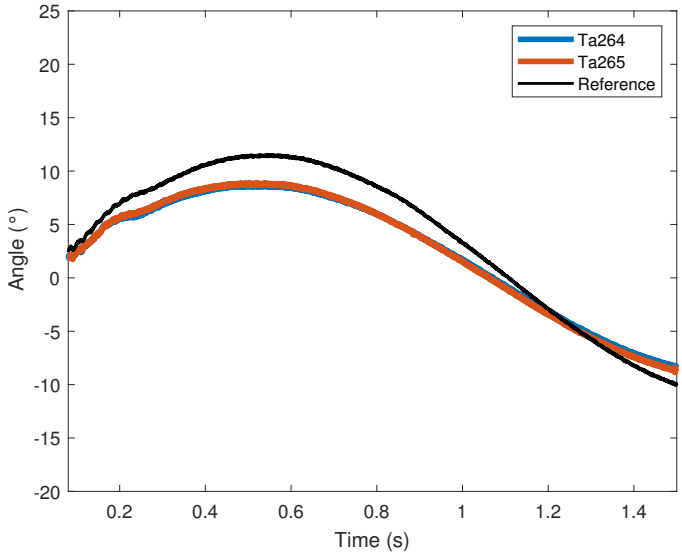

Figure A.14: Elévation angulaire du pendule pour une structure remplie d'eau avec quatre ouvertures de diamètre 100, comparaison à la valeur de référence

(a) t = 41.317 ms, début de l'éjection de l'eau avant mise en mouvement du pendule

(b) t = 60.317 ms, éjection de l'eau avant mise en mouvement du pendule

(c) t = 91.317 ms, éjection d'eau dirigée

(d) t = 245.317 ms, mouvement du pendule une fois que la majeure partie du fluide est éjectée

Figure A.15: Images de la caméra haute vitesse de la première oscillation du pendule pour l'expérience Ta265

Des résultats préliminaires montrent que ce concept offre un bon potentiel de réduction de la quantité de mouvement transférée par le souffle à une structure. Ce dispositif expérimental représente une première étape vers l'intégration sur un véhicule d'une structure remplie de fluide permettant une éjection dirigée de ce fluide. La première phase de cette étude a consisté à mettre en place un dispositif expérimental fonctionnel et à résoudre les problèmes principalement liés à l'étanchéité d'une structure remplie de fluide installée sur un pendule à blast. Les premiers résultats expérimentaux montrent une réduction de l'élévation angulaire du pendule lorsqu'il est équipé d'une structure remplie de fluide et démontrent le potentiel d'une telle solution pour la réduction de la quantité de mouvement.

Conclusions et perspectives

Dans cette étude, l'utilisation de structures remplies de fluides permettant la protection contre l'effet de souffle, en particulier la transmission de la quantité de mouvement, a été étudiée. À cette fin, deux dispositifs expérimentaux ont été utilisés.

Les effets de l'utilisation d'un fluide sur la transmission de l'impulsion à une cible ont été étudiés à l'aide d'un conteneur rempli de fluide et équipé d'un capteur de pression. Le fluide contenu dans ce conteneur a été soumis à un chargement provenant d'un tube à choc actionné par un explosif. Il a été démontré que l'utilisation d'un fluide dans une protection permet un étalement de l'impulsion et donc de la réduire localement. Un lien a été établi entre la surface libre permettant au fluide d'être éjecté hors de la protection et cet étalement d'impulsion.

Pour l'étude de la transmission globale de la quantité de mouvement, il a fallu utiliser un dispositif expérimental permettant la mise en mouvement d'une structure remplie de liquide. Pour ce faire, un pendule à blast sur lequel a été placé une structure remplie d'eau a été utilisé. L'angle d'élévation maximal atteint par le pendule a pu être comparé pour une structure remplie d'eau et une valeur de référence de masse équivalente sans eau. Différentes configurations expérimentales ont été testées pour répondre à un certain nombre d'exigences liées au confinement de l'eau avant l'explosion, ainsi qu'à son temps d'éjection et à sa direction une fois que l'onde de souffle interagit avec la structure.

En ce qui concerne les conclusions tirées de cette étude, il est possible d'explorer des perspectives d'études académiques futures et des perspectives d'intégration si une telle structure venait à être utilisée sur un véhicule.

L'influence des propriétés du fluide utilisé devrait être étudiée. Il serait judicieux d'étudier des fluides déjà présents à bord du véhicule, comme le liquide de refroidissement ou le liquide de frein par exemple. Ceci permettrait de protéger le véhicule contre les effets de souffle tout en évitant une trop grande augmentation de la masse du véhicule. Cela pourrait se faire en modifiant les propriétés des matériaux dans les simulations numériques établies au cours de cette étude. En outre, des simulations numériques du pendule à blast et de la structure remplie de fluide associée devraient être établies pour faciliter les processus de conception futurs.

Dans le cas d'une intégration de la solution de protection sur un véhicule, l'influence de sa conception partic-

ulière et de sa géométrie sur la propagation des ondes à l'intérieur du fluide devra être évaluée. D'une manière générale, il faudra trouver des solutions techniques aux directives de conception telles que le besoin d'éjection ou de confinement du fluide établi dans cette étude, tout en tenant compte des exigences d'encombrement souvent restrictives dans un véhicule.

A.2 Deutsch

Einleitung

Bei der Detonation einer Sprengladung unter dem Boden eines Fahrzeugs, z. B. einer vergrabenen Mine oder eines improvisierten Sprengkörpers, treten zwei Haupteffekte auf: die Verformung oder Zerstörung des Fahrzeugbodens durch die vom Blast übertragene Belastung und die allgemeine vertikale Beschleunigung des Fahrzeugs. Diese kann aufgrund des auf das Fahrzeug übertragenen Impulses zu einem Überschlag führen. Viele Studien über Fahrzeugschutz in der einschlägigen Literatur befassen sich mit der Übertragung der Belastung und haben zum Ziel, die Verformung des Fahrzeugbodens zu verringern. Es befassen sich aber nur sehr wenige Studien mit der Übertragung des Impulses und damit der Änderung des Bewegungsmoments. Die Verwendung von Flüssigkeiten, insbesondere Wasser, wurde als potenzielles Mittel zur Beeinflussung der Impulsübertragung identifiziert. Die wenigen in der Literatur vorhandenen Studien konzentrieren sich jedoch auf die Wirkungen des Vorhandenseins von Wasser innerhalb der Schutzstruktur. Sie bewerten die Reduzierung des auf das Ziel übertragenen Impulses im Hinblick auf den Verformungsgrad des Ziels. Diese Arbeit hat zum Ziel, die in der Flüssigkeit stattfindenden Phänomene zu identifizieren, die sich auf die Impulsübertragung auswirken. Dafür wird also vor dem Ziel gemessen. Es wurden experimentelle Studien durchgeführt, bei denen ein Explosivstoff enthaltendes Stoßrohr einen Blast überträgt, welcher der Stoßwelle einer vergrabender Mine nahe kommt. Dabei wird der Blast auf einen mit Wasser gefüllten Behälter übertragen. Diese experimentellen Studien wurden durch numerische Simulationen ergänzt, wodurch einige Einschränkungen, wie die Anzahl der Messpunkte, überwunden werden konnten. Es wurde gezeigt, dass die Verwendung einer Flüssigkeit in einer Schutzstruktur gegen Druckwellen zu einer Ausbreitung des Impulses und damit zu einer lokalen Abnahme des Impulses führt. Es wurde ein Zusammenhang zwischen der freien Fläche, aus welcher die Flüssigkeit aus der Schutzvorrichtung ausgestoßen wird, und der Impulsausbreitung hergestellt. Für ein umfassenderes Verständnis des Vorgangs wurde ein Blast-Pendel verwendet, um die Wirkungen einer Flüssigkeit in einer Schutzstruktur auf das Bewegungsmoment zu beobachten. Mit diesem zweiten Versuchsaufbau kann untersucht werden, wie sich die Ausstoßrichtung der Flüssigkeit in Bezug auf die ursprüngliche Belastung durch den Blast auswirkt.

Untersuchung der Impulsausbreitung

Beschreibung des experimentellen Versuchsaufbaus und der numerischen Simulation

Es wurde ein Versuchsaufbau konzipiert, um eine mit Flüssigkeit gefüllte Struktur, welche einer Stosswelle ausgesetzt ist, zu untersuchen (siehe A.16). Diese Struktur beinhaltet ein vertikales, Explosivstoff enthaltendes Stossrohr, welches eine flache Stosswelle generiert. Hierzu wird eine 50 mm vom Rohreingang platzierte Sprengladung mit 15 oder 30 Gramm C4 verwendet. Der Rohrinnendurchmesser beträgt 80 mal 80 mm und die Rohrlänge 1750 mm.

Am unteren Ende des Rohrs befindet sich eine Stahlplatte mit den Massen 100 mal 100 mm und einer Dicke von 1,5 oder 3 oder 5 mm. Vor Auftreffen der Stosswelle ist diese Stahlplatte mit einem Klebeband am Rohr befestigt. Aufgrund der Wechselwirkung zwischen dieser Platte und der durch das Rohr generierten Stosswelle wird die Platte in einen mit Wasser gefüllten Container ausgestossen. Dieser Container hat eine Grösse von 200 mal 200 mm und eine Tiefe von 50 oder 100 mm. Bei experimentellen Untersuchungen kann der zeitliche Druckverlauf mit Hilfe eines PCB-Drucksensors, welcher mittig auf dem Boden des Containers angebracht ist, gemessen werden. Während des Experiments konnte der Druckwellenverlauf im Wasser mit Hilfe einer Hochgeschwindigkeitskamera sichtbar gemacht werden.

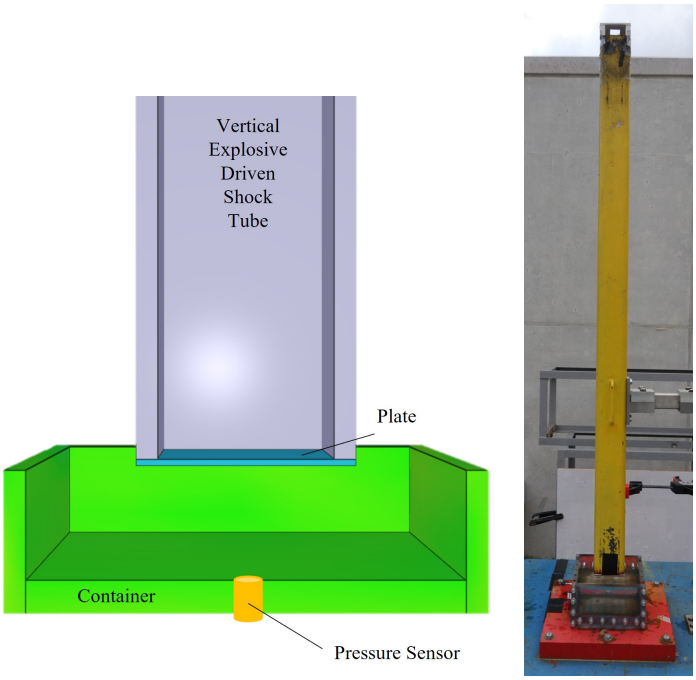

Figure A.16: Versuchsaufbau

Der Versuchsaufbau wurde durch die Möglichkeit verschiedener Flüssigkeits-Einschlussgrade erweitert. Hierfür wurde der Container mit einem Deckel versehen. Dieser bewirkt, dass der Ausstoss der Flüssigkeit aus dem Container mehr oder weniger eingeschränkt werden kann (siehe A.17).

(a) a) Schematische Darstellung unterschiedlicher Flüssigkeits-Einschlussgrade. Von links nach rechts: 0 %, 50 % und 100 %.

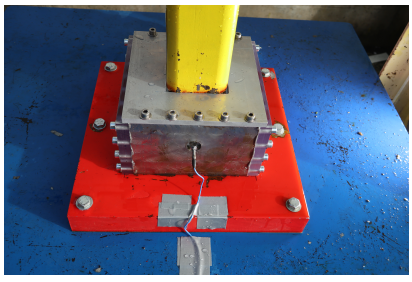

(b) b) 100 % Flüssigkeits-Einschluss

Figure A.17: Erweiterter Versuchsaufbau für die Untersuchung des Einflusses des Flüssigkeits-Einschlusses

Anhand von Experimenten konnte ein Referenzwert für die Ladung, mit welcher die Platte beaufschlagt wurde, ermittelt werden. Hierfür wurde das Ende des Explosivstoff enthaltenden Stossrohrs unmittelbar mit dem Drucksensor in Berührung gebracht . Somit konnte das Druckprofil unter perfekten Reflexionsbedingungen bestimmt werden. Das am Boden des mit Wasser gefüllten Containers gemessene Drucksignal wird dann mit dem Referenzwert verglichen, um die Effizienz der Schutzwirkung der mit Wasser gefüllten Struktur zu bewerten. Fig. A.18 zeigt die Kurven für den Druck-Zeit-Verlauf und den Impuls-Zeit-Verlauf für einen solchen Referenzwert für 15 g C4.

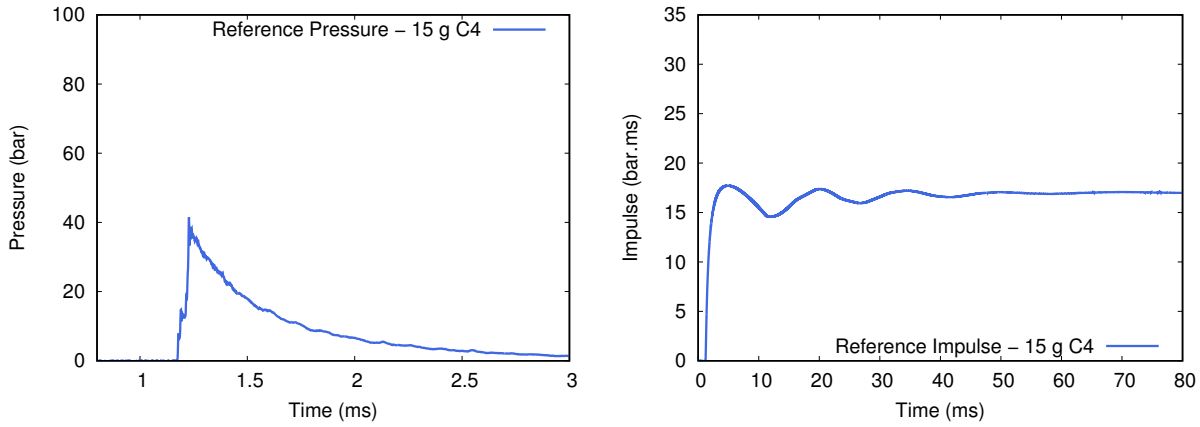

(a) Referenz Druck - 15 g C4

(b) Referenz Impuls - 15 g C4

Figure A.18: Stosswellenbelastung der Platte mit dem Explosivstoff enthaltenden Stossrohr zur Ermittlung eines Referenzwerts, 15 g C4

Die mit dem beschriebenen Versuchsaufbau durchgeführten Versuche wurden mit LS-Dyna simuliert. Das numerische Modell simuliert sowohl Luft und Wasser mit der Arbitrary-Lagrangian-Eulerian-Methode (ALE) als auch die Platte mit einer lagrangeschen Formulierung. Zur Optimierung der Rechenzeit beinhaltet das numerische Modell nur eine Teilsimulation, d.h. das Rohr und der Explosivstoff werden nicht modelliert. Vielmehr wird das experimentell bestimmte Druckprofil des Referenzwerts direkt auf die Knoten an der Oberfläche der Platte angewandt. Zur weiteren Optimierung der Rechenzeit werden Symmetrien des Versuchsaufbaus genutzt. Dies ermöglich die Simulation eines Viertels des Modells. Zur Ermittlung der Randbedingungen entsprechend den Containerwänden und den Einschlussgebieten werden unbewegliche Knotennetze verwendet. Die experimentellen Einschränkungen mit nur einem Messpunkt konnten mit Hilfe des numerischen Modells überwunden werden: Hier waren Sensoren über den gesamten Containerboden verteilt. Im Rahmen dieser Arbeit wurden insbesondere Sensoren entlang der Diagonale des Containerbodens angebracht (siehe Bild A.19). Hierbei befand sich der Sensor T1 in der Mitte des Containers und der Sensor T121 am weitesten von der Containermitte entfernt.

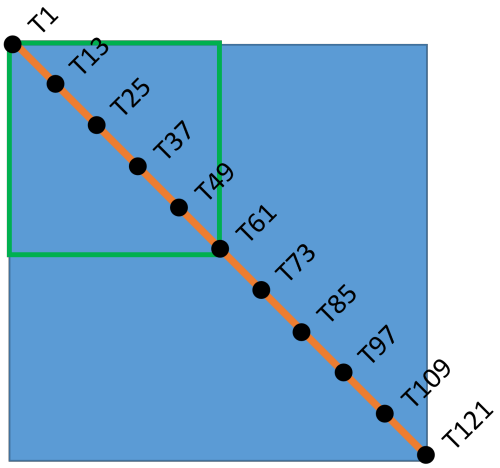

Figure A.19: Anordnung der in der Simulation benutzten Sensoren entlang der Diagonale des Containerbodens

Untersuchung unterschiedlicher Plattengeschwindigkeiten

Um herauszufinden, inwieweit Wasser die Impulsverteilung am Boden des Containers beeinflussen kann, wurden unterschiedlich starke Druckwellen generiert. Hierfür wurde die Platte mit unterschiedlichen Geschwindigkeiten in das Wasser ausgestossen.

Die unterschiedlichen Plattengeschwindigkeiten wurden durch verschieden dicke und somit unterschiedlich schwere Platten erreicht. Ein Vergleich der Druck-Zeit-Kurven (Fig. A.20a) zeigt, dass - in der Mitte des Containerbodens - eine erste Überdruckspitze entweder höher oder gleich hoch wie der maximale Überdruck des Referenzsignals gemessen wird. Die Impulsmessung von Figur A.20b zeigt, dass für alle Plattengeschwindigkeiten eine lokale Impulsverringerung erreicht werden konnte. Während die 1,5 mm-Platte und die 3 mm-Platte eine gleich hohe Impulsverringerung aufweisen, bewirkt die langsamere 5 mm-Platte offensichtlich einen stärkeren lokalen Impuls.

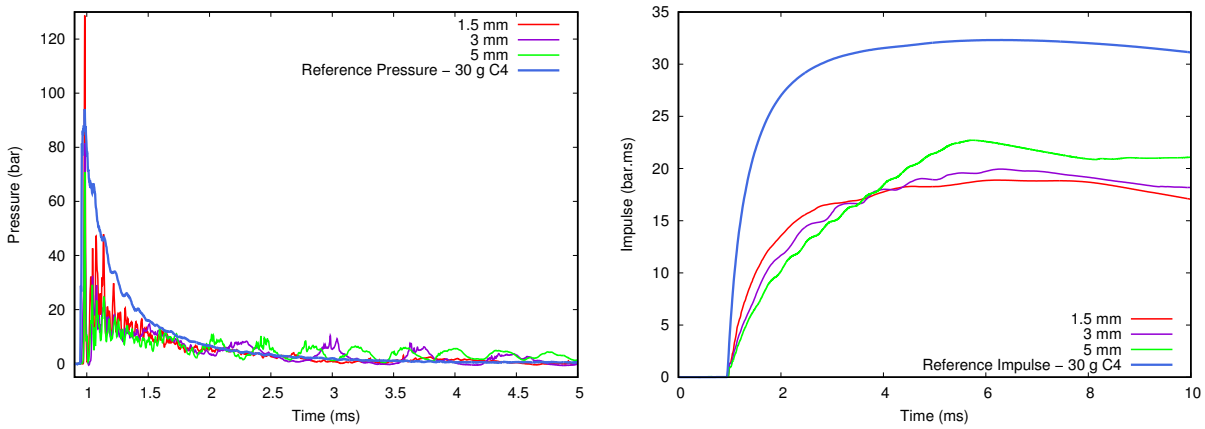

(a) Lokale Druckmessung

(b) Lokale Impulsmessung

Figure A.20: Vergleich lokaler Messungen in der Mitte des Containerbodens für verschiedene Plattenggeschwindigkeiten und Vergleich mit dem Referenzwert für eine Explosivstoffmenge von 30 g C4.

Wie in Figur A.21 ersichtlich, kann mit dem numerischen Modell die Impulsverteilung über den gesamten Containerboden für verschiedene Explosivstoffmassen und unterschiedlich dicke Platten dargestellt werden. Figur 4.6 zeigt eine 3D-Darstellung des Impulses am Containerboden nach gänzlicher Übertragung der Stosswelle auf die Flüssigkeit. Die Tiefe des Containers betrug hierbei 50 mm. Der Impuls breitete sich entlang der Diagonale des Containers aus und war in der Containermitte am stärksten, während er in Richtung der Containerränder allmählich abnahm. Die numerische Simulation zeigt, dass sich die Plattengeschwindigkeit nicht wesentlich auf die Form der Impulsausbreitung entlang des Containerbodens auswirkt.

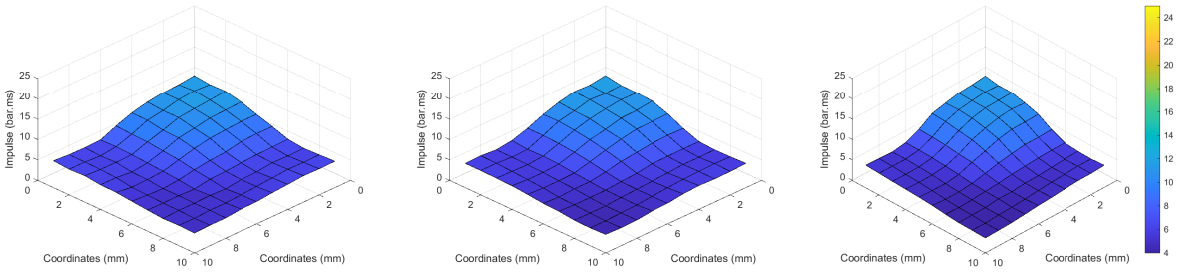

(a) 1.5 mm Platte - 15 g C4 (b) 3 mm Platte - 15 g C4 (c) 5 mm Platte - 15 g C4

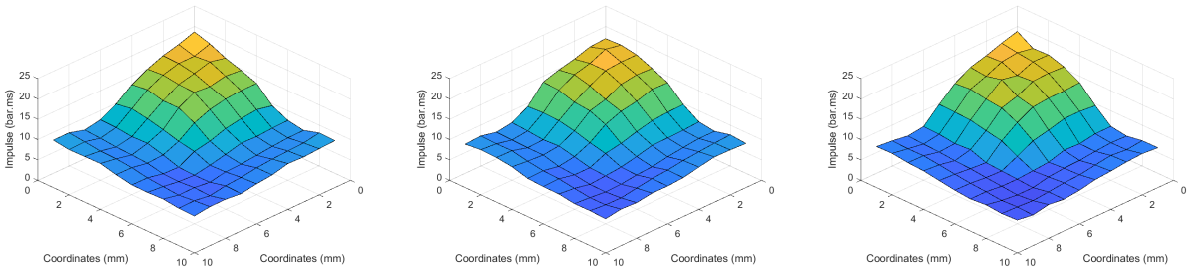

(d) 1.5 mm Platte - 30 g C4 (e) 3 mm Platte - 30 g C4 (f) 5 mm Platte - 30 g C4

Figure A.21: Impulsverteilung am Containerboden für verschiedene Explosivstoffmassen und Plattendicken; Zeit = 8 ms – 0 % Flüssigkeits-Einschluss, 50 mm Containertiefe

Untersuchung des Flüssigkeits-Einschlusses und der Flüssigkeits-Tiefe

Bei den Experimenten mit verschiedenen Plattengeschwindigkeiten wurde eine grosse Menge des im unverschlossenen Container vorhandenen Wassers ausgestossen. Daher wurden Messungen am Containerboden durchgeführt, um den Einfluss des Einschlussgrades des Wassers auf Impulsverteilung zu bestimmen . Drei verschiedene Grade des Flüssigkeits-Einschlusses wurden untersucht: 0 %, 50 % und 100 %.

Bei der experimentellen Studie wurde der Einfluss des Einschlussgrades auf den lokalen Impuls am Boden des Containers untersucht, wobei die Explosivstoffmasse 15 g, die Plattendicke 3 mm und die Containertiefe 50 mm betrugen (siehe Fig. A.22). Beobachtungen ergaben, dass die lokale Impulsverringerung ähnlich ist, wenn die Flüssigkeit gar nicht im Container eingeschlossen ist oder die Wasseroberfläche zu 50 % frei liegt. Beim gänzlich verschlossenen Container wurde dagegen keinerlei Impulsverringerung gemessen. Dies weist ganz offensichtlich darauf hin, wie wichtig es ist, dass die Flüssigkeit aus dem Container ausgestossen werden kann.

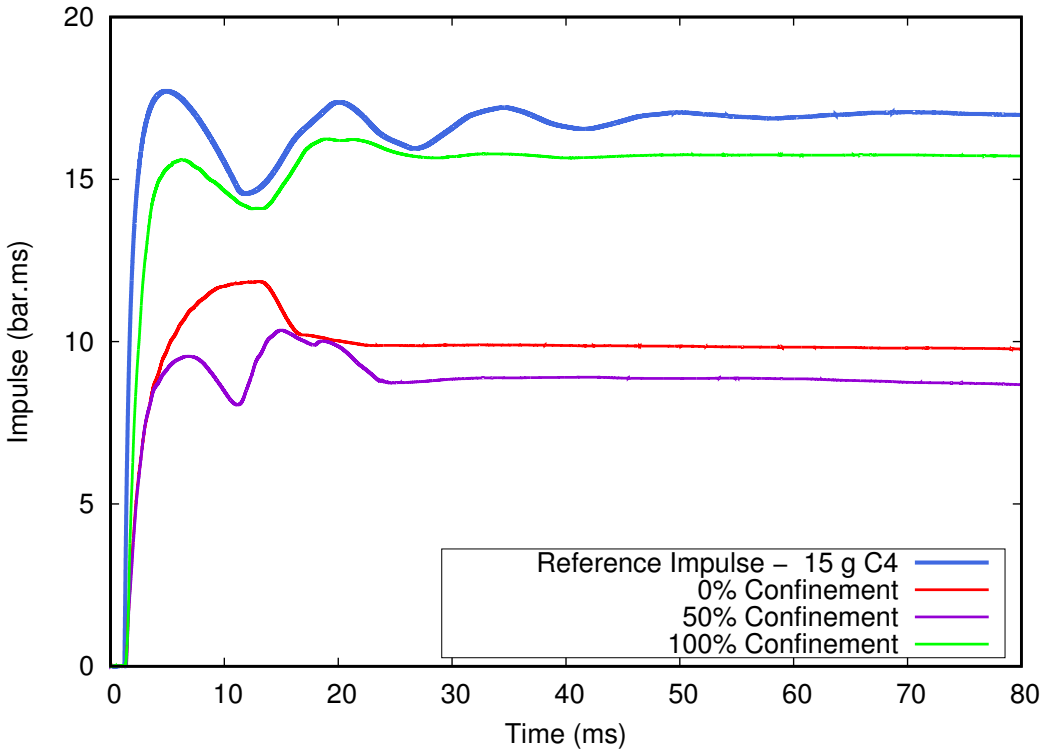

Figure A.22: Experimentelle lokale Impulsmessungen für verschiedene Grade des Flüssigkeits-Einschlusses

Die numerische Modellierung der Experimente mit einem Wassereinschluss von jeweils 0 %, 50 % und 100 % untersuchte die Impulsausbreitung entlang der Diagonale des Containerbodens (siehe A.23). Bei einer uneingeschlossenen Flüssigkeit breitet sich der Impuls entlang der Diagonale des Containerbodens aus (siehe Bild A.23a). Der stärkste Impuls wird hierbei in der Mitte des Containers gemessen. Der Impuls verringert sich allmählich, je mehr man sich den Rändern des Containers nähert. Für einen Wassereinschluss von 50% (siehe Figur A.23b) ist die lokale Impuls-veringerung ähnlich wie im Fall der uneingeschlossenen Flüssigkeit. Jedoch ist die Impuls-verbreitung entlang der Diagonale des Containerbodens weniger stark. Da bei der gänzlich eingeschlossenen Flüssigkeit keine Impulsausbreitung stattfindet (siehe Fig. A.23c), ist davon auszugehen, dass dies auf die Einschlussbedingungen zurückzuführen ist.

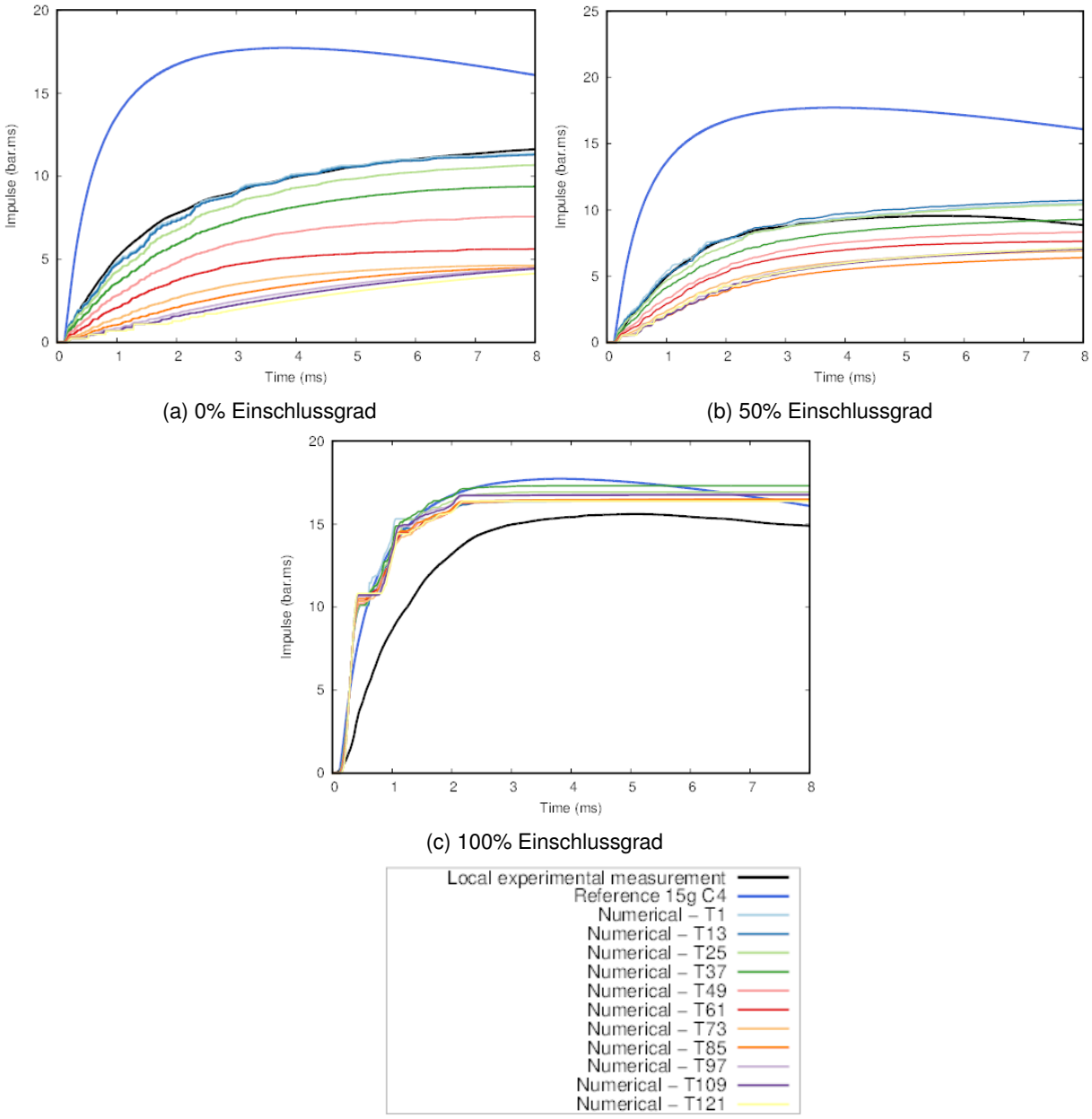

(a) 0% Einschlussgrad

(b) 50% Einschlussgrad

(c) 100% Einschlussgrad

Figure A.23: Impuls entlang der Diagonale des Containerbodens für unterschiedliche Flüssigkeits-Einschlussgrade – 15 g C4, 3 mm-Platte, 50 mm Containertiefe

Es wurde auch ein Versuchsaufbau mit einer Containertiefe von 100 mm untersucht. Ergebnisse, welche mit dem 50 mm tiefen Container erzielt wurden, ließen sich auch bei einer grösseren Flüssigkeitshöhe beobachten. Da die Druckwelle in der Flüssigkeit sphärisch ist, bewirkt die grössere Flüssigkeitshöhe, dass sich die sphärische Druckwelle etwas länger ausbreitet und einen größeren Radius erhält. Somit bewirkt sie eine Glättung der lokalen Impulsveränderungen am Containerboden. Auch wenn die Form der Impulsverteilung am Containerboden weniger ausgeprägt ist, ist immer noch eine lokale Impulsverringerung messbar.

Lokale Messungen ergaben, dass sich die erste Überdruckspitze mit gesteigerter Plattengeschwindigkeit erhöhte. Hinsichtlich des lokalen Impulses zeigte sich, dass sich eine erhöhte Plattengeschwindigkeit nicht bemerkbar macht. Die numerischen Simulationen führten zu weiteren Ergebnissen bezüglich der Impulsverteilung am Containerboden. Insbesondere verteilt sich der Impuls nicht einheitlich auf dem Containerboden, sondern es ist eine Impulsausbreitung feststellbar. Hierbei ist der Impuls in der Mitte des Containers am grössten und an den Rändern des Containers am geringsten.
Bei diesem Versuchsaufbau wird der Impuls gänzlich an den Boden des Containers übertragen, da dieser sich nicht bewegen kann. Somit kann der Einfluss einer Flüssigkeit auf die Impulsausbreitung gut beobachtet werden. Um Kenntnisse über die Übertragung des globalen Bewegungsmoments zu erlangen, muss eine mit Flüssigkeit gefüllte Schutzstruktur, welche in Bewegung versetzt werden kann, untersucht werden. Aus diesem Grund wird eine weitere Versuchsanordnung mit einem Blast-Pendel entwickelt. Diese Anordnung eignet sich sehr gut, um die Übertragung des Bewegungsmoments zu erforschen.

Übertragung des Bewegungsmoments

Versuchsaufbau

Mit einem Blast-Pendel kann ein Zusammenhang zwischen der Drehbewegung des Pendels und der Impulsbelastung einer Struktur nach der Detonation eines Explosivstoffs hergestellt werden. Das am ISL verwendete Pendel ist in Figur A.24 dargestellt. Bei dieser Untersuchung kann ein Zusammenhang zwischen dem größten Ausschlagwinkel des Pendels (bei der ersten Schwingung) und der höchsten vertikalen Beschleunigung des Ziels nach der Detonation einer Explosivstoffladung unter einem Fahrzeug hergestellt werden. Der maximale Ausschlagwinkel des Pendels welches eine mit Flüssigkeit gefüllten Struktur enthält wird mit einem Referenzwert verglichen. Bei diesem Referenzwert hat das Pendel das gleiche Gewicht wie ein Pendel mit Flüssigkeit. Bei dieser Untersuchung entspricht der Referenzwert der Verwendung von 840 g C4 bei einem Abstand von 1 m vom Pendel, welches eine Gesamtmasse von 215 kg aufweist. Die Bewegung des Blast-Pendels wurde mit einer Hochgeschwindigkeitskamera aufgezeichnet. Ein Rotationssensor war auf der Achse des Pendels angebracht.

Bei diesem Versuchsaufbau befand sich die Flüssigkeit in einem Wasserbeutel, welcher zwischen einer Vorder- und einer Rückplatte angebracht war (siehe Fig. A.25a). Somit befand sich das Wasser nicht in einer geschlossenen Architektur, so dass es sich seitlich ausbreiten kann, wenn es von der sich bewegenden Vorderplatte weggedrückt wird. Damit der Massenmittelpunkt des gesamten Aufbaus sich im Zentrum des Pendels befindet, wurden an der gegenüberliegenden Seite Stahlplatten zum Gewichtsausgleich angebracht (siehe Fig A.25b).

Figure A.24: Versuchsaufbau

(a) Vorderplatte, wassergefüllter Beutel und Rückplatte

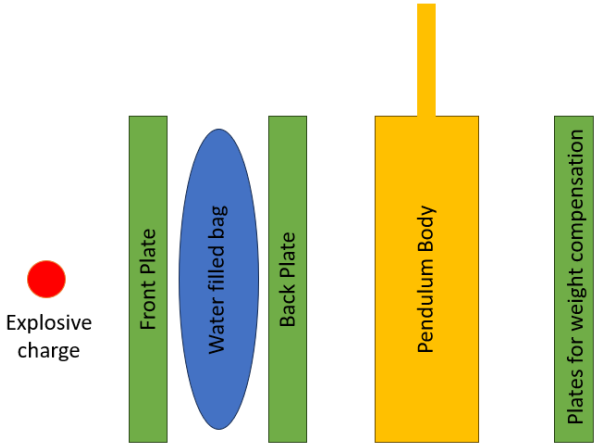

(b) Schematische Darstellung des Versuchsaufbaus

Figure A.25: Anbringung von Wasserbeuteln am Blast-Pendel

Veränderung der Wassermasse und der Plattenkonfiguration

Um zu ermitteln, wie viel Wasser gebraucht wird, um den Ausschlagwinkel des Pendels zu verringern, wurde jeweils unterschiedlich viel Wasser in den Wasserbeutel gegeben. Dieser war zwischen einer Vorder- und einer Rückplatte platziert. Es wurden Wassermassen von 7,85 kg, 9,81 kg und 11, 78 kg verwendet, welche jeweils 4,9 %, 6 % und 7,3 % der gesamten Pendelmasse entsprachen. Bei allen drei Konfigurationen wurde das Gesamtgewicht des Pendels konstant gehalten und entsprach stets dem Pendelgewicht des Referenzwerts. Um die größere oder kleinere Wassermasse zu berücksichtigen, wurden die Dicken der Vorder- und Rückplatten angepasst. Figur A.26 zeigt die Versuchsergebnisse für die Konfiguration mit 11,78 kg Wasser. Es konnte beobachtet werden, dass sich der maximale Ausschlagwinkel des Pendels nicht verringert. Diese Beobachtung traf auf alle verwendeten Wassermassen zu.

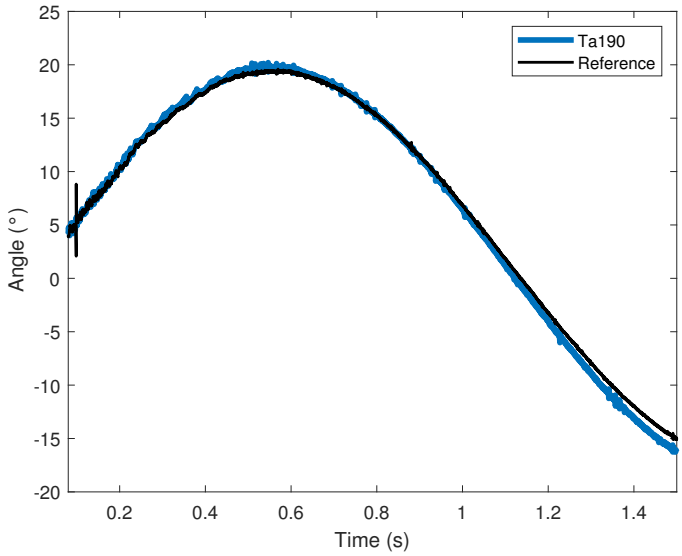

Figure A.26: Ausschlagwinkel des Pendels für eine Wassermasse von 11,78 kg zwischen einer Vorder- und einer Rückplatte; Vergleich mit dem Referenzwert

Die Aufnahmen mit der Hochgeschwindigkeitskamera ergaben, dass es erst dann zum Ausstoß von Flüssigkeit kam, nachdem das Pendel durch den Blast in Bewegung versetzt worden war, da das Wasser zwischen Vorder- und Rückplatte festgehalten war. Daher wurde in einer zweiten Versuchsanordnung die Vorderplatte entfernt, so dass das Wasser eine höhere Bewegungsfreiheit erlangt. Für diese zweite Versuchsreihe wurden dieselben Wassermengen verwendet. Bei dieser Anordnung konnte ein kleinerer maximaler Ausschlagwinkel des Pendels festgestellt werden (siehe Figur A.27). Dieser nimmt offensichtlich mit steigender Wassermasse ab. Bei der Auswertung der Ergebnisse ist jedoch Folgendes zu berücksichtigen: Wenn keine Vorderplatte vorhanden ist, wird das nach der Detonation frei gesetzte Wasser direkt gegen die Sprengladung ausgestoßen, wobei sich die Wassertropfen vermutlich dämpfend auf den Feuerball auswirken. Somit verringert sich der auf das Pendel übertragene Gesamtimpuls.

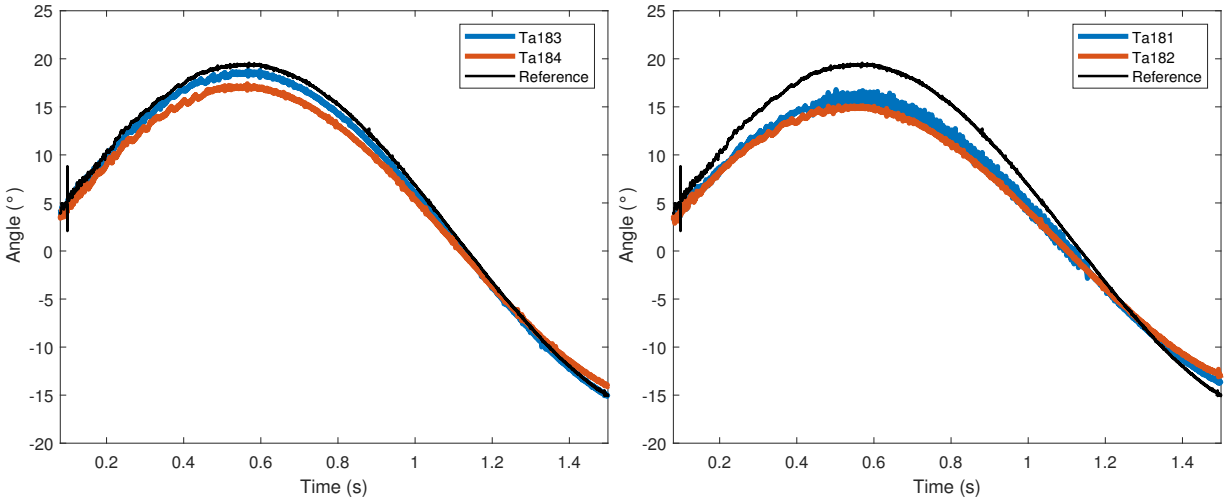

(a) 7.85 kg Wassermasse

(b) 11.78 kg Wassermasse

Figure A.27: Ausschlagwinkel des Pendels beim Versuchsaufbau ohne Vorderplatte; Vergleich mit dem Referenzwert

Änderung des Versuchsaufbaus

Nach Vorliegen der ersten Versuchsergebnisse wurde der Versuchsaufbau geändert, mit dem Ziel, den Flüssigkeitsausstoß aus der Struktur mit Vorder- und Rückplatte zu verbessern. Das Wasser muss in dieselbe Richtung wie die Stoßwelle ausgestossen werden, so dass der durch die vertikale Beschleunigung des Fahrzeugs erzeugte Geschwindigkeits Vektor mit dem durch den Massenausstoß erzeugten Geschwindigkeits Vektor in Wechselwirkung tritt (3. Newtonsches Gesetz: Wechselwirkungsprinzip).

Die zuvor beschriebene Pendelkonfiguration wurde so verändert, dass ein Rohr für den Wasserausstoß durch die Pendelstruktur angebracht wurde. Figur A.28a zeigt die Anordnung eines Rohres, mit welchem der Wasserausstoß in die gewünschte Richtung gelenkt werden kann. Hierfür müssen Löcher in die Rückplatte und die Pendelstruktur eingebracht werden. Für den seitlichen Flüssigkeitseinschluss wurde das Wasser mit einem Aluminiumrahmen umgeben. Hierdurch entsteht eine geschlossene, mit Flüssigkeit gefüllte Struktur, deren einzige Öffnungen in den Rohren bestehen (siehe Figur A.28b). Bei diesem Versuchsaufbau entfallen die Wasserbeutel; die Flüssigkeit wird hier unmittelbar durch eine Öffnung im Aluminiumrahmen in die Struktur gefüllt. Außerdem mussten geeignete Lösungen gefunden werden um die Struktur dicht zu machen. Aufgrund des veränderten Versuchsaufbaus musste ein neuer Referenzwert aufgestellt werden, um das höhere Gewicht zu berücksichtigen. Bei dieser Versuchsanordnung beträgt das Gesamtgewicht des Pendels 231 kg. Die Flüssigkeitsmaße von 16 kg entspricht 6,92 % des gesamten Pendelgewichts.

Die Versuche mit dieser veränderten speziellen Versuchsanordnung sind noch nicht abgeschlossen. Erste Ergebnisse mit vier Öffnungen eines Durchmessers von 100 mm liegen vor (siehe Figur 3.23). Aufnahmen mit der Hochgeschwindigkeitskamera zeigen, dass Wasser ausgestoßen wird, bevor das Pendel in Bewegung versetzt

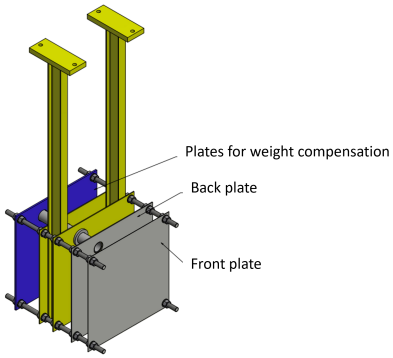

(a) Schematische Darstellung, der Aluminiumrahmen ist nicht dargestellt

(b) Neuer Versuchsaufbau mit Aluminiumrahmen

Figure A.28: Neuer Versuchsaufbau mit Wasserausstoß durch Rohre

wird (Fig. A.30). Der maximale Ausschlagwinkel beträgt $4°$ (Figur A.29), was 35% des Referenzwertes entspricht.

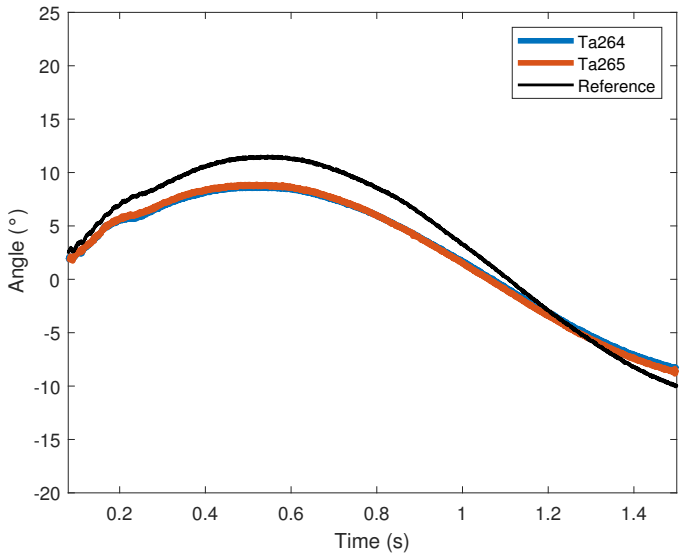

Figure A.29: Ausschlagwinkel des Pendels beim Versuchsaufbau mit vier Öffnungen eines Durchmessers von 100 mm; Vergleich mit dem Referenzwert

(a) t=41.317 ms, beginnender Wasserausstoß, bevor das Pendel in Bewegung versetzt wird

(b) t=60.317 ms, Wasserausstoß, bevor das Pendel in Bewegung versetzt wird

(c) t=91.317 ms, gerichteter Wasserausstoß

(d) t=245.317 ms, Pendelbewegung, nach Ausstoß eines Großteils der Flüssigkeit

Figure A.30: Aufnahmen mit der Hochgeschwindigkeitskamera: erste Pendelbewegung beim Versuch Ta265

Erste Ergebnisse zeigen, dass sich dieses Konzept gut eignet, um das globale Bewegungsmoment, welches durch eine Blastwelle auf die Struktur übertragen wird, zu verringern. Dieser Versuchsaufbau ist ein erster Schritt hin zu einer mit Flüssigkeit gefüllten Struktur in einem Fahrzeug, wobei diese Struktur einen zielgerichteten, durch Rohre gelenkten Flüssigkeitsausstoß beinhaltet. In einem ersten Schritt wurde ein funktionierender Versuchsaufbau entwickelt. Dabei mussten insbesondere Lösungen für eine wasserdichte, mit Flüssigkeit gefüllte Struktur erarbeitet werden, die auf einem Blast-Pendel angebracht werden konnte. Erste experimentelle Ergebnisse zeigen, dass der Ausschlagwinkel des Pendels kleiner ist, wenn eine mit Flüssigkeit gefüllte Struktur vorhanden ist. Dieser Lösungsansatz weist ein hohes Potenzial zur Verringerung des globalen Bewegungsmoments auf.

Schlussfolgerungen und Perspektiven

Diese Arbeit hat die Verwendung von Flüssigkeiten in Schutzstrukturen gegen die Wirkungen von Stoßwellen zum Gegenstand. Insbesondere wird die Übertragung des Bewegungsmoments untersucht. Hierfür wurden zwei Ver-

suchsaufbauten eingesetzt.

Anhand eines mit Flüssigkeit gefüllten und mit Drucksensoren ausgestatteten Containers wurden die Wirkungen der Flüssigkeit auf die Übertragung eines Impulses auf ein Ziel erforscht. Die Flüssigkeit im Container war einer Stoßwelle ausgesetzt, welche von einem Stoßrohr mit Explosivstoff generiert wurde. Es konnte gezeigt werden, dass sich der Impuls durch die Flüssigkeit in der Schutzstruktur ausbreitet. Dies führt zu einer lokalen Impulsverringerung. Es wurde erkannt, dass ein Zusammenhang zwischen der freien Oberfläche, durch welche die Flüssigkeit aus der Schutzstruktur ausgestoßen wird, und der Impulsausbreitung besteht.

Für die Untersuchung der globalen Übertragung des Bewegungsmoments wurde ein Versuchsaufbau eingesetzt, mit welchem eine mit Flüssigkeit gefüllte Schutzstruktur in Bewegung versetzt werden kann. Dieser Beschleunigung geht eine Wechselwirkung mit einer Blastwelle voraus. Besagte Versuchsanordnung enthält ein Blast-Pendel an dem eine Flüssigkeit enthaltenden Schutzstruktur angebracht wurde. Der maximale Ausschlagwinkel des Pendels konnte für eine mit Wasser gefüllte Struktur mit einem Referenzwert äquivalenter Masse verglichen werden. Um einer Vielzahl von Anforderungen gerecht zu werden, wurden verschiedene Versuchskonfigurationen geprüft. Hierbei ging es um den Einschluss des Wassers vor der Stoßwellenbelastung sowie um die Ausstoßzeit und –richtung, sobald die Blastwelle mit der Schutzstruktur in Wechselwirkung tritt.

In Anbetracht der Schlussfolgerungen dieser Studie kann ein Ausblick für künftige akademische Studien und die spätere Integration einer mit Flüssigkeit gefüllten Schutzstruktur in ein Fahrzeug gegeben werden.

Auch die Art der verwendeten Flüssigkeit sollte untersucht werden. Hierbei sollten Flüssigkeiten benutzt werden, welche sich schon an Bord eines Fahrzeugs befinden, wie z.B. Kühlwasser oder Bremsflüssigkeit. Bei den numerischen Simulationen sind die jeweils unterschiedlichen Materialeigenschaften zu berücksichtigen. Außerdem sollten numerische Simulationen des Blast-Pendels und der darauf angebrachten mit Flüssigkeit gefüllten Struktur durchgeführt werden, um mit den erworbenen Kenntnissen künftige Designprozesse effizient zu unterstützen.

Bei Implementierung der untersuchten Schutzlösung in ein Fahrzeug, ist der Einfluss des speziellen Designs und der betreffenden Geometrie auf die Wellenausbreitung in der Flüssigkeit zu bewerten. Ganz allgemein müssen technische Designkonzepte erarbeitet werden, welche den in dieser Arbeit ermittelten Anforderungen an den Flüssigkeitsausstoß und den Flüssigkeitseinschluss entsprechen. In diesem Zusammenhang ist zu bedenken, dass in Fahrzeugen häufig nur begrenzt Raum zur Verfügung steht.

A.3 English

Introduction

Following the detonation of an explosive charge, such as a buried mine or an improvised explosive device, under a vehicle floor, two main effects occur: the rupture or deformation of the vehicle floor due to the loading transmitted by the blast wave and a global vertical acceleration leading in the worst-case scenario to the overturning of the vehicle, due to the impulse being transmitted. For protection purposes, numerous studies have been conducted in literature regarding load transmission in order to reduce target deformation but very few studies focus on impulse transmission, and thus change in momentum. The use of fluids, and in particular water, has been identified as a possible means on acting on impulse transmission. However, the few studies available in the literature focus on the effects of water being included in the protective structure. Therefore, they evaluate the reduction in transmitted impulse to a target by its reduction in deformation. The aim of this work is to identify the phenomena taking place in the fluid itself acting on impulse transmission, placing the investigation upstream of a potential target. Experimental investigations using an explosive driven shock tube allowing the transmission of a blast wave similar to that of a buried mine to a fluid filled container were carried out. These experimental studies were supplemented by numerical simulations, allowing to overcome certain limitations such as the number of measuring points. It was shown that the use of a fluid in a protection against the effects of blast allows the impulse to be spread out, and therefore its local reduction. A link was established between the free surface allowing the fluid to be ejected out of the protection and this impulse spreading. For a more global comprehension of the phenomenon, a blast pendulum was used to observe the effects of fluid filled protection on momentum. This second experimental setup was used to study the effect of the direction of fluid ejection in relation to the origin of the blast loading.

Investigation of impulse spreading

Description of the experimental and numerical setup

An experimental setup was designed to allow the study of a fluid filled cladding under blast loading and is shown in Figure A.31. It comprises a vertically placed explosive driven shock tube generating a planar blast wave with an explosive charge of 15 or 30 grams of C4 placed at a stand-off distance of 50 mm from the entrance of the tube. The tube has an internal section of 80 by 80 mm and a total length of 1750 mm. On the lower end of the tube, a 100 by 100 mm steel plate of a thickness of 1.5, 3 or 5 mm is held into place with adhesive tape. Upon interaction between this plate and the planar, uniform, blast wave generated by the tube, the plate is projected into a water filled container. This container has a dimension of 200 by 200 mm and a depth of 50 or 100 mm. During a given experiment, a PCB pressure sensor located at the center of the bottom of the container gives a local pressure-time history. A high speed imaging camera allowed the visualization of the compression wave in the water during the

experiment.

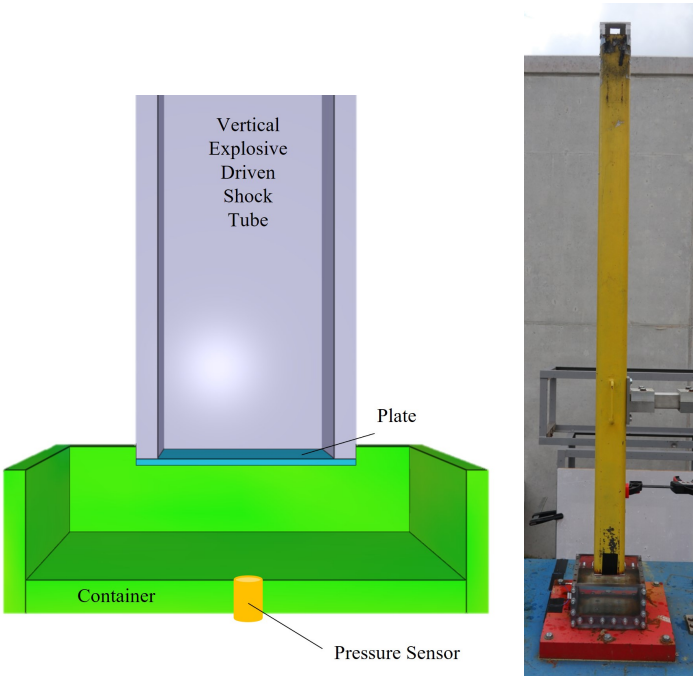

Figure A.31: Experimental setup

The experimental setup was expanded by adding the possibility of having different levels of fluid confinement by adding a lid to the container, allowing or restricting the ability of the fluid of being ejected out of the container as shown in Figure A.32.

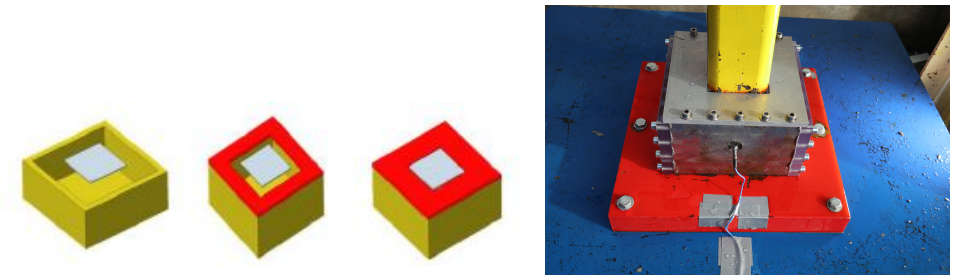

(a) Schematic representation of different water confinement levels. From left to right 0, 50 and 100%.

(b) Illustration of 100% water confinement.

Figure A.32: Expansion of the experimental setup allowing the study of the influence of water confinement.

A reference value describing the load applied to the plate was experimentally acquired. This was done by placing the end of the explosive driven shock tube directly in contact with the pressure sensor, thus determining the pressure profile under perfect reflection conditions. The comparison between the pressure signal measured at the bottom of the water filled container and this reference value will be used to asses the efficiency of the water filled structure for protection purposes. Figure A.33 shows the pressure-time and impulse-time curves for such a reference when 15 grams of C4 are used.

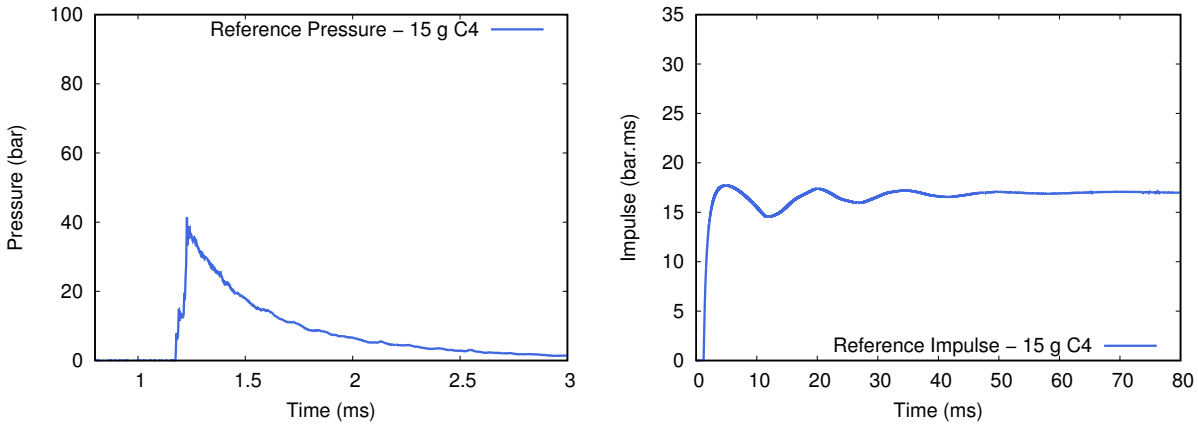

(a) Reference Pressure - 15 g C4

(b) Reference Impulse - 15 g C4

Figure A.33: Blast loads applied to the plate by the explosive driven shock tube serving as reference values, 15 g of C4

This experimental setup was reproduced numerically in LS-Dyna. The numerical model simulates both fluids domains (air and water) using the Arbitrary Lagrangian Eulerian element formulation and the plate using a Lagrangian element formulation. In order to improve calculation time, the numerical model is only a partial simulation as the tube and the explosive charge are not modeled. Rather, the experimentally determined pressure profile of the reference is applied directly to the top nodes of the plate. To further improve calculation time, symmetries of the experimental setup are exploited, allowing the simulation of a quarter of the model. Fully constrained node sets are used for boundary conditions for the container walls as well as confinement areas. The numerical model allowed to overcome the experimental limitation of having only one sensor location, allowing the placement of sensors on the entirety of the container bottom. For this work, a particular interest is taken to the sensors located on the diagonal of the container bottom, shown in Figure A.34, with T1 being the sensor in the middle of the container and T121 the sensor furthest away from the center.

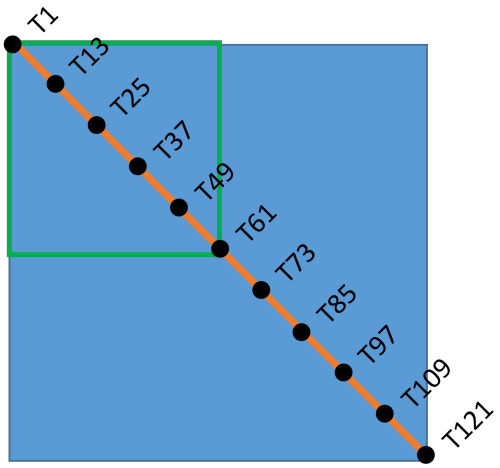

Figure A.34: Database tracer placement along the diagonal of the container bottom in the numerical model

Investigation of the variation of the plate velocity

In order to investigate the capabilities of water to act on the impulse distribution on the bottom of the container, it was chosen to vary the intensity of the compression wave by varying the velocity at which the plate was projected into the water.

This variation could be achieved by using different plate thicknesses, and thus plate weights. The comparison of the pressure-time curves (Figure A.35a) shows that, at the center of the container bottom, a first overpressure peak is either higher or matches the maximal overpressure of the reference signal. However when considering impulse, Figure A.35b shows that a local impulse reduction could be achieved for all plate velocities. Whilst the 1.5 mm and 3 mm plates offer an equivalent level of impulse reduction, the slower plate of 5 mm appears to provide a higher level of local impulse.

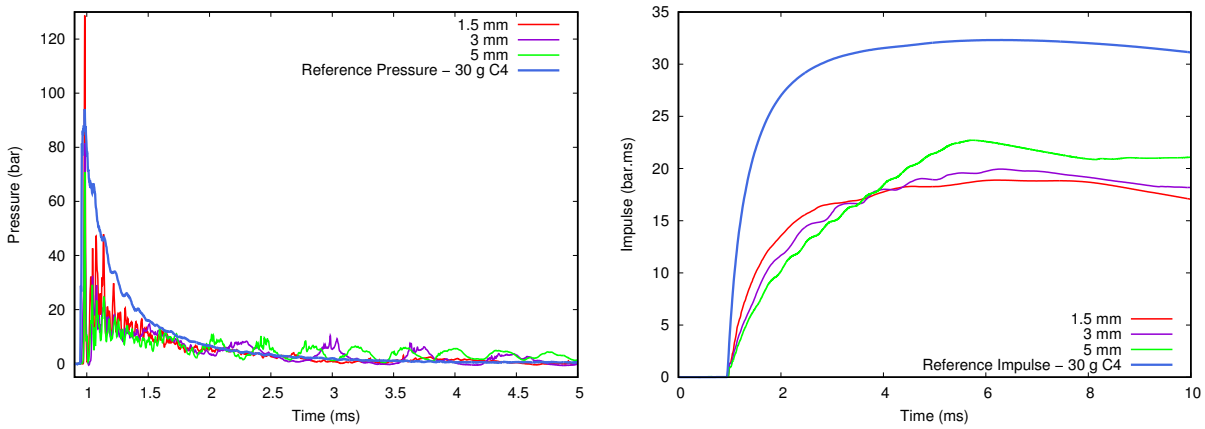

(a) Local pressure measurement

(b) Local impulse measurement

Figure A.35: Comparison of the local measurements at the center of the container bottom for three different plate velocities and comparison to the reference value for 30 g of C4

The numerical model allows to plot impulse distribution on the entirety of the bottom of the container as shown in Figure A.36 for different charge masses and plate thicknesses. Figure A.36 shows a 3D mapping of the impulse on the container bottom once the blast loading has been fully transmitted to the fluid for a container depth of 50 mm. A spreading of impulse occurs along the diagonal of the container, with the highest impulse measured at the center of the container and a gradual decrease when moving towards the edges of the container. The numerical results show that plate velocity does not have a significant influence on the shape of the spreading phenomenon along the bottom of the container.

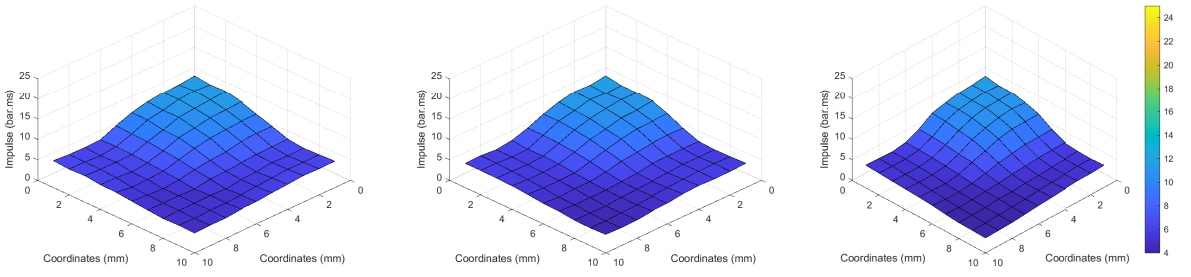

(a) 1.5 mm plate - 15 g C4 (b) 3 mm plate - 15 g C4 (c) 5 mm plate - 15 g C4

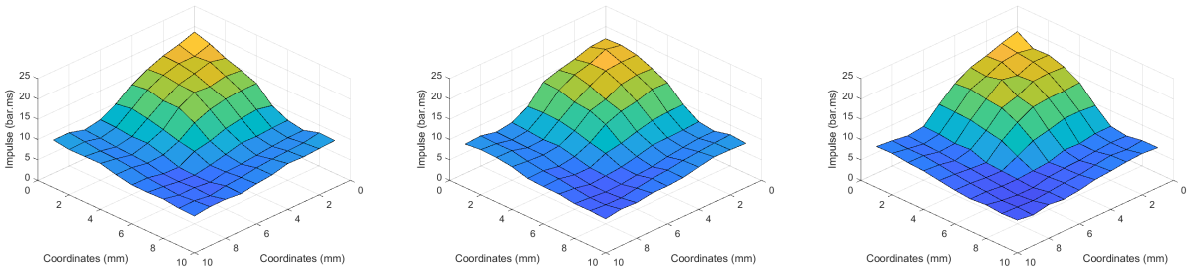

(d) 1.5 mm plate - 30 g C4 (e) 3 mm plate - 30 g C4 (f) 5 mm plate - 30 g C4

Figure A.36: Impulse distribution on the bottom of the container for different charge masses and plate thicknesses, time = 8 ms - 0% confinement, 50 mm fluid depth

Investigation of the fluid confinement and depth

During the experiments with varying plate velocity, a large quantity of the fluid initially present in the container was ejected due to the free water surface. Thus, the influence of fluid confinement on the measurements made at the bottom of the fluid filled container was investigated. This investigation was made with three different levels of water confinement (0, 50 and 100 %).

Experimentally, the influence of the confinement level on local impulse measurements on the bottom of the container was investigated with a charge mass of 15 g, a plate thickness of 3 mm and container depth of 50 mm (Figure A.37). It can be observed that a similar local reduction in impulse is achieved when the fluid is fully unconfined or when 50% of the water surface is free. However, for a fully confined fluid there is no reduction in the measured impulse. These very interesting local observations seem to point in the direction of the high importance of the ability of the fluid to be ejected out of the container.

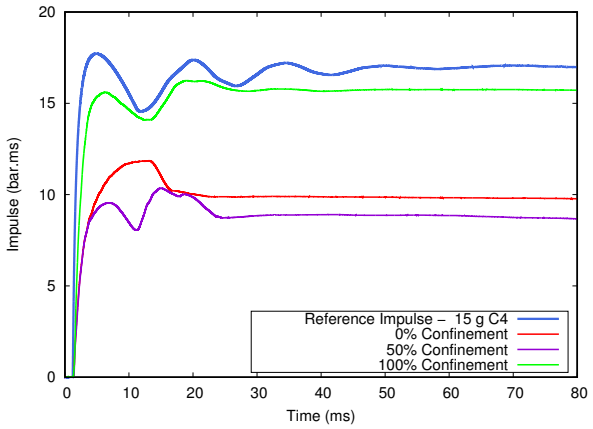

Figure A.37: Experimental local impulse measurements for different degrees of water confinement - 15 g C4, 3 mm plate, 50 mm fluid depth.

A numerical model of the experimentally investigated levels of water confinement of 0, 50 and 100% allowed to look at the impulse spreading along the diagonal of the bottom of the container (Figure A.38). In the case of an unconfined fluid (Figure A.38a), impulse spreading occurs along the diagonal of the container, with the highest impulse measured at the center of the container and a gradual decrease when moving towards the edge of the container. For a level of fluid confinement of 50% (Figure A.38b), impulse reduction occurs similarly to the case of a fully unconfined fluid. However, the spreading of impulse along the diagonal of the container bottom is less pronounced. As the spreading does not occur when the fluid is fully confined, as shown in Figure A.38c, it can be concluded that it is most likely due to the boundary conditions.

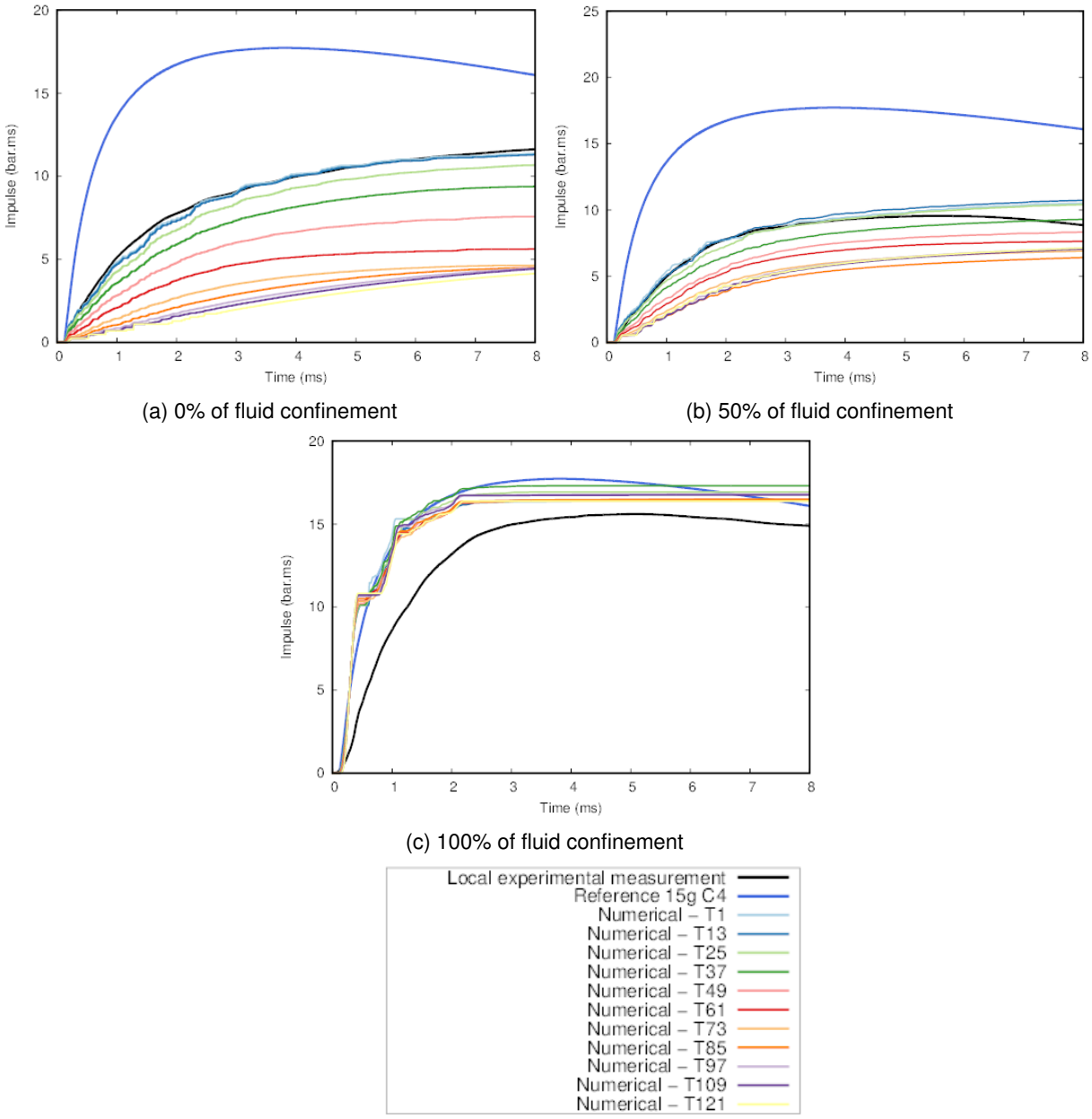

(a) 0% of fluid confinement

(b) 50% of fluid confinement

(c) 100% of fluid confinement

Figure A.38: Impulse along the diagonal of the container bottom for different levels of fluid confinement - 15 g C4, 3 mm plate, 50 mm fluid depth.

An experimental setup with an increased fluid depth of 100 mm was also investigated. Previous conclusions established with the 50 mm deep container could be observed with an increased water height. However, as the compression wave inside the fluid is of spherical shape, the additional water height allows time for this spherical shape to reach a larger radius, thus smoothing the local variations observed at the bottom of the container. Even though the shape of the impulse distribution at the bottom of the container is less pronounced, local reduction in impulse are still measured.

Through local measurements, it was found that a higher plate velocity increased the first overpressure peak. Regarding local impulse, there did not seem to be an effect of an increasing plate velocity when the thickness of the plate was varied. The numerical results enabled us to gain additional insight on the impulse distribution in the bottom plate. In particular, the impulse is not homogeneously distributed on the bottom plate, but spreading was observed, with a maximal value at the center and a minimum at the corners of the container. With this experimental setup, the impulse is fully being transmitted to the bottom of the container as it is rigid and fixed in space. This allowed to make observations on the influence of a fluid on impulse spreading. To gain understanding regarding global momentum transmission, a fluid filled structure that can be set into motion has to be tested. Therefore, another experimental setup is developed including a blast pendulum for the understanding of momentum transmission.

Momentum transmission

Experimental setup

A blast pendulum is an experimental device that allows to establish a link between the rotational movement of the pendulum and the impulse that was transmitted to its structure following the detonation of an explosive charge. The pendulum used at ISL is shown in Figure A.39. In the case of this investigation, the maximal angle of elevation of the pendulum (occurring during the first oscillation) can be assimilated to the maximum vertical displacement of a target following the detonation of an explosive charge below a vehicle. Thus, the maximal angle of elevation of fluid filled structures will be compared to the reference value where the pendulum has an equal weight without fluid. In the case of this investigation, this reference value corresponds to the use of 840 grams of C4 at a stand-off distance of 1 m from the pendulum having a total mass of 215 kg. The motion of the blast pendulum was recorded with a high speed imaging camera and rotation sensor placed in the axis of the pendulum.

Figure A.39: Pendulum used at ISL

The fluid for this experimental setup was placed in between a front and a back plate inside a water bag as shown

in Figure A.40a. By not restricting the water in a closed architecture, this design should allows the water to spread on the side as it is pushed by the front plate during its deformation. To ensure that the center of mass of the entire setup is positioned in the center of the pendulum body, steel plates were placed on the opposite side for weight compensation (Figure A.40b).

(a) Front plate, water filled bag and back plate

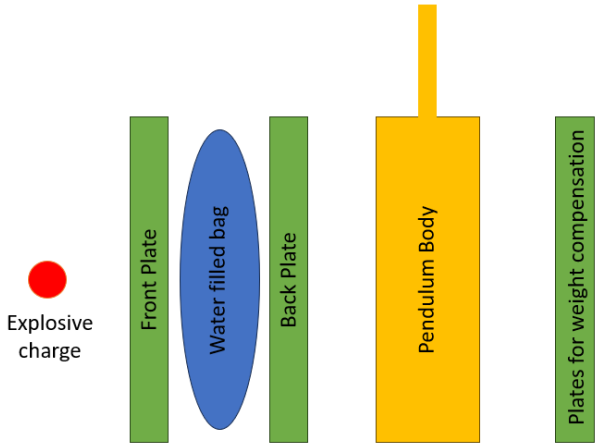

(b) Schematic representation of the experimental setup

Figure A.40: Placement of water bags on the blast pendulum

Variation of water mass and plate configuration

In order to investigate the quantity of water needed for a reduction in the angle of elevation of the pendulum, the water mass present in the fluid filled bag, placed in between a front and a back plate was varied. Water masses of 7.85 kg, 9.81 kg and 11.78 kg were used, these water masses correspond respectively to 4.9, 6 and 7.3 % of the total pendulum mass. For all three configurations, the total weight of the pendulum was kept constant and equal to the weight of the pendulum of the reference value. To account for an increased or decrease water mass, the thickness of the front and back plates surrounding the water bag were adjusted accordingly. The experimental results for the configuration with 11.78 kg of water is shown in Figure A.41. It can be observed that no reduction in the maximal angle reached by the pendulum occurs, this observation is true for all water masses tested.

Looking at the images provided by the high speed camera, it could be observed that the fluid ejection occurs only after the pendulum was set into motion by the blast as it is trapped in between the front and back plate. Therefore, the front plate was removed in a second experimental configuration to allow more freedom of motion to the water. The same water quantities were used in this second set of experiments. In that configuration, a reduction of the maximal angle of elevation of the pendulum occurs (Figure A.42). This reduction seemed to increase when the water mass used increased. However, for the interpretation of these results it has to be noted that, as no front plate is present, the water ejection following the detonation can be directly projected towards the explosive charge, thus possibly mitigating the fire ball with the water droplets and therefore reducing the total impulse being transmitted to

the pendulum.

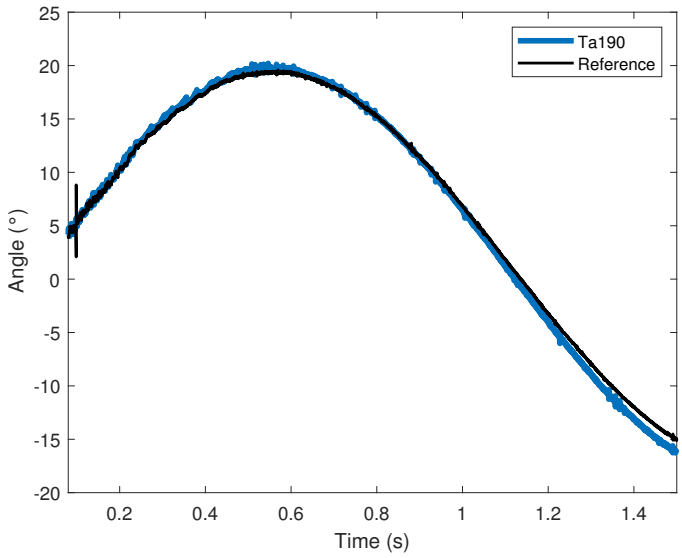

Figure A.41: Angular elevation of the pendulum for a water mass of 11.78 kg placed in between a front and a back plate, comparison to the reference value

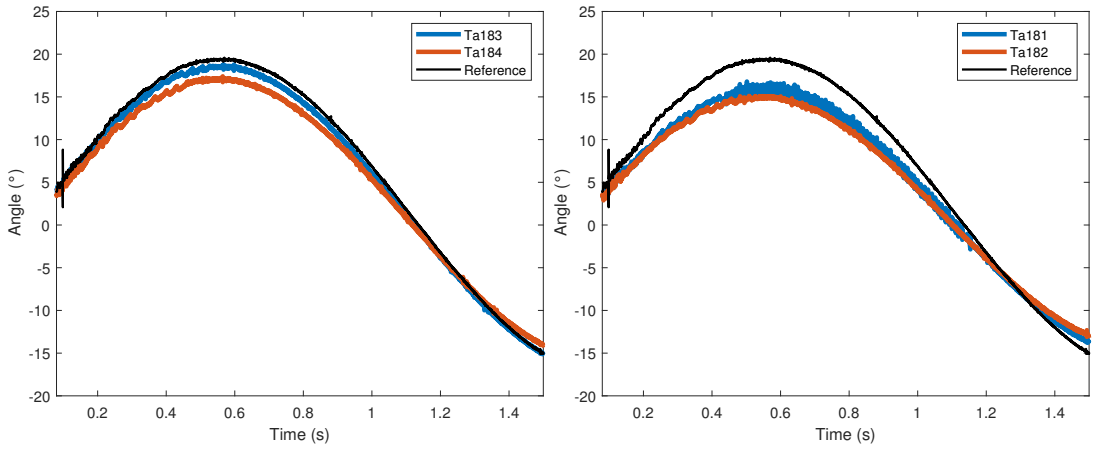

(a) Water mass of 7.85 kg

(b) Water mass of 11.78 kg

Figure A.42: Angular elevation of the pendulum for the experimental configuration where the front plate has been removed, comparison to the reference value

Modification of the experimental setup

Following these first experimental observations, the setup was modified to improve the ejection of the fluid out of a structure with both a front and back plate. The direction of ejection of the water mass needs to be in the same direction as the blast loading in order for the velocity vector generated by the vertical acceleration of the vehicle to be counteracted by the velocity vector generated by the ejection of the mass accordingly to Newton's third law of motion.

The previously presented pendulum had to be modified to allow the passage of a tube serving for water ejection through the body of the pendulum. Figure A.43a illustrates the placement of the tube forcing the direction of water ejection, requiring holes to be made in the back plate and the body of the pendulum. For the side confinement of the fluid, a frame was added in between the front and back plate, allowing for a closed fluid filled structure where the only openings are provided by the tubes (Figure A.43b). In this case, the water was no longer placed into a water bag as water was filled directly intro the structure by an opening in the aluminum frame. The main difficulty of this investigation consisted in finding appropriate solutions to prevent water leakage from the structure. As the experimental setup was modified, a new reference value was established to take into account the weight increase due to the addition of the aluminum frame. For this experimental configuration, the total weight of the pendulum is of 231 kg and the fluid mass of 16 kg represented 6.92 % of the total pendulum mass.

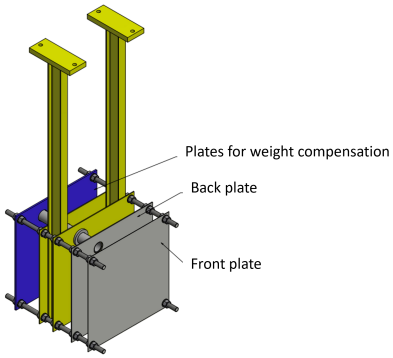

(a) Schematic representation, the aluminum frams is not shown

(b) New experimental setup with aluminum frame

Figure A.43: New experimental configuration allowing the ejection of water through tubes

The experimental investigations for this particular configuration are ongoing. A first result with four openings of a diameter of 100 mm can be shown. The images provided by the high speed camera shows that in this case, water ejection occurs before pendulum motion (Figure A.45). A reduction of the maximal angular elevation of around 4° can be observed (Figure A.44), which corresponds to 35% of the maximal angle of the reference.

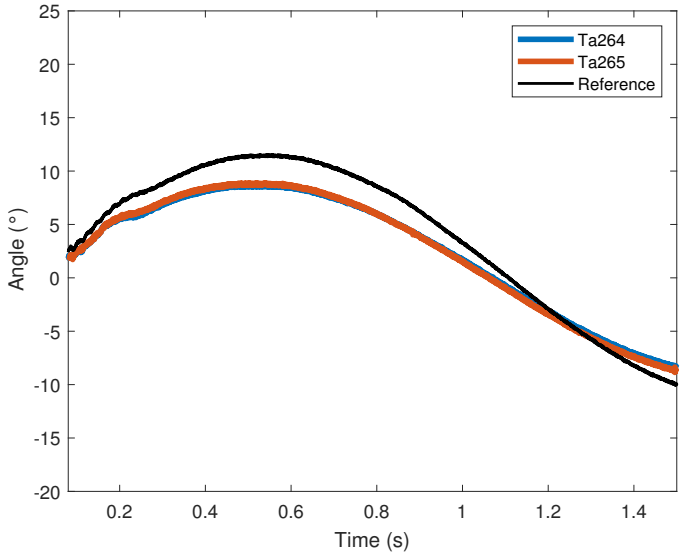

Figure A.44: Angular elevation of the pendulum for a fluid filled structure with 4 openings of diameter 100 mm, comparison to the reference value

(a) t=41.317 ms, start of the water ejection before pendulum motion

(b) t=60.317 ms, water ejection before pendulum motion

(c) t=91.317 ms, directed water ejection

(d) t=245.317 ms, pendulum motion once the majority of the fluid is ejected

Figure A.45: High speed camera images of the first oscillation of the pendulum for experiment Ta265

Preliminary results show that this concept has a good potential for reduction of the global momentum transferred by the blast to the structure. The experimental setup represents a first step towards integration of a fluid filled structure in a vehicle with an intentional path for fluid ejection through tubes. A first phase of this investigation consisted in establishing a working experimental setup and solving issues mainly related to the sealing of a fluid filled structure installed on a blast pendulum. First experimental results show a reduction of the angular elevation of the pendulum when equipped with a fluid filled structure and show the potential of such a solution for global momentum reduction.

Conclusions and perspectives

In this investigation, the use of fluids in protective structures against the effect of blast, especially momentum transmission, were investigated. For this purpose, two experimental setups were used.

The effects of the use of a fluid on the impulse transmission to a target were investigated using a fluid filled container equipped with pressure sensors. The fluid in this container was subjected to blast loading from an explosive driven shock tube. It was shown that the use of a fluid in a protection allows the impulse to be spread out, and therefore its local reduction. A link was established between the free surface allowing the fluid to be ejected out of the protection and this impulse spreading.

For the investigation of global momentum transmission, an experimental setup allowing a fluid filled structure to be set into motion following an interaction with a blast wave had to be used. This was done using a blast pendulum onto which fluid filled structures could be placed. The maximal angle reached by the pendulum could be compared for a water filled structure and a reference value of equivalent mass established using steel plates. Different experimental configurations were tested to address a number of requirements related to the containment of water prior to the blast, as well as its ejection time and direction once the blast interacts with the structure.

With regards to the conclusions drawn following this study, perspectives for future academic investigations and perspectives for vehicle integration should water filled protective structure be implemented on a vehicle can be explored.

The influence of the type of fluid used should be investigated, with the goal of making use of fluids already on board a vehicle such as cooling or brake fluid for example. This would allow to improve vehicle protection against the effects of blast without increasing vehicle mass too much. This could be done by changing the material properties in the numerical simulations established in the course of this investigation. Furthermore, a numerical simulations of the blast pendulum and the associated fluid filled structure should be established to aid in future design processes.

In the case of an integration of the protective solution onto a vehicle, the influence of the particular design and its geometry on the wave propagation inside the fluid will have to be assessed. Generally speaking, technical solutions to design guidelines such as the need for fluid ejection or fluid confinement established in this study will have to be found whilst taking into account often restrictive space requirements in a vehicle.

Bibliography

[1] International Campaign to Ban Land Mines. *LANDMINE MONITOR 2022*. 2022. ISBN: 9782970147626. URL: www.the-monitor.org/cp.

[2] Huon Adam Bornstein. “Physical Mechanisms for Near-Field Blast Mitigation with Fluid-Filled Containers”. PhD thesis. RMIT University, 2018.

[3] G.S. Langdon et al. “Fracture of aluminium foam core sacrificial cladding subjected to air-blast loading”. In: *International Journal of Impact Engineering* 37.6 (2010). Impact Loading of Lightweight Structures, pp. 638–651. ISSN: 0734-743X. DOI: https://doi.org/10.1016/j.ijimpeng.2009.07.006.

[4] Zhenyu Xue and John W. Hutchinson. “A comparative study of impulse-resistant metal sandwich plates”. In: *International Journal of Impact Engineering* 30 (2004), pp. 1283–1305.

[5] John W. Hutchinson and Zhenyu Xue. “Metal sandwich plates optimized for pressure impulses”. In: *International Journal of Mechanical Sciences* 47.4 (2005). A Special Issue in Honour of Professor Stephen R. Reid’s 60th Birthday, pp. 545–569. ISSN: 0020-7403. DOI: https://doi.org/10.1016/j.ijmecsci.2004.10.012.

[6] A.G. Hanssen, L. Enstock, and M. Langseth. “Close-range blast loading of aluminium foam panels”. In: *International Journal of Impact Engineering* 27.6 (2002), pp. 593–618. ISSN: 0734-743X. DOI: https://doi.org/10.1016/S0734-743X(01)00155-5.

[7] M.D. Theobald and G.N. Nurick. “Numerical investigation of the response of sandwich-type panels using thin-walled tubes subject to blast loads”. In: *International Journal of Impact Engineering* 34.1 (2007). International Conference on Impact Loading of Lightweight Structures, pp. 134–156. ISSN: 0734-743X. DOI: https://doi.org/10.1016/j.ijimpeng.2006.04.003.

[8] Martien Teich and Norbert Gebbeken. “Analysis of FSI effects of blast loaded flexible structures”. In: *Engineering Structures* 55 (2013). Analysis and Design of Protective Structures, pp. 73–79. ISSN: 0141-0296. DOI: https://doi.org/10.1016/j.engstruct.2011.12.003.

[9] N. Kambouchev, L. Noels, and R. Radovitzky. “Nonlinear compressibility effects in fluid-structure interaction and their implications on the air-blast loading of structures”. In: *Journal of Applied Physics* 100.6 (2006), p. 063519. DOI: 10.1063/1.2349483.

[10] Amin Paykani et al. “Dynamic analysis and design of V-shape plates under blast loading”. In: *Journal of Vibroengineering* 15 (2013), pp. 971–978.

[11] S. Chung Kim Yuen et al. “Response of V-shape plates to localised blast load: Experiments and numerical simulation”. In: *International Journal of Impact Engineering* 46 (2012), pp. 97–109. ISSN: 0734-743X. DOI: https://doi.org/10.1016/j.ijimpeng.2012.02.007.

[12] Huon Bornstein, Shannon Ryan, and Adrian Mouritz. “Physical mechanisms for near-field blast mitigation with fluid containers: Effect of container geometry”. In: *International Journal of Impact Engineering* 96 (2016), pp. 61–77. ISSN: 0734-743X. DOI: https://doi.org/10.1016/j.ijimpeng.2016.04.015.

[13] Michel Arrigoni. *Ondes de choc dans la matière condensée, Cours ENSIETA 3. Année*. 2009.

[14] *LS-DYNA Keyword User's Manual, Version 971 R6.1.0, Vol.2*. Livermore Software Technology Corporation (LSTC), 2012.

[15] Gilbert Ford Kinney and Kenneth Judson Graham. *Explosive Shocks in Air*. Springer Science Business Media, 1985. ISBN: 9783642866845. DOI: 10.1007/978-3-642-86682-1.

[16] C.E. Needham. *Blast Waves, Shock Wave and High Pressure Phenomena*. Springer Verlag Berlin Heidelberg, 2010. ISBN: 9783642052873.

[17] B Hopkinson. *British ordnance board minutes. Rerport 13565*. British Ordonance Office, 1915.

[18] C Cranz. *Lehrbuch der Ballisitk, Zweiter Band*. Springer Verlag Berlin Heidelberg 1926, 1926. ISBN: 978-3-642-52558-2. DOI: 10.1007/978-3-642-52612-1.

[19] G.I. Taylor. “The formation of a blast wave by a very intense explosion I. Theoretical discussion”. In: *Proceedings of the Royal Society of London. Series A. Mathematical and Physical Sciences* (1950), pp. 159–174.

[20] John Von Neumann. *John Von Neumann: Collected Works. Theory of games, astrophysics, hydrodynamics and me- teorology*. 6th ed. Pergamon Press, 1963.

[21] L I Sedov. “Propagation of strong shock waves”. In: *Journal of Applied Mathematics and Mechanics* (1946).

[22] Nayden Kambouchev. “Analysis of Blast Mitigation Strategies Exploiting Fluid-Structure Interaction”. PhD thesis. Massachusetts Institute of Technology, 2007.

[23] T. Schunck et al. *Mitigation of Blast in a Water Mist, 31st International Symposium on Shock Waves 2*. Springer International Publishing, 2019, pp. 711–718. ISBN: 978-3-319-91017-8.

[24] Samuel E Rigby. “Blast Wave Clearing Effects on Finite-Sized Targets Subjected to Explosive Loads”. PhD thesis. University of Sheffield, Department of Civil and Structural Engineering, 2014, p. 192. DOI: 10.1088/1741-2560/8/4/046017. URL: https://www.researchgate.net/profile/Sam_Rigby/publication/281861546_Blast_wave_clearing_effects_on_finite-sized_targets_subjected_to_explosive_loads/links/55fc0a8a08aeba1d9f3a6bb0.pdf.

[25] Ludovic Blanc, D. Lebaillif, and A. Bufalo. “Experimental analysis of fluid–structure interaction between a blast wave and a sandwich add-on armor”. In: *AIP Advances* 12 (May 2022), p. 055105. DOI: 10.1063/5.0082336.

[26] Denis Bergeron, Robert Walker, and Clay Coffey. *Detonation of 100 gram anti personnel mine surrogate charges in sand*. Defence research establishement suffiled, 1998.

[27] N Heider et al. “Vehicle Protection Against Global IED Effects”. In: *27th International Symposium on Ballistics* (2013).

[28] H. Ousji et al. “Air blast response of sacrificial cladding using low density foams: Experimental and analytical approach”. In: *Internatioal Journal of Mechanical Sciences* 128-129 (2017), pp. 459–474.

[29] Yun Chen, Wei Huang, and Shlomi Constantini. “Blast Shock Wave Mitigation Using the Hydraulic Energy Redirection and Release Technology”. In: *PLOS ONE* 7.6 (2012). DOI: 10.1371/journal.pone.0039353.

[30] Laurence Young et al. *A Fluid Helmet Liner for Protection Against Blast Induced Traumatic Brain Injury*. Tech. rep. Massachusetts Institute of Technology, Office of Naval Research, 2010.

[31] V. Denefeld et al. “Reduction of global effects on vehicles after IED detonations”. In: *Defence Technology* 10.2 (2014), pp. 219–225. ISSN: 22149147. DOI: 10.1016/j.dt.2014.05.005.

[32] Janet Crumrine Wolfson. “Blast damage mitigation of steel structures from near-contact charges”. PhD thesis. UC San Diego, 2008, p. 214.

[33] Huon Bornstein, Shannon Ryan, and Adrian P. Mouritz. “Blast mitigation with fluid Containers: Effect of mitigant type”. In: *International Journal of Impact Engineering* 113 (2018), pp. 106–117. ISSN: 0734-743X. DOI: https://doi.org/10.1016/j.ijimpeng.2017.11.012.

[34] Sophie Trelat. “Impact de fortes explosions sur les bâtiments représentatifs d’une installation industrielle”. PhD thesis. Université d’Orléans, 2006.

[35] I. Sochet, T. Lamy, and J. Brossard. “Experimental investigation on the detonability of non-uniform gaseous mixtures”. In: *Shock Waves* 10.5 (Nov. 2000), pp. 363–376. DOI: 10.1007/s001930000066. URL: https://hal.science/hal-01833463.

[36] Guanbing Cheng. “Contribution à l’étude de la Transition Déflagration Détonation (TDD) dans les Mélanges Gazeux Binaires”. PhD thesis. Ecole Nationale Superieure de Mecanique et d’Aerotechnique, 2012. ISBN: 561E598D5658693.

[37] W. Van Paepegem et al. “Blast performance of a sacrificial cladding with composite tubes for protection of civil engineering structures”. In: *Composites Part B: Engineering* 65 (2014). Damage Mechanics, pp. 131–146. ISSN: 1359-8368. DOI: https://doi.org/10.1016/j.compositesb.2014.02.004. URL: https://www.sciencedirect.com/science/article/pii/S135983681400081X.

[38] Sivakumar Palanivelu. “Energy Absorption of Crushable Tubes for Protective Structures under Static, Impact and Blast Loading Sivakumar Palanivelu”. PhD thesis. University Ghent, 2010. ISBN: 9789085784388.

[39] Björn Zakrisson, Bengt Wikman, and Hans-Åke Häggblad. “Numerical simulations of blast loads and structural deformation from near-field explosions in air”. In: *International Journal of Impact Engineering* 38.7 (2011), pp. 597–612. ISSN: 0734-743X. DOI: https://doi.org/10.1016/j.ijimpeng.2011.02.005. URL: https://www.sciencedirect.com/science/article/pii/S0734743X11000200.

[40] Marek Świerczewski, Grzegorz Sławiński, and Piotr Malesa. “Modelling and the FEM Analysis of the Effects of the Blast Wave on the Floor of a Vehicle According to the AEP-55 Vol. 2 Methodology”. In: *Mechanisms and Machine Science, Springer Science and Business Media B.V.* 75 (2020), pp. 1157–1168. ISSN: 22110992. DOI: 10.1007/978-3-030-27053-7_99.

[41] *AEP-55 Procedures for evaluating the protection level of logisitic or light armoured vehicles*. Vol. 2. NATO, 2011.

[42] M Vieille. “Étude sur le role des discontinuités dans les phénomènes de propagation”. In: *J. Phys. Theor. Appl* 9 (1 1900). DOI: 10.1051/jphystap:019000090062100. URL: https://hal.science/jpa-00240479.

[43] K. Kitagawa et al. “Attenuation properties of blast wave through porous layer”. In: *Hannemann, K., Seiler, F. (eds) Shock Waves. Springer, Berlin, Heidelberg.* (2009), pp. 73–78.

[44] Michael W Seitz and Beric W Skews. “Effect of Compressible Foam Properties on Pressure Amplification During Shock Wave Impact”. In: *Shock Waves* 15 (3 2006), pp. 177–197. ISSN: 1432-2153. DOI: 10.1007/s00193-006-0033-2. URL: https://doi.org/10.1007/s00193-006-0033-2.

[45] Amy C. Courtney, Lubov P. Andrusiv, and Michael W. Courtney. “Oxy-acetylene driven laboratory scale shock tubes for studying blast wave effects”. In: *Review of Scientific Instruments* 83 (4 Apr. 2012). ISSN: 00346748. DOI: 10.1063/1.3702803.

[46] Ronald A Segars and Marina G Carboni. *A Shock Tube for Downselecting Material Concepts for Blast Protection*. U.S. Army Natick Soldier Research, Development and Engineering Center Natick, Massachusetts 01760-5000, 2008.

[47] M.A. Louar et al. “Explosive driven shock tube loading of aluminium plates: experimental study”. In: *International Journal of Impact Engineering* 86 (2015), pp. 111–123. ISSN: 0734-743X. DOI: https://doi.org/10.1016/j.ijimpeng.2015.07.013. URL: https://www.sciencedirect.com/science/article/pii/S0734743X15001682.

[48] Army TM 5-1300, Navy NAVFAC P-394, and Air Force AFR 88-22. *Unified Facilities Criteria, UFC 3-340-02, Structures to resist the effects on accidental explosions*. 1990. URL: http://dod.wbdg.org/..

[49] L.F. Henderson et al. “Refraction of a shock wave at an air-water interface”. In: *Fluid Dynamics Research* 5.5-6 (1990), pp. 337–350. ISSN: 01695983. DOI: 10.1016/0169-5983(90)90003-H.

[50] Phillip J. Peckham. *Air to water blast wave transfer*. Tech. rep. Naval Surface Weapons Center, 1976.

[51] Benjamin Robins. *New Principles of Gunnery*. Richmond Publishing Co. Ltd., 1742.

[52] I M Snyman and T Van Dyk. “The imparted impulse of a PMN anti-personnel mine”. In: *2010 National Ballistics Symposium of South Africa* (2010).

[53] B Reck et al. “Ballistic Pendulum for Blast Wave Impulse measurement, Analysis and Optimization”. In: *Military Aspects of Blast and Shock, Oslo, Norway* (2008).

[54] Martin Larcher and Folco Casadei. “Explosions in Complex Geometries - A Comparison of Several Approaches”. In: *International Journal of Protective Structures* 1 (2 2010).

[55] Ludovic Blanc. “Numerical modelling of sacrificial cladding”. In: *Agence Innovation Defense, Grant agreement DGA/ISL No. 2021.65.0008 (T4-05)* (2022).

[56] Jose A Sanchidrian et al. “Determination of the JWL Constants for ANFO and Emulsion Explosives from Cylinder Test Data”. In: *Central European Journal of Energetic Materials* 12 (2 2015), pp. 177–194. ISSN: 1733-7178.

[57] L. Olovsson et al. “A particle-based approach to close-range blast loading”. In: *European Journal of Mechanics - A/Solids* 29.1 (2010), pp. 1–6. ISSN: 0997-7538. DOI: https://doi.org/10.1016/j.euromechsol.2009.06.003. URL: https://www.sciencedirect.com/science/article/pii/S0997753809000783.

[58] Jérôme Limido et al. “Modeling of the Hypervelocity Impact Experiments using Gamma-SPH Technique”. In: *Proceedings of the ASME 2017 Pressure Vessel and Piping Conference PVP2017* (2017).

[59] Alexander L Kozak et al. “Validation of the ALE Methodology by Comparison with the Experimental Data Obtained from a Sloshing Tank”. In: *LS-DYNA User Conference* (2016), pp. 1–14.

[60] O. M. Faltinsen. *Sloshing*. Cambridge University Press, 2017. ISBN: 10000992. DOI: 10.6052/1000-0992-16-017.

[61] Todd B Silvester and Paul W Cleary. “Wave-Structure Interaction Using Smoothed Particle”. In: *Fifth International Conference on CFD in the Process Industries* (December 2006), pp. 1–8. URL: http://www.cfd.com.au/cfd_conf06/PDFs/026Sil.pdf.

[62] M Gomez-Gesteira. *SPHERIC SPH Benchmark test cases: Test 1 - Force exerted by a schematic 3D dam break on a square cylinder*. 2006. URL: http://cfd.me.umist.ac.uk/sph/TestCases/SPH_Test1.html.

[63] B M Dobratz and P C Crawford. *Properties of Chemical Explosives and Explosive Simulants*. LLNL Explosives Handbook, 1985.

[64] *LS-DYNA Keyword User's Manual, Version 971 R6.1.0, Vol.1*. Livermore Software Technology Corporation (LSTC), 2012.

[65] C Bisagni and M S Pigazzini. "Modelling strategies for numerical simulation of aircraft ditching". In: *International Journal of Crashworthiness* 0.0 (2018), pp. 1–18. ISSN: 1358-8265. DOI: 10.1080/13588265.2017.1328957.

[66] Dong-Myung Bae and Ahmad Zakki. "Comparisons of Multi Material ALE and Single Material ALE in LS-DYNA for Estimation of Acceleration Response of Free-fall Lifeboat". In: *Journal of the Society of Naval Architects of Korea* 48 (Dec. 2011). DOI: 10.3744/SNAK.2011.48.6.552.

[67] R. Byron Bird et al. *Transport Phenomena*. John Wiley and Sons Inc., 2002, p. 895. ISBN: 0471410772.

université PARIS-SACLAY
ÉCOLE DOCTORALE
Sciences mécaniques et énergétiques, matériaux et géosciences (SMEMAG)

Titre: Protection contre les ondes de souffles à l'aide de fluide

Mots clés: Effet de souffle, Equipement de protection, Expérimental

Résumé: Lors de la détonation d'une charge explosive sous le plancher d'un véhicule, telle qu'une mine enterrée ou un engin explosif improvisé, deux effets principaux se produisent : la déformation ou rupture du plancher due à la contrainte transmise par le blast et l'accélération verticale globale du véhicule pouvant mener à son retournement due à l'impulsion qui lui est transmise. Dans un but de protection, de nombreuses études dans la littérature se concentrent sur la transmission du chargement afin de réduire les déformations du plancher mais très peu d'études se concentrent sur la transmission d'impulsion, et donc de variation de quantité de mouvement. L'utilisation de fluides, en particulier l'eau, a été identifié comme pouvant potentiellement permettre d'agir sur cette transmission d'impulsion. Néanmoins, les quelques études présentes dans la littérature se focalisent sur les effets de la présence de l'eau dans la protection. Elles évaluent ainsi la réduction d'impulsion transmise à une cible par la déformation de celle-ci. Ainsi, ces travaux proposent d'identifier les phénomènes ayant lieu dans le fluide en lui-même agissant sur la transmission d'impulsion, se plaçant donc en amont de la cible. Des études expérimentales utilisant un tube à choc explosif permettant de transmettre un blast proche de celui généré par une mine enterrée à un conteneur rempli d'eau ont été réalisées. Ces études expérimentales ont été complétées par des simulations numériques, permettant de surmonter certaines limitations tel que le nombre de points de mesure. Il a été montré que l'utilisation d'un fluide dans une protection contre les effets de souffle permet un étalement de l'impulsion, et donc sa diminution locale. Un lien entre la surface libre permettant au fluide d'être éjecté de la protection et cet étalement d'impulsion a été établi. Pour une compréhension plus globale du phénomène, un pendule à blast a été utilisé pour observer les effets d'un fluide dans une protection sur la quantité de mouvement. Ce second dispositif expérimental a été utilisé afin d'étudier l'effet de la direction d'éjection du fluide par rapport à l'origine du chargement par le blast.

Title: Blast protection with fluids

Keywords: Blast load, Protective equipment, Experimental

Abstract: Following the detonation of an explosive charge, such as a buried mine or an improvised explosive device, under a vehicle floor, two main effects occur: the rupture or deformation of the vehicle floor due to the loading transmitted by the blast wave and a global vertical acceleration leading in the worst-case scenario to the overturning of the vehicle, due to the impulse being transmitted. For protection purposes, numerous studies have been conducted in literature regarding load transmission in order to reduce target deformation but very few studies focus on impulse transmission, and thus change in momentum. The use of fluids, and in particular water, has been identified as a possible means on acting on impulse transmission. However, the few studies available in the literature focus on the effects of water being included in the protective structure. Therefore, they evaluate the reduction in transmitted impulse to a target by its reduction in deformation. The aim of this work is to identify the phenomena taking place in the fluid itself acting on impulse transmission, placing the investigation upstream of a potential target. Experimental investigations using an explosive driven shock tube allowing the transmission of a blast wave similar to that of a buried mine to a fluid filled container were carried out. These experimental studies were supplemented by numerical simulations, allowing to overcome certain limitations such as the number of measuring points. It was shown that the use of a fluid in a protection against the effects of blast allows the impulse to be spread out, and therefore its local reduction. A link was established between the free surface allowing the fluid to be ejected out of the protection and this impulse spreading. For a more global comprehension of the phenomenon, a blast pendulum was used to observe the effects of fluid filled protection on momentum. This second experimental setup was used to study the effect of the direction of fluid ejection in relation to the origin of the blast loading.

Titel: Blast Schutz mit Fluiden

Schlüsselwörter: Blast load, Schutzstruktur, Experimentell

Zusammenfassung: Bei der Detonation einer Sprengladung unter dem Boden eines Fahrzeugs, z. B. einer vergrabenen Mine oder eines improvisierten Sprengkörpers, treten zwei Haupteffekte auf: die Verformung oder Zerstörung des Fahrzeugbodens durch die vom Blast übertragene Belastung und die allgemeine vertikale Beschleunigung des Fahrzeugs. Diese kann aufgrund des auf das Fahrzeug übertragenen Impulses zu einem Überschlag führen. Viele Studien über Fahrzeugschutz in der einschlägigen Literatur befassen sich mit der Übertragung der Belastung und haben zum Ziel, die Verformung des Fahrzeugbodens zu verringern. Es befassen sich aber nur sehr wenige Studien mit der Übertragung des Impulses und damit der Änderung des Bewegungsmoments. Die Verwendung von Flüssigkeiten, insbesondere Wasser, wurde als potenzielles Mittel zur Beeinflussung der Impulsübertragung identifiziert. Die wenigen in der Literatur vorhandenen Studien konzentrieren sich jedoch auf die Wirkungen des Vorhandenseins von Wasser innerhalb der Schutzstruktur. Sie bewerten die Reduzierung des auf das Ziel übertragenen Impulses im Hinblick auf den Verformungsgrad des Ziels. Diese Arbeit hat zum Ziel, die in der Flüssigkeit stattfindenden Phänomene zu identifizieren, die sich auf die Impulsübertragung auswirken. Dafür wird also vor dem Ziel gemessen. Es wurden experimentelle Studien durchgeführt, bei denen ein Explosivstoff enthaltendes Stoßrohr einen Blast überträgt, welcher der Stoßwelle einer vergrabender Mine nahe kommt. Dabei wird der Blast auf einen mit Wasser gefüllten Behälter übertragen. Diese experimentellen Studien wurden durch numerische Simulationen ergänzt, wodurch einige Einschränkungen, wie die Anzahl der Messpunkte, überwunden werden konnten. Es wurde gezeigt, dass die Verwendung einer Flüssigkeit in einer Schutzstruktur gegen Druckwellen zu einer Ausbreitung des Impulses und damit zu einer lokalen Abnahme des Impulses führt. Es wurde ein Zusammenhang zwischen der freien Fläche, aus welcher die Flüssigkeit aus der Schutzvorrichtung ausgestoßen wird, und der Impulsausbreitung hergestellt. Für ein umfassenderes Verständnis des Vorgangs wurde ein Blast-Pendel verwendet, um die Wirkungen einer Flüssigkeit in einer Schutzstruktur auf das Bewegungsmoment zu beobachten. Mit diesem zweiten Versuchsaufbau kann untersucht werden, wie sich die Ausstoßrichtung der Flüssigkeit in Bezug auf die ursprüngliche Belastung durch den Blast auswirkt.

Université Paris-Saclay
Espace Technologique / Immeuble Discovery
Route de l'Orme aux Merisiers RD 128 / 91190 Saint-Aubin, France